UNIVERSITY OF SOUTHAMPTON

SIGNALLING CASCADES INDUCED BY TYPE I AND II ANTI-CD20 MONOCLONAL ANTIBODIES

Claire Anne Walshe BSc. (Hons)

Doctor of Philosophy

Cancer Sciences Division
Faculty of Medicine, Health and Life Sciences

May 2006

UNIVERSITY OF SOUTHAMPTON

ABSTRACT

FACULTY OF MEDICINE, HEALTH AND LIFE SCIENCES
CANCER SCIENCES DIVISION

Doctor of Philosophy

Signalling cascades induced by Type I and II anti-CD20 monoclonal antibodies

Claire Anne Walshe BSc. (Hons)

CD20 is a non-glycosylated phosphoprotein exclusively expressed on B lymphocytes and the target for the highly successful immunotherapeutic drug, Rituximab. Rituximab (Ritux) is an anti-CD20 monoclonal antibody (mAb) and has been successfully used to treat over a half a million Non Hodgkin's lymphoma patients. However, not all patients respond to Ritux treatment. The reason for this is currently unclear. Furthermore, although Rituximab and other anti-CD20 mAb are known to deplete B cells through complement dependent cytotoxicity (CDC), antibody dependent cellular cytotoxicity and direct signalling of programmed cell death (PCD) and growth arrest, which of these predominate and whether they are the same for each mAb remains unclear. In particular, the signalling cascades evoked by ligating CD20 are poorly understood. Therefore, one of the aims of this project is to dissect the signalling cascades induced by anti-CD20 mAb in order to better understand the mechanisms of CD20-directed therapy.

Using a range of different techniques we demonstrated that some but not all anti-CD20 mAb could redistribute CD20 in the plasma membrane into Triton-X 100 insoluble raft domains. The mAb which were good redistributors of CD20, like Ritux, were also effective mediators of CDC yet were poor inducers of PCD. These mAb were classed as Type I. In contrast, mAb which were poor redistributors of CD20 were also ineffective at mediating CDC, yet induced effective PCD. These mAb were classed as Type II mAb. Type I, but not Type II, mAb induced a calcium signalling cascade upon CD20 ligation in both B-lymphoma cell lines and primary B cells. This event was found to be dependent on the B cell receptor (BCR) complex. Importantly, we demonstrate that even though Type I and Type II mAb bind the same target, they induce distinct signalling cascades. Further knowledge of these signalling pathways and their operation in primary tumour cells may provide the means to better understand the critical parameters involved in patient response to CD20-directed therapy.

To my wonderful Parents
Tony & Joan

LIST OF CONTENTS

Chapter 1: Introduction

Chapter 2: Materials and Methods

Chapter 3: Activation of complement lysis by anti-CD20 mAb

Chapter 4: Association of CD20 with lipid raft micro-domains

Chapter 5: Calcium Signalling induced by anti-CD20 mAb

LIST OF TABLES

Chapter 1

Chapter 2

Chapter 3

Chapter 4

Chapter 5

Chapter 6

Appendix I

ACKNOWLEDGEMENTS

I would like to thank Prof. Martin Glennie for giving me this opportunity and for all his helpful guidance and encouragement and indeed the great insight into fishing in Ireland.

Most hearty thanks must go to the Dr. Mark 'Speedy Gonzales' Cragg, who I was lucky enough to have as my supervisor. His great leadership and infinite enthusiasm and optimism were at the very least, inspirational.

To all in Tenovus research laboratory who have made my time in Southampton a great pleasure; to Chris, Juliet and Fernanda for all the not-so-scientific discussions and of course Claude, Alison, Ruth, Weng and Mo for their time, patience and kindness. A big thanks in particular to Dr. Steve Beers for all his time and fortitude in wading through my Irish colloquialisms with that dreaded red pen!

I also need to thank my sponsors Tenovus Cancer Charity, Cardiff and all the people who kindly provided cells, antibodies and advice throughout my project.

There are always so many people one would like to thank for their time and patience, but invariably there is never enough space! However, one person I owe a dept of gratitude to is Mrs M. Noonan, my science teacher at St. Mary's Secondary School, who sowed the seeds of scientific interest in a way that only a great teacher can.

I am also deeply grateful to Ryan for so many things but in particular for his unending support and understanding and always being able to bring a smile to my face when I needed it most.

Finally, I would like to thank my family for their constant love and support. To Adrian and Louise for always giving me something to aspire to and to Mum and Dad for everything and so much more.

'Tús maith leath na hoibre'

Publications

Cragg MS, Walshe CA, Ivanov AO, Glennie MJ. The biology of CD20 and its potential as a target for mAb therapy. **Current Directory Autoimmunity**. 2005;8:140-74.

Chan HT, Hughes D, French RR, Tutt AL, Walshe CA, Teeling JL, Glennie MJ, Cragg MS. CD20-induced lymphoma cell death is independent of both caspases and its redistribution into triton X-100 insoluble membrane rafts. **Cancer Research** 2003 Sep 1;63(17):5480-9.

Walshe CA, Beers S, French RR, Chan HT, Glennie MJ and Cragg MS. Cytosolic calcium flux evoked through CD20 engagement is dependent upon its association with the BCR. **In preparation.**

Presentations

Parts of this work has been presented at:

Walshe CA, Chan HT, Hughes D, French RR, Tutt AL, Teeling JL, Glennie MJ, Cragg MS. CD20-induced lymphoma cell death is independent of both caspases and its redistribution into triton X-100 insoluble membrane rafts. Poster Presenstation. Keystone Symposia, Lymphocyte Signalling conference, January 2004

C.A. Walshe, M.S. Cragg, R.R. French, M.J. Glennie. Different signalling cascades of Type I and II anti-CD20 monoclonal antibodies. Poster Presentation. Keystone Symposia, Cellular Senescence conference, March 2005

C.A. Walshe, M.S. Cragg, R.R. French, M.J. Glennie. Different signalling cascades of Type I and II anti-CD20 monoclonal antibodies. Oral presentation; Postgraduate Conference, University of Southampton, June 2005.

ABBREVIATIONS

ADCC:	Antibody dependent cytotoxicity
AIF:	Apoptosis inducing factor
ALL:	Acute lymphoblastic leukaemia
ARL:	AIDS-related lymphoma
BCR:	B cell receptor
BL:	Burkitt's lymphoma
BLNK:	B-cell linker protein
Btk:	Bruton's tyrosine kinase
BSA:	Bovine serum albumin
$[Ca^{2+}]_{cy}$	Cytosolic calcium,
CDC:	Complement dependent cytotoxicity
CDR:	Complementarity determining region
CHO:	Chinese Hamster Ovary
CHOP:	Cyclophosphamide, Doxorubicin, Vincristine and Prednisone
CLL:	Chronic lymphocytic leukaemia
CR:	Complete response
DAG:	Diacylglycerol
DCs:	Dendritic cells
DMSO:	Dimethyl sulfoxide
DRM:	Detergent resistant microdomain
EBV:	Epstein Barr virus
EM:	Electron microscopy
ER:	Endoplasmic reticulum
ERK:	Extracellular signal regulated kinase
FACS:	Fluorescent activated cell sorter
FCS:	Foetal calf serum
FDA:	Food and drug administration
FITC:	Flourescein isothiocyanate
FL:	Follicular lymphoma
FRET:	Fluorescence resonance energy transfer
FSC:	Forward scatter
GAM:	Goat anti-mouse
GPI:	Glycosylphosphatidyl inositol
HACA:	Human-anti-chimeric-antibody
HAMA:	Human anti-mouse antibody
HARA:	Human anti-rabbit/rat antibody

HRP:	Horse Radish Peroxidase
IAP:	Inhibitors of apoptosis
I_{CRAC}:	Calcium release activated current
Id:	Idiotype
Ig:	Immunoglobulin
IP_3	Inositol 1,4,5-triphosphate
ITAM	Immuno-receptor tyrosine-based activation motif
JNK-1:	c-jun NH2-terminal kinase
mAb:	Monoclonal antibodies
MAC:	Membrane attack complex
MAH:	Mouse anti-human Fc antibody
MAPK:	Mitogen activated protein kinases
MCD:	Methyl-β-cyclodextrin
MDR:	Multidrug-resistance
MHC:	Major histocompatibility complex
NFAT:	Nuclear Factor of Activated T cells
NFκB:	Nuclear factor κB
NHL:	Non-Hodgkin's lymphoma
NHS:	Normal human serum
NK:	Natural killer cells
NT:	Non-treated
OR:	Objective response
PAG:	Phosphoprotein associated with glycospingolipid rich microdomains
PAGE:	Polyacrylamide gel electrophoresis
PBA:	PBS/BSA/sodium azide
PBS:	Phosphate buffered saline
PCD:	Programmed cell death
PI:	Propidium iodide
PI3K:	Phosphoinositide 3-kinase
PIP_2:	Phosphatidlyinositol (3,4)-bisphosphate
PKC:	Protein kinase C
PLC:	Phospholipase C
PMA:	Phorbol 12-myristate 13-acetate
PS:	Phosphatidyl serine
PTK:	Protein tyrosine kinases
RIT:	Radio-immunotherapy
Ritux:	Rituximab
ROS:	Reactive oxygen species
SDS:	Sodium dodecyl sulphate

SHIP:	SH2-domain containing inositol phosphatase
SSC:	Side scatter
Syk:	Splenic tyrosine kinase
TBS:	Tris buffered saline
TNF:	Tumour necrosis factor
TX:	Triton X

CHAPTER ONE

1.0 Introduction

1.1 General introduction

One in three of us will develop cancer. After heart disease, cancer is the second highest cause of death in the western world. The development of cancer is a multi-step process resulting in a breakdown of the normal mechansims that govern cell behaviour. Cancers are derived from normal cells that have undergone malignant transformation resulting in dysregulated proliferation, invasion of normal tissues and metastasis to distant sites. Metastasis is the major property which leads to death of the host. Tumours which do not progress to this stage are said to be benign [1].

Cancer is caused by the mutation of cellular DNA. These mutations can either be inherited or, more commonly, induced by a variety of mechanisms such as viruses, random spontaneous mutations or external carcinogens such as chemicals and radiation. As every nucleated cell has the potential to become malignant, a broad spectrum of neoplasia can occur where over 100 distinct cancers and their tumour subtypes have been identified. Tumours are classified according to the origin of the tissue from which they are derived [2].

Lymphomas are a heterogenous group of lymphoid tumours, mainly of B-cell origin, which are grouped based on morphological criteria into two categories: Hodgkin's disease or Non-Hodgkin's lymphoma (NHL), where the latter makes up four in five lymphomas. NHL is the fifth most common malignancy in the United States and is the leading cause of cancer-related death of people between 20 and 40 years of age [3]. Treatment of NHL with conventional therapeutic approaches such as chemotherapy and radiotherapy are not always successful and can lead to high patient toxicity. Therefore other avenues of research such as immunotherapy are actively being explored.

1.2 The immune system and cancer immunotherapy

All multicellular organsims have evolved to defend themselves against the invasion of pathogenic organsims by means of an immune response. The immune system comprises of two parallel but interrelated systems - the innate and the adaptive immune systems. Both systems work together to provide protection against a diverse and evolving array of pathogens. In general, innate immunity is a non-specific, inducible response to pathogens primarily mediated by neutrophils, macrophages and natural killer cells. It is immediate in action, yet short-lived. On the other hand, the adaptive immune system is much more specific, but takes longer to activate. Adaptive responses comprise of both cellular and humoral elements which result from clonal expansion of antigen specific T and B lymphocytes, respectively. In the humoral immune response, soluble proteins called antibodies or immunoglobulins function as recognition elements that bind to foreign molecules. These responses mainly protect the host against extracellular bacteria and toxins. In the cellular immune response, cytotoxic T lymphocytes kill host cells that have been infected with foreign pathogens such as intracellular bacteria and viruses. The adaptive immune response features immunological memory, giving enhanced responses after a second exposure to the same antigen.

The concept of cancer immunotherapy is based on the use of the body's immune system to fight cancer. Even though most human malignancies express tumour-associated or tumour-specific antigens, they often lack sufficient immunogenicity to generate an effective immune response [4, 5]. Therefore the immune system often requires an extra boost to potentiate an effective immune response against tumours. Numerous stratagies, or immunotherapies, have evolved to try to augment these immune responses to generate effective tumour immunity. The first reported attempt was made by an American surgeon Willam Coley over 100 years ago who treated sarcoma patients with bacterial toxins to remarkable success [6]. Since then there have been considerable advances in our understanding of the immune system and the host response to tumour.

In general, cancer immunotherapy can be either active or passive. Vaccines and the use of certain cytokines such as IL-2 are classed as active therapies as they aim to

induce the body to produce a natural adaptive immune response against tumours. In contrast, passive therapies such as antibody infusion or adoptive transfer of cytotoxic cells, provide the end products of the immune response directly into the patient instead of inducing the body to mount an immune response itself (reviewed in [7]). All of these approaches have been demonstrated to be effective in the treatment of neoplasia. However, to date it is primarily monoclonal antibody (mAb) mediated therapies that have gained approval from the food and drug administration (FDA) for the treatment of cancer.

1.2.1 Monoclonal antibody-mediated therapy

The use of highly specific mAb has been generally welcomed due to their low toxicity allowing patients in poor clinical condition to be treated without life-threatening toxicity [8]. However, the concept that mAb could be used in the treatment of various malignancies took over 15 years to be realised.

The first indication that mAb might have significant therapeutic potential was in 1982 when Levy and colleagues reported that a patient treated with anti-Idiotype (Id) mAb achieved a complete and durable response with no significant toxicity [9]. An idiotype is the part of the variable domain of an immunoglobulin (Ig) molecule which is immunogenic and unique to a particular Ig (See Section 1.3.1). Targeting this region of the surface Ig (sIg) with an anti-Id mAb can result in depletion of malignant B cells. The downfall of this therapy was that each anti-Id mAb had to be custom made for each patient, making it unfeasible for routine use. Since 1982, hundreds of clinical trials were performed to assess the therapeutic efficacy of mAb targeted to different tumour antigens. Unfortunately, these trials on the whole were disappointing. One of the main factors thought to be contributing to poor efficacy was that most of the mAb utilised were of murine, rabbit or rat origin and so patients often generated a humoral immune response against these foreign mAb, referred to as HAMA (human anti-mouse antibody) or HARA (human anti-rabbit/rat antibody). Such responses resulted in a short half life ($t_{1/2}$) of the therapeutic mAb in circulation. To minimise immunogenic responses to the mAb, chimeric antibodies were subsequently produced through genetic engineering. Chimeric mAb consist of the constant regions from human mAb and the variable domain of the original murine

mAb (see Figure 1.2). These engineered mAb are potentially more effective in achieving therapeutic responses than murine mAb as they are less immunogenic (a human-anti-chimeric-antibodies (HACA) response is rarely observed), they contain a human Fc domain (generally IgG1) allowing more efficient interaction with human (host) effector systems and they have a longer $t_{1/2}$ in circulation (reviewed in [8]). With the use of these chimeric mAb and through the selection of more suitable antigens as targets, the therapeutic potential of mAb became clear with the arrival of Rituximab and campath-1H (which target CD20 and CD52, respectively), demonstrating good therapeutic potential in the treatment of lymphoma and leukaemia. Therapeutic efficacy has also been achieved using antibodies that target other tumour cell surface antigens. To date, eight mAb have gained FDA approval for the treatment of various cancers, these are outlined in Table 1.1. Five of these reagents have been approved for treatment of B cell malignancies.

MAb name	Commercial name	Target	Target malignancy
Rituximab	Rituxan	CD20	B-cell lymphoma
Trastuzumab	Herceptin	HER2/neu	Breast cancer
Gemtuzumab	Mylotarg	CD33	Acute myeloid leukaemia
Alemtuzumab	Campath	CD52	B-Chronic lymphocytic leukaemia
Ibritumomab tiuxetan	Zevalin	CD20	B-cell lymphoma
Tositumomab	Bexxar	CD20	B-cell lymphoma
Cetuximab	Erbitux	EGFR	Colorectal cancer
Bevacizumab	Avastin	VEGFR	Colorectal cancer

Table 1.1: FDA approved mAb for the treatment of cancer.

1.3 B Lymphocytes

B cells are the principal cellular mediator of the humoral immune system, allowing the host to effectively defend their environment from invading pathogens [10]. B cell development takes place in distinct differentiation steps that can be characterised by

the expression pattern of various differentiation makers, such as the B cell receptor (BCR)

Early B-cell development occurs in the bone marrow and concludes when a B-cell precursor successfully rearranges its Immunoglobulin (Ig) heavy- and light-chain genes and is equipped with a functional surface BCR (illustrated in Figure 1.1). Cells that express a functional and non-autoreactive BCR (i.e. do not bind to self-antigens), differentiate into mature naïve B cells and migrate from the bone marrow into the periphery. Mature B cells can then be activated by foreign antigen and become an antibody-secreting plasma cell or a memory B cell which will respond more quickly to a second exposure to the antigen. B cells which fail to successfully complete B cell development undergo programmed cell death or apoptosis (for a detailed overview refer to [10]).

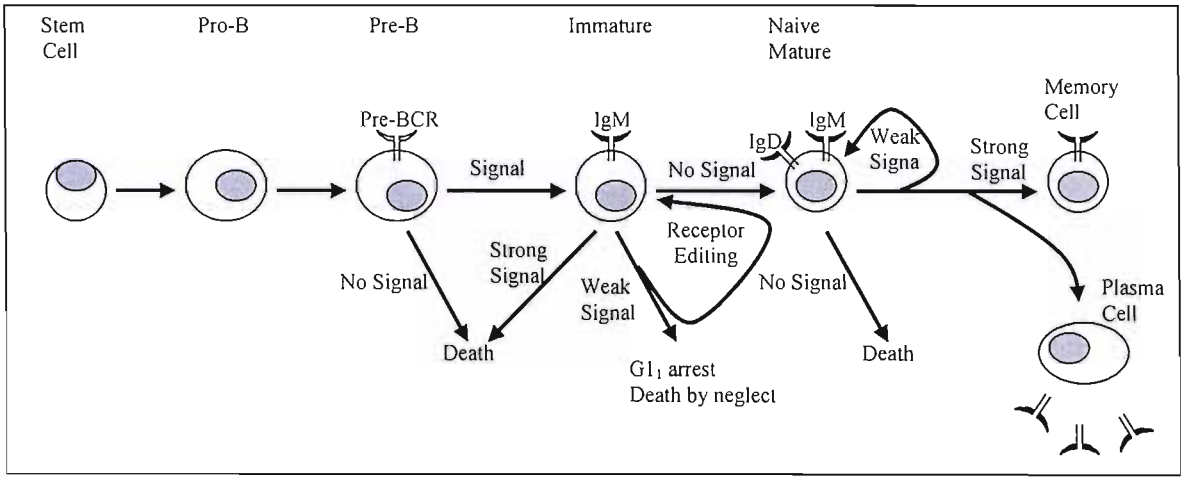

Figure 1.1: The Developmental progression of B cells. B cells originate in the bone marrow from stem cells, differentiate into pro-B cells and then into pre-B cells that express a pre-BCR. From the pre-B cell stage it is thought that signals derived from the BCR drives B cell differentiation allowing cells to mature. BCR signalling pathways are also important in selecting B cells that only recognise and react to foreign antigen allowing the production of high affinity Ab secreting plasma cells against the target.

1.3.1 Antibodies

Antibodies, or immunoglobulins, are soluble glycoprotein molecules that are secreted by plasma cells in response to the presence of foreign molecules in the body. The

structure of an IgG antibody is shown in Figure 1.2. It is composed of three globular units; consisting of two identical Fab arms and an Fc tail. The characteristic structure consists of four polypeptide chains; two identical heavy (H) chains (50-70kD) and two identical light (L) chains (23kD) linked through non-covalent and disulphide interactions. Both the heavy and light chains can be divided into two distinct domains, the constant (C) and variable (V) domains. The V regions of both the H and L chains combine to form a specific antigen binding pocket. Comparisons of the amino acid sequences of the variable regions show that most of the variability resides in three regions called the hypervariable or complementarity determining regions (CDRs). These CDR regions provide the unique specificity of the Ab which is identical for each Fab arm. These V regions also contain the idiotype of the Ab, an immunogenic region specific to each Ab which can be used to generate an Ab against the original Ab. As mentioned earlier in Section 1.2.1, anti-idiotype mAb have been successfully used in the clinic for the treatment of NHL.

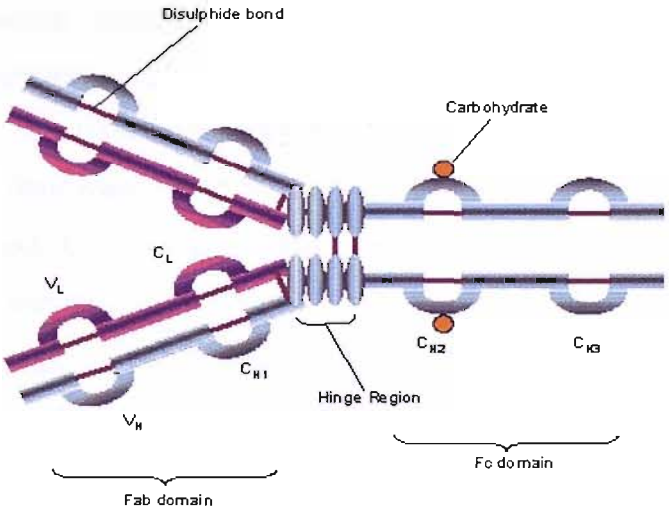

Figure 1.2: Overview of antibody structure. Antibodies are composed of three globular domains – two Fab domains and an Fc domain which are connected by the hinge region. The specificity of the antibody is determined by the binding pockets located in the variable regions of the Fab domains. The Fc domain is primarily involved in the recruitment of cellular effectors.

Digestion with papain cleaves the Ab molecule into three globular domains; two Fab domains and the Fc domain. Moreover, digestion with pepsin can digest the Ab just below the point where the two Fab arms join, known as the hinge region, to form a $F(ab')_2$ fragment and Fc fragment [11]. The $F(ab')_2$ fragment produced therefore maintains the specificity and binding affinity of the original Ab without the ability to engage effector mechanisms through the Fc domain. The Fc portion of the molecule

consists of the constant domains of the two heavy chain molecules. It determines the isotype of the antibody and serves as a binding site for complement and effector cells [12].

1.3.2 B cell receptor signalling

The BCR consists of a membrane bound immunoglobulin (primarily IgM, IgD or IgG) which is non covalently associated with the CD79 alpha (α) and beta (β) heterodimer in the membrane. It plays a fundamental role in the regulation of B cell development and in the activation of the B cell in response to foreign antigen [10]. The structure of the BCR is similar to the antibody structure outlined in Section 1.3.1. The main difference between the structures of secreted and membrane bound Ig lies in the length of the Fc region with membrane bound forms possessing an additional transmembrane domain allowing for insertion into the plasma membrane. In addition, the membrane bound forms also possess an intracellular tail, which varies according to isotype; for example sIgM has 3 intracellular amino acid residues compared to sIgG which has 28 intracellular amino acids. . Surface Igs are not capable of signal transduction on their own but require the association of CD79α and CD79β. These molecules contain cytoplasmic immunoreceptor tyrosine-based activation motifs (ITAMs) which can transmit signals following sIg cross-linking [13]. Depending on the differentiation stage of the B cell and on the activation of other B cell surface receptors that modulate BCR signalling, the activated B cell might be induced to proliferate, die and/or undergo further differentiation steps [14].

Cross-linking of the BCR with multivalent antigen or artificially with mAb causes receptor aggregation and leads to activation of intracellular protein tyrosine kinases (PTK), release of intracellular calcium and the activation of nuclear transcription factors. The resting BCR is associated with Src family PTKs such as Blk, Lyn and Fyn. The association of these kinases with the receptor is mediated through a binding motif located in the intracellular domain of CD79α. Syk kinase is also thought to be weakly associated with the resting BCR complex. Tyrosine phosphorylation of the ITAM motifs of CD79 drives Syk recruitment which is believed to be the primary kinase involved in the initiation of downstream signalling cascades involving phospholipase C gamma (PLCγ) and Ras which lead to the activation of transcription

factors such as nuclear factor κB (NFκB), c-jun and Nuclear Factor of Activated T cells (NFAT) [15, 16]. These pathways are overviewed in Figure 1.3 and reviewed in [14].

1.3.2.1 BCR mediated calcium signalling

One of the earliest intracellular responses to BCR activation along with protein tyrosine phosphorylation is the increase in concentration of intracellular calcium [17]. Upon BCR activation, the ITAMs become phosphorylated by Src family kinases and Syk is recruited. Simultaneous with phosphorylation of the ITAMs, B-cell linker protein (BLNK) is recruited to the CD79α chain. BLNK is an adaptor protein and therefore has no intrinsic signalling ability but serves as a scaffold for the recruitment of other signalling molecules. Once localised to the membrane through its recruitment by CD79α, BLNK associates with Bruton's tyrosine kinase (Btk) where it can become phosphorylated by Src family kinases such as Lyn or Fyn [18] (see Figure 1.3). It is thought that BLNK co-ordinates the localisation of Btk and Syk to facilitate rapid and effective activation of phospholipase Cγ2 (PLCγ2) [19]. Phosphatidylinositol 3-kinase (PI3-kinase) is also required for activation of PLCγ2 [20]. Activated PI3K phosphorylates PIP_2 to produce phosphoinositol 3,4,5-trisphosphate ($PIP_{3,}$), which is critical for the recruitment of pleckstrin homology (PH) domain-containing proteins to the membrane, most importantly, the Tec family kinases and PLCγ [20, 21]. Activation of PLCγ2 results in the cleavage of phosphatidlyinositol (3,4)-bisphosphate (PIP_2) to inositol 1,4,5-triphosphate (IP_3) and diacylglycerol (DAG) [22]. IP_3 can then bind to receptors expressed on the surface of the endoplasmic reticulum (ER), causing the release of Ca^{2+} from intracellular calcium stores [17]. The other cleavage product of PIP_2, DAG, can lead to the activation of protein kinase C-β (PKC-β) in the presence of calcium [23]. This can ultimately result in the downstream activation of NFκB [16]. A recent report by Singh et al [24] suggested that the BCR-mediated Ca^{2+} flux employs a positive feedback loop involving Src Family kinases and reactive oxygen species (ROS). Upon BCR cross-linking in Murine A20 cells, a low level of Src family PTK phosphorylation and Ca^{2+} flux occurs. However, during this initial cross-linking, ROS are also generated which is dependent on Src kinase phosphorylation. The investigators elegantly demonstrated that ROS can induce an up-regulation in Src phosphorylation by the inhibition of phosphatases which in turn leads to an up-regulation in Ca^{2+} flux generation. As both Ca^{2+} flux and ROS appear co-dependent,

they suggest that a positive feedback loop is involved in BCR-mediated calcium signalling.

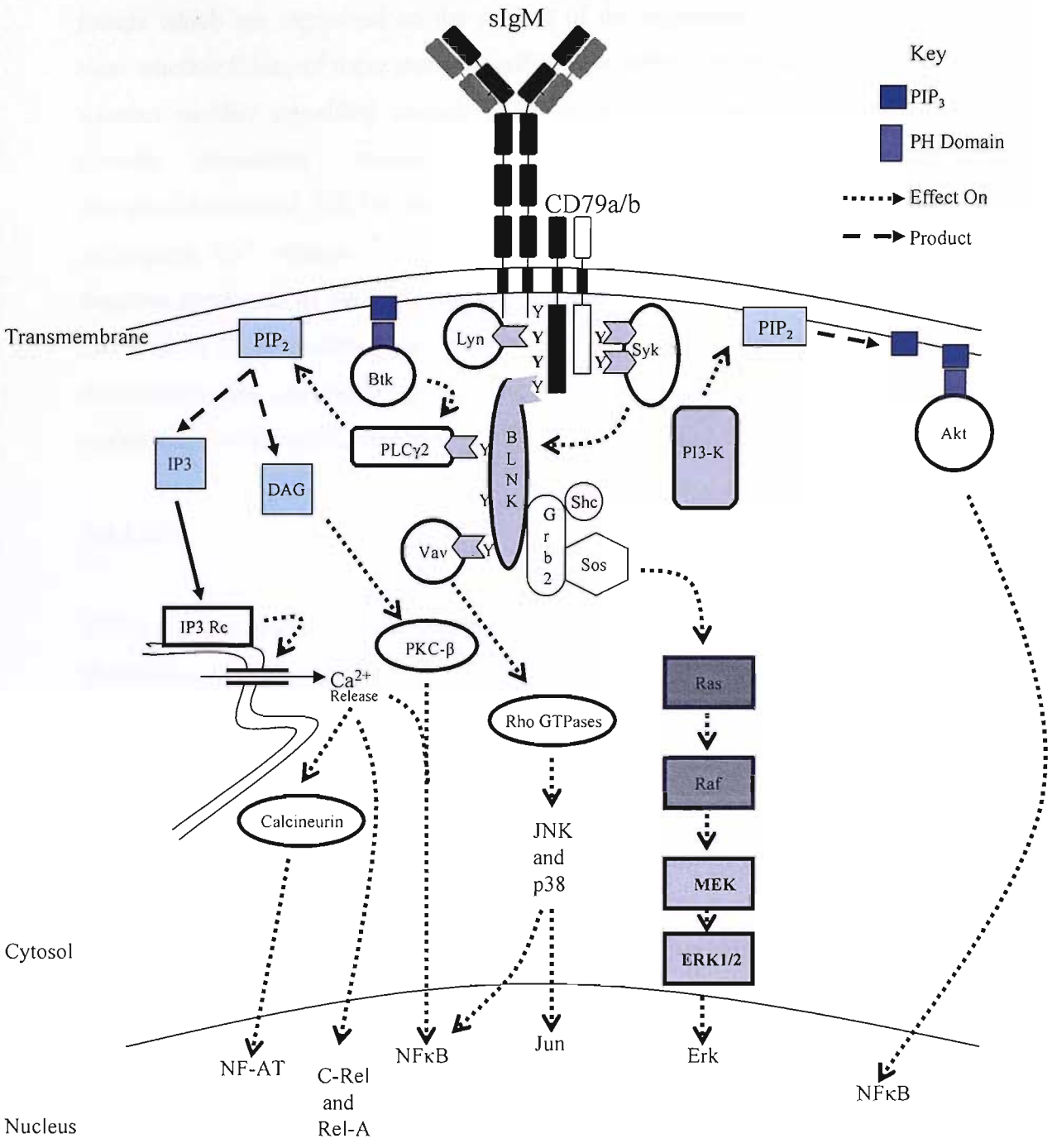

Figure 1.3: Activation of Intracellular Signalling Pathways. Cross-linking of the BCR on the surface of B cells in response to Ag leads to the activation of a variety of PTKs. Activation of these PTKs leads to the activation of intracellular signalling pathways ultimately leading to the activation of nuclear transcription factors within the cell nucleus.

Upon Ca^{2+} entry from the extracellular space, it is thought that the intracellular stores are replenished by the action of SERCA (sarco(endo)plasmic reticular calcium) pumps which are expressed on the surface of the endoplasmic reticulum. It is not clear whether filling of these stores is sufficient to signal for cessation of Ca^{2+} entry or whether another signalling cascade is involved. It has been suggested that SH2-domain containing inositol phosphatase (SHIP) can dephosphorylate phosphatidylionsitol 3,4,5-triphosphate (PIP_3) which can hinder Btk activity and subsequent Ca^{2+} release [18, 25]. Another molecule reported to be involved in the negative regulation of the Ca^{2+} flux is Src family kinases. Cornall et al [26] found that the level of BCR-mediated Ca^{2+} flux was exaggerated in Lyn-deficient mice. This observation was supported by the finding that membrane depolarization of store operated Ca^{+} channels activated by the BCR was mediated by Lyn kinase [27].

1.4 CD20

CD20 is a pan B-cell marker which has proven to be of great clinical importance for the treatment of malignant disease. Testament to this fact is that three out of the eight mAbs approved by the FDA for cancer immunotherapy (see Table 1.1) target this surface antigen. The CD20 molecule illustrated in Figure 1.4 is a 33-37 kDa, trans-membrane, non-glycosylated phosphoprotein, expressed on greater than 95% of normal and neoplastic B cells. CD20 belongs to the recently described MS4A family which includes the β chain of the high-affinity receptor for IgE and the myeloid and lymphoid specific protein HTm4 [28, 29]. Two separate groups cloned and isolated the CD20 gene simultaneously in 1988 [30, 31]. From analysis of the cDNA sequence, four transmembrane domains were proposed with both the amino and carboxyl termini residing in the cytoplasmic region and two potential extracellular loops. Only the second (larger) domain is believed to be the available for mAb binding [32]. This loop is composed of approximately 43 amino acid residues residing between the third and fourth transmembrane regions. From transfection studies in *E. coli*, Ernst et al [33] recently reported that a disulphide bond linking two cysteines in this loop is important for maximal mAb binding. Furthermore, Polyak and colleagues [32] demonstrated that even though there are 43 amino acids available for mAb binding, the loop contains only one main epitope, an alanine-x-proline motif where 'x' can be any amino acid residue, which is crucial for mAb binding to human CD20.

Interestingly, the homology between the family of MS4A genes is focussed in the transmembrane regions with little or no homology observed in the extracellular loop. This suggests that it is the transmembrane regions that play a pivotal role in the function of these proteins yet the extracellular loops may provide specificity for ligand interactions.

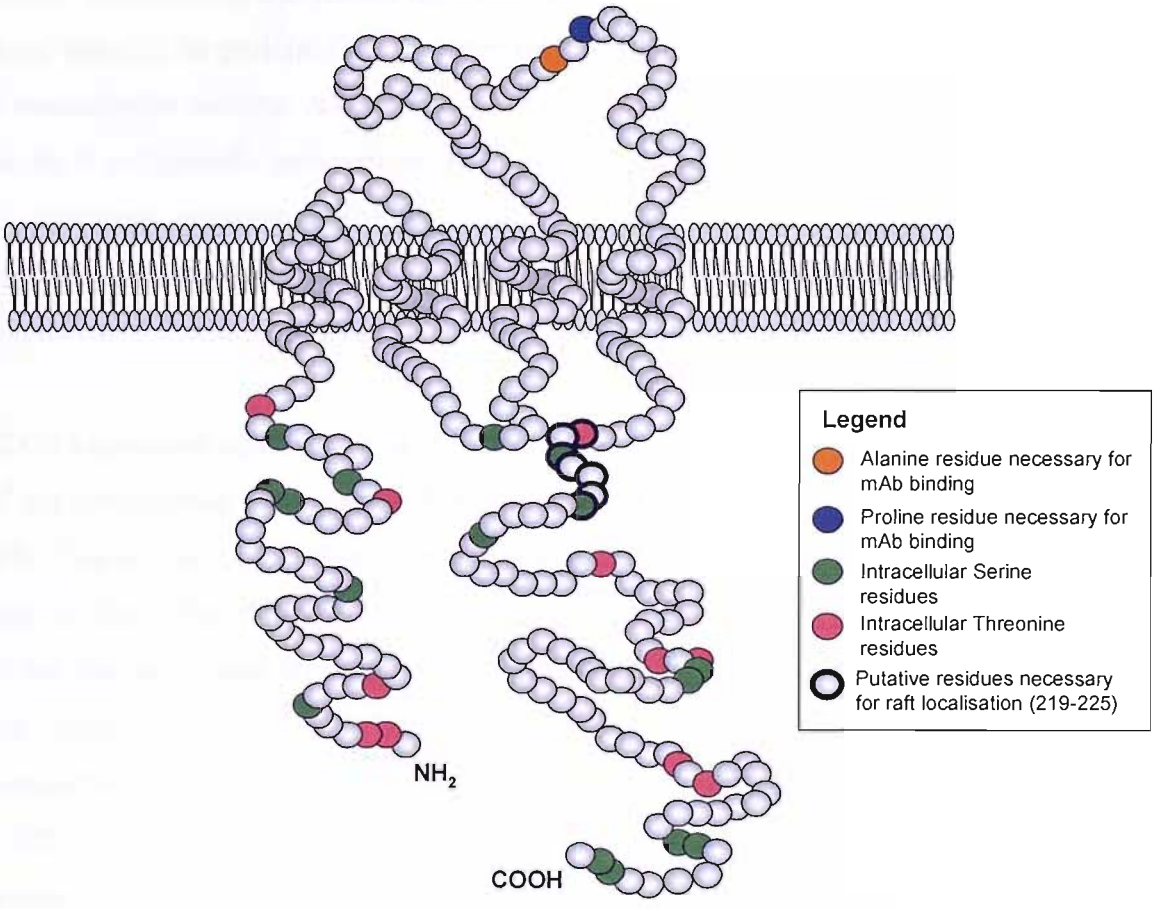

Figure 1.4: Predicted structure of CD20 as it lies in the membrane. The conformation of CD20 allows only one extracellular loop for binding and both N and C termini reside in the cytoplasm.

1.4.1 Transcriptional regulation of the CD20 gene

CD20 is expressed in a lineage-specific and developmentally regulated manner. The CD20 gene is 16kB in length and located on chromosome 11q12-q13.1 [31, 34]. Genes similar to CD20 have also been identified in rat and mouse genomes. Recent work by Tedder et al [29] identified 16 new human and mouse genes that display good homology (23-29%) to CD20, these genes have been grouped together to form the MS4A gene

family. Of the human genes, 7 of the 9 genes including HTm4 are mapped to the same 11q12-q13.1 chromosomal location.

The CD20 gene contains eight exons however as the gene lacks a classical TATA box, it appears to have several minor initiation sites such that transcription could start at several different points in exon 1 and 2 resulting in mRNA lengths from 2.6 to 3.4Kb. Despite this, translation appears to always commence in exon 3 resulting in a single form of the protein. CD20 gene expression appears to be regulated by a number of transcription factors. A BAT box at –225 to –201 contains an octamer binding site for the B cell specific transcription factors Oct-2 and the ubiquitously expressed Oct-1 [35]. However, mutation of the BAT box only resulted in a 40% reduction in CD20 transcription indicating that other regions are of more critical importance in the regulation of CD20 production [35].

CD20 expression commences at the early pre-B cell stage just before the expression of the cytoplasmic μ H chain and is lost upon terminal differentiation into a plasma cell. The control of CD20 to coincide with B cell development is not understood but may be due to the PU.1/Pip transcription factor complex. PU.1 and Pip are members of the Ets family and are important regulators of other B cell-specific genes such as the immunoglobulin light chain and CD72. *In vivo* footprint analysis by Himmelmann et al [36] identified a PU.1/Pip binding site in the proximal end of the CD20 promoter (-160). The appearance of this complex corresponds to the expression of CD20, it is absent in non-B cell lines and CD20-negative pre-B cell lines, up-regulated during B-cell progression followed by down-regulation upon terminal differentiation into a plasma cell [36].

In addition to the PU.1/Pip complex binding site, a binding site for basic helix-loop-helix-zipper (bHLHZ) family proteins was found at position –45. This site binds μE3 specific transcription factors such as TFE3 and USF which are found expressed in most cell types. Intriguingly, co-transfection experiments with mouse fibroblast cells demonstrated that even though the μE3 proteins are not B cell specific, they are the most potent at inducing CD20 expression causing a 9 fold increase in expression compared to a 2 fold increase with the presence of either Oct-2 or PU.1/Pip

complexes [36]. However, the lack of apparent potency of the B cell-specific transcription factors may be due to the absence of other proteins in the mouse fibroblast cells as previous experiments have shown that members of the Ets family are poor transcriptional activators and often function as part of a multi-protein complex [37].

Another regulatory region in the CD20 promoter contains a binding site for the B-cell-specific activator protein (BSAP). This protein is encoded by the Pax5 gene which itself is highly regulated and is required for B cell commitment [38]. BSAP is involved in the regulation of CD19 amongst other B cell specific genes. How or what BSAP interacts with to induce CD20 expression is not fully understood although it has been demonstrated that BSAP and members of the Ets family can interact to induce translation of Igα [38].

In summary, the major site of promoter activity of the CD20 gene is believed to be in the region of –40 to –450. Within these 400 bases at least four regulatory regions have been identified. How these transcription factors interact either in complexes or individually to control CD20 expression is still unclear. However, it is evident that CD20 is regulated both by transcription factors that are involved in B cell specific differentiation and also by ubiquitously expressed proteins which are not dependent on the stage of B cell development.

Furthermore it should be noted that although CD20 expression is generally restricted to B cells, aberrant expression on T cells has been reported in rare cases of T cell acute lymphoblastic leukaemia (ALL), NHL and chronic lymphocytic leukaemia (CLL) [39-40].

1.4.1.2 Modulation of CD20 expression

A number of studies have reported the effect of cytokines on the expression of CD20. For example, interleukin-4 (IL-4) and tumour necrosis factor-α (TNF-α) were found to up-regulate CD20 in cell samples derived from CLL patients [41, 42]. Interferon –α (IFN-α) induced a significant up-regulation of CD20 on cells from B-CLL patients

with no increase observed in normal patients [43]. In support of this, Bryostatin-1 a PKC inhibitor which can induce expression and secretion of IFN-γ was shown to up-regulate CD20 in Ramos B cells through ERK dependent mechanisms [44].

1.4.2 Sub-cellular location of CD20

Once expressed, much evidence has accumulated to suggest that CD20 does not reside in cell membranes in monomeric form but most likely forms multimers, possibly tetramers. Immunoprecipitation experiments yielded products of 33kDa, 70kDa and 140kDa suggesting that CD20 proteins exists as dimers and tetramers [32, 45]. Furthermore, it has been suggested that CD20 associates with other signalling molecules such as CD40, MHC class II and can transiently reside with the BCR [46, 47]. How CD20 interacts with these molecules is not fully understood. A recent study by Li and colleagues [48] demonstrate that CD20 localises to microvilli in the membrane where both the BCR [49] and MHC Class II [50] are also known to localise suggesting that the actin cytoskeleton may play an important role in CD20 associations and function.

1.4.3 Putative physiological function of CD20

The physiological role of CD20 remains elusive. However, there is strong evidence to suggest that it may function as a calcium ion channel. The first demonstration of this came from a study by Bubein et al [45] who demonstrated that transfection of CD20 into human T and mouse lymphoblastoid cells resulted in an increase in the level of cytosolic calcium, $[Ca^{2+}]_{cy}$ in resting cells.

The potential of CD20 to function as a Ca^{2+} ion channel may explain its putative role in the regulation of cell cycle progression. It has been demonstrated that CD20 ligation with mAb prevents cell cycle progression from G1 to S-G2/M and can induce cell death [51-53]. However, this is not always observed upon CD20 mAb ligation as it has also been demonstrated that stimulation with anti-CD20 mAb IF5 can induce B cell proliferation and suppress apoptosis of germinal centre B cells [54, 55]. The reason why such apparently conflicting cellular effects are induced could possibly be explained by the different calcium flux profiles generated by the various mAb. Bubein et al [45] demonstrated that stimulation of Daudi cells with the anti-CD20 mAb

B1 induced a slow, steady increase of $[Ca^{2+}]_{cy}$, whereas IF5 caused an acute increase in transmembrane conductance. More recent studies performed by Shan et al [56] demonstrated a difference in flux observed in Ramos cells when CD20 was hyper cross-linked with anti-CD20 mAb B1, 2H7 and IF5. The profiles observed were somewhat different to that reported by Bubien in that there was no acute rise in $[Ca^{2+}]_{cy}$ upon IF5 ligation. However it should be noted that the cell line and the system used to assess calcium changes were different, in Bubien's studies whole cell patch-clamp analysis was employed and a calcium dye system was used in the latter report.

The studies mentioned above refer to the ability of CD20 to induce a calcium flux upon mAb ligation. CD20 however has no known ligand. Therefore in a more physiological setting, it is probable that CD20 functions as part of a signalling pathway initiated by ligand binding to other surface antigens. It has been suggested that CD20 may play a role in BCR-mediated Ca^{2+} flux [48, 57]. Recent work by Uchida and colleagues [57] suggested that the calcium flux observed upon BCR or CD20 stimulation is reduced in CD20 knockout mice. However, upon more thorough investigation of their results, this conclusion is questionable due to the reduced expression of IgM on the surface of B cells from CD20-knockout mice ($CD20^{-/-}$). In addition it was suggested that these cells displayed a lower calcium flux upon CD19 ligation. Even though no down regulation of CD19 was observed, it would be tenable that a reduced expression of IgM could lead to a reduced amount of CD19/BCR complexes and hence reduced calcium flux profile. The lack of a distinct phenotype in $CD20^{-/-}$ was disappointing however, as calcium flux is such an important cellular process, it is possible that other members of the MS4A family or other calcium regulators may compensate for the loss of CD20, therefore masking an obvious phenotype. Further work with the use of conditional knockouts may resolve this issue.

Avoiding the difficulties with CD20 knockout mice, Li et al [48] demonstrated a clear link between CD20 and BCR induced calcium flux where knockdown of CD20 expression in BJAB cells using siRNA resulted in a marked decrease in the calcium flux generated upon IgM stimulation. Importantly, this effect was implicated to be due to a reduction in store operated channel (SOC) opening [48]. In cells there are two

main classifications of ion channels - voltage-operated and non-voltage operated channels. Voltage operated channels are usually found in excitable cells such as neuronal and muscle cells and are dependent upon the potential across the membrane. Conversely, SOC generate Icrac (Ca^{2+} release activated Ca^{2+}) currents. Such currents are biphasic in nature. The first phase involves the release of calcium from intracellular stores, generally from the endoplasmic reticulum. This in turn activates the second phase which involves the activation of plasma membrane ion channels to facilitate calcium influx from the extracellular milieu and subsequent repletion of these stores (reviewed in [58]). The mechanism involved in the activation of SOC is not fully understood, however several hypotheses have been proposed; the use of secondary messengers, transportation of ion channels to the surface via vesicles and physical docking of the ER with the plasma membrane (reviewed in [17]).

In B lymphocytes, the two phases of calcium mobilisation are thought to be coupled to different signalling pathways where a release from intracellular stores is sufficient to activate NFκB but is insufficient for the activation of NFAT which requires a sustained increase in calcium [59]. Even though CD20 is reported to mediate Ca^{2+} flux through store operated channels the possibility of the involvement of other ion channels should not be ruled out as recently, channels that demonstrate L-type voltage-gated characteristics have been associated with BCR-mediated calcium flux [60].

The exact nature of the involvement of CD20 as a SOC in IgM-mediated Ca^{2+} flux is not clear. There is strong evidence to indicate that CD20 forms part of the SOC ion channel itself. First, it has been shown that the intensity of calcium flux after store depletion is proportional to the CD20 expression level [48]. Second, CD20 shows good structural homology to other ion channels (in being a tetraspan molecule and found in oligomeric complexes in the membrane [34, 45]). Third, CD20 transfection into Chinese Hamster Ovary cells and Jurkat T cells significantly enhanced cytosolic calcium levels [48]. Finally, studies in Hairy Cell Leukaemia revealed that CD20 is over expressed and hyper-phosphorylated and that cytosolic calcium levels are elevated in these cells compared to normal B cells [61].

In addition to its role as a SOC in IgM signalling, calcium flux may also be evoked by ligation of CD20. Interestingly, CD20 phosphorylation in resting cells is up-regulated upon mAb stimulation suggesting that phosphorylation of CD20 may play a role in the regulation of CD20-mediated calcium flux. Incubation of cells with the calcium ionophore Ionomycin, induced a time dependent phosphorylation of CD20 which was detectable within 5 seconds and plateaued after 2 minutes [61]. Furthermore, treatment of Ramos B cells with PP2 (a Src family tyrosine kinase inhibitor) resulted in abrogation of calcium flux observed with cross-linked anti-CD20 mAb 2H7 or ritux [56, 62]. Another important cellular protein phosphorylated upon CD20 stimulation is phospholipase C gamma-2 (PLCγ2) [63]. As mentioned briefly in Section 1.3.2.1, this enzyme can cleave membrane-bound PIP_2 into IP_3 and DAG. IP_3 can diffuse to the ER and stimulate calcium release (see Figure 1.3). The other cleavage product, DAG, is a substrate for protein kinase C (PKC). This kinase also has a substrate binding site on the intracellular domain of CD20. Interestingly, PKC has been linked to the down regulation of other cell signalling pathways [58, 64] and has been suggested to decrease Ca^{2+} flux associated with CD20 mAb stimulation [45].

These data have all lead to the suggestion that the calcium flux generated after anti-CD20 mAb cross-linking is due to opening of a SOC channel, although the direct evidence for this is not readily apparent. For this reason there has been limited work investigating the possibility of involvement of a signalling pathway in CD20-mediated Ca^{2+} flux. Recently, two groups have suggested that in B-cell lines redistribution of CD20 into lipid rafts (discussed in the next section) by anti-CD20 mAb is a pivotal first step for the generation of a Ca^{2+} flux [62, 65].

1.4.4 CD20 association with lipid rafts

There have been several reports demonstrating that CD20 can be redistributed into lipid rafts upon mAb binding [62, 66-68]. Lipid rafts are tightly packed, highly ordered domains, rich in glycosphingolipids and cholesterol which are estimated to contain <1% of membrane proteins (for reviews see [69-71]). Important signalling molecules such as G proteins and Src kinases are thought to constitutively reside within these domains with some non-resident raft proteins, for example the BCR, being

demonstrated to localise with rafts upon cross-linking [72]. These domains are postulated to form important signalling platforms in some signal transduction pathways where compartmentalisation of receptors into and out of rafts can result in new micro-environments, facilitating modification of the receptor's phosphorylation state by local kinases and phosphatases, thereby modulating downstream signalling. It was originally thought that redistribution of CD20 by mAb ligation was necessary to associate CD20 with lipid rafts, where the rafts are characterised by their insolubility in Triton X-100 (TX-100) detergent at 4°C [66]. However, it is now thought that CD20 is constitutively present in "mini" rafts which, on their own are solubilised by TX-100, but remain insoluble in less stringent detergents such as Brij 58 and CHAPS [68]. Therefore, cross-linking CD20 with certain mAb to confer TX-100 insolubility is likely to be a consequence of the clustering of mini-rafts.

The affinity of proteins for lipid rafts can be increased by certain post-translational modifications, such as the addition of glycosylphosphatidyl inositol (GPI) groups or long chain fatty acids (s-acylation or palmitoylation) [73]. CD20 does not appear to have any such modifications. However, the membrane proximal region of the cytoplasmic C-terminal domain of CD20, residues 219-252 (see Figure 1.4), has been shown to be important for translocation of CD20 into TX-100 rafts [74] [52]. Apart from proteins which are constitutively associated with lipid rafts like the dually acylated Src family PTKs [75] and adapter proteins like phosphoprotein associated with glycospingolipid rich microdomains (PAG) which is thought to be palmitoylated [76], the propensity of proteins without these post-translational modifications to translocate into TX-100 rafts upon ligation is relatively rare. Filatov and colleagues [72] found that only 3 out of 24 antigens studied (CD5, CD20 and sIgM) were able to redistribute into TX-100-insoluble fractions after incubation with mAb.

Whether a biochemical event is involved in the redistribution of CD20 into lipid rafts is unknown. A recent review [77] has highlighted the possibility that these domains could be formed by the spontaneous association of ceramide rich microdomains. These ceramide micro-domains are derived from the action of acid spingomyelinase which hydrolyses sphingomyelin in the plasma membrane to release its ceramide moiety. These ceramide molecules are then free to spontaneously associate [77]. Interestingly, it has been reported that Rituximab (ritux) can activate acid

sphingomyelinase in Daudi cells however more work is required to fully understand the implications of this event [78].

1.4.4.1 Isolation of lipid rafts

The main technique utilised to isolate lipid raft fractions is based on their detergent insolubility. Brown and colleagues [79] initially used this technique in 1994 where they isolated detergent resistant microdomains (DRMs) and these were termed lipid raft domains. Detergents work by solubilising membrane components via micelle formation. Above a certain detergent concentration (termed the critical micelle concentration (CMC)), detergent molecules spontaneously self-associate engulfing membrane components in micelles making them water-soluble. Depending on the stringency of the detergent, lipid raft domains can be impervious to this micelle formation and remain insoluble, therefore when separated on a density gradient, they remain buoyant and are localised in the low density fractions [80].

Even though detergent analysis is the most common method used to investigate lipid rafts there have been several arguments over the validity of this technique [80-82]. A summary of these concerns is that the contents of the lipid raft domains can vary greatly and are highly dependent on the cell type and the detergent used. Another major criticism is that detergents are used at 4°C, where lipid packing and redistribution may not reflect the situation in the plasma membrane at 37°C. In addition, detergent insoluble domains cannot determine whether two or more proteins identified in the DRMs are in one distinct raft or in separate ones. Therefore, the identification of two proteins in a raft fraction only indicates that both are in raft domains but does not necessarily imply that they are associated or even localised together. Furthermore, detergent lysis results in a loss in the plasma membrane integrity and therefore cannot be used to detect rafts in living cells. To quell these concerns, it is now common practice to assess lipid rafts using several different detergents and complementary detergent-less methods such as flow cytometry or fluorescent microscopy.

1.4.4.2 The significance of CD20 association with lipid rafts

The significance of the ability of CD20 to redistribute into TX-100 insoluble rafts is unclear. Recent work by Li and colleagues [48] suggests that association of CD20 with lipid rafts is necessary for CD20-mediated calcium flux. Deletion of residues 219-225 in the cytoplasmic tail of CD20, which is important for the association with TX-100 rafts but not for oligomerisation, resulted in a reduction of Ca^{2+} influx. As the suggestion that CD20 can constitutively reside in lipid rafts is a recent one, most work to date has focussed on the significance of CD20 redistribution into TX-100 insoluble rafts. However, Li et al did demonstrate that treatment of cells with methyl-β-cyclodextrin (MCD) which disrupts CD20's constitutive association with rafts also resulted in a decreased flux [48]. Aside from calcium flux generation, work by our group suggests that the clustering of CD20 into TX-100 rafts is an important step in the activation of complement. We found that the mouse anti-CD20 mAb B1 (a poor inducer of CD20 redistribution and complement lysis) and IF5 (a good inducer of raft redistribution and complement lysis) differed in their ability to induce complement even though both are of the same mAb isotype (IgG2a) [67].

Conversely, CD20 clustering does not appear to be essential for all CD20-mediated events. We have reported that one of the most effective inducers of CD20-mediated cell death is B1 mAb which does not stimulate this redistribution into TX-100 insoluble domains [52]. As such, CD20 induced cell death does not seem to depend upon lipid rafts. A similar scenario has also been observed in BCR-mediated apoptosis where Trijillo et al [83] demonstrated that clustering of the BCR into TX-100 rafts is not required for the induction of apoptosis.

1.4.4.3 Cholesterol in lipid rafts

Brown and colleagues [82] demonstrated that rafts isolated in 1% TX-100 contained 32% cholesterol compared to approximately 12% in the rest of the membrane. Cholesterol depletion is often used as a method to disrupt raft integrity. It has been demonstrated that treatment of cells with MCD, a drug that extracts cholesterol, prevents the recruitment of the BCR to lipid rafts [84]. The importance of cholesterol for CD20 mAb binding was first indicated by Polyak et al [85] who demonstrated that

an epitope recognised by the anti-CD20 mAb FMC7, was cholesterol dependent. Work by our group supported these findings and reported that in fact most anti-CD20 mAb required cholesterol for optimal mAb binding suggesting that CD20 is dependent on its plasma membrane micro-environment to provide optimal spatial orientation for mAb binding [86].

1.4.5 Association of CD20 with the actin cytoskeleton

One of the earliest events in some receptor signalling pathways is changes in the actin cytoskeleton. Actin polymerisation occurs by the conversion of monomeric globular (G)-actin to polymeric filamentous (F)-actin [87]. It has been suggested that cytoskeleton-associated proteins are among the most abundant proteins found in rafts and the actin cytoskeleton itself has been implicated in the compartmentalisation of raft domains [88].

Several membrane proteins important in B cell signalling have been reported to be associated with actin filaments such as MHC class II [89] and the BCR [90]. Intriguingly, it has now been revealed that CD20 also associates with microfilaments [68]. This association however does not appear to be important for the redistribution of CD20 into lipid rafts as disruption of actin polymerisation with various inhibitors does not affect the presence of CD20 in the TX-100 insoluble domain. As the actin cytoskeleton plays such a central role in signal transduction, further work is required to fully understand the importance of its association with CD20.

1.4.6 Association of CD20 with other surface antigens

CD20 is reported to be associated with several important signalling molecules such as the BCR [47], MHC class II and CD40 [46] molecules. Deans and colleagues [47] demonstrated that the BCR can co-localise with CD20 on the surface of stimulated B cells until just before BCR internalisation, when rapid dissociation occurs. Furthermore, Mathas et al [91] found that anti-CD20 and BCR-mediated cell death utilise similar signalling pathways and the sensitivity of cell lines to this death was the same for both, independent of the expression level. Other studies have directly linked

CD20 and the BCR by demonstrating that stimulation of IgM results in enhanced phosphorylation of CD20 [47] and can lead to a down-regulation of CD20 expression [92].

Immunoprecipitation studies have also suggested that CD20 is physically and functionally coupled to MHC class II and CD40 [46]. CD40 is critically involved in B cell proliferation and differentiation and stimulation with CD40 ligand or anti-CD40 mAb can protect cells from receptor-stimulated apoptosis [93]. Interestingly, it has been shown that CD20 stimulation can lead to a decrease in CD40 expression [94] indicating a possible mechanism through which anti-CD20 mAb signal for cell death. MHC Class II plays an important role in antigen presentation to $CD4^+$ T cells with mAb ligation of MHC Class II inducing high levels of apoptosis [95]. The pathway involved appears similar to that of CD20 with calcium chelation and Src family kinase inhibition resulting in a significant decrease in the level of cell death occurring.

Furthermore, it has been shown recently that cross-linking of some cell surface antigens on leukaemia cells may lead to an increase (e.g.CD95, CD80) or decrease (e.g. CD32) of CD20-mediated cell death [96]. How CD20 interacts with these molecules to achieve such opposing biological outcomes of cell death and cell survival has yet to be fully understood.

1.4.6.1 Association of CD20 with protein kinases

CD20 itself can be phosphorylated on serine and threonine residues upon mAb stimulation accounting for the different molecular weights (33, 35 and 37 KDa). This phosphorylation is believed to be partially mediated through PKC, evidence for which comes from studies where the activation of PKC by PMA resulted in increased CD20 phosphorylation. Interestingly, use of the PKC inhibitor H-7 also resulted in enhanced phosphorylation of CD20 but on different residues to that induced by PMA [30]. In addition to CD20 itself becoming phosphorylated upon anti-CD20 mAb ligation, other cellular proteins are also known to become phosphorylated such as PLCγ1 and PLCγ2 however this phosphorylation does not occur on serine/threonine but on tyrosine residues indicating a direct link between CD20 and tyrosine kinase activity [56, 97].

Deans et al [98] revealed that CD20 was associated with members of the Src-family PTKs, Lyn, Fyn and Lck. Src kinases serve as molecular switches that regulate a variety of cellular events such as cell growth, division and differentiation. Src PTKs are strictly regulated by the phosphorylation of two tyrosine residues, auto-phosphorylation of a tyrosine (Tyr416) in the kinase domains is required for full activity, whereas phosphorylation of tyrosine 527 located in the C-terminal region abolishes activity. When the C-terminal tyrosine is phosphorylated this causes binding of an internal SH2 domain and results in a closed conformation of the enzyme. Dephosphorylation results in release of the SH2 domain, an open conformation and enzyme activation [99]. The main kinase activity of CD20 is mediated by Lyn [98]. Src family kinases are not directly associated with CD20 but are linked by an adaptor protein known as PAG which also binds to the major negative regulator of Src kinases, C-terminal Src kinase (Csk) [100]. How PAG associates with CD20 is not known, however there is strong evidence to suggest that it is most likely within the transmembrane domain as deletion of a large proportion of the cytoplasmic domain of CD20 did not abolish CD20-mediated phosphorylation [74]. The interaction between CD20, PAG and Lyn is not fully understood, however, the association of these molecules with lipid rafts may be important.

1.5 CD20-directed therapy in the treatment of Non Hodgkin's Lymphoma

CD20 has been highly successful as a target for immunotherapy of B-cell malignancies. This success can be attributed to several factors; firstly, it is ubiquitously and exclusively expressed at high surface densities on normal and malignant human B cells. Secondly, it is not internalised or modulated after mAb binding [101]. Thirdly, rituximab therapy rarely develops CD20 negative disease [7], allowing for patient re-treatment. Moreover, CD20 is not expressed on stem cells or plasma cells, therefore even though patients show a significant drop of plasma IgM levels, they do not become severely immunocompromised as the presence of pro-B cells facilitates repletion of B cells after treatment and the continuation of plasma cells restores the level of circulating antibodies [102].

Several anti-CD20 mAb have been assessed for their therapeutic efficacy. In 1997, the anti-CD20 chimeric antibody Rituximab (Rituxan, IDEC Pharmaceuticals, San Diego, CA) was the first therapeutic mAb to be approved by the US food and drug administration (FDA) for the treatment of cancer. Since then, two CD20-directed radionuclide-labelled mAb, ^{90}Y-ibritumomab tiuxetan and ^{131}I-Tositumomab have also gained approval from the FDA for the treatment of lymphoma.

Rituximab has found its widest application in the treatment of patients with NHL, particularly follicular lymphoma (FL). NHL is a heterogeneous group of neoplasias. These lymphomas are typically separated into indolent or low-grade (small lymphocytic, marginal zone, follicular centre cell grades I and II), intermediate grade (e.g. diffuse large cell) and high grade (lymphoblastic, Burkitt's) subtypes [103]. Patients with low grade lymphoma have a median survival of 10 years but the disease is considered incurable with current therapeutic options [104]. Patients with more aggressive lymphomas such as diffuse large cell lymphoma are potentially curable. Even in the advanced stages of the disease, treatment can achieve long-term remission in 30-50% of cases. For relapsed patients, high-dose chemotherapy and stem cell rescue is often successful. However, relapse with the development of drug resistance remains a major problem [105]. Thus, highlighting the need for other treatment modalities such as immunotherapy.

The typical treatment regime for Rituximab is 375 mg/m^2 administered intravenously weekly for four consecutive weeks [106]. Treatment related toxicity is generally mild and occurs most often with the first infusion of mAb. Initial success was achieved in relapsed or chemorefractory low grade and follicular NHL. Now treatments have diverged to involve ritux as a first line therapy i.e. in previously untreated patients, and in combination with CHOP (cyclophosphamide, doxorubicin, vincristine and prednisone) chemotherapy. Presently, a vast number of clinical studies are in progress to assess the efficacy of ritux in a range of different scenarios. A summary of selected trials are shown in Table 1.2.

Treatment Regimen	Lymphoma	No. of Patients	Response	Median PFS	Reference
Rituximab (Post chemotherapy)	Relapsed or refractory low-grade NHL	166	50% OR 6% CR	13 months	[102]
Rituximab (First Line)	Low-grade lymphoma	49	73% OR 27% CR	34 months	[106]
Rituximab (extended treatment of 8 weeks)	Relapsed or refractory low-grade or follicular NHL	37	57% OR 5% CR	13 months	[107]
Rituximab combined with CHOP	Relapsed low-grade lymphoma	40	95% OR 55% CR	> 40 months	[108]
Rituximab combined with IL-2	Relapsed or refractory follicular NHL	20	55% OR	> 30 months	[109]
Zevalin (^{90}Y-ibritumomab tiuxetan)	Relapsed or refractory follicular, low grade or transformed lymphoma	143	80% OR 30% CR	14.2 months	[110]
Bexxar (^{131}I-Tositumomab)	Relapsed or refractory follicular, low grade or transformed NHL	24	87% OR 81%CR	> 50 months	[111]

Table 1.2: Summary of CD20 directed therapies. OR: overall response CR: complete response PFS: progression free survival

One of the most effective therapy regimes is when ritux is administered in combination with chemotherapy. Greater therapeutic efficacy is believed to be a consequence of the lymphoma cells becoming sensitised to cytotoxic drugs following exposure to the anti-CD20 mAb (see Section 1.6.6). Czuczman et al [102] demonstrated in a trial of 40 patients with low grade B-cell lymphoma who had relapsed after a response to ritux therapy, 95% had an objective response with 55% complete response (CR) rate. The median progression free survival was greater than 40 months and the toxicity observed was similar to CHOP alone. However, conventional chemotherapy regimens achieve long term remission in fewer than 40% of patients with aggressive NHL [112] and fewer than 5% of patients with indolent lymphomas [113]. Because lymphomas are inherently sensitive to radiation, radioimmunotherapy (RIT) is now proving to be a highly effective method for the treatment of NHL. As already

mentioned, two radiolabelled anti-CD20 mAb are currently in use, ^{90}Y-ibitumomab tiuxetan which consists of the murine 'parent' of ritux (C2B8) and ^{131}I-Tositumomab which consists of the murine anti-CD20 mAb, B1. Therefore, cells are being subjected to two modes of cell death, firstly from the direct effects of the mAb such as programmed cell death, antibody dependent cytotoxicity (ADCC) and complement dependent cytotoxicity (CDC) and also the effects from irradiation. Irradiation of cells can result in chromosomal damage and subsequent activation of a p53 mediated apoptotic pathway. RIT has the added advantage that a 'bystander' or 'cross-fire' effect can occur from the irradiation, resulting in the depletion of neighbouring cells inaccessible to antibody or with insufficient antigen expression [114].

Even though good progress has been made in the treatment of NHL, it is evident from Table 1.2 that, to date no curative treatment has been developed for the treatment of low grade lymphoma. Therefore, in the last few years several novel approaches have been employed. One such approach is the combination of ritux with the anti-CD22 mAb Epratuzumab. It has been reported that complete response rates are better when this combination is used compared to ritux on its own [115]. Another novel approach currently being explored is to engineer cytotoxic T cells to express a modified receptor which consists of a single chain Fv (ScFv) antibody fragment (i.e. the variable domains of a Fab arm tethered together by a small linker region) specific to CD20 fused to the CD3 zeta chain [116]. This targets the cytotoxic T cell to the malignant cell, resulting in its destruction. T cells may be more advantageous than soluble mAb as they are highly efficient at mounting a cytotoxic response, can readily move in and out of lymph nodes, lyse multiple targets and persist in circulation for long periods of time. However, this therapy is in the very preliminary stages and more research is required before it can become a tenable treatment option.

1.5.1 Rituximab resistance

Although ritux therapy has significantly improved the treatment outcome of NHL patients, only 50% of patients respond. Various mechanisms have been postulated for ritux resistance and have been recently reviewed by Maloney et al [105], with the main reasons being suggested as transient CD20 down regulation [117] and expression of complement inhibitors [118]. A more recent suggestion is that CD20 is removed from

the surface of B-cells ligated with ritux by the action of macrophages when large numbers of tumour cells are in circulation. Beum and colleagues [119] elegantly demonstrated that when cells from B-CLL patients (which have large numbers of circulating tumour cells) were opsonised with ritux and incubated with FcγR expressing monocytes, CD20:ritux complexes were 'shaved' from the B cells. The loss of CD20 did not appear to be due to internalisation of ritux-bound CD20 but removal of the CD20:ritux complexes through the interaction of the Fc domain of ritux with FcγR receptors on monocytes leading to the endocytosis of these complexes into the monocytes. This report is supported by a recent study demonstrating that depletion of B cells by ritux in CD20 transgenic mice is primarily achieved by macrophages in the liver [120].

1.5.2 The use of ritux in the treatment of other B cell disorders

As is evident from Table 1.2, the primary focus of ritux therapy has been in low-grade NHL, however ritux has also been evaluated for therapeutic efficacy in a range of different lymphomas and other CD20 positive diseases. Large B-cell lymphomas have been shown to be sensitive to CD20 directed therapy. Akhtar et al [121] reported a 97% OR rate with 73% CR using ritux in combination with CHOP chemotherapy where long term follow-up is not yet available. The feasibility of using CD20 related therapies for several other lymphomas such as Waldenstroms macroglobulinemia and mantle cell lymphoma have also been assessed [122, 123]. As B cells play a pivotal role in the adaptive immune response, the efficacy of ritux treatment in a range of auto-immune diseases has also been investigated. These have in some cases proven to be adequately convincing to initiate clinical trials, such as for systemic lupus erythematosus (SLE) [124], AIDS [125], and rheumatoid arthritis [126].

1.6 Effector mechanisms evoked by anti-CD20 mAb

Anti-CD20 mAb are well established as effective immunotherapeutic agents. The main effector mechanisms evoked by CD20 mAb are believed to be complement dependent cytotoxicity (CDC) [118, 127], antibody dependent cellular cytotoxicity (ADCC) [128] and direct induction of growth arrest and programmed cell death (PCD) [51, 129] as illustrated in Figure 1.5. In addition, ritux has been postulated to sensitise

chemoresistant cells [130, 131] and limited evidence suggests a role in direct stimulation of an immune response [132, 133]. The study of CD20-directed B cell depletion has been significantly aided by the recent generation of anti-mouse(m) CD20 mAb [57]. Prior to this, as anti-mCD20 mAb were not available, transgenic mice expressing human CD20 were used to study normal B cell depletion. From these studies with anti-mCD20 mAb in C57BL/6 mice, it was shown that B cells are rapidly depleted from the blood and bone marrow followed by the spleen and other lymphoid tissues. However, B cells in non-lymphoid tissues like the peritoneal cavity were protected from CD20-directed depletion. The effector mechanisms that predominate in CD20-directed therapy remains a topic of debate, Tedder et al [134] reported that ADCC was more important than CDC but did not assess the involvement of direct cell death induction. Furthermore, these studies focus on the depletion of normal as opposed to malignant B cells and it is now becoming apparent that the mode of B cell depletion may depend on its type, origin, location as well as the anti-CD20 mAb employed. The potential mechanisms engaged by anti-CD20 mAb and evidence for their involvment are highlighted in more detail below.

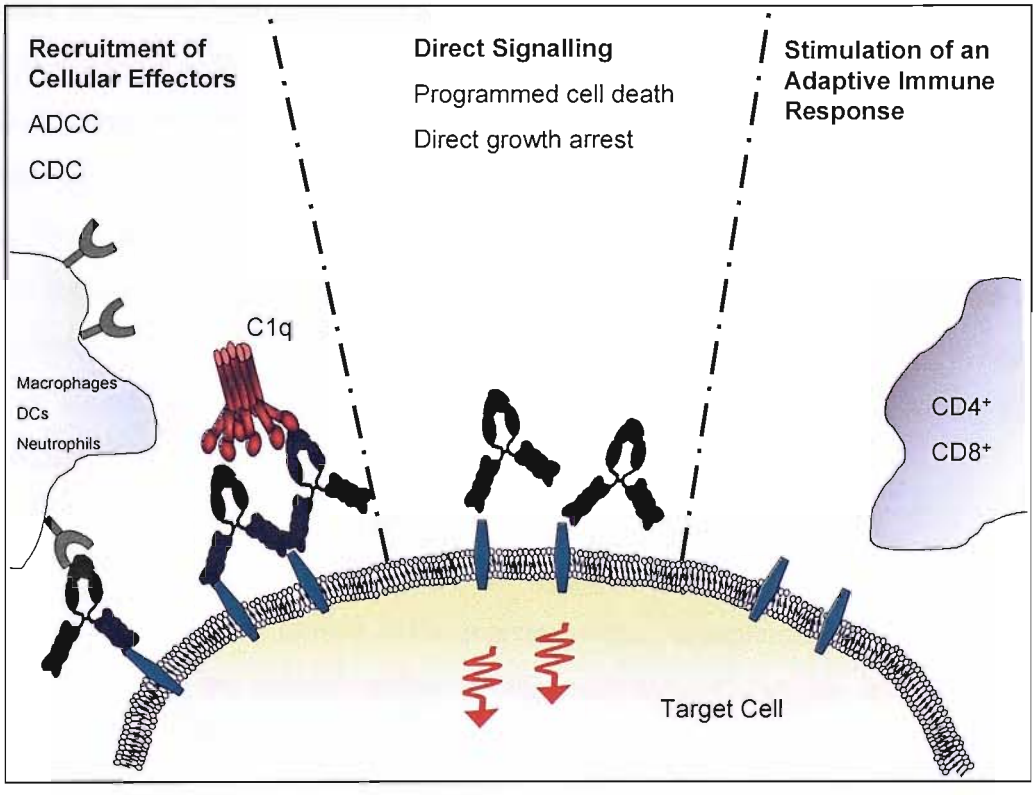

Figure 1.5: Effector mechanisms believed to be evoked upon CD20 ligation with mAb

1.6.1 Complement Dependent Cytotoxicity

Complement is a highly regulated enzymatic cascade that can be activated in three ways, known as the classical, alternative and lectin pathways. In mAb-mediated immunotherapy, it is believed that CDC is mediated through the classical pathway. The complement cascade begins with the formation of antigen-antibody complexes on the surface of cells to which C1q can bind (Figure 1.6, reviewed in [135]). C1q is composed of six globular arms and therefore requires at least two antibody Fc domains in close proximity on the cell surface and in the correct orientation for stable binding. In the presence of calcium ions, C1q binds constitutively present serum proteins C1r and C1s to form a stable complex. C1s can then cleave C4 and C2. C4 is cleaved to release C4a and a larger fragment C4b, which attaches to the cell surface along with the cleavage product of C2, C2a. The complex C4b2a is known as C3 convertase. A single C3 convertase can generate over 200 molecules of C3b from the cleavage of C3, hence the formation of C3 convertase is a critical step in the amplification of the complement cascade. Some of the C3b formed can associate with C4b2a to form C5 convertase which cleaves C5 into C5a and C5b. C5b can then go on to associate with other serum proteins C6, C7, C8 and C9 to form the membrane attack complex (MAC). This complex displaces the membrane phospholipids, forming a large transmembrane channel that disrupts the membrane permeability of the target cell leading to lysis. In addition to direct lysis of cells, during the complement cascade, the smaller cleavage products C3a, C4a and C5a can act as anaphylatoxins mediating an inflammatory response. Furthermore, C3b and to a lesser extent C4b can opsonise the cell for binding complement receptor bearing cytotoxic effector cells such as macrophages and NK cells.

Clearly the complement cascade, if not tightly regulated, is a potentially harmful process and therefore human cells express several complement defence molecules which intervene at critical points in the complement cascade to limit aberrant activation and destruction of host cells. Complement defence proteins CR1 and CD55 accelerate the decay of C3- and C5-convertase, CD59 binds to complement proteins C8 and C9 hindering MAC formation whilst CD46 acts as a co-factor which binds to C3b and C4b converting them into fragments that cannot support further complement activation [136].

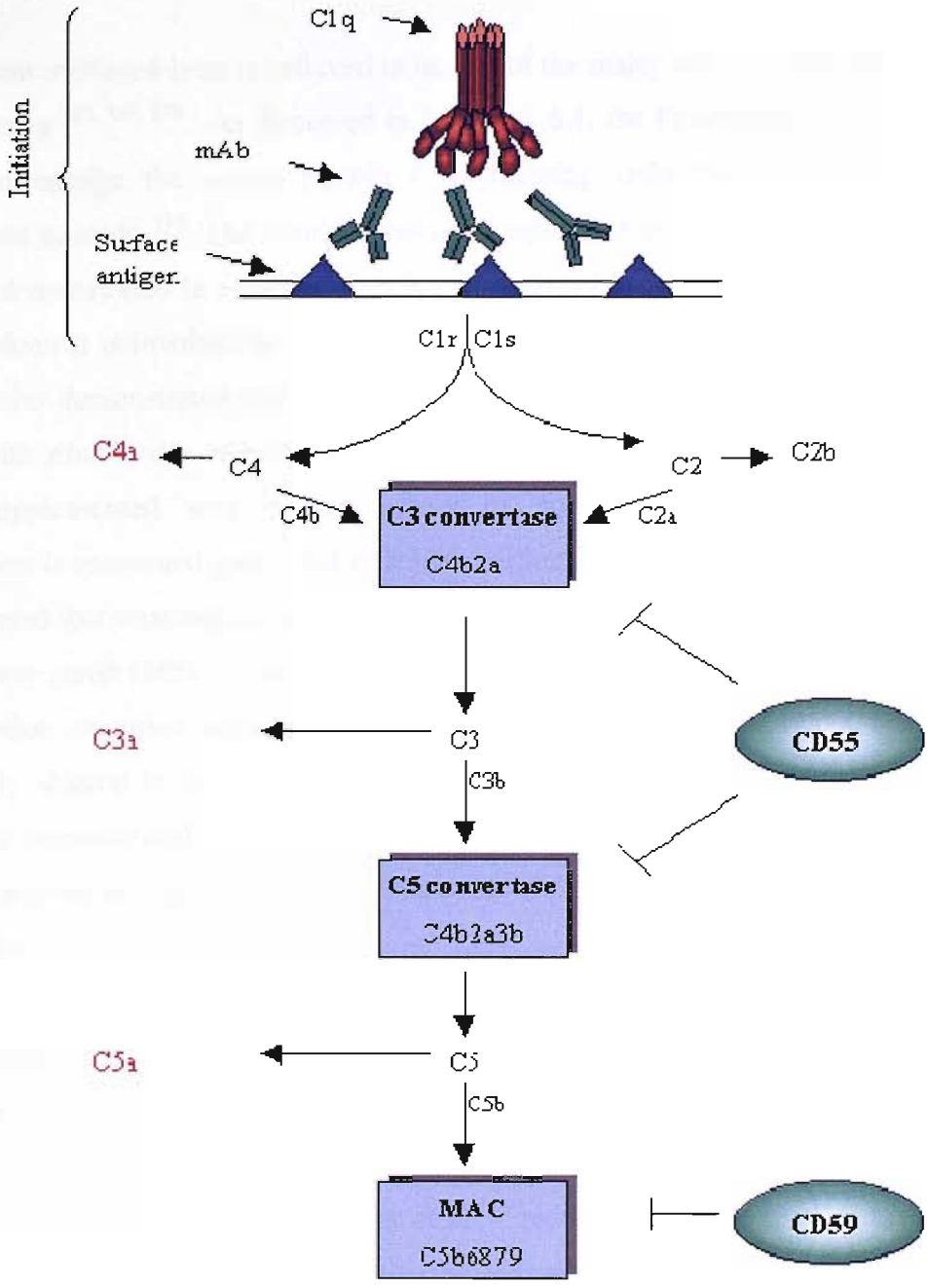

Figure 1.6: Summary of the classical pathway of complement. The pathway is activated upon C1q binding to the Fc domain of antibody:antigen complexes. In the presence of calcium ions, C1s and C1r bind to C1q forming an esterase which can cleave both C4 and C2. This leads to the binding of a cleaved fragments from both molecules to form C3 convertase which subsequently leads to the generation of C5 convertase and formation of the membrane attack complex (MAC). Some of the cleaved fragments produced during the cascade (highlighted in red) act as soluble mediators to recruit and activate immune effector cells with C5a being the most effective. To prevent abberant activation of complement, host cells can express complement defence proteins such as CD55 and CD59.

1.6.1.1 CD20-mediated CDC

Complement mediated lysis is believed to be one of the major effector mechanisms of CD20 therapy [127, 137, 138]. As discussed in Section 1.6.1, the Fc domain of Rituximab is able to engage the serum protein C1q allowing induction of the classical complement cascade [139]. The involvement of complement in CD20-directed therapy has been demonstrated in vitro and in vivo. Possibly the most persuasive evidence that complement is involved in ritux therapy comes from a recent study by Kennedy et al [140] who demonstrated that the sera of chronic lymphocytic leukaemia patients treated with ritux had a reduced ability for C3b to opsonise and kill $CD20^+$ cells unless supplemented with normal serum or component C2, indicating that complement is consumed upon ritux treatment. Other evidence from an animal model demonstrated that treatment of mice with either ritux or 1F5 one day after inoculation with tumour cured 100% of the animals. The therapeutic efficacy was not effected by the depletion of either natural killer (NK) cells or neutrophils or both but was completely ablated in knockout mice lacking C1q [127]. Furthermore, work in our laboratory demonstrated that depletion of complement by cobra venom factor led to a notable decrease in the therapeutic efficiency of 1F5 and ritux in lymphoma-bearing SCID mice [141].

The importance of complement defence proteins in CD20-mediated CDC remains controversial. Several groups have investigated the relationship between complement defence molecules CD59 and CD55 with CD20 expression level. In a study of cells isolated from 33 B-CLL patients, Golay et al [118] reported that the expression level of CD20 and complement inhibitors CD55 and to a lesser extent CD59 were determinants in the clinical response of patients. Furthermore, ritux therapy of follicular lymphoma can be enhanced by pre-incubation with a CD59 blocking mAb [118]. In addition, it has been shown that the surviving tumour cells in some patients treated with ritux have increased CD59 expression [142]. However, other studies have found no such association and an investigation of 29 ritux-treated patients with follicular lymphoma showed no significant correlation between the expression of CD55 and CD59 and ritux-induced CDC [143]. Further studies are required to delineiate the exact role of complement defence molecules in CD20-mediated CDC.

Even though the ability of ritux to activate CDC is now well established, limited work has been performed in understanding what makes CD20 a particularly good mediator of complement lysis. Work in our group suggests that CD20 redistribution into TX-100 insoluble lipid rafts upon mAb ligation, may play an important role [67].

1.6.2 Antibody Dependent Cellular Cytotoxicity

Antibody dependent cellular cytotoxicity, or ADCC, relies on recruitment of accessory cells such as NK cells, Macrophages, Neutrophils, Eosinophils and Platlets through engagement of the Fc domain of bound IgG mAb. In mammalians, there are four main groups of Fc receptors for IgG (FcγR); the inhibitory receptor, FcRII (CD32) which possesses an immunoreceptor tyrosine-based inhibitory motif (ITIM) and the activatory receptors, FcRI (CD64) and FcRIII (CD16), and the recently described, FcRIV receptors which all contain ITAM motifs. Co-expression of both activatory and inhibitory FcγRs on cells of the immune system regulates the cytotoxic response to invading pathogens which can become opsonised with IgG [7, 144].

As ADCC is dependent on interaction with Fc, the isotype of the mAb is a determining factor in the efficency of induction. Studies have shown that mouse IgG2a is the most active subclass in ADCC, especially with activated macrophages where it is the most effective isotype at prolonging survival of tumour-bearing mice [145, 146]. The signalling events leading to the death of the cell are currently unclear. It is believed that release of cytotoxic granules occurs. These granules, present in the cytoplasm of resting effector cells, fuse with the plasma membrane in response to target cell recognition, releasing their cytotoxic contents at the target cell interface. These granules contain enzymes such as granzymes, perforin, myeloperoxidase, acid hydrolases and lysozyme which cause degradation, toxic oxygen radical build-up and ultimately death of the target cell [147].

1.6.2.1 CD20-mediated ADCC

Investigations into the B cell depletion mechanism employed by anti-mCD20 mAb in mice and anti-CD20 mAb in transgenic mice expressing human CD20 suggest that ADCC plays a pivotal role in CD20-directed B cell depletion. Uchida et al [148]

reported that B cell depletion by anti-CD20 mAb could still occur in C3-deficient mice. Furthermore, it has been demonstrated that FcR$\gamma^{-/-}$ nude mice, that lack FcγRI and III, have a significantly reduced anti-tumour activity with ritux than wild type mice. Additionally, this activity can be substantially increased by the disruption of FcγRIIb, an inhibitory Fc receptor [149]. Perhaps the most convincing evidence that ADCC is an important effector function of ritux in human immunotherapy comes from an investigation by Cartron et al [150] who recently revealed that the clinical response of FL patients to ritux treatment correlates to a favourable polymorphism in the FcγRIIIa receptor of accessory cells. The study assessed the significance of a polymorphism at residue 158 of FcγRIIIa, which can either be valine (V) or phenylalanine (F). It has been shown that human IgG1 favours binding of the V variant. Patients homozygous for valine (V/V) at residue 158 had a better response to ritux treatment when compared to patients carrying the F variant, either V/F or F/F. Interestingly another study on patients with CLL found no such correlation [151], however FL and CLL have different genomic and immunophenotypic profiles, one of the most notable differences being CLL generally express lower levels of CD20. Furthermore, a recent study by Hamaguchi et al [144] demonstrated that in mice, the mode of B cell depletion by anti-CD20 mAb was different for circulating B cells compared to those found in tissues such as the spleen. Clearance of B cells from the latter is thought to be more dependent on ADCC than circulating B cells thereby suggesting a possibly reason for the difference observed between FL (more tissue related) and CLL (blood) diseases.

1.6.3 Induction of programmed cell death

Apoptosis or programmed cell death is a normal, physiological process which is fundamental to tissue homeostasis and embryonic development. In addition to its role in developmental control processes, apoptosis can be induced by toxic insult and the triggering of cell surface receptors such as Fas and other members of the tumour necrosis factor (TNF) family [152].

The 'classical' apoptotic pathway follows a characteristic pattern of events in which the fate of a cell is determined by the interplay of various signal transduction

pathways (see Figure 1.7). The process can be divided into three stages; the initiation stage, where death receptors such as Fas and TNFR are stimulated or the cell undergoes toxic insult such as irradiation or chemotherapy; the execution stage where the cell becomes commited to die and the final destruction phase where the cell undergoes several characteristic morphological changes such as DNA fragmentation and cell shrinkage.

Even though the signalling pathways involved in apoptotic induction are not fully elucidated, the morphological changes are well defined and are generally the most reliable marker used to identify an apoptotic cell. Typical morphological events include exposure of phosphatidyl serine (PS) to the surface of the cell membrane, DNA condensation followed by fragmentation, cell shrinkage and membrane blebbing. These cell changes occur following a cascade of signalling events where caspase involvement is a primary indicator that a cell is undergoing apoptosis (reviewed in [153]).

Caspases are cysteine proteases, using the sulfur atom in cysteine to cleave polypeptide chains next to aspartate amino acids. It is believed that caspase activation is the principal program of cell death in many developmental and physiological settings. Presently 13 human caspases have been identified which share similarities in amino acid sequence, structure and substrate specificity [154]. All are expressed as proenzymes which upon cleavage form a smaller (~10kDa) and larger subunit (~20KDa). These two subunits associate to form a heterodimer which associates with another heterodimer to become an active protease. Not all of the 13 caspases identifed are functionally defined, two (-11 and -1) have a role in inflammation and seven are important in apoptosis induction. These seven caspase members can be divided into two groups; the initiator caspases, -2, -8, -9 and -10 and the executioner caspases which include caspase-3, -6 and -7. As seen in Figure 1.7, activation of executioner caspases can result in a myriad of events such as the inactivation of anti-apoptotic proteins, activation of nucleases such as DFF (DNA fragmentation factor) and reorganisation of the cell structure through the cleavage of several proteins involved in cytoskeletal regulation such as the F-actin and nuclear lamins [155, 156].

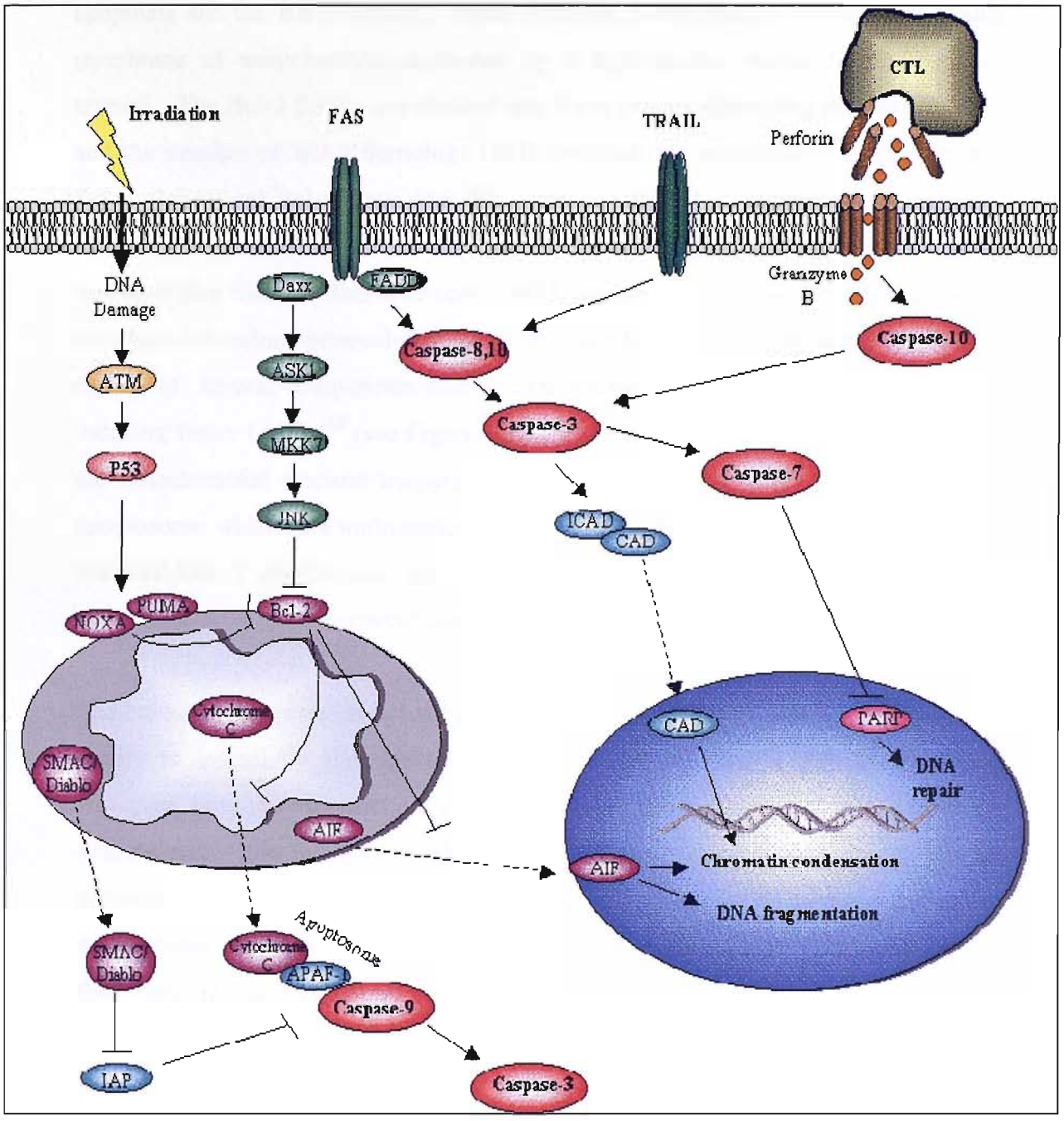

Figure 1.7: Illustration of some of the signalling pathways involved in apoptosis or PCD. The programmed cell death process can be split into three stages; the initiation phase where the apoptotic pathway is induced by various stimuli such as ligation of various surface antigens or by irradiation. The execution phase involves several signal transduction pathways which can be mediated through caspases and other cellular proteins and can be regulated by members of the Bcl-2 family proteins. This ultimately leads to the destruction phase where a cell displays defined morphological changes such as DNA fragmentation and membrane blebbing.

Another key family of proteins involved in the orchestration and regulation of apoptosis are the Bcl-2 family. These proteins predominantly reside in the outer membrane of mitochondria, anchored by a hydrophobic stretch within their C' termini. The Bcl-2 family are divided into three groups depending on their function and the number of Bcl-2 homology (BH) domains; the anti-apoptotic members e.g. Bcl-2, Bcl-x_L and Bcl-w have four BH domains (BH 1-4) whereas the pro-apoptotic members Bax and Bak possess three BH domains (BH 1-3) and some pro-apoptotic members like Bid and Bim have only a BH3 domain (reviewed in [157]). Pro-apoptotic members can induce permeabilisation of the mitochondrial membrane resulting in the release of several components such as cytochrome c, Smac/DIABLO and apoptosis inducing factor (AIF) [158] (see Figure 1.7) . Cytochrome c, an essential compound of the mitochondrial electron transport chain, is also instrumental in formation of the apoptosome which is a multimeric structure involved in the activation of caspase-9. Smac/DIABLO counteracts the inhibitors of caspases known as inhibitors of apoptosis (IAPs). IAPs prevent caspase action by blocking their cleavage.

The balance of expression between the pro and anti-apoptotic members of the Bcl-2 family is essentially the deciding factor between whether a cell lives or dies. However, how they interact on a molecular level to regulate each other is still not entirely clear. It is thought that the pro-apoptotic proteins such as Bax and Bak are hindered by the binding of anti-apoptotic proteins like Bcl-2 [158]. In the presence of a death stimulus, the level of BH3 only proteins increase. These BH3 only proteins then bind the anti-apoptotic proteins bound to Bak and Bax releasing them to orchestrate cell death [158].

For many years the terms apoptosis and programmed cell death (PCD) were utilised interchangably. However, recent evidence suggests that cells can undergo PCD which is caspase-independent and therefore would not be classified as 'classical' apoptosis (see Section 1.6.4).

1.6.3.1 CD20-mediated cell death

The third mechanism implicated in CD20-mediated anti-tumour responses is through direct transmembrane signalling resulting in the induction of PCD [51, 129]. The ability

of anti-CD20 mAb to induce cell death has been widely demonstrated in vitro [51, 105, 128, 159] and is now emerging that direct induction of cell death through anti-CD20 mAb can occur in vivo [129]. Cragg et al demonstrated that in a mouse xenograft model therapeutic efficacy was possible with B1 $F(ab')_2$ fragments [141]. As the Fc domains were absent, the anti-CD20 mAb was not able to engage cellular effector mechanisms suggesting that cell death was primarily achieved through direct intracellular signalling. Furthermore, a recent investigation of the mononuclear cells of CLL patients treated with ritux showed that the classical indicators of apoptosis, caspases -9, -3 and PARP cleavage along with down-regulation of XIAP and Mcl-1 anti-apoptotic proteins was observed [129].

The involvement of caspases in CD20-mediated cell death remains unclear. Several groups have demonstrated that caspase 3 is activated upon CD20 ligation [56, 63, 91]. However, inhibition of caspase activity was only able to reduce the level of cell death induced by anti-CD20 mAb but did not completely abrogate the killing. Furthermore, in line with our findings from a recent study [52], Van der Kolk and colleagues [160] concluded that although mitochondrial triggering and caspase activation takes place upon CD20 cross-linking, these events are not essential for the cell to die. Other conflicting reports on the mechanism involved in the induction of CD20-mediated cell death seem to relate to the cross-linking process. Several groups have found that cross-linking of the murine mAb B1 and other anti-CD20 mAb significantly increases the level of cell death achieved in Burkitt's lymphoma B cell lines [51, 161, 91] whereas other groups investigating some of the same cell lines reported no significant differences were observed with cross-linking [162, 52].

Full elucidation of the cell death pathway employed by anti-CD20 mAb is crucial as it is possible that intracellular signalling is central to achieving a maximal therapeutic response [163]. A putative pathway involving calcium signalling and Src family kinases is emerging where calcium chelation with EDTA and EGTA resulted in a significant decrease in cell death as did the use of specific Src family kinases inhibitors [56 63]. However, the investigation into CD20-mediated cell death is made difficult by the heterogeneous nature of the cell lines where this laboratory and others have demonstrated that some cells lines are more sensitive to CD20 mediated cell death than others [52, 162].

Chromosomal translocations often occur in B cell lymphomas which can potentially have a direct effect on the efficacy of therapeutic treatments. Translocations involving the Bcl-2 gene are characteristic of follicular lymphoma. The translocation t(14:18)(q32:q21) places the Bcl-2 gene under the control of the immunoglobulin heavy chain Eμ enhancer leading to high expression of the anti-apoptotic Bcl-2 protein [164], possibly explaining why some patients are resistant to a range of treatments including ritux therapy. However, the significance of Bcl-2 over expression on CD20-mediated cell death is unclear. Shan et al [56] found no difference in the level of cell death in Ramos cells expressing low levels of Bcl-2 compared to cells expressing high levels of Bcl-2 when treated with anti-CD20 mAb. Similar results were obtained from work in our group [52]. Furthermore, Shan et al assessed the involvement of EBV infection in CD20-mediated cell death. EBV infection can result in resistance to apoptosis, the molecular-basis of which is still not totally understood, although such resistance appears to be associated with the expression of some viral proteins, such as latent membrane protein 2A and the upregulation in Bcl-2[165]. Shan and colleagues [56] found that EBV infection did not protect Ramos cells from anti-CD20 mAb induced cell death. However, it has been demonstrated the ritux treatment can lead to decreased expression of Bcl-2 and sensitisation to chemotherapy [166]. Furthermore, it has been reported that down-regulation of Bcl-2 by anti-sense oligonucleotides enhances ritux efficacy in AIDS related lymphoma and post transplant lymphoproliferative disorder [167].

P53 is a transcription factor involved in cell cycle regulation which has a high frequency of mutation in malignant cells. Mutations of p53 in lymphomas tend to be single nucleotide changes in conserved regions that are part of the sequence encoding the DNA binding region [168]. P53 has an essential role in DNA damage control which when operating normally, identifies DNA damage via G1 and S phase check points and repairs that damage or alternatively can induce apoptosis of cells which have undergone severe cellular insult, hence reducing the likelihood that damaged cells will survive and propagate [169] [170]. The effects that such genetic mutations have on the sensitivity of cells to CD20-induced cell death are currently unknown.

1.6.4 Non classical apoptosis

As described in Section 1.6.3, apoptosis is a highly regulated process which is generally mediated by the activation of caspases and Bcl-2 family proteins. However, it is now emerging that cell death triggered by cell stress and other stimuli may be signalled through caspase independent pathways. In extreme circumstances of cell stress necrosis may be induced.

Necrosis is a rapid, energy independent process which has distinct morphological features (reviewed in [171]). Cells undergoing necrosis first swell and then lose membrane integrity resulting in the efflux of cell constituents into the extracellular space which in vivo would initiate an inflammatory response. In a physiological setting, necrosis can be induced by various stimuli such as bacterial toxins, NK cells and Macrophages. Furthermore, necrosis can be stimulated by various receptors such as members of the TNF family (Fas and TRAIL) and cytokines such as IFN-γ and TNF-α [172-174].

Initially it was believed that necrosis and "classical" apoptosis were two very distinct cell death pathways, however it is now believed that these two pathways represent the extreme ends of a wide range of possible morphological and biochemical deaths, more loosely termed programmed cell death pathways [175]. Distinction between these pathways is made difficult for several reasons. Firstly, both apoptotic and necrotic pathways can signal through similar pathways. In various cell stress environments, both cell death pathways can utilise early stress kinases e.g. JNK and p38 [176], mitochondrial proteins e.g. Bax and Bcl-2 [177], secondary messengers e.g. Ca^{2+} [178] and even, caspases [179]. Secondly, both pathways can share similar morphological features such as exposure of phosphatidyl serine and cytoplasmic shrinkage [175]. Furthermore, apoptosis and necrosis are almost indistinguishable in vitro as apoptotic cells culminate in plasma membrane permeabilisation (termed "secondary necrosis"). This does not appear to occur in vivo as apoptotic bodies are engulfed by circulating macrophages or surrounding cells before the plasma membrane becomes disrupted.

However, one proposed approach to distinguish between the various cell death pathways is based on the chromatin condensation that occurs with death. Jaatalia et al [175] has divided non-classical apoptotic pathways into two main groups; Apoptosis-like PCD which results in less compact chromatin than classical apoptosis and necrotic PCD which can occur in the complete absence of chromatin condensation.

1.6.4.1 CD20-induced PCD

Even though it is commonly reported that CD20 induces cell death through apoptosis [51, 63, 91], there is evidence to suggest that CD20 induced cell death may be mediated through a more necrotic-like PCD. Killing induced by anti-CD20 mAb demonstrate some of the classical morphological changes associated with apoptosis such as the exposure of phosphatidyl serine. However, Shan and colleagues [51] comment on the inconsistency of DNA fragmentation and Chan et al [52] found no DNA fragmentation with ritux treatment (in the absence of cross-linking). Furthermore, caspase activation has been linked to CD20 mediated cell death however this does not automatically indicate an apoptotic pathway. We have previously shown that even though cleavage of pro-caspase 3 occurs upon anti-CD20 mAb binding, inhibition of this and other caspases with ZVAD appears to have no effect on the level of cell death being induced [52]. Our findings have been supported by a recent report by Daniels et al [180] who demonstrated that in a range of Burkitt's lymphoma B cell lines, rituximab could induce cell death which showed some of the characteristics of apoptosis such as exposure of phosphatidyl serine and depolarisation of the mitochondrial membrane but caspase involvement was not required for effective cell death. Understanding the cell death pathways employed by anti-CD20 mAb will be crucial to maximising the potential of CD20-directed therapy.

1.6.5 Direct stimulation of an immune response

Intriguingly, efficacy with ritux in patients is often not observed for up to two weeks post-treatment. The reason for this is currently unknown. Selenko and colleagues [181] suggest that ritux induced programmed cell death not only kills B-cells but also promotes the uptake and cross-presentation of lymphoma cell-derived peptides by antigen-presenting Dendritic cells (DCs), induces the maturation of DCs and allows

for the generation of specific cytotoxic T-lymphocytes. Therefore it is postulated that a specific T-cell response may play an important role in ritux therapy. How this response may be initiated is not known, however the fact that CD20 is associated with different molecules involved in T cell activation such as MHC class II, CD40 and CD81, may play a role [46, 173, 182].

1.6.6 Sensitisation of cells to chemotherapy

The use of Rituximab as a first line therapy is successful for the treatment of NHL patients. However, the most successful regimen to date is the use of Rituximab in combination with chemotherapy (see Section 1.5). The reasoning behind was that both 'arms' of the therapy can work separately increasing the patients response. However, recent studies have suggested that ritux acts a chemosensitising agent possibly sensitising cells which would have otherwise been non-responsive to chemotherapy [130, 166]. There is substantial evidence to indicate that the transcripton factor NF-κB regulates oncogenesis giving rise to chemo-resistance and tumour progression in a variety of malignancies. Genes encoding NF-κB-family members such as p52/p100, Rel and RelA are frequently rearranged or amplified in human lymphomas and leukemias [183, 184]. NFκB has been reported to activate various anti-apoptotic proteins such as Bcl-2 and IAP family members which have also been demonstrated to confer resistance to cytotoxic drugs [185]. Therefore inhibition of NFκB activation could be of great therapeutic benefit. Bonavida and colleagues [166, 186, 187] performed pioneering work to link ritux therapy to the down-regulation of NFκB activity via ERK1/2 inhibition which they suggest in turn leads to the down-regulation of Bcl-2. In addition, they have revealed that IL-10 can be down-regulated in AIDS-related lymphoma (ARL) cells by ritux treatment [130]. This led to the down-regulation of the anti-apoptotic protein Bcl-2 resulting in sensitisation of the cells to apoptosis. Whether similar pathways are in operation in Non-AIDS lymphoma cells is not yet clear.

Another cause of chemoresistance is the emergence and selective outgrowth of drug-resistant variants with a multidrug-resistant (MDR) phenotype. Ghetie et al (in press) suggest that ritux may disable the permeability glyco-protein (P-gp) pump in MDR by

inducing translocation of P-gp out of rafts however more work will need to be performed to fully understand the significance of this event

1.7 Differential effects of anti-CD20 mAb

In 1980 the first anti-CD20 mAb, B1, was characterised. Since then, a considerable panel of mAb which bind to CD20 has been generated. Based on blocking experiments it was originally thought that the approximately 43 amino acid extracellular loop of CD20 (Figure 1.4) only contained two distinct epitopes, one recognised by the vast majority of anti-CD20 mAb and the second recognised by 1F5. However Deans and colleagues [32] revealed that the large extracellular loop offers a more diverse binding platform and that 16 mAb can be categorised into 4 groups depending on their abilities to bind a crucial alanine-x-proline motif, induce homotypic aggregation and translocate CD20 into TX-100 insoluble lipid rafts.

Several groups have reported that the potency of CD20-mediated CDC or cell death is dependent on the mAb employed. The differential effect of anti-CD20 mAb are summarised in Table 1.3. It is interesting to note that mAb which are effective inducers of complement are poor at evoking CD20-mediated cell death and vice versa. The reasons for this disparity and underlying mechanisms are currently unknown.

MAb	Isotype	Induction of cell death	Induction of CDC	Homotypic Adhesion	Immunoprecipitates Src-family kinase activity	CD20 Translocation into Tx100 rafts	References
B1	mIgG2a	+++	-	+++	+	-	52, 56, 67, 98
AT80	mIgG1	++	+	++	ND	++	52, 67
Ritux	hIgG1	+	+++	+	+++	+++	52, 62, 63, 67, 98
1F5	mIgG2a	-	+++	-	++	+	52, 67, 159
2H7	mIgG2b	-	++	-	+++	+++	52, 66, 67, 98

Table 1.3: Characteristics of selected anti-CD20 mAb.

1.8 Aims of the project

The B cell antigen CD20 is of great clinical significance with the anti-CD20 mAb Rituximab successfully treating over 500,000 NHL patients to date. On the basis of this success ritux is now being investigated in the treatment of a range of other B cell malignancies and auto-immune diseases. However, not all patients respond to ritux therapy and the key effector mechanisms involved are not yet resolved. Furthermore, the key properties of anti-CD20 mAb have not yet been delineated and the importance of CD20 raft redistribution remains unclear. From Table 1.3 it is interesting that even though all anti-CD20 mAb bind the same target they can induce very different responses. Therefore, the aim of this thesis was to investigate the different effector mechanisms and signalling cascades induced by a range of anti-CD20 mAb. The four key aims of this project were 1) to assess a panel of anti-CD20 mAb for their ability to induce CDC and PCD in B cell lines, 2) to investigate whether different signalling cascades were employed by anti-CD20 mAb in achieving cell death, 3) to establish the importance of CD20 redistribution into lipid rafts and 4) to understand why different malignancies respond in different ways to CD20-directed therapy. To this end, we utilised a large panel of anti-CD20 mAb, an array of B cell lymphoma lines and primary tumour material in search of answers to these questions.

CHAPTER TWO

2.0 Materials and Methods

2.1 Chemicals

All chemicals and materials were purchased from either Sigma, UK or BDH, Poole, UK laboratories unless otherwise stated.

2.1.1 Cell culture materials

All human cell lines were cultured in RPMI 1640 medium (Invitrogen, Gibco, UK), supplemented with 2mM L-glutamine (Invitrogen, Gibco, UK), 1mM pyruvate (Invitrogen, Gibco, UK) and 10% foetal calf serum (FCS; Invitrogen, Gibco, UK). Murine NS/0 cells transfected with CD20 were cultured in DMEM (L-glutamine free, SIGMA, UK) supplemented with 10% dialysed FCS (First Link, UK) and 1X glutamine synthetase supplement (JRH, UK).

2.2 Buffers

The main buffers used in this project are outlined in Table 2.1.

Name	Contents
Phosphate Buffered Saline (PBS)	0.124 M NaCl, 0.0058 M KH_2PO_4 and 0.024 M Na_2HPO_4
PBA	PBS supplemented with 1% BSA and 20 mM sodium azide
MES buffer	25 0mM MES (2-[N-morpholine]ethanesulphonic acid), 1.5 M Sodium Chloride, titrated to pH 6.5 with sodium hydroxide
Lysis buffer	5ml of MES buffer, 1% Triton X-100 (or another detergent), 5.75mM PMSF, 0.06% aprotonin (w/v) and, 0.025 mM EDTA (ethylenediaminetetraacetic acid)
Resolving buffer	1.5M Tris Base pH 8.7 stock solution, 10% acrylamide, 0.05% (v/v) N'-Tetramethylethylenediamine (TEMED), 0.4% (v/v) Ammonium persulphate (APS, 10% stock solution), 0.5% (v/v) sodium dodecyl sulphate (SDS, 10% stock solution)
Stacking buffer	0.5M Tris base pH6.8 stock solution yielding a final acrylamide concentration of 3.0%, 0.1% (v/v) TEMED, 1% APS (10% stock), 0.5 % (v/v) SDS (10% stock).
3X SDS Loading buffer (reducing)	30% glycerol (w/v), 9% SDS (w/v), 0.1875 M Tris-cl, 0.03% (w/v) Bromophenol blue and 10% 2-ME (v/v) pH6.8
Electrode buffer	0.77 M glycine, 0.1 M tris-base and 0.015 M SDS titrated to pH8.3
Transfer buffer	20% (v/v) Methanol, 25 mM Tris, 192 mM glycine
TBS-T	1X Tris buffered saline (10X stock solution containing 0.5M Tris base, 9% SDS, pH7.6) with 0.1% (v/v) Tween-20 (TBS/T)
Stripping buffer	2% (w/v) SDS, 100mM 2 beta-mercaptoethanol, 20 mM Tris, pH 6.8
Sodium carbonate buffer	0.008 M Sodium carbonate and 0.067 M sodium bicarbonate, pH 9.3
MACS buffer	De-gassed PBS supplemented with 2mM EDTA and 0.5% (w/v) BSA

Table 2.1: The buffers used in this project.

2.3 Cell lines

The cell lines used and their tumor of origin are outlined below.

Cell line	*Cell type*
MHH PRE B-1	B-NHL
ARH77	MM
Tanoue	ALL
SUDHL4	B-NHL
EHRB	BL
Ramos	BL
Akata	BL
BL60	BL
Raji	BL
Daudi	BL

Table 2.2: Human B cell lines used in this project. NLH= Non Hodgkin's lymphoma; MM= multiple myeloma; ALL=Acute lymphoblastic leukemia; BL=Burkitts lymphoma

These cell lines along with the murine NS/0 transfected cells were maintained in culture at 37°C in a 5 % CO_2 humidified incubator. Media was replaced every 2-3 days.

2.4 Cell quantification

Cell concentrations were determined using Coulter Industrial D Cell counter (Coulter Electronics, Bedfordshire).

2.5 Antibodies

A list of the mAb used in the project and their source is given in Table 2.3.

mAb	Specificity	Isotype	Source
IF5	CD20	IgG2a	ECACC Hybridoma
B1	CD20	IgG2a	Coulter, Miami, FL
Ritux	CD20	Chimeric Hu Fcγ1	IDEC, San Francisco, CA
AT80	CD20	IgG1	In-house
LT20	CD20	IgG1	In-house
11B8	CD20	Hu Fcγ1	Genmab, Utrecht, Holland
7D8	CD20	Hc Fcγ1	Genmab, Utrecht, Holland
FMC7	CD20	IgM	Serotec, UK
F3.3	MHC II	IgG1	In-house
A9-1	MHC II	IgG2a	In-house
L243	MHC II	IgG2a	ATCC
1B4	CD38	IgG2a	Fabio Malavasi
WR17	CD37	IgG2a	Keith Moore
M15/8	BCR (IgM)	IgG1	In-house
SB2H2	BCR (IgG)		In-house
LOB 3/11	CD95	IgG1	In-house
Clone 26	CD55	IgG1	Serotec, UK
MEM-43	CD59	IgG2a	Serotec, UK
HB202	LFA-1		A. Smith
JG 13.2	4-1BB	Hu Fcγ1	Juliet Gray
ZL16/1	Ramos idiotype		In-house

Table 2.3: The specificity, isotype and source of mAb used in this project

2.5.1 Antibodies used for Western Blotting

Specificity	*mAb name*	*mAb conc*	*Supplier*
Phospho ERK1/2 (Thr 202/Tyr 204)	197G2	1:1000	Cell Signalling Technology (CST New England Biolabs UK)
ERK1/2	N/A	1:5000	Promega UK
Phospho-IκBα (Ser 32/36)	12C2	1:1000	CST
β-Actin	N/A	1:15000	Sigma, UK
PAG (MEM 255)	MEM 255	1:1000	Vaclov Herejsi
CD20 (7D1)	7D1	1:200	Serotec, UK

Table 2.4: Antibodies used for western blotting. N/A: not applicable.

2.5.2 Labelled antibodies used for detection in flow cytometry or Western blot assays

Secondary antibodies used were SB2H2-FITC labelled (mouse anti-human Fc (MAH), in-house), goat anti-mouse IgM-FITC (GAM, Jackson immunoresearch USA) and goat $F(ab')_2$- mouse Ig-FITC labelled (Dako, UK). For western blotting, anti-mouse Ig-HRP labelled (Amersham Biosciences, UK) and goat anti-Rabbit $F(ab')_2$ HRP (Pierce, Perbio sciences UK) were employed and goat anti-human IgG labeled with 15nM gold (Agar UK) was used for electron microscopy labelling.

2.6 Measurement of expression level of surface antigens

$1x10^6$ cells were resuspended in 1ml PBA. For direct staining; cells were incubated with 10μg/ml FITC labeled mAb for 15 minutes in the dark at room temperature before being washed and anlaysed by flow cytometry. For indirect analysis; cells were incubated with 10μg/ml mAb for 15 minutes at room temperature. The samples were washed twice in PBA and 50μl of 1:40 FITC-conjugated GAM (Dako Corp., CA, USA) or 10μg/ml MAH (SB2H2) was added to each sample. Samples were incubated in the dark for 15 minutes at room temperature before being washed in PBA and analysed by flow cytometry using a

FACScan flow cytometer with CellQuest software (BD Biosciences, CA, USA) with a 488 nm argon laser for excitation and a 560 nm dichroic mirror and 600 nm band pass filter (bandwidth 35 nm) for detection.

2.7 CDC assay

Human serum for complement-mediated lysis was prepared as follows: blood from normal volunteers was allowed to clot at room temperature for 30-60 minutes and then centrifuged at 900 x g for 20 min. Serum was harvested and then either used fresh or stored at -80°C. To determine the CDC activity of the various mAb, elevated membrane permeability was assessed using a rapid and simple propidium iodide (PI) exclusion assay, as previously described [143]. Cells were resuspended in RPMI (containing 1%BSA) to a concentration of $1x10^6$cells/ml. 20µl of RPMI (1% BSA) was added to each well of a 96-well plate except the top row where 25µl of mAb (of 500µg/ml stock in PBS) was added. From the wells in the top row 5µl was taken and added to the second row and so on until 1/5 dilution was completed down the plate (50, 10, 2 and 0.4µg/ml respectively). To each well 100µl of cells, 40µl of serum (20% v/v) and 40µl RPMI (1%BSA) was added and incubated at 37°C for 30 minutes.

The plate was kept at 4°C until analysis. 150µl of each cell sample was then added to 100 µl of PI solution (10 µg/ml in PBS) in a FACS tube. The samples was assessed immediately by flow cytometry. At least 7,500-10,000 events were collected for analysis with cell debris excluded by adjustment of the forward scatter (FSC) threshold parameter.

When analysing NS/0 cells for complement lysis the same method was used with two modifications; firstly, the top concentration of mAb was 10µg/ml and secondly, the final concentration of serum (human) was 1%.

2.8 Investigation of lipid rafts

2.8.1 SDS PAGE analysis

2.8.1.1 Lipid Raft isolation using density gradients

2.8.1.1.1 Sucrose gradients

To allow the detection of specific proteins in lipid raft membranes, cell lysates were separated through sucrose density gradients. $1x10^8$ cells were washed and re-suspended in 1ml of complete media. The relevant mAb was added at a final concentration of 25μg/ml to the cells for 30 minutes at 37°C. Cells were washed once in complete medium then immediately lysed in 750μl of cold lysis buffer (Section 2.2) for 40 minutes on ice. The lysed cell solution was mixed with an equal volume of 80% sucrose (w/v in MES buffer) and transferred into a 5ml ultracentrifuge tube (Sorvall, UK) and over-laid with 750μl of 30% sucrose, 500μl of 20% sucrose, 500μl of 10% sucrose and filled to the top of the tube with 5% sucrose (all w/v in MES buffer). Layered samples were separated at 45,000g for 16 to 18 hours at 4°C.

2.8.1.1.2 Optiprep gradients

For Optiprep gradients, 416μl of lysed cell sample was added to 833μl of optiprep (Axis-Shield, Norway) in a 5ml ultracentrifuge tube to achieve 40% w/v, this was overlaid with 1ml 35%, 1ml 30%, 0.75ml 25%, 0.75ml 20% optiprep and filled to the top of the tube with MES buffer. The tube was centrifuged as outlined above.

Separated samples were removed in 500μl aliquots, the first removed denoted fraction 1, and stored at -20°C until ready for use. When ready for analysis, samples were mixed with an equal volume of 3X SDS-loading buffer and separated using SDS-PAGE (see Section 2.8.1.3)

2.8.1.2 Isolation of lipid rafts with different detergents using the pellet/lysate assay

$1.5x10^7$ cells were resuspended in 7.5mls of RPMI (1% BSA). 500µl of cells were treated with 10µg/ml of the relevant mAb for 15 minutes at room temperature and washed in RPMI. Samples were resuspended in 200µl RPMI and treated or not 10mM methyl-β-cyclodextrin (MCD) for 15 minutes at room temperature before being washed twice in RPMI. Samples were lysed in 40µl of either 0.5% TX-100, 1% CHAPS or 1% Brij 58 made up in lysis buffer (as outlined in the Section 2.2) for 15 minutes on ice. The samples were then centrifuged on a bench-top centrifuge at maximum speed (16,000g) for 15 minutes at 4°C. The supernatant, containing the lysate, was removed and mixed 1:1 with 3X SDS-loading buffer. The pellet was washed 3X with lysis buffer, each time ensuring that the pellet was gently resuspended in the buffer before centrifugation. After washing, the pellet was mixed 1:1 with 3X SDS-loading buffer. Proteins from both the pellet and lysate were resolved using SDS-PAGE.

2.8.1.3 SDS PAGE gel preparation

SDS PAGE was performed using a mini-gel system (Biorad, UK) according to the method of Laemmli [188]. 12.5% acrylamide resolving gel (Section 2.2) was left to set in a 1.5mm plate for over 30 minutes at room temperature. Once the resolving gel had set, stacking gel (Section 2.2) was overlaid, a 15 tooth comb inserted and left to set at room temperature. When the gel was completely polymerized, the gel was immersed in electrode buffer (Section 2.2) in the electrode tank as per manufacturer guidelines and the comb removed.

Samples were boiled at 95°C for 5 minutes in a heat block and 20µl loaded into each well. Gels were run at a constant current of 20 mA or constant voltage of 100V per gel, until samples had entered the resolving gel. This was increased to 40 mA or 200V until markers (High-range Rainbow markers; Amersham Biosciences, UK) had reached their desired position, Gel running apparatus was water cooled throughout.

2.8.1.4 Western blotting

For Western analysis, proteins were transferred onto Polyvinylidene diflouride (PVDF) membranes (millipore) that had been pre-activated by immersing in 100% methanol for 15 seconds, followed by immersion in deionised water for two minutes. Proteins were transferred in transfer buffer (Section 2.2) for one hour at 400mA (constant current) using an immersed transfer system (TE 22 system; Hoeffer, Germany). The tank was water cooled throughout transfer. Following transfer, gels were coomassie stained to determine relative levels of loaded protein and the efficiency of the transfer. Transfer was deemed to have been successful in the presence of visible Rainbow markers on the PVDF membrane.

The PVDF membrane was blocked overnight at 4°C, in 5% dried low-fat milk powder or bovine serum albumin (BSA, Sigma), in TBS-T (Section 2.2) with constant rotation using a roller mixer (Spiramix; Jencons) to prevent non-specific binding.

Following blocking, the membrane was rinsed twice in TBS-T, followed by a further 15 minute and two 5 minute washes. The primary antibody was diluted to the desired concentration in TBS-T (containing 1% milk) and incubated with constant rotation for two hours at room temperature or overnight at 4°C. Following primary antibody incubation, the membrane was washed as described above before incubation with the relevant secondary antibody conjugated to Horse Radish Peroxidase (HRP), at the desired concentration in TBS-T (containing 1% milk) for one hour at room temperature with rotation.

The membrane was then washed in TBS-T for one 15 minute wash and 2 further 5 minute washes before the addition of Supersignal Chemiluminescent reagent (Pierce, UK); Supersignal substance was left on the membrane on a flat surface for 5 minutes. Following incubation, excess reagent was removed and the membrane was placed in an appropriate film cassette (Kodak), and protein bands visualised by exposing light sensitive film paper (Hyperfilm; Amersham Biosciences, UK) for the desired length of

time under safe light conditions. Films were exposed and developed by an automatic developer (Compact X4, Xograph imaging systems, UK)

2.8.2 Assessment of raft-associated antigen by TX-100 insolubility

As a rapid assessment of antigen presence in raft microdomains, we utilized a flow cytometric method based on TX-100 insolubility at low temperatures, as described previously [67]. Cells were washed in RPMI/1 % bovine serum albumin (BSA) and resuspended to 2.5 x 10^6/ml. Cells were then incubated with FITC-conjugated mAb (10μg/ml) for 15 minutes at 37°C, washed in cold PBA buffer. One half of the sample was maintained on ice to allow calculation of 100 % surface antigen levels, the other was treated with 0.5 % TX-100 for 15 minutes on ice to determine the proportion of antigens remaining in the insoluble raft fraction. Cells were maintained at 4°C throughout the assay, washed once in PBA, re-suspended and assessed by flow cytometry using a FACScan flow cytometer and CellQuest Pro software analysis. Various pre-treatment conditions and harvesting times were used in different assays such as cholesterol depletion (Section 2.7.4), inhibition of actin polymerization (Section 2.16) or extended time points. These are detailed in the text/figure legends.

2.8.3 Fluorescence resonance energy transfer (FRET)

2.8.3.1 Preparation of Cy3- and Cy5-conjugated mAb

Monoclonal Ab were directly conjugated to bisfunctional NHS-ester derivatives of Cy5 (Amersham Biosciences UK Ltd) as described in the manufacturer's instructions. Briefly, one vial of dye was dissolved in 10μl H_2O, and 2.5μl immediately added to 0.2ml of the mAb (mAb were dialysed in sodium carbonate buffer (section 2.2), and incubated at room temperature in the dark for 30 min. The labelled mAb was separated from the unconjugated dye by gel chromatography using a PD10-Sephadex G25 column (Amersham, UK) equilibrated in PBS. Molar ratios of coupling were determined using a spectrophotometer from ε_{650} =250/mM/cm for Cy5 and ε_{280} =170/mM/cm for protein, and ranged from 5- to 8-

fold excess dye:protein. Monoclonal Ab were microcentrifuged at 10,000 x g to remove aggregates.

2.8.3.2 FRET Analysis

According to the method described by Pfeiffer [189] FRET analysis was carried. Cells were resuspended at $3x10^6$ cells/ml in PBS /0.1% (w/v) BSA which contained 1% (v/v) heat-inactivated mouse and human serum (to block non-specific binding). For each experiment 6 tubes were setup as outlined in Table 2.5, in this example the homo-association of ritux in B cells was being investigated. Samples A-C were setup to assess the non-specific binding (OKT3 is an irrelevant mAb which binds CD3). Samples D-F measure the actual FRET signal generated by ritux homo-association.

Cell Sample	Contents
A	OKT3 FITC +OKT3 cold
B	OKT3 CY5 + OKT3 cold
C	OKT3 FITC + OKT3 CY5
D	Ritux FITC + Ritux cold
E	Ritux Cy5 + Ritux cold
F	Ritux FITC + Ritux Cy5

Table 2.5: Tube contents of samples required to measure FRET signal by Ritux homo-association. All contents are at a final concentration of 10μg/ml

Cells were incubated for 20 minutes at 37°C and then washed in PBA. To assess the homo-association of labelled antigen, flow cytometric FRET measurements were carried out using a FACSCalibur (BD Biosciences, CA, USA). The fluorescence intensities at 585 nm (FL2) and 650 nm (FL3), both excited at 488nm, and the fluorescence intensity at 661 nm (FL4), excited at 635 nm, were detected and used to calculate FRET according to the equation below, where A is acceptor (Cy5), and D is donor (FITC). All values obtained were corrected for autofluorescence:

$$FRET = FL3(D,A) - FL2(D,A)/a - FL4(DA)/b$$

Where: $a = FL2(D)/FL3(D)$, and $b = FL4(A)/FL3(A)$

Correction parameters were obtained using data collected from single-labelled cells (samples D and E), and side angle light scattering was used to gate out debris and dead cells. The necessary parameters were collected for 10,000 cells. FRET between donor and acceptor mAb derivatives on the dually-labelled cells are expressed in terms of acceptor sensitised emission at 488 nm [190]. Larger FRET efficiencies suggest a closer physical association of the donor- and acceptor-labelled antibodies or a higher density of acceptor-labelled mAb in the vicinity of donor-labelled mAb [190].

Various modifications have been made to the assay during this project such as changes in the incubation period, temperature and concentration of mAb. These modifications are outlined in the text/figure legends.

2.8.4 Cholesterol depletion/repletion of cells

For cholesterol depletion, cells were washed and resuspended at $1x10^6$ cells/ml in RPMI containing 1% (w/v) BSA. 100µl of cells were treated with either 2.5 or 10mM MCD for 15 minutes at room temperature. For cholesterol repletion, cells were treated with MCD as outlined above, washed twice in RPMI/BSA and incubated with 12.5µg/ml water soluble cholesterol (SIGMA) for 1 hour at room temperature, shaking every 10-15 minutes. For cholesterol loading, cells were washed and resuspended as outlined for cholesterol depletion and incubated with 12.5µg/ml water soluble cholesterol (SIGMA, UK) for the same conditions as outlined for cholesterol repletion.

To investigate the effect of cholesterol depletion/repletion on mAb binding, after the relevant treatment of cholesterol depletion/repletion/loading, samples were washed twice, resuspended in 100µl RPMI(1%BSA) and incubated with 10µg/ml mAb for 15 minutes at room temperature (with the exception of FMC7 which was incubated for 45 minutes as it is an IgM mAb and therefore has slow binding). Samples were washed 2X and incubated with

the relevant secondary mAb, either GAM-FITC (50µl 1:40), mouse anti-human SB2H2-FITC (10µg/ml) or GAM-IgM-FITC (50µl, 1:50) for 15 minutes at room temperature before being washed and analysed by flow cytometry using a FACScan cytometer. To investigate the effect of cholesterol depletion/repletion on TX-100 insolubility after MCD treatment cells were treated as outlined in Section 2.8.2.

2.8.5 Electron Microscopy

$5x10^6$ cells were resuspended in 1 ml complete media and treated with either ritux, 11B8 or an isotype matched irrelevant control (JG 13.5, anti-41BB) at 10µg/ml for 45 minutes at 4°C and transferred to a 37°C water bath for a further 15 minutes. Samples were washed twice in serum free media and resuspended in 65ul of RPMI (10% serum). 5µl was removed to check binding levels using SB2H2-FITC, incubated for 15 minutes at room temperature, washed once in PBA and assessed by flow cytometry. To the remaining 60µl, 3µl (1:20) of goat anti-human IgG $F(ab')_2$-gold labelled (15nm, AGAR Scientific, UK) was added for 45 minutes at 4°C and transferred to a 37°C water bath for a further 15 minutes. The samples were washed twice in serum free media, all the supernatant was removed and the pellets were resuspended in 200µl fixative (3% gluteraldehyde, 4% para-formaldehyde in 0.1M PIPES). Cells were processed by Dr. Anton Page in the Biomedical Imaging department, School of Medicine, University of Southampton. Briefly, cells were embedded in an alginate matrix and sectioned in 70nm slices. Sections were then transferred to a copper grid ready for analysis using a transmission electron microscope (Hitachi H7000). Images are taken using a digital camera (Megaview 3) and image archiving software (soft imaging systems) at a recorded magnification.

2.9 Calcium Signalling

2.9.1 Indo-1 labelling

$1x10^7$ cells were washed twice in serum free RPMI. The pellet was resuspended by flicking and 1µl of 5mM Indo-1-AM (Sigma, made up with 0.2% plurionic-F127) was added. The cell solution was slowly re-suspended to 500µl in serum free RPMI and incubated at 37°C for 30 minutes with gentle shaking every 10 minutes. After this cells

were washed twice in serum free RPMI and re-suspended in 5ml RPMI (containing 10% FCS). Cells were left to rest for 30 minutes in the dark at room temperature before use.

2.9.2 Analysis of Ca^{2+} flux generation

Cells were maintained in the dark at room temperature until required. RPMI (supplemented with 10% FCS), FACS tubes and mAb were kept in an incubator at 37°C. For analysis, 300µl RPMI and 200µl cell sample were added to a FACS tube and incubated at 37°C for 2 minutes before analysis using a FACS Vantage flow cytometer with UV excitation at 365nm and CellQuest software analysis (BD Biosciences, CA, USA). The FL5 and FL4 values in non-stimulated were set to a level of 0-10 MFI for FL5 and 300-500 MFI for FL4. Increase in free Ca^{2+} ions in the presence of Indo-1 led to an increase in FL5 MFI and a decrease in FL4 MFI. Analysis was performed using the FL5/FL4 ratio. Before cell stimulation a baseline FL5/FL4 ratio was obtained over 60 seconds. Cells were then stimulated with the desired mAb or Ionomycin (warmed to 37°C) and the FL5/FL4 ratio was recorded over 6-10 minutes. Time scale shown is seconds

Different pre-treatment of Indo-1 labelled cells such as with kinase inhibitors, calcium chelators or MCD treatment was carried out. The details of these are outlined in the figure legend.

2.10 Knockdown of CD20 using siRNA

Silencer RNA (siRNA) was used to reduced the expression of CD20 in cell lines according to the method of McManus et al [191]. The optimised protocol supplied with the Amaxa Nuclefector Kit (Amaxa, Germany) was used for each cell line. Firstly, the appropriate number of wells in a 12-well plate were filled with 1.5 ml media (RPMI supplemented with 10% serum) and maintained at 37°C. $2x10^6$ cells for each sample were spun down at 1500 RPM for 5 minutes, the supernatant was decanted off and the residual medium was removed by pipette before the clls were resusupended in 100 µl of Solution T (provided by manufacturer). It was important that the cells did not remain in the

nucleofector solution for longer than 15 minutes as this reduces the viability and gene transfer efficiency of the cells. The appropriate amount of siRNA was added to the 100 µl of the cells, see Table 2.6, and transferred to an Amaxa certified cuvette, whilst trying to avoid air bubbles in the solution. The nucleofector program was set to G16 (found to be optimum for Ramos and SUDHL4 cells (A. Ivanov personal communication)). After nucleofection, the cuvette was removed and 500 µl of the pre-warmed media was added. The cells were then transferred from the cuvette using mini-pasteur pipettes provided by the manufacturer to the well which had the 500 µl removed. The cells were cultured in an incubator at 37°C/5% CO_2 for 24-48hrs. Nucleofection efficiency was assessed using a pmaxGFP-labelled RNA - instead of siRNA, 2 µg of pmaxGFP was added to the 100 µl of cells and nucleofected. The efficiency was measured by the percentage of FL1 positive cells when analysed by flow cytometry. To determine the efficency of the siRNA induced knockdown, 100µl of the 1.5 ml samples were labelled with FITC labelled mAb, either Ritux for CD20 levels or for the BCR, M15/8 (Ramos) or SB2H2 (SUDHL4) for 15 minutes at room temperature before being washed and analysed by flow cytometry as outlined in Section 2.6.

Target	Sequence
CD20	5'-CCACUCUUCAGGAGGAUGU-3'
Control	5'-GCGCGCUUUGUAGGAUUCG-3'

Table 2.6: siRNA probe sequence against CD20.

2.11 Isolation of normal B cells

The magnetic cell separation MACS B cell isolation kit (Miltenyi Biotech, UK) was used to isolate B cells as per the manufacturer guidelines. 50ml of normal human blood was diluted 1:1 with PBS. 12mls of lymphoprep^{TM} (Axis Shield) was added to four universals and was over-layed with blood/PBS. The universals were centrigued at 2000 rpm for 10 minutes at room temperature with no braking. After centrifugation a lymphocyte band formed at the interface. This band was removed by a pasteur pipette and transferred to a clean universal. The lymphocytes were washed twice in PBS by centrifugation at 150 rpm for 5 minutes. The pellet was resuspended by flicking and all

the pellets were pooled and topped up to 1.1ml. 100µl was removed and the cells were counted using a Coulter Counter. Following this, cells were centrifuged and resuspended at 10^7/80µl of MACS Buffer (Section 2.2). 10µl of Biotin-antibody cocktail (cocktail of biotin conjugated mAb against CD2, CD14, CD16, CD27, CD36, CD43 and CD236a) per 10^7 cells was added and incubated at 4°C for 10 minutes. 30µl of MACS buffer and 20µl of anti-biotin MicroBeads were added per 10^7 cells and incubated at 4°C for a further 15 minutes. Labelled cells were then washed once in MACS buffer and resuspended in 500µl of buffer. B cells were separated using the MS seperation column as per manufacturer guidelines. Briefly, the column was equilibriated by passing 500µl MACS buffer. 500µl of magnetically labelled cells was added and allowed to fully enter the column before 500µl of buffer was added. The effluent was collected in a FACS tube. The column was then washed a further two times by the addition of 500µl of buffer. The purity of B cells was assessed by CD20 and BCR FITC direct staining and flow cytometry (Section 2.6). If further purification was required, the effluent collected in the FACS tube was spun down, resuspended in 500µl buffer and passed through another MS separation column.

2.12 Inhibition of BCR internalisation

Inhibition of BCR internalisation was carried out according to the method by Stevenson et al [192]. $2x10^6$ cells were resupended in 1ml RPMI or in 1ml RPMI supplemented with 15mM sodium azide and 50mM 2-deoxyglucose. $2x10^5$ cells in both RPMI and supplemented RPMI were stimulated with 10µg/ml M15/8 (anti-sIgM), ritux (anti-CD20) or polyclonal anti-IgM (goat anti-human IgM $F(ab)_2$ Jackson Immunoresearch) at 37°C for 15, 30 and 60 minutes. After which, cells were washed, resuspended in 100µl of PBS and incubated with FITC labelled anti-idiotype (ZL16/1), specific for Ramos B cells. After 15 minutes at room temperature, samples were washed and assessed by flow cytometry.

2.13 Investigation of ERK and IκBα phosphorylation

2.13.1 Western Blot analysis of phosphorylation

For analysis of ERK phosphorylation, 5-10x10^6 cells were washed and re-suspended in 1ml RPMI (10% FBS) and transferred to a 1.5ml micro-centrifuge tube. Cells were stimulated with 10μg/ml anti-CD20 (ritux, 11B8), anti-sIgM (M15/8) or anti-sIgG (SB2H2). For ritux and 11B8 cross-linked samples; cells were stimulated with 10μg/ml mAb for 15 minutes at room temperature before being washed twice in RPMI and 20μg/ml MAH added for the desired time (2, 15 or 60 minutes) at 37°C. After which, samples were pelleted in a bench-top centrifuge. The supernatant was removed and 75μl of NP40 lysis buffer was added (Section 2.2) for 30 minutes on ice. Samples were then spun in an ultracentrifuge at 27000 rpm for 15 minutes at 4°. 2.5μl of the supernatant was used to quantify the amount of protein in the sample using a BCA assay (Section 2.13.2). 66μl of the supernatant was added to 33μl of 3X loading buffer (reducing) and boiled at 95°C for 5 minutes in preparation for SDS-PAGE analysis. SDS-PAGE and western blot analysis was carried out as outlined in Sections 2.8.1.3 and 2.8.1.4. 30μg of protein was loaded onto each lane. The same method was used for analysis IκBα phosphorylation except that the mAb stimulation periods were 1 and 12 hours.

For membrane blotting, the membrane was blocked in TBS-T with 5% BSA for one hour at room temperature or overnight at 4°C. Membranes were washed as outlined in Section 2.8.1.4 and incubated with 5ml 1:1000 rabbit anti-phospho ERK1/2 (CST) in TBS-T/1% BSA on a roller overnight at 4°C. Membranes were washed and incubated with 1:5000 goat anti-rabbit HRP labelled Ab in TBS-T/1%BSA for 1 hour on a roller at room temperature before being washed and developed at outlined in Section 2.8.1.4.

Membranes were stripped of surface-bound immunoglobulin by immersing the membrane in stripping buffer (Section 2.2) for 30 minutes at 50°C with intermittent shaking. Membranes were washed 5 times in TBS-T before re-probing. For ERK1/2 detection, membranes were incubated with 1:5000 anti-ERK1/2 in TBS-T/1%BSA overnight on a roller at 4°C. After washing (1x15 minutes, 2x5 minutes), membranes were incubated with

1:5000 goat anti-rabbit HRP labeled Ab in TBS-T/3% BSA for 1 hour on a roller at room temperature. The membrane was developed as outlined in Section 2.8.1.4.

2.13.2 Protein quantification by the BCA assay

Protein concentrations were determined using a method based on that of Smith et al [193] which utilises the increase in absorbance at 562nm caused by the biuret reaction - the reduction of Cu^{2+} to Cu^{+} by protein in a concentration dependent manner. The kit was obtained from Pierce and used according to their instructions.

2.13.3 Flow cytometry analysis of ERK phosphorylation

$5x10^5$ cells were re-suspended in 0.5ml of complete media and treated with 10μg/ml ritux (anti-CD20), 11B8 (anti-CD20), M15/8 (anti-sIgM), SB2H2 (anti-sIgG) for 15 minutes at 37°C. For ritux and 11B8 cross-linked samples, cells were treated with 10μg/ml mAb for 15 minutes at room temperature, washed twice and 20μg/ml MAH added for a further 15 minutes at 37°C. Samples were fixed by the addition of 1ml 3% formaldehyde (made up in PBS) and incubated for 10 minutes at room temperature. Cells were pelleted and re-suspended in 1ml 90% methanol (ice cold) for 30 minutes on ice. After which, the cells were washed twice in PBA and re-suspended to 100μl. 10μl of Alexa-Fluor-488 conjugated anti-phospho-ERK 1/2 (BD Bioscience, UK) was added to 50μl of cell sample and incubated for 60 minutes at room temperature. Samples were washed once in PBA and assessed by flow cytometry using the FACScan for flourescence in FL1.

2.14 General cell death assay

Cells were washed and resuspended in complete medium at $5x10^5$ cells/ml. 500μl of cells were added to wells containing 500μl of complete medium with 20μg/ml mAb (final mAb concentration of 10μg/ml). For hyper cross-linking experiments 500μl of cells were stimulated with 5μg/ml anti-CD20 mAb for 15 minutes at 37°C before the addition of 25μg/ml MAH (SB2H2). At the designated time (usually 4 or 24 hours), cells were

assessed for homotypic adhesion using a light microscope (Olympus, Japan) before being harvested for analysis.

2.14.1 Detection of programmed cell death:

2.14.1.1 AnnexinV/PI assay

Samples were washed, resuspended in binding buffer (10mM HEPES, pH 7.4, 140 mM NaCl, 2.5mM $CaCl_2$), containing 1 μg/ml FITC-AnnexinV. 10 μg/ml of propidium iodide (PI) was also added to the samples to distinguish between early apoptosis and secondary necrosis. Subsequently, cells were assessed by flow cytometry using the FACScan for flourescence in FL1 and FL2 as detailed by Vermes et al [194].

2.14.1.2 DioC6 assay

DioC6 (Molecular Probes, Cambridge, UK) is a mitochondrial reporter dye, which determines whether cells have undergone the membrane permeability transition, a classical sign of a cell entering cell death. Cells were setup and harvested as outlined in Section 2.14, 10-20 nM of DioC6 was added to 2.5 x 10^5 cells and then incubated for 15-30 minutes at 37°C in the dark. The cells were pelleted, washed and resuspended in PBS before being analyzed by flow cytometry (FL1).

2.14.1.3 DNA Fragmentation

Samples were analysed as per the method of Nicoletti et al. [195]. Briefly, samples of 5x10^5 cells were taken and centrifuged for 5 minutes at 500g. Samles were washed once in PBS, re-suspended in hypotonic fluorochrome solution (50μg/ml Propidium Iodide (PI), 0.1% Sodium citrate, 0.1% (v/v) Triton X-100) and stored in the dark at 4°C overnight. Analysis of samples was performed on FACScan flow cytometer.

2.14.2 Inhibition of anti-CD20 mAb mediated cell death

2.14.2.1 Disruption of homotypic aggregation

$2.5x10^5$ cells were resuspended in complete medium and incubated with 10μg/ml anti-LFA-1 mAb (HB202) for 15 minutes at 37°C before addition of 10μg/ml anti-CD20 mAb. After 6 or 24 hours samples were assessed for homotypic aggregation under a light microscope (4X) before being harvested and analysed by annexinV/PI assay.

2.14.2.2 Removal of mitochondria: Generation of cell cytoplasts

Cell cytoplasts were generated as previously described by Roos et al [196]. Briefly, cells were separated through a discontinuous Ficoll-70 (Sigma, UK) gradient (12.5%, 16%, 25%) pre-warmed to 37°C which contained 5-10 μg/ml cytochalasin B by ultra-centrifugation at 81,000g. After centrifugation, the top band of cellular material was collected. This band was composed of cytoplasts, which was confirmed by lack of mitochondrial staining with Dioc6 (see above). Cytoplasts were incubated at 1 x 10^6/ml in the presence or absence of 10 μg/ml mAb for 16 hours at 37°C before being assessed by the annexin V assay (PI was omitted as cytoplast formation usually results in extraction of the nucleus from cells).

2.14.2.3 Cellular inhibitors

Inhibitors were reconstituted in DMSO to a concentration at least 10x higher than the working concentration. The most appropriate inhibitor and dose was selected based on cytotoxicity assays. Inhibitors studies were performed for the investigation of cell death and calcium signaling pathways. For cell death analysis, $1\text{-}2.5x10^5$ cells were treated with the relevant inhibitor for 15-30 minutes before addition of anti-CD20 mAb (10μg/ml). Cells were assessed after 6 or 24 hours for homotypic adhesion and cell death by the Annexin V/PI assay as outlined in Section 2.15.1.1. For calcium signaling analysis, Indo-1 labelled cells were treated with the desired inhibitor for 20 minutes at room temperature before mAb stimulation as outlined in Section 2.9. The inhibitors used in this project to date are outlined in Table 2.7 below.

Selectivity	Source	Inhibitor	Final working conc.
Src family PTKs	Calbiochem (Merck UK)	PP1 PP2 PP3	10μM
Caspases	Calbiochem	ZVAD-fmk VDVAD	10μM
Actin polymerisation	Calbiochem Sigma, UK Sigma	Jasplakinolide Cytochalasin D Latruculin A	10, 50, 100ng/ml 1, 10μM 1, 10μM
Syk kinase	Calbiochem	Syk Inhibitor I	10μM
ERK 1/2	Calbiochem Promega, UK	PD98059 UO126	10μM
PI3 kinase	Calbiochem	LY294002	10μM
P38	Calbiochem	SB203580	10μM
Calcium chelator	BDH, UK	EGTA	1.5mM

Table 2.7: The specificity and concentration of inhibitors used in this project to investigate signaling pathways stimulated by anti-CD20 mAb.

CHAPTER THREE

3.0 Complement Dependent Cytotoxicity

3.1 Introduction

The effector mechanisms predominating in CD20-mediated immunotherapy of a malignant disease is a controversial issue. To date, evidence has implicated complement dependent cytotoxicity (CDC) [118, 140], antibody-dependent cellular cytotoxicity (ADCC) [120, 134] and programmed cell death [91, 129] as important mechanisms but the predominance of one mechanism over another is unclear. In this chapter we examine the ability of anti-CD20 mAb to evoke complement dependent lysis of various target cells. As rituximab (ritux) is in prevalent use in the clinic, most studies to date have focused on the ability of this chimeric mAb to activate complement [118, 139, 140]. However, since CD20 was first characterized in the 1980s, a large panel of anti-CD20 mAb has been established and clearly the activity of ritux may not reflect the potency of all anti-CD20 to induce cell death. Therefore, a panel of anti-CD20 mAb were assessed for their ability to induce complement lysis.

The complement pathway involves a complex series of proteins that operate in a sequential cascade which is outlined in detail in Section 1.6.1. The classical pathway is thought to be the main complement pathway utilised in mAb mediated immunotherapy. The pathway is initiated by the complement protein C1q binding to juxtaposed bound mAb as illustrated in Figure 3.1. This results in C3 convertase activation and subsequent formation of the membrane attack complex (MAC) leading to cell lysis.

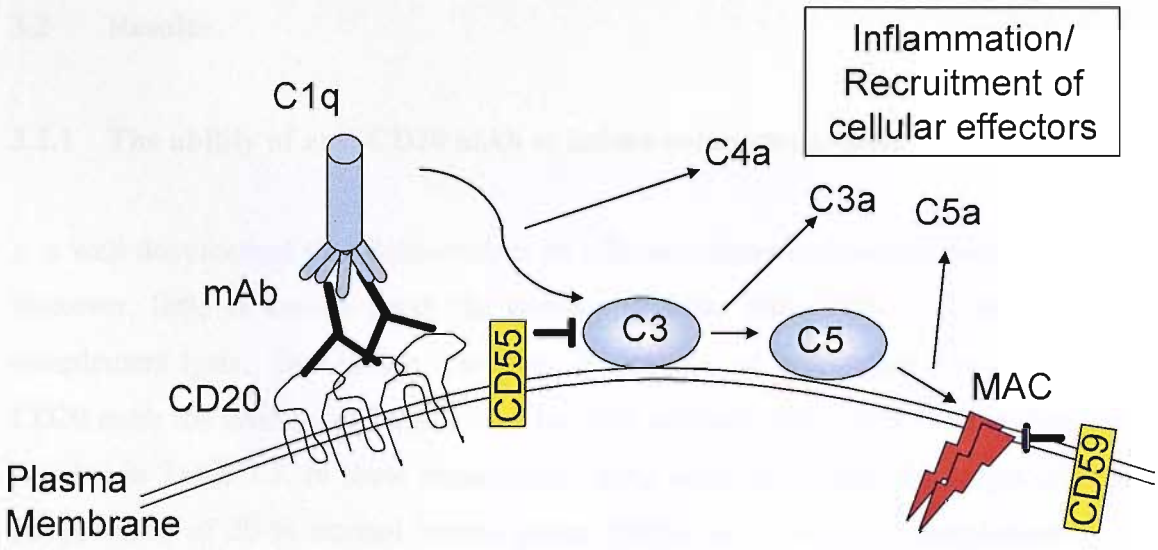

Figure 3.1: Overview of complement activation. C1q binds to juxtaposted Fc domains on the cell membrane. This results in recruitment of cellular proteins leading to formation of C3 convertase (C3) and C5 convertase (C5) and eventually the MAC complex and soluble mediators of inflammation. This pathway is inhibited at various points by CD55 and CD59. See section 1.6.1 for a more detailed overview.

In this chapter we assessed the importance of several factors for the induction of CD20-mediated CDC. Firstly, as C1q binds the Fc domain of mAb, the importance of mAb isotype was investigated. Furthermore, C1q is a globular protein which requires at least two Fc domains need to be sufficiently juxtaposed for stable binding. Due to this requirement, we assessed a range of different B cell lymphoma lines and cells transfected with different levels of CD20 to determine whether CD20 expression correlates with cytolytic activity. Complement is part of the innate immune system and is therefore rapid and not as highly specific as the adaptive immune response. To minimize aberrant activation on normal host cells, the cells express complement defence molecules such as CD55 and CD59 on their surface (see Figure 3.1). CD55 binds to C3b and C4b and accelerates the decay of C3 and C5 convertase whereas CD59 binds to C8 and C9 and prevents pore formation by the MAC (ref see Section 1.6.1 for more details). The importance of these molecules in the regulation of CD20-mediated lysis was also analysed.

3.2 Results

3.2.1 The ability of anti-CD20 mAb to induce complement lysis

It is well documented that Rituximab is an efficient inducer of complement [67, 118, 140]. However, little is known about the potency of other anti-CD20 mAb in inducing complement lysis. Due to this limitation, we decided to investigate a panel of anti-CD20 mAb for their cytolytic ability. The mAb utilized, along with their isotype are detailed in Table 3.1. In these experiments, mAb were incubated with target cells in the presence of 20 % normal human serum (NHS) as a source of complement (i.e. soluble proteins which circulate in the blood which are involved in the complement cascade such as C1q, C4, C2 etc), at 37°C for 30-45 minutes. The cells were then assessed for lysis utilising propidium iodide (PI). Propidium iodide is a fluorescent dye which can permeate the nucleus only upon loss of nuclear membrane integrity indicating the demise of the cell. This assay has been compared to more traditional methods of target cell lysis such as Cr^{51} release [197], and shown to give comparable results (V Anderson, Personal Communication). A typical assay is illustrated in Figure 3.2 where ritux-treated and non-treated cells are compared. The difference between the two samples is evident in the flow cytometry profiles of both the forward scatter (FSC) and the MFI of FL2 (PI staining). Forward scatter reflects the physical size of the cell, when a cell becomes lysed its FSC is reduced. In Figure 3.2 it is evident that the majority of ritux treated cells have a low FSC compared to non-treated control cells. Furthermore, the level of PI staining is reflected in the mean FL2 value. In ritux treated cells, 48.1% of the cells have high PI staining compared to only 3.7% in control cells; this value is taken as the level of lysis induced by ritux.

A relatively short 30 minute incubation period was used for these experiments for two reasons; firstly, almost all complement mediated cell lysis is complete during this time (V. Anderson, PC) and secondly, this timeframe was selected to minimize cell death occurring through other mechanisms such as apoptosis. For comparative purposes, some experiments were performed in the absence of active complement using heat-inactivated serum, i.e. serum which has been heated to 56°C for 30 minutes, resulting in denaturisation of complement proteins rendering complement inactive [198].

mAb	Isotype	Source
IF5	IgG2a	In house
B1	IgG2a	Coulter Corp.
Ritux	Chimeric Hu Fcγ1	Genentech, CA
11B8	Hu Fcγ1	Genmab, Denmark
7D8	Hu Fcγ1	Genmab, Denmark

Table 3.1: Panel of anti-CD20 mAb investigated for their potency of complement activation

Initially we focused on three anti-CD20 mAb that have previously been used in the clinic (ritux, B1 and 1F5 see Section 1.5). These mAb were assessed for the effect of mAb concentration on the potency of CDC induction. It is evident from Figure 3.3A that the ability of the three anti-CD20 mAb to induce complement lysis are quite different where ritux and 1F5 are good inducers compared to B1 which failed to lyse to cells to any notable level above control cells. The value shown above the M1 gate is the complement lysis induced in the presence of normal human serum and mAb minus the background lysis (% PI positive cells in medium only). The lysis which occurs with serum alone is due to the constitutive low level of complement activated by the alternative pathway. This usually does not affect cell lines as they are generally grown in heat inactivated serum. However from the data in Figure 3.3B it is apparent that when cells were incubated with active NHS a low level of lysis occurs, generally between 5-10% of total cells. To ensure that the increased cell death was mediated by complement activation, a comparative study was performed between cells incubated with heat inactivated NHS and active NHS. It is evident from the lack of lysis detected when cells are incubated in heat inactivated serum that cell death is mediated through CDC activity.

The data in Figure 3.3C demonstrates that the potency of CDC induction is related to the mAb concentration. This experiment was repeated twice. CDC by ritux, 1F5 and B1 was dependent on mAb concentration. 7D8 induced lysis is not as sensitive to a reduced mAb concentration indicating that it is a more potent inducer of complement mediated lysis , inducing maximal lysis with only 2μg/ml mAb. As the complement protein C1q binds the Fc domains of juxtaposed mAb bound to the cell surface, the

isotype of the mAb is an important factor. Both murine and human mAb are reported to effectively engage human complement, however the extent of this depends on the isotype with human IgG1, mouse (m) IgG2a and mIgG3 reported as good mediators compared to mIgG1 and mIgG2b which are considered as poor activators [12].. It is apparent from Figure 3.3C however that the efficacy of anti-CD20 mAb at inducing complement lysis was not entirely dependent on isotype as both B1 and 1F5 are murine IgG2a and ritux and 11B8 are human IgG1 (Table 3.1). These isotypes are characteristically good mediators of complement activation yet only 1F5, 7D8 and ritux hold true to their classification compared to B1 and 11B8 which induce little if any, lysis.

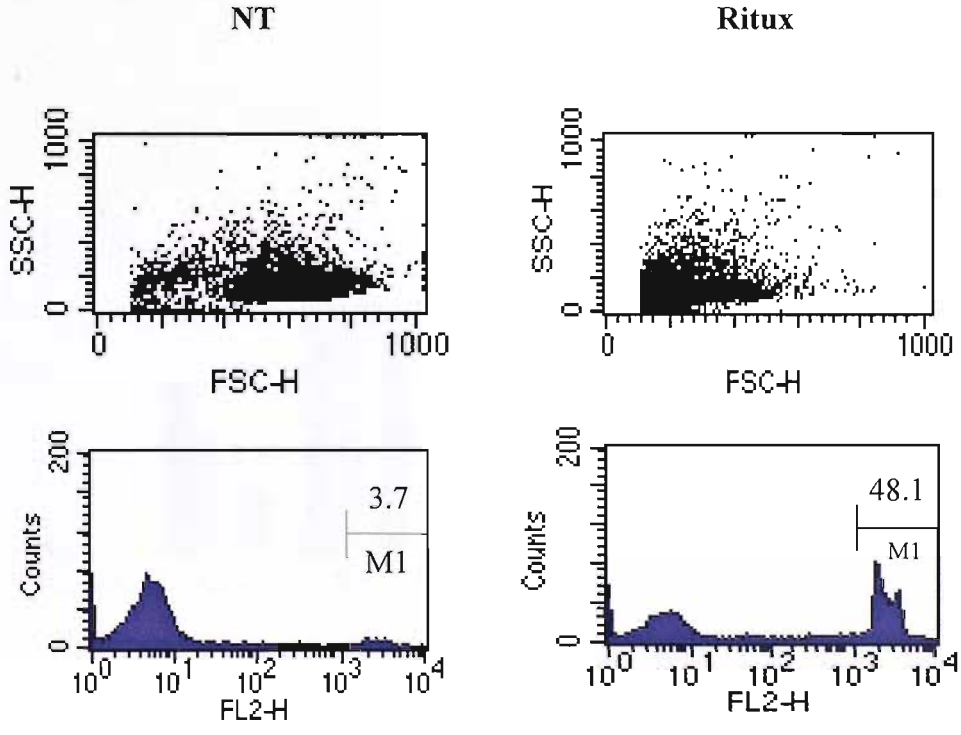

Figure 3.2: Illustration of a complement assay. $1x10^5$ cells were coated or not with 10 μg/ml ritux and incubated in 20% NHS (v/v) for 30 minutes at 37°C. The cells were then analyzed for lysis by flow cytometry using PI staining. FSC/SSC profiles are shown to demonstrate the physical change of the cells after complement lysis. M1 gates for PI positive cells. The values shown in the top right hand corner of the histogram is the number of cells gated in M1 expressed as a percent of the total number of cells and is taken to represent lysed cells.

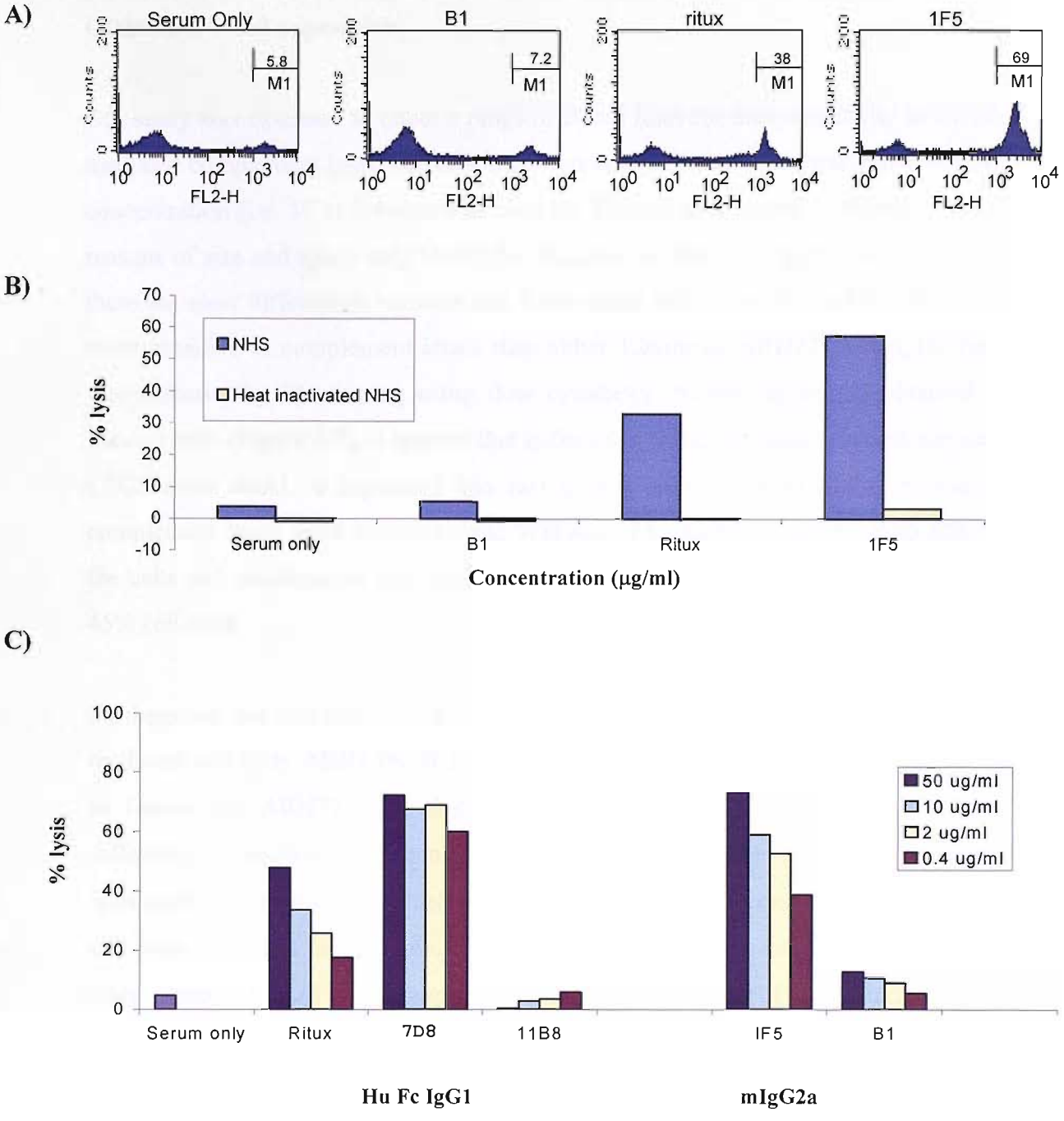

Figure 3.3: CD20-mediated complement lysis is dependent on mAb concentration and less dependent on mAb isotype. A) $1x10^5$ Tanoue cells were treated or not (serum only) with 10 µg/ml ritux, 1F5 or B1 in the presence of 20% NHS (v/v) for 30 minutes at 37°C. Samples were then incubated with 2µg/ml PI and analysed by flow cytometry. The values shown over the M1 gate is the % lysis (% of total population that are PI positive). This value is adjusted for background lysis by subtracting the lysis in the presence of media alone. **B)** Tanoue cells were treated as outlined above. Briefly, cells were incubated with 50 µg/ml mAb in the presence of either NHS or heat inactivated NHS (20%) for 30 minutes at 37°C before being assessed by the PI assay. **C)** The dose response of anti-CD20 mAb was assessed in Tanoue cells. The same procedure as outlined in A was employed where cells were incubated, or not, with 50, 10, 2 and 0.4 µg/ml mAb. The data is representative of two independent experiments.

3.2.2 The sensitivity of cell lines to CD20-induced CDC is dependent on CD20, CD55 and CD59 expression

Our study was extended to cover a range of B cell lines for their sensitivity to CD20-mediated complement lysis. All cell lines were assessed using the same range in mAb concentration (i.e. 50 to 0.4μg/ml) as used for Tanoue cells shown in Figure 3.3. For reasons of size and space only results for 10μg/ml are shown. Figure 3.4 reveals that there are clear differences between cell lines where MHH Pre B-1 and SUDHL4 are more sensitive to complement attack than either Tanoue or ARH77. Again, the lysis was assessed by PI staining using flow cytometry. Similar to results obtained in Tanoue cells (Figure 3.3), it appears that in the other three cell lines assessed, the anti-CD20 mAb could be separated into two groups based on their ability to induce complement lysis; good inducers ritux, 7D8 and 1F5 which lyse greater than 60% of the cells and moderate to poor inducers, 11B8 and B1 which demonstrate less than 45% cell lysis.

Furthermore, the cell lines could also be divided based on their sensitivity to CD20-mediated cell lysis. MHH Pre B-1 and SUDHL4 cells are highly sensitive compared to Tanoue and ARH77 cells which demonstrate notably lower levels of lysis. The difference in sensitivity between the cell lines is less apparent with good inducers of lysis such as 7D8 and 1F5 which at 10μg/ml achieve approximately 70% lysis in all cell lines tested but becomes more pronounced on analysis of ritux and B1 mediated lysis. Ritux mediated lysis is approximately 75% in both MHH Pre B-1 and SUDHL4 cells but in Tanoue and ARH77 cells, lysis is less than 50%. Similarly, in MHH Pre B-1 and SUDHL4 cells B1 induces approximately 40% cell lysis compared to less than 10% in Tanoue and ARH77 cells.

The reason why some cell lines are more sensitive to CD20-mediated lysis than others could be related to the expression of complement defence molecules as discussed previously in Section 1.6.1. Complement defence molecules such as CD59 and CD55 play an important role in limiting non-specific activation of complement [199]. We assessed whether the four cell lines used in this investigation, expressed CD55 and CD59 proteins.

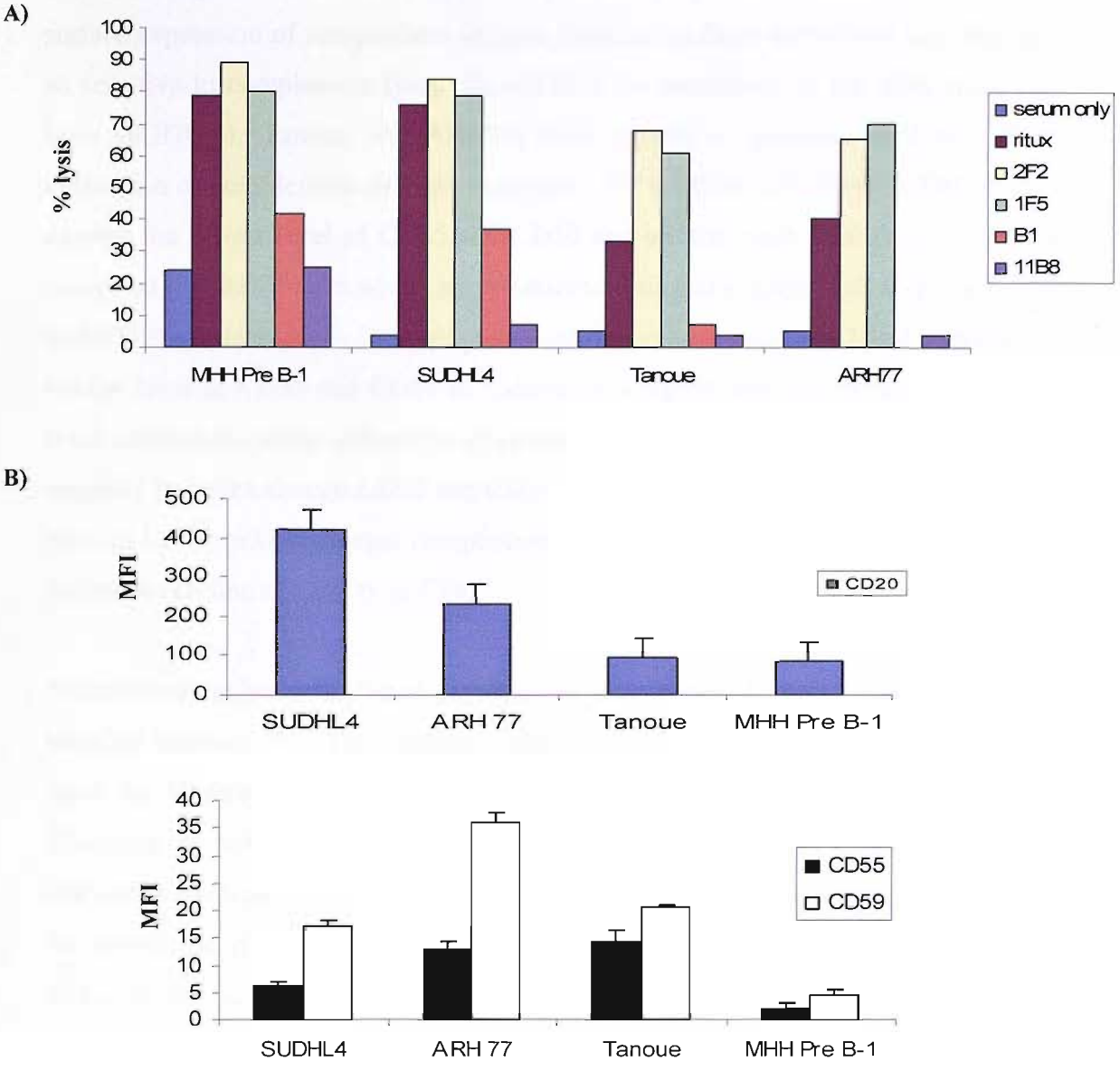

Figure 3.4: B cell lines have different sensitivities to CD20-mediated complement lysis. A) Cells were assessed for complement lysis using the method as outlined in materials and methods Section 2.7. Briefly, MHH Pre B-1, SUDHL4 and ARH77 cells were stimulated with 10μg/ml mAb and incubated with 20% NHS (v/v) at 37°C for 40 minutes. The cells were then analyzed for lysis by flow cytometry using the PI assay. All values have the background lysis subtracted, which is the % lysis in the absence of serum and mAb. The data is representative of two independent experiments **B)** Expression levels of CD20 (1F5) CD55 (clone 26) and CD59 (Mem43) are determined by indirect labelling and flow cytometry as outlined in Section 2.6. Briefly, $1x10^5$ cells were incubated with 10 μg/ml mAb at room temperature for 15 minutes. The samples were then washed twice and labelled with 50μl 1:40 GAM (Goat anti-mouse FITC labelled, DAKO) for 15 minutes before being washed and analyzed by flow cytometry. Data shown is the mean and standard deviation of three independent experiments. MFI: Mean fluorescent intensity.

From analysing the surface expression of CD55 and CD59 proteins in the different cell lines (Figure 3.4B and see Appendix I), it can be seen that MHH Pre B-1 lacks surface expression of complement defence proteins, perhaps explaining why they are so sensitive to complement lysis. In addition, the sensitivity of the other three cell lines (SUDHL4, Tanoue and ARH77) also appears to correlate well with their expression of complement defence molecules. Of the three cell lines, SUDHL4 cells express the lowest level of CD55 and CD59 and are the most sensitive to cell lysis compared to ARH77 cells which are resistant to lysis and express high levels of CD55 and CD59 proteins. It is interesting to note that even though SUDHL4 expresses a similar level of CD55 and CD59 to Tanoue, it is significantly more sensitive to cell lysis, particularly when induced by ritux and B1 (See Figure 3.4A). This observation suggests that even though CD55 and CD59 expression can influence the sensitivity of cells to CD20 mAb-mediated complement lysis, it is not the only factor which can influence cell line sensitivity to CDC.

Monoclonal antibody mediated complement lysis generally progresses through the classical pathway [199]. This pathway requires the activation of C1q which depends upon the binding of juxtaposed Fc domains of cell-bound mAb (see Figure 3.1). Therefore, as mAb bind to a specific surface antigen on the cell surface, it is likely that surface antigen expression level is of critical importance in inducing cell lysis. To investigate if CD20 expression level is important in anti-CD20 mAb-mediated CDC, the four cell lines detailed previously were analysed for CD20 expression. The data in Figure 3.4B demonstrates that at an MFI of 400, SUDHL4 cells express CD20 at a 3-4 fold higher level than the other cell lines. This high expression appears to be reflected in the high sensitivity of the cells to complement lysis induced by anti-CD20 mAb. From Figure 3.4A, it appears that SUDHL4 and MHH Pre B-1 are lysed to relatively the same extent by anti-CD20 mAb. However, if the inherent sensitivity of the cells is taken into account and the specific lysis by anti-CD20 mAb is only assessed (i.e. subtracting the lysis induced by serum alone) it becomes apparent that SUDHL4 is the most sensitive cell line and that MHH Pre B-1 and Tanoue which have similar CD20 expression levels, have in turn similar sensitivities to anti-CD20 mAb-mediated complement lysis.

In order to clarify whether CD20 expression level is an important factor in inducing complement lysis, NS/0 cells were transfected with human CD20. These are murine cells and therefore normally lack expression of human CD20. A number of clones were selected based on their CD20 expression level. These clones were obtained from collaboration with GenMab (Utrecht, Holland). As NS/0 clones are murine cells, only 1% NHS was used as a source of active complement in these assays as lack of human complement defence molecules on NS/0 cells makes them highly sensitive to CDC induction. It is evident from Figure 3.5A that the NS/0 clones express different levels of CD20, with expression increasing from clone 8 to 21 and with ritux binding at a higher level than B1 mAb. Taking data from Figure 3.5A and B, it becomes apparent that CD20 expression level is an important factor in determining the sensitivity of cells to CD20-mediated lysis where the level of lysis correlates strongly with the level of CD20 expression. Once again, the differences in potency of the various mAb were evident, with 1F5 and ritux being the most potent compared to B1 which induces a moderate level of cell lysis. It is of interest to note that the level of CD20 expression does not interfere with the inherent sensitivity of the clones to complement lysis as can be seen from the relatively consistent background lysis achieved with serum alone. To confirm this correlation linear regression analysis was applied. On plotting the data shown in Figure 3.5C, the R^2 was calculated at 0.88 which demonstrates a high degree of correlation and a threshold response to the concentration of mAb.

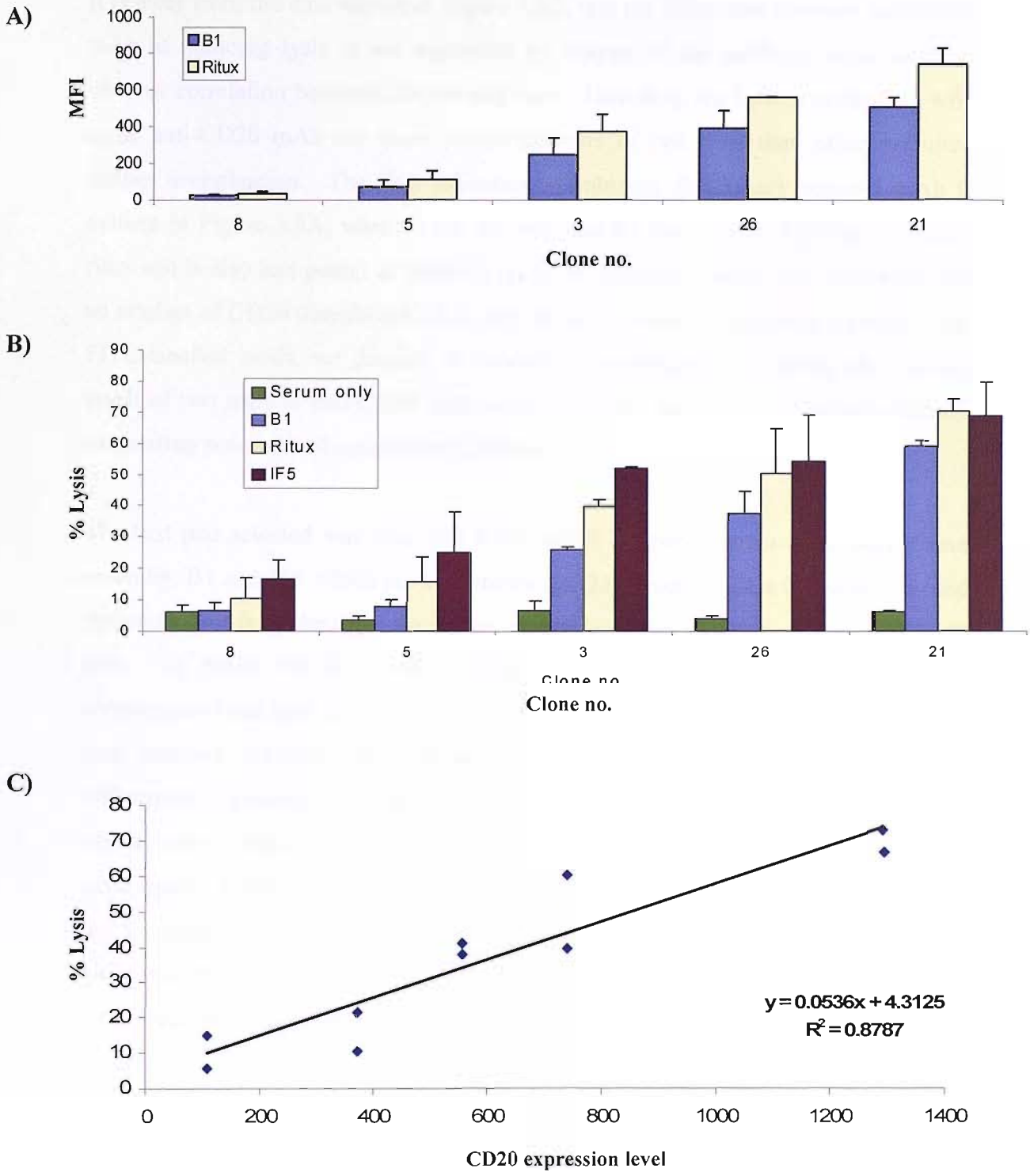

Figure 3.5: CD20 expression level correlates with the level of complement lysis. A) $1x10^5$ cells were incubated with 10 μg/ml FITC labelled B1 or ritux for 30 minutes at 37°C before being washed and analysed by flow cytometry. **B)** $1x10^5$ cells were treated, or not, with 10μg/ml mAb in the presence of 1% NHS for 30 minutes at 37°C. The cells were then analyzed for lysis by the PI assay as outlined in Section 2.6. **C)** Linear regression was performed using EXCEL. Data is based on 10μg/ml ritux FITC binding and % lysis induced by the same concentration of ritux in a range of NSO clones. Data is from two independent experiments.

3.2.3 Binding profiles of anti-CD20 mAb

It is clear from the data shown in Figure 3.3C, that the difference between anti-CD20 mAb at inducing lysis is not explained by isotype of the antibody alone with no obvious correlation between isotype and lysis. Therefore, the factors underlying why some anti-CD20 mAb are more potent inducers of cell lysis than others required further investigation. The first indication of inherent differences between mAb is evident in Figure 3.5A, where it can be seen that B1 has a lower binding level than ritux and is also less potent at inducing lysis. To analyse whether this difference was an artefact of CD20 transfected NS/0 cells or due to different dye:protein ratios of the FITC-labelled mAb, we decided to extend the investigation to assess the binding levels of two pairs of anti-CD20 mAb which share the same isotypes but demonstrate contrasting potencies of complement induction.

The first pair selected was ritux and 11B8 which are both human IgG1 isotype and secondly, B1 and 1F5 which are both mouse IgG2a. From the data in Figure 3.6 (and Appendix I) it is evident that the earlier observation was not just an artefact of NS/0 cells. In MHH Pre B-1 cells, efficient inducers of anti-CD20 mAb-mediated complement lysis such as ritux and 1F5 bind at a higher level when compared to the poor inducers, B1 and 11B8, which bind at approximately half this level. These differences in binding level are not affected by expression level, as SUDHL4 cells which express almost 4 fold higher levels of CD20 than MHH Pre B-1 depict the same result. Furthermore, from other work performed in our laboratory [200], it appears that the difference in mAb potency may be linked to the off rate of the mAb where it was found that anti-CD20 mAb with slower off rate like ritux and 7D8 were more effective at engaging complement.

Despite good inducers of complement-mediated lysis such as ritux binding at higher levels to the cells, this does not appear to be the determining factor in explaining why they are good activators of complement. From Figure 3.7 it is evident that at 10 μg/ml, both 1F5 and ritux bind at a higher level than B1 in NS/0 clone 3 (Fig 3.7B) and 26 (Fig 3.7D). However in Clone 3, 2μg/ml B1 binds at a higher level than 0.08μg/ml ritux yet the corresponding lysis shown in panel A is still lower. Similarly

in Clone 26 at 0.08μg/ml all mAb bind at the same level yet again B1 gives the lowest lysis of the three.

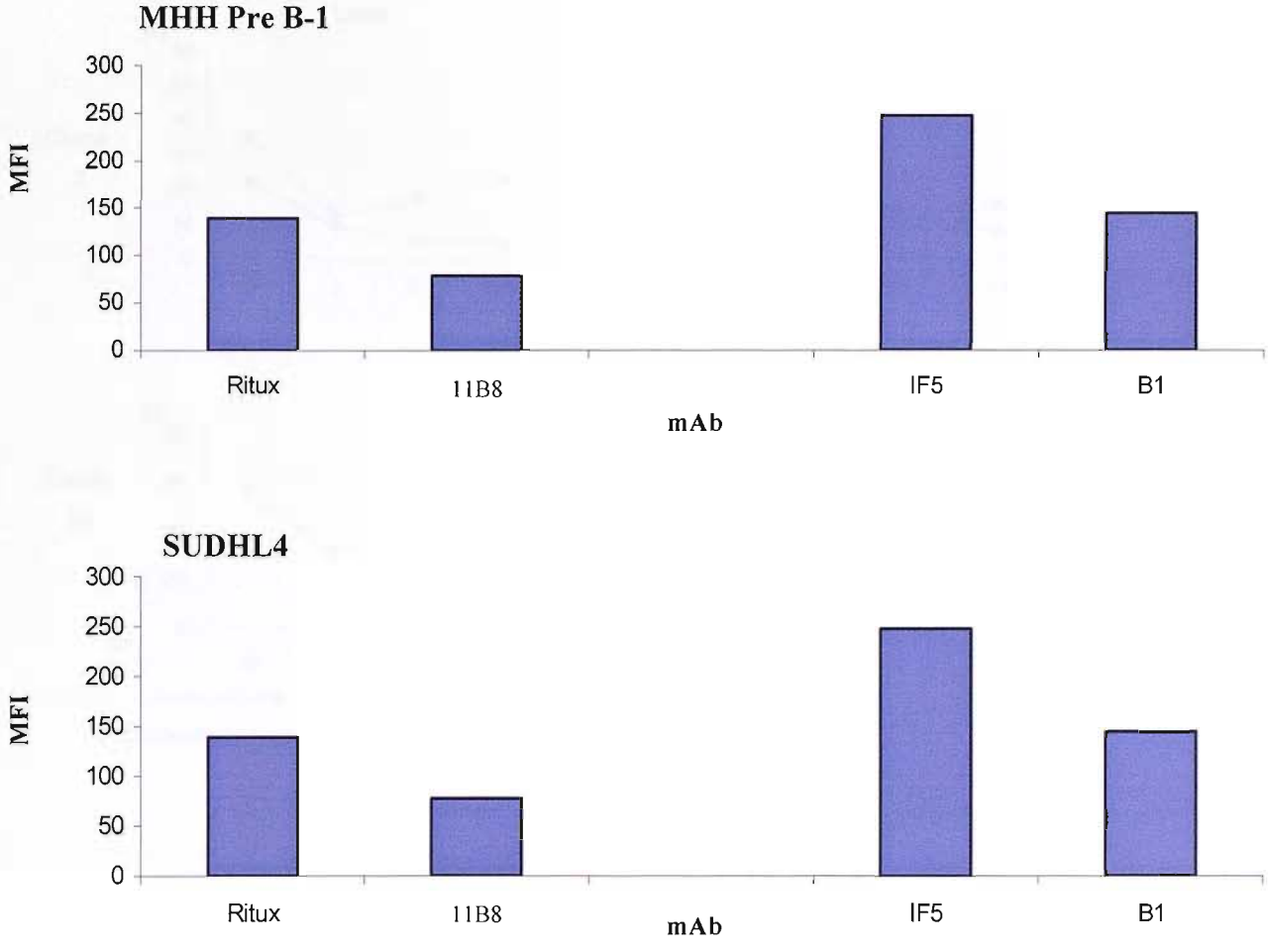

Figure 3.6: The binding profiles of Anti-CD20 mAb. $1x10^5$ cells were incubated with 10 μg/ml mAb for 15 minutes at room temperature. Samples were then washed twice and incubated with the appropriate FITC labelled secondary mAb, either 50μl 1:40 GAM or 10 μg/ml SB2H2 which is mouse anti-Human Fc FITC for 15 minutes at room temperature before being washed and analysed by flow cytometry.

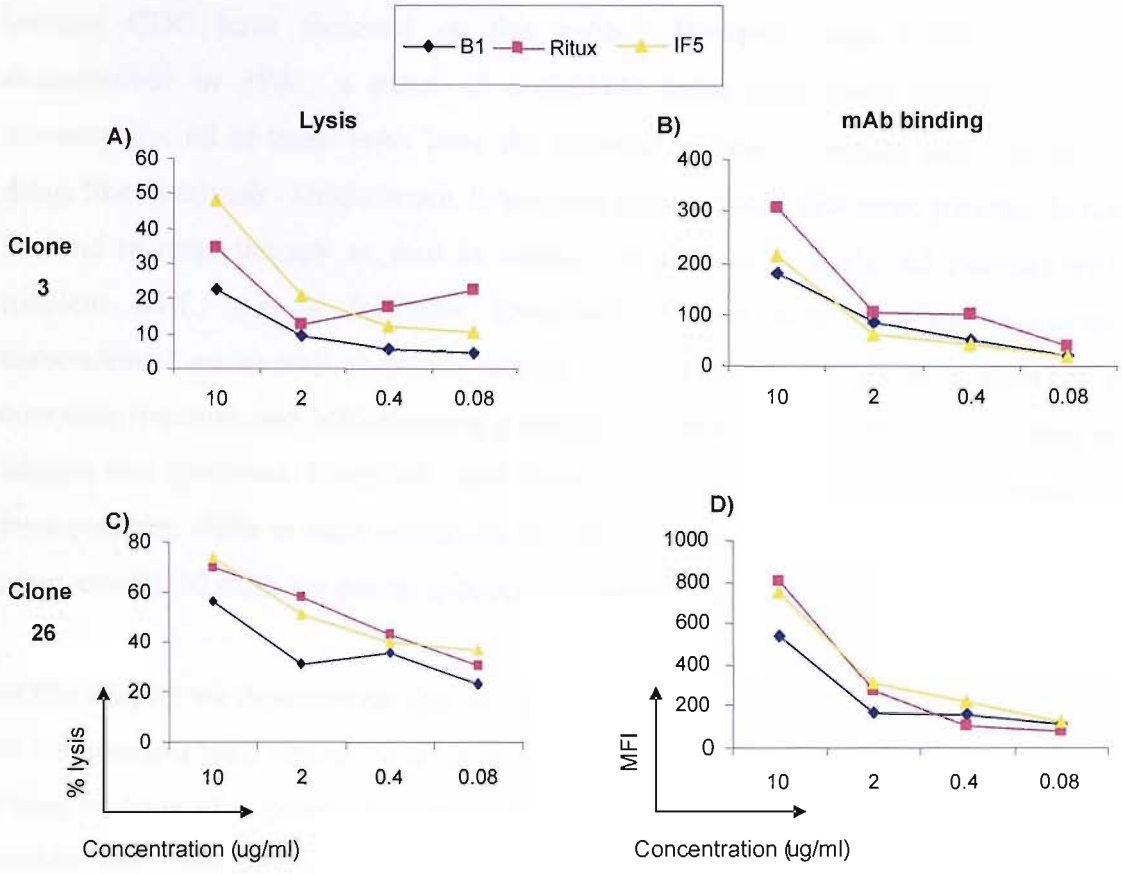

Figure 3.7: Comparison of mAb binding with complement lysis. A) $1x10^5$ NS/0 clone 3 cells were treated, or not, with 10, 2, 0.4 or 0.08 µg/ml B1 (diamonds), ritux (squares) or 1F5 (triangles) in the presence of 1% NHS for 30 minutes at 37°C. The cells were then analyzed for lysis by the PI assay as outlined in materials and methods Section 2.6. B) $1 x10^5$ NS/0 clone 3 cells were incubated with 10, 2, 0.4 or 0.08 µg/ml FITC labelled mAb in the absence of NHS for 30 minutes at 37°C. Cells were harvested and assessed by flow cytometry as outlined in Section 2.5. C) NS/0 clone 26 cells were treated as outlined in A. D) NS/0 clone 26 cells were treated as outlined in B.

3.3 Discussion

Complement dependent cytotoxicity is postulated to be an important effector mechanism in ritux mediated therapy [118, 140, 141]. As ritux is currently the main mAb employed in CD20-directed therapies, the majority of investigations on CD20-induced CDC have focussed on this mAb. However since CD20 was first characterised in 1980, a panel of anti-CD20 mAb have been established and theoretically, all of these mAb have the potential to become potent immunotherapy drugs like rituximab. Furthermore, it has been demonstrated that some patients do not respond to ritux therapy as well as others. In a phase II study, 62 patients with indolent NHL, mainly follicular lymphoma, treated with first-line rituximab demonstrated an overall response rate of 73% with 37% of patients showing a complete response and 36% showing a partial response [102]. Therefore, we wanted to address two questions, firstly why cell lines (which originate from tumours extracted from patients) differ in their sensitivity to CD20-induced CDC and secondly, whether other anti-CD20 mAb are potent inducers of complement lysis.

In this chapter we demonstrate that not all anti-CD20 mAb generate significant levels of complement lysis where the level of cytolytic activity seen is depends on the mAb. From analysis of a panel of 5 anti-CD20 mAb, it emerged that the mAb could be divided into two groups; firstly, good inducers of complement lysis 1F5, ritux and 7D8 and secondly poor inducers of a cytolytic response B1 and 11B8. This data is in agreement with a study performed by Cardarelli et al [162] who reported that B1 induced a lower level of activity against CDC-sensitive cells Daudi and Ramos cells compared to ritux. We found that within the groups there was a notable difference in the ability of mAb to induce cell lysis. 7D8 was the most potent of all the mAb assessed achieving almost maximal potency at 0.4 μg/ml on all cell lines tested (similar to Tanoue data shown in Figure 3.3) compared to the ritux and 1F5 mAb where their efficacy was reduced upon reduction of mAb concentration. The cell death induced by the anti-CD20 mAb was confirmed to be due to CDC activity by the absence of cell death when cells were incubated in the presence of heat inactivated NHS.

In addition to differences in mAb potency, it was observed that cell lines varied in their sensitivity to CD20 mAb-induced CDC (Figure 3.4). In our study, we assessed

four B-cell lymphoma cells lines of various tumour origins (see Table 2.2). A report by Manches and colleagues [128] suggests that depending on their tumour origins, lymphoma cells exhibit differential sensitivity to ritux-mediated CDC. Ritux induced high levels of CDC in FL cells, whereas diffuse large B-cell lymphoma and mantle cell lymphoma were moderately sensitive and small lymphocytic lymphoma were almost resistant. Various agents have been reported to enhance CD20 mAb-mediated CDC in vitro. Kennedy et al [140] utilised a mAb directed at the C3b breakdown product which increases C3 deposition on lymphoma cells enhancing the efficacy of ritux-induced complement lysis. Several investigators have reported an increase in ritux potency in the presence of mAb against complement defence proteins in lymphoma and multiple myeloma cell lines [118, 122, 137]. In support of these reports, a study of circulating cells of CLL patients treated with ritux revealed that surviving tumour cells have elevated expression of the complement defence proteins CD55 and CD59 [143]. Therefore, in an attempt to explain the heterogeneity between the cell lines, the expression levels of CD55 and CD59 were assessed. We found that the expression level of CD55 and CD59 was indeed a determining factor in the sensitivity of the cells to CDC. MHH pre B-1 have a low expression level of complement defence proteins and were highly sensitive to CD20 mAb-induced CDC in our studies. In contrast, ARH77 cells, which express similar levels of CD20 to MHH Pre B-1 cells, express higher levels of CD55 and CD59 and were relatively resistant to anti CD20 mAb-induced CDC. This data reports from Golay et al [118], suggest a possible mechanism for patient resistance to ritux therapy.

Another determining factor in anti CD20 mAb-mediated CDC is the expression level of CD20 itself. When comparing SUDHL4 and Tanoue cells, it was found that SUDHL4 cells had a significantly higher CD20 expression and were consequently more sensitive to lysis. For example, using ritux at 10μg/ml, 80% lysis of SUDHL4 cells was achieved compared to 35% for Tanoue cells. The importance of CD20 expression in CD20-induced CDC was confirmed by the use of NS/0 cells expressing different levels of CD20 where the sensitivity of the different clones to lysis was strongly correlated to the level of CD20 expression. These differences are probably due to the requirement for C1q binding. The C1q binding motif located in the Fc domain (human IgG1) of ritux has been reported to be pivotal for efficient CDC induction [139]. C1q requires at least two juxtaposed Fc domains to be in close

proximity to one another for stable binding and activation of the classical pathway of complement [199]. Therefore at a higher expression level of CD20 there is a greater probability that Fc domains of bound mAb will be in sufficient proximity for effective C1q binding to take place. Taken together, this data suggests that the difference in sensitivity of cell lines to CD20 mAb-mediated CDC is dependent on the expression of complement defence proteins CD55 and CD59 and the expression level of CD20.

It was demonstrated that even with a high CD20 expression level, the various anti-CD20 mAb investigated differed in their ability to induce CDC. There is a well established hierarchy of mAb isotypes with regard their ability to activate complement [12]. Human IgG1, mouse (m) IgG2a and mIgG3 are reported to be efficient mediators of complement compared to mIgG1 and mIgG2b which are poor activators. However, not all anti-CD20 mAb investigated demonstrated the characteristic potency of their isotype. Most notable was the apparent lack of CDC induced by 11B8. 11B8 possess the same human IgG1 Fc domain as ritux which has been reported to be pivotal for the binding of C1q and activation of CDC [139]. Therefore, it would be expected that 11B8 would be a potent mediator of CDC effectively engaging human C1q. It is in fact the least potent of all anti-CD20 mAb assessed achieving less than 10% lysis at saturating concentrations in most cell lines in marked contrast to other huIgG1 mAb, ritux and 7D8, assessed which achieve 80% lysis at the same concentration. Similarly, B1 a mIgG2a isotype would be expected to induce high levels of CDC like 1F5 also a mIgG2a. However at 50 μg/ml B1 lyses 10% Tanoue cells compared to 1F5 which achieves 70% lysis.

In an attempt to explain the different cytolytic potencies of anti-CD20 mAb, the binding profiles of the mAb were assessed. This analysis revealed when mAb of the same isotype were compared, some mAb demonstrated an almost two fold higher binding level compared to mAb of the same isotype. It appeared that mAb which bound at the higher level, such as ritux and 1F5 were characteristic of their isotype and good inducers of CDC. These mAb were classified as type I mAb. The mAb which bound at a lower level B1 and 11B8, were poor inducers of CDC relative to their isotype and were classified as type II mAb. The reason for the difference in levels of mAb saturation could possibly be explained by modes of mAb binding. CD20 is believed to provide one epiptope for mAb binding, located in the large

extracellular loop of the tetraspan molecule [32]. The conformation of type I mAb binding may only allow for univalent binding i.e. one "arm" of the mAb can only bind a CD20 epitope. In contrast, the conformation of type II mAb upon binding may facilitate bivalent binding where the two "arms" of the mAb could engage two CD20 epitopes. Thus explaining why type II mAb show an almost 50% lower level of binding compared to type I mAb. An important point to note is that, it is not just the increased binding level that makes type I mAb good mediators of CDC. From analysis of the NS/0 cells it is apparent that even when 1F5 and B1 are bound at the same level, the lysis induced is higher with 1F5.

The ability of type II mAb like B1 to induce CDC was not improved by increasing the mAb concentration to well over the saturation concentration of approximately 10μg/ml in most normal B cell lines. In Tanoue cells, on comparison of 50 μg/ml 11B8 (type II) with 0.4 μg/ml 7D8 (type I), a concentration which would not be expected to achieve saturation binding, 11B8 achieved 5% lysis compared to 70% for 7D8. A similar result was observed in all other cell lines assessed. This data suggests that it is not the binding level of the mAb itself that is the crucial factor but the binding mode where type I mAb, but not type II, somehow orientate their Fc domains to facilitate stable binding of C1q. This theory is supported by the observation that at high CD20 expression levels (NS/0 clone 21), type II mAb are almost as effective at inducing lysis as type I mAb. This is in marked contrast to cells with low CD20 expression levels where a more favourable orientation of Fc would be required and therefore type II mAb do not activate complement. At high CD20 expression levels presumably CD20 molecules would be in close proximity to each other such that when mAb binds, the requirement for optimal orientation of their Fc domains to engage C1q stably would be reduced. Hence, type II mAb can effectively mediate CDC at high CD20 expression levels but not when expression of CD20 is low.

The reason why CD20 is such a good mediator of CDC is not fully understood. The three main advantageous characteristics of CD20 for CDC induction are; Firstly, it has a small extracellular loop which may allow the complement cascade to be focused close to the cell surface. Secondly, CD20 is not internalised on mAb binding therefore the anti-CD20 mAb required for C1q binding would remain on the surface to sustain C1q binding and activation of the complement cascade. Finally, CD20 is expressed at

high levels on B cells which as demonstrated by our data is a crucial factor for efficient lysis. Previous work by our group assessed the ability of other surface antigens which share some of the favourable characteristics of CD20 such as CD37 which is a tetra-span molecule with a small extracellular loop and MHC Class II which is highly expressed on B cells. When comparing he complement lysis induced by anti-CD37, -MHC class II and –CD20 (ritux) it was found that even though both anti-CD37 and MHC class II effectively induced CDC, the anti-CD20 mAb ritux was still the most potent (M Cragg, personal communication).

In conclusion, high levels of cytolytic activity can be induced by some but not all anti-CD20 mAb. We have shown that high CD20 expression is a necessary requirement for efficient cell lysis and that complement defence proteins CD55 and CD59 regulate the CD20 induced complement cascade. In addition, we have demonstrated that anti-CD20 mAb can be classified by their potency to induce CDC. Type I mAb demonstrate the CDC potency predicted by their isotypes and achieve high levels of cytolytic activity whereas type II mAb even though they are of the same isotypes, they induce low levels of CDC. We suggest that the difference in potencies of type I and type II mAb could possibly be explained by different binding modes to CD20. This hypothesis is explored further in the next chapter.

CHAPTER FOUR

4.0 Investigation into the localisation of CD20 in lipid raft domains.

4.1 Introduction

In the previous chapter we introduced the idea that even though all anti-CD20 mAb bind the same target, their downstream effects can be quite different. It was found that certain anti-CD20 mAb are more potent inducers of complement lysis than others. Indeed mAb can be divided into two groups based on these differences; type I such as ritux and 1F5 which are good mediators of cytolytic activity and type II like B1 which are poor inducers of complement activation. The classical complement pathway is initiated upon C1q activation, which requires at least two Fc domains of mAb to be sufficiently juxtaposed for binding. Therefore we decided to investigate whether the varying ability of anti-CD20 mAb to cause CDC was related to their ability to redistribute CD20 differently in the plasma membrane.

In 1998, Deans et al [66] demonstrated that some anti-CD20 mAb could redistribute CD20 into Triton X-100 (TX-100) insoluble micro-domains in plasma membranes. Around this time Brown et al [79] suggested that these TX-100 insoluble domains, also known as detergent insoluble micro-domains (DRMs), might represent lipid 'raft' structures which may play an important role in transmembrane signal transduction (see Section 1.4.4). These rafts are thought to be small islets (<70 nm) in the plasma membrane of most cell types that are enriched in glycosphingolipids, sphingomyelin, and cholesterol [82]as shown in Figure 4.1.

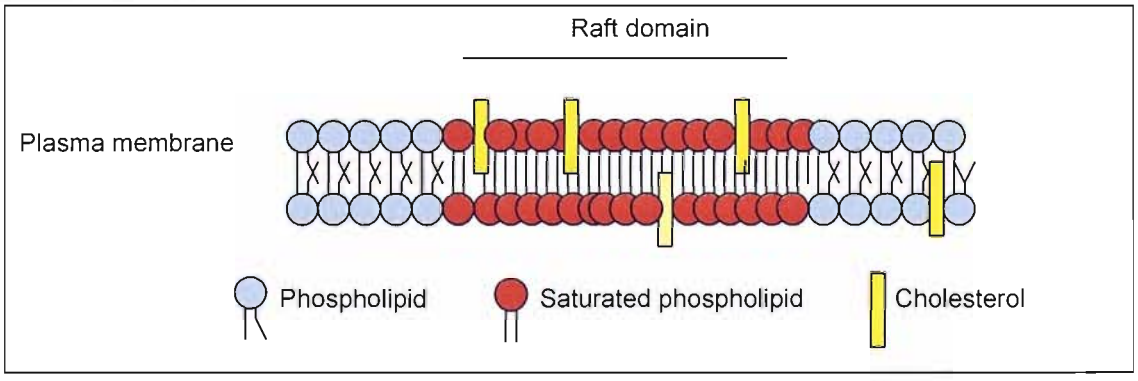

Figure 4.1: Diagrammatic representation of lipid raft domains. Lipid raft domains are postulated to be membrane microdomains which are rich in saturated phospholipids, glycosphingolipids and cholesterol. This domain is highly ordered compared to the rest of the normally fluid plasma membrane, allowing for a tightly packed structure.

Their main distinguishing feature is their tightly packed "liquid ordered phase" which separates it from the less-ordered bulk membrane. This tight packing presumably occurs because of their high content of cholesterol and lipids possessing saturated acyl chains. Conveniently, because of their high lipid content, DRMs can be isolated by detergent extraction and density gradient ultracentrifugation [69, 81]. These "rafts" are generally characterized by their insolubility in 0.5-1% TX-100 at low temperature[82]. Proteins that localize to these domains are usually glycosylphosphatidylinositol (GPI) anchored such as CD59 and CD48 or dually acylated like the Src family kinases.

As lipid rafts are suggested to be important signalling platforms, we were interested in whether CD20 associates with these domains and whether this association is important for the induction of complement lysis. To this end, the ability of CD20 mAb to translocate CD20 was analysed by various methods utilising western blotting, flow cytometry and electron microscopy. In addition to assessing the potency of mAb to redistribute CD20, the dynamics of CD20 redistribution was also assessed.

TX-100 insolubility is the most common biochemical method employed to analyse lipid rafts. However, other detergents such as Brij 58 and CHAPS are now being used and it appears that proteins which are solubilised by TX-100 can be insoluble to these different detergents [68]. Therefore, we decided to compare the CD20 distribution when lysed in TX-100 and Brij 58. Furthermore, as cholesterol is an important component of lipid raft domains, we also analysed the effects of cholesterol depletion on mAb binding and CD20 redistribution.

4.2 Results

4.2.1 Investigation of CD20 redistribution in the plasma membrane by density gradients with ultra centrifugation

The ability of anti-CD20 mAb to induce redistribution of CD20 into TX-100 insoluble domains was assessed by several methods. Firstly, sucrose density gradients of detergent lysates were used which identifies the raft domains by their buoyancy in such gradients. Daudi B-cells were incubated with or without anti-CD20 mAb before lysis in 0.5-1% TX-100 for 40 minutes on ice. The lysed cells were added to the

bottom of the tube and centrifuged at 26,000RPM through a sequential, discontinuous sucrose density gradient varying from 5-40%, for 16 hours at 4°C. After this ultracentrifugation, ten 500µl fractions (F) were removed representing the gradients of 5% (F1-3), 10% (F4), 20% (F5), 30% (F6-7) and 40% (F8-10) sucrose and these fractions were analysed by SDS-PAGE and western blotting. In general it is considered that F1-5 represent the insoluble, buoyant fractions (low density) and F7-10 the soluble fractions (high density).

On analysis of the coomasie-stained gel (Figure 4.2) it can be seen that most of the protein lysate remain in the high-density fractions and only a small proportion resides in low density fractions that would be expected to contain rafts. This distribution was not found to be changed with different mAb treatments (data not shown).

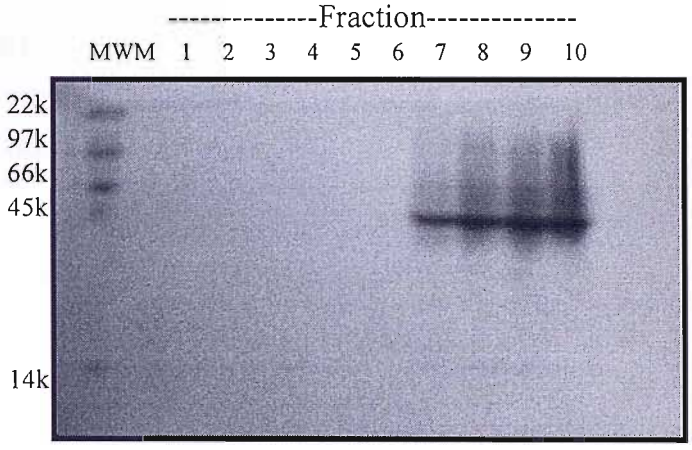

Figure 4.2: Coomasie stained SDS gel of raft fractions from a sucrose density gradient. $5x10^7$ Daudi cells were treated with mAb (25 µg/ml) for 20 min at 37°C and then lysed with 1% TX-100 on ice for 40 minutes. Lysed cells were separated via sucrose density gradient centrifugation and resolved on SDS-PAGE. The above gel was stained over night at room temperature with Coomasie blue stain and then destained. MWM: molecular weight marker.

Figure 4.3 demonstrates that CD20 does not constitutively reside in TX-100 insoluble domains as in unstimulated cells (NT), CD20 remains in the soluble fractions 7-10. Upon stimulation with ritux or 7D8, CD20 was redistributed into the insoluble domain and therefore found in the buoyant fractions. In marked contrast, B1 and 11B8 only shifted the localization of CD20 to a very small extent. As such, it appears that type I mAb (good inducers of CDC) redistribute CD20 whereas type II (poor mediators of CDC) do not. The anti-CD20 mAb 7D8 resulted in complete redistribution of CD20 to Fraction 5 whereas ritux caused a redistribution of CD20 to

fraction 4 and 5. This was a reproducible finding but the significance of which is unclear. To confirm the findings from above we also performed gradient experiments using another commonly used, commercially available gradient called optiprep and found comparable distribution patterns with type I and type II mAb treatment (data not shown).

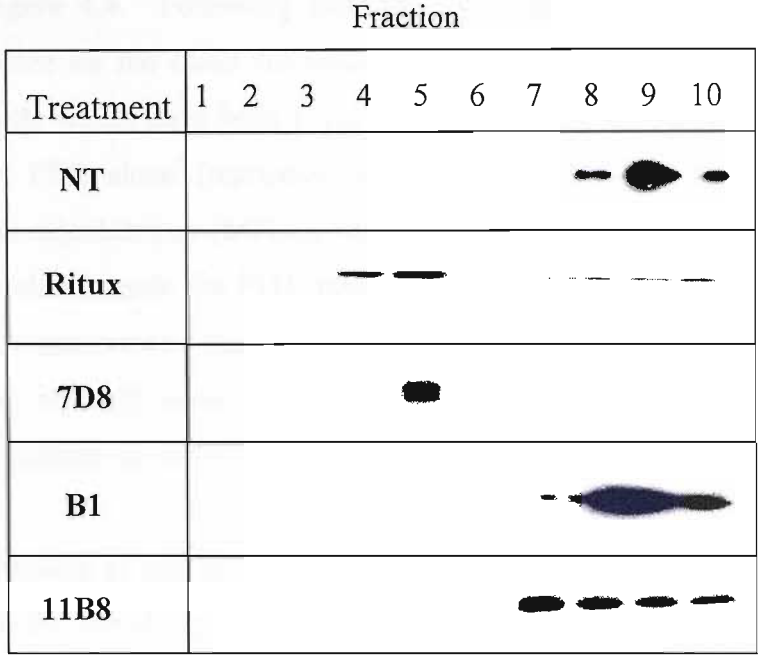

Figure 4.3: CD20 can translocate in or remain outside of lipid rafts upon mAb binding. $5x10^7$ Daudi cells were treated with mAb (25μg/ml) for 30 minutes at 37°C and then lysed with 1% TX-100 on ice for 40 minutes. Lysed cells were separated via sucrose density gradient centrifugation, resolved on SDS-PAGE and western blotted for CD20 using 7D1 mAb.

4.2.2 Analysis of the localization of CD20 to TX-100 insoluble domains by flow cytometry

Sucrose density gradients are a laborious and time consuming technique. The process takes three days to complete, requires a large number of cells and any physical disruption of the gradient, such as accidental shaking of the tubes, can result in a loss of gradient integrity making reproducibility of the assay difficult. Therefore, an alternative rapid and semi-quantitative method was developed. In this method the ability of mAb to translocate CD20 into TX-100 insoluble domains was determined by flow cytometry (Figure 4.4). This assay determines how potent mAb are at redistributing target antigens into TX-100 insoluble domains by the level of mAb binding remaining after TX-100 lysis, expressed as % insolubility. Briefly, cells are

incubated or not with 10μg/ml FITC labelled mAb for 15 minutes at room temperature before being split into two, one half incubated with PBS and the other with in 0.5% TX-100 on ice for 15 minutes before washing and assessing by flow cytometry. Significant physical changes were seen in the cells after incubation with TX-100 as shown by the lower forward (FSC) and side (SSC) scatter properties shown in Figure 4.4. Following flow cytometry analysis the % insolubility was calculated based on the mean fluorescent intensity (MFI) difference between mAb binding to cells which have been lysed in 0.5% TX-100 and those which have been incubated in PBS alone (representing maximal binding of the mAb). The % insolubility is calculated as $(MFI_{lysed}/MFI_{PBS})x100$. Therefore, if CD20 redistributes into the insoluble domain the FITC labelled mAb binding will not be highly affected by detergent treatment and the MFI will be similar to the unlysed cells giving a high %. However, if CD20 is not present in the insoluble domain it will be solubilised, reducing the amount of anti-CD20 mAb FITC signal resulting in a low % insolubility.

The ability of mAb to redistribute CD20 as measured by this assay is consistent with the data from the density gradient assays where again a clear division between type I and type II mAb can be seen in Figure 4.4 and 4.5. As such ritux was a good inducer of CD20 translocation and B1 and 11B8 were poor inducers. These experiments were also preformed in Raji or MHH pre-B1 B cell lines and similar results were observed in both. It is notable that there is a slight discrepancy between the density gradient and flow cytometry assays. In the density gradient analysis (Figure 4.3) 7D8 demonstrated a 100% redistribution of CD20, yet in the TX-100 flow cytometry assay (Figure 4.5) it only demonstrates 70%. The difference could be accounted for by the loss of CD20 during the washing step which takes place in the flow cytometry technique and which is not required for the density gradient assay.

Next we decided to investigate whether antibody-induced TX-100 insolubility was common for other tetra-span molecules or for other surface antigens that are highly expressed on B cells. To this end, the % TX-100 insolubility was obtained for CD38 (which is a type II transmembrane protein), CD37 (which has a similar structure to CD20 in that it is a tetraspan molecule with a small extracellular loop) and MHC class II (which is highly expressed in B cells). In accordance with Filatov and colleagues [72], Figure 4.6 suggests that redistribution into TX-100 insoluble domains is not a

common phenomena where neither CD37, CD38 nor MHC class II appear to become insoluble upon mAb binding.

From this data and the data in Section 4.2.2, we demonstrated that the anti-CD20 which are good inducers of complement lysis (type I mAb) are also efficient redistributors of CD20 into lipid rafts. Conversely, type II mAb like B1 are poor mediators of complement lysis and do not redistribute CD20 into lipid rafts.

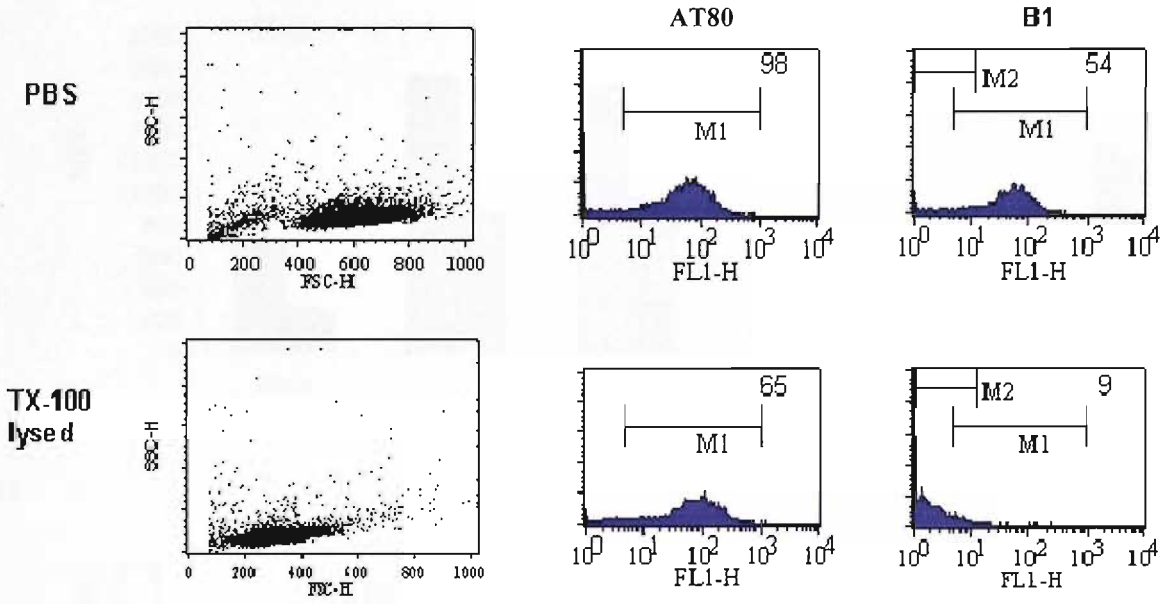

$$\% \text{ TX-100 insolubiltiy for AT80} = MFI_{lysed}/MFI_{PBS} \times 100$$
$$= 65/98 \times 100$$
$$= 66.5\%$$

Figure 4.4: Example of TX-100 flow cytometry assay. Raji cells were treated with 10 μg/ml FITC labelled anti-CD20 mAb for 15 minutes at 37°C before washing and dividing the sample in two. One half was maintained on ice in PBS, allowing calculation of 100% binding levels, whilst the other was treated with 0.5% TX-100 for 15 minutes on ice. Cells were then washed once, resuspended in PBA and assessed by flow cytometry. The MFI for each histogram is shown in the top right hand corner. Calculation of the % TX-100 insolubility is outlined for AT80 only.

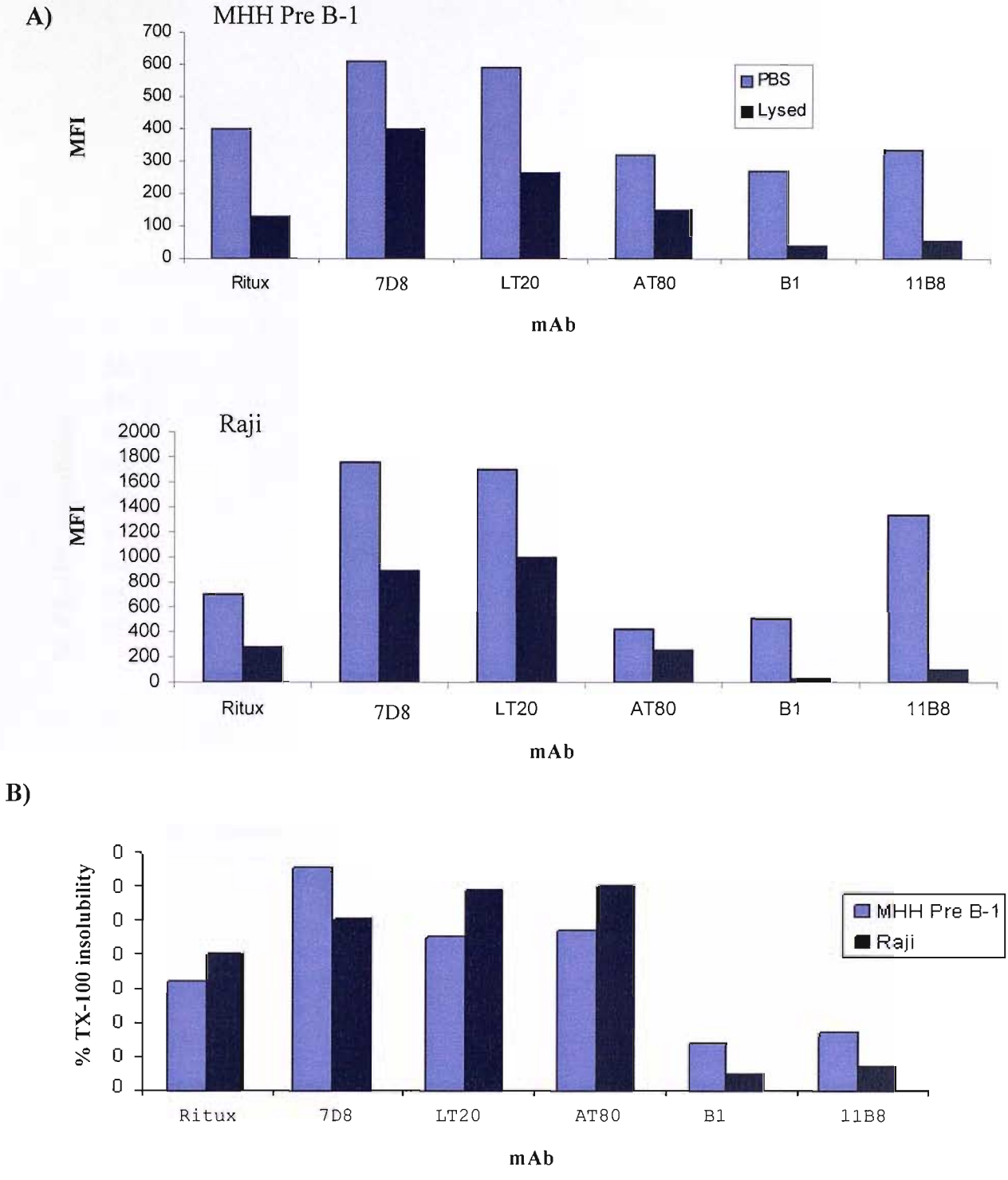

Figure 4.5: TX-100 insolubility of CD20 after binding of anti-CD20 mAb. $2.5x10^6$ cells (MHH Pre B-1 and Raji) were treated with 10 µg/ml FITC labelled mAb for 15 minutes at 37°C before washing and dividing the sample in half. One half was maintained in PBS on ice, whilst the other was treated with 0.5% TX-100 for 15 minutes on ice. Cells were then washed once, resuspended and assessed by flow cytometry. Shown are **A)** MFI values and **B)** the % TX-100 insolubility calculated from A.

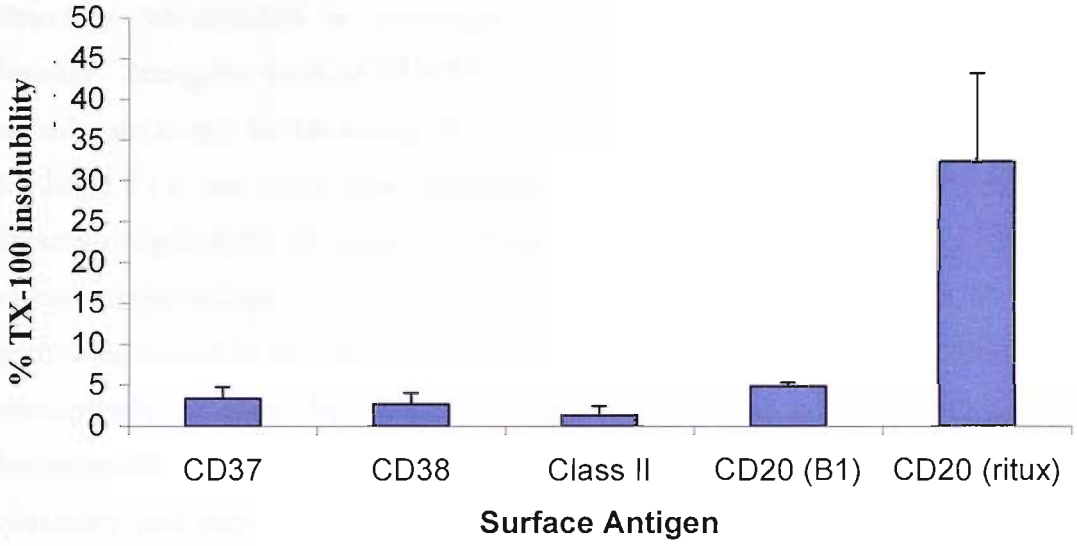

Figure 4.6: Redistribution of surface antigens upon mAb ligation. The same procedure was used as outlined in Materials and Methods Section 2.8.2. Briefly, Raji cells were treated with FITC labelled anti-CD37 (WR17), CD38 (IB4), Class II (A9-1) and CD20 mAb for 15 minutes at 37°C before being lysed or not in 0.5% TX-100 for 15 minutes on ice. Samples were then washed and analysed by flow cytometry. Data shown is mean and standard deviation of three independent experiments

4.2.3 The association of CD20 with lipid rafts when assessed by different detergents

The previous two sections have both utilised TX-100 insolubility to demonstrate CD20 redistribution in the membrane upon mAb binding. However, as 1% TX-100 treatment is a relatively harsh treatment, only membrane domains which are highly compact will withstand lysis with this detergent. Furthermore, as TX-100 is such a stringent detergent it is conceivable that the CD20 redistribution observed in the presence of this detergent is unrepresentative of the physiological situation. Therefore, we decided to investigate the distribution of CD20 when lysed by "weaker" detergents such as CHAPS and Brij 58 [68, 81]. For this analysis we used a pellet/lysate assay. In this assay, cells were lysed as per normal procedure outlined in Section 2.8.1.2 but rather than separating the lysates through a density gradient by ultracentrifugation for 16 hours at 27000RPM, the lysed cells were spun at 16,000g in a bench top centrifuge for 30 minutes. This pelleted all insoluble material, leaving the solubilised matter in the supernatant (lysate). The resultant pellets and lysates were subsequently assessed by SDS-PAGE and western blot analysis. Figure 4.7A demonstrates that inTX-100 treated cells the pellet/lysate assay, like the flow cytometry and sucrose density gradients, distinguish between the redistribution of CD20 when cells are treated with either type I and type II mAb with CD20 being found in the pellet (insoluble, raft domain) of type I ritux treated Ramos cells compared to the lysate (soluble, non-raft domain) in type II, B1 treated cells.

To determine if the redistribution of CD20 differs with different detergents we have compared the CD20 distribution in Raji cells when lysed in 1% Brij 58 to that in 0.5% TX-100. Figure 4.7B demonstrates that there is a difference in CD20 localisation when analysed with Brij 58 compared to TX-100. The presence of CD20 in the pellet, which is representative of its insolubility in these detergents, is evident in unstimulated cells when lysed in Brij 58. In marked contrast, CD20 was not detected in the pellet of unstimulated cells lysed in TX-100.

Cholesterol is reported to predominantly reside in highly-ordered domains in the plasma membrane such as lipid rafts. We further probed the distribution of CD20 using a cholesterol sequestering drug called methyl-β-cyclodextrin (MCD). This is a cyclodextrin specific for cholesterol that encapsulates the hydrophobic sterol into a

central cavity allowing it to become soluble in aqueous solution. The effect of MCD treatment on CD20 distribution in non-treated cells lysed in Brij 58 in Figure 4.7B suggests that the insolubility of CD20 in Brij 58 is indeed due to CD20 residing constitutively in an ordered-domain, possibly a raft structure which is lost upon MCD treatment. Interestingly, when ritux is bound to the cells and lysed in Brij 58, treatment with MCD does not appear to have any effect with CD20 remaining associated with the pellet fraction. The reason for this is currently unclear although it may be linked to the stabilising effect of ritux cross-linking CD20, making it resistant to "weaker" detergents.

When cells are assessed with TX-100, similar results to the density gradients and TX-100 flow cytometry assay were observed. CD20 is only found in the pellet upon ritux binding, where it is evident in Figure 4.7B that a high proportion of CD20 translocates into the pellet. Upon MCD treatment this association with the pellet fraction is lost and CD20 is found only in the lysate. This is possibly due to ritux clustering CD20-containing micro-domains which upon MCD treatment are disrupted, essentially making them less compact and more soluble. When lysed in TX-100, these larger domains are solubilised due to the strength of the detergent. As CD20 is found in the insoluble fraction of untreated cells lysed with Brij 58 and not TX-100, it suggests that CD20 is constitutively present in rafts and that the association of CD20 with TX-100 insoluble domains upon mAb ligation is representative of clustering of these mini-rafts.

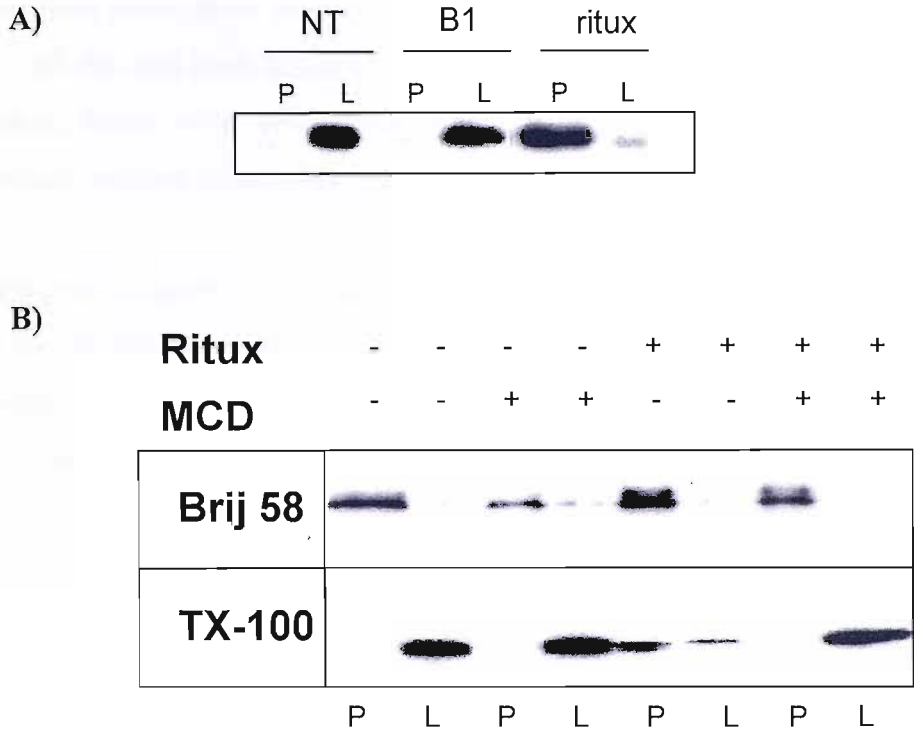

Figure 4.7: Effect of different detergents on CD20 association with lipid raft fractions. A) Ramos cells were washed and resuspended at $2x10^6$ cells/ml in RPMI (1% BSA). $1x10^6$ cells were treated or not with 10 μg/ml B1 or ritux for 15 minutes at room temperature. Samples were then lysed with 0.5% TX-100 for 15 minutes on ice before being pelleted at 16,000g in a benchtop centrifuge. The resulting supernatant forms the lysate (L). The pellet (P) is washed 3x in lysis buffer and resuspended and 30μl of each loaded onto an SDS/PAGE gel and CD20 detected using 7D1 mAb and western blot. **B)** Raji cells were treated as outlined in A. Except that before mAb binding, cells were treated or not with 10mM MCD for 15 minutes at room temperature before being washed, treated with mAb and after 15 minutes lysed in either TX-100 or 1% Brij 58.

4.2.4 The dependence of anti-CD20 mAb binding on cholesterol

From the data in the last section we have suggested that CD20 constitutively resides in lipid rafts microdomains. A characteristic feature of raft domains is their high cholesterol content which is found intercalated between the phospholipids [82]. The initial indication that anti-CD20 mAb may be effected by changes in cholesterol composition came from Polyak and colleagues [85] who demonstrated that FMC7, an IgM mAb that has been utilized in the clinic to phenotype some lymphoproliferative disorders, binds to a cholesterol dependent epitope of CD20. We decided to investigate whether this cholesterol dependency is true of other anti-CD20 mAb.

Initially, we assessed Daudi and Ramos B-cell lines with a large panel of anti-CD20 mAb for the effect of MCD treatment (Figure 4.8). In these experiments cells were treated with 2.5 or 10mM MCD for 15 minutes at room temperature and then washed twice in serum free media. Samples were then incubated with mAb for 15 minutes at room temperature except for FMC7 which is incubated for 45 minute. FMC7 is an IgM, consequently has slower binding. Samples were then washed and incubated with an appropriate secondary labelled FITC mAb before being analysed by flow cytometry. Figure 4.8 demonstrates that most anti-CD20 mAb are affected by cholesterol depletion. The most sensitive mAb is certainly FMC7 but all the other mAb appear to be effected to some extent or other with the notable exception of 7D8 in Ramos cells. However the data does indicate that some mAb are more sensitive than others, particularly it would appear the murine mAb. Interestingly, the sensitivity of the mAb to cholesterol appears to correlate with mAb off rates where ritux and 7D8 are of higher affinity compared to B1 and 1F5 and therefore not as stably bound to the cell (R. French, personal communication).

A)

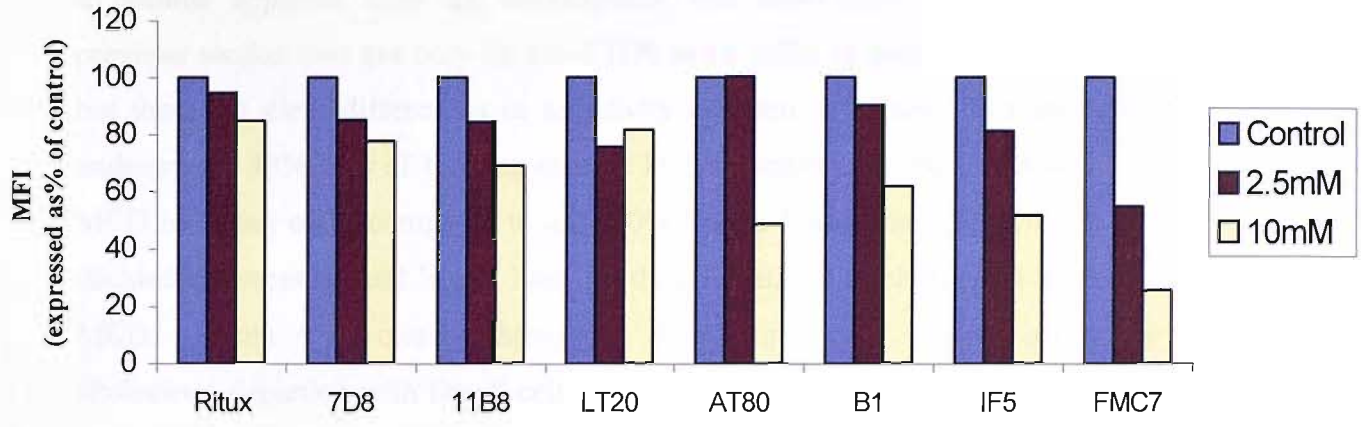

B)

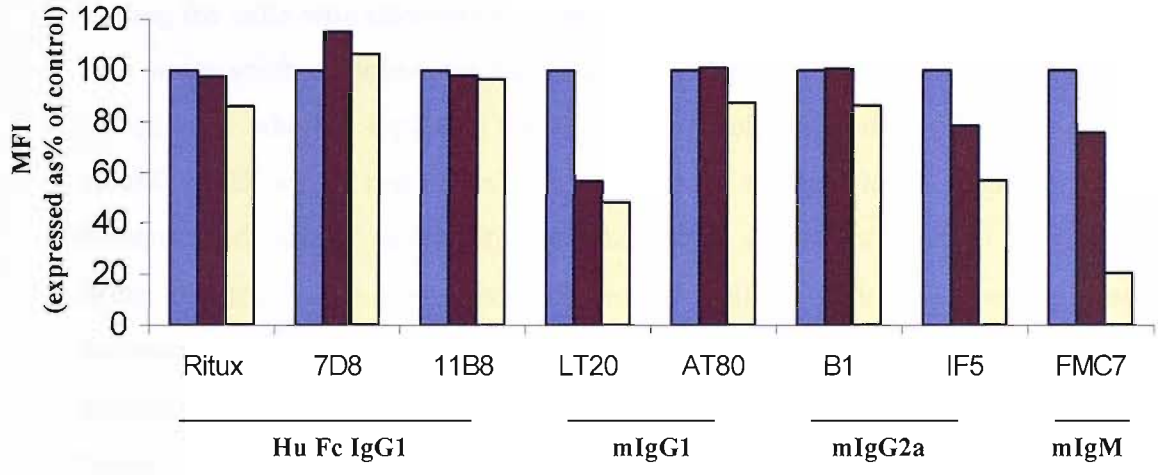

Figure 4.8: The effect of MCD treatment on a panel of anti-CD20 mAb. A) Daudi cells at $1x10^6$/ml were resuspended in RPMI with 1% BSA. Cells were treated or not (control) with 2.5 or 10mM MCD for 15 minutes at room temperature. Samples were then washed twice and incubated with 10 μg/ml mAb for 15 minutes at room temperature, except for FMC7 which was incubated for 45 minutes. Samples were washed twice and incubated with a suitable FITC labelled secondary mAb, either 50 μl 1:40 GAM, 10 μg/ml SB2H2 (anti-HuFc) or 50 μl 1:50 goat anti-mIgM (Jackson immunoresarch) for 15 minutes at room temperature. All samples were washed before being analysed by flow cytometry. The values shown are the MFI expressed as a % of control (mAb binding to non-treated cells). **B)** The same method as outlined in A was used to assess Ramos cells

4.2.5 The sensitivity of cell lines to cholesterol depletion

It became apparent from the investigation into anti-CD20 mAb binding in the previous section that not only do anti-CD20 mAb differ in their sensitivity to MCD, but there are clear differences in sensitivity between cell lines. For example, B1 undergoes a 40% loss of binding relative to the control after treatment with 10mM MCD in Daudi cells, compared to only 20% loss in Ramos cells. Therefore, it was decided to assess several B cell lines for their sensitivity to cholesterol depletion by MCD. Figure 4.9A clearly shows that B cell lines vary in their sensitivity to cholesterol depletion with Daudi cells demonstrating a 40-50% loss of binding of the murine mAb and an 80% loss for FMC7. However in SUDHL4 cells, only 10% loss of the murine mAb binding occurred and 30% loss of FMC7 binding.

As mAb binding was sensitive to cholesterol depletion, we considered whether loading the cells with cholesterol might enhance binding. Daudi cells were incubated with water-soluble cholesterol for 60 minutes at room temperature. Furthermore, we investigated whether repleting the cells with cholesterol after prior depletion with 10mM MCD would restore mAb binding to its original level. Both B1 and IF5 demonstrated similar sensitivities to cholesterol depletion/repletion (Figure 4.9B). When the cells were loaded with cholesterol neither mAb demonstrated a notable increase in binding. However, when the cells were treated with 10mM MCD, the binding level of both mAb dropped to 60% of that shown by control cells (mAb bound to untreated cells). This reduction in mAb binding was completely ablated upon repletion of cholesterol. In contrast, FMC7 binding was much more sensitive to cholesterol loading, where its binding was seen to increase to 180% of that on control cells. However, upon cholesterol depletion, mAb binding dropped to 10% of the control and was only increased to ~40% of the original binding level when repleted with cholesterol. From this data, we suggest that cholesterol is important for the binding of all anti-CD20 mAb, the extent of this dependence is determined by the mAb and the cell line used.

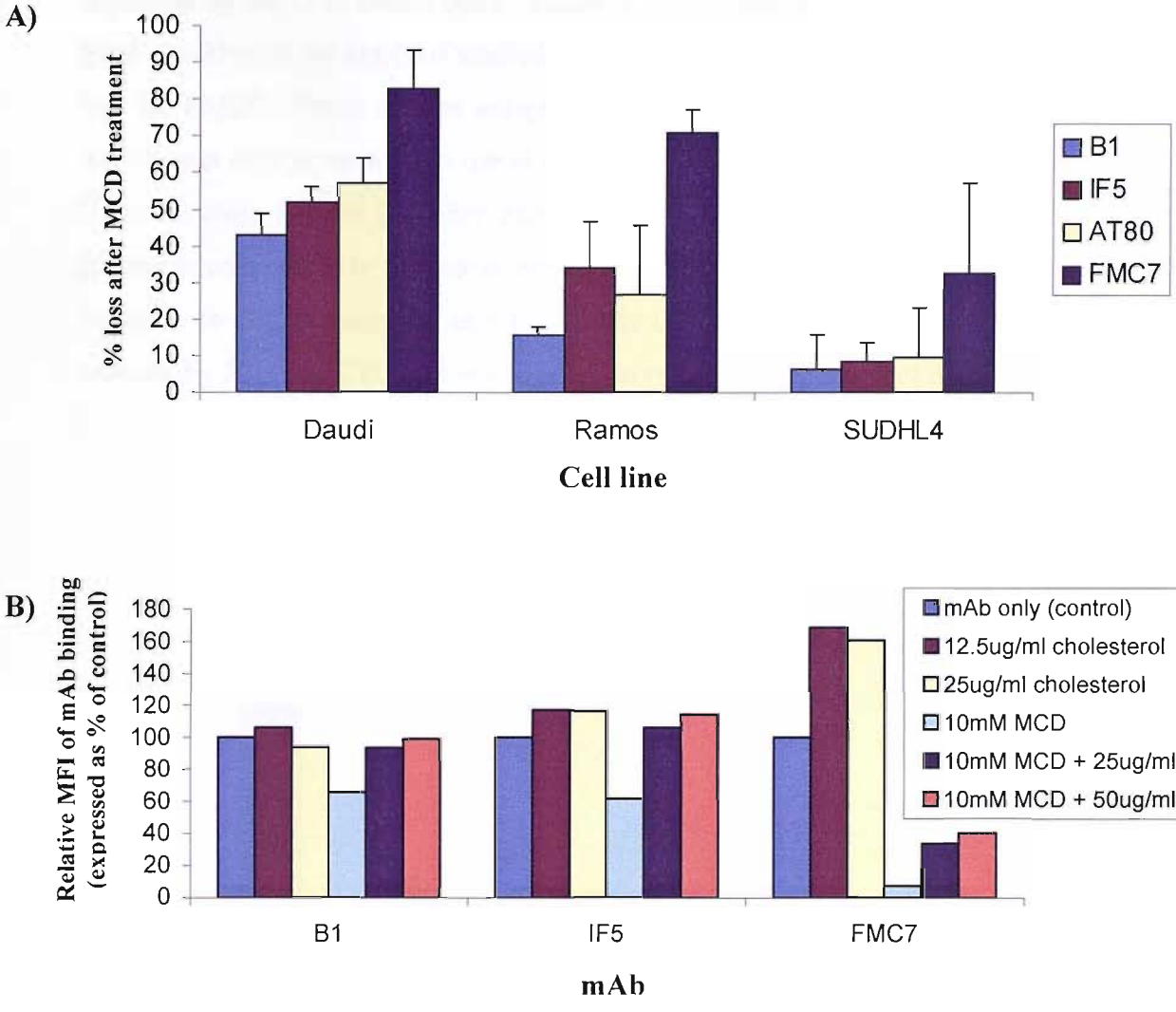

Figure 4.9: A) Sensitivity of anti-CD20 mAb binding to cholesterol depletion is cell line dependent. Daudi, Ramos and SUDHL4 cells were treated with 10mM MCD as outlined in Materials and Methods Section 2.8.4. Values shown are the % loss which was calculated using the following formula: % loss = $[1-(MFI_{sample}/MFI_{control})]x100$. Values are based on the mean and standard error of the mean of at least two independent experiments. **B) The effect of cholesterol loading on MCD treatment.** $1x10^5$ Daudi cells were treated or not with 10mM MCD for 15 minutes at room temperature. Samples were then washed twice and incubated with either 0, 12.5, 25 or 50 μg/ml cholesterol (SIGMA) for 1 hour. Samples were washed again and incubated with 10 μg/ml B1, IF5 or FMC7 for 15 or 45 minutes at room temperature before being washed twice and incubated with the appropriate secondary FITC labelled mAb, either GAM or goat anti-mIgM FITC for 15 minutes at room temperature. Samples are then further washed and analysed by flow cytometry. Expression level is shown as a % of mAb binding on non-treated (control) cells.

4.2.5.1 Effect of cholesterol depletion on mAb binding to other surface antigens

As cholesterol forms such a vital part of the cell membrane, we decided to investigate whether other surface antigens in addition to CD20 were susceptible to cholesterol depletion by MCD in Daudi cells. Figure 4.10 demonstrates that CD20 is by far the most sensitive of the antigens studied with a loss of 33% for B1, 37% IF5 and a 90% loss for FMC7. Other surface antigens were assessed for various reasons; the BCR was chosen as it is reported to translocate into lipid rafts which are rich in cholesterol [47], MHC class II as it is highly expressed on B cells and CD55 as due to its GPI linkage it constitutively resides in rafts [79]. However, none of these antigens were as sensitive to MCD treatment as CD20, both Class II and BCR mAb binding were reduced by 20% and CD55 appeared insensitive to MCD cholesterol depletion.

.

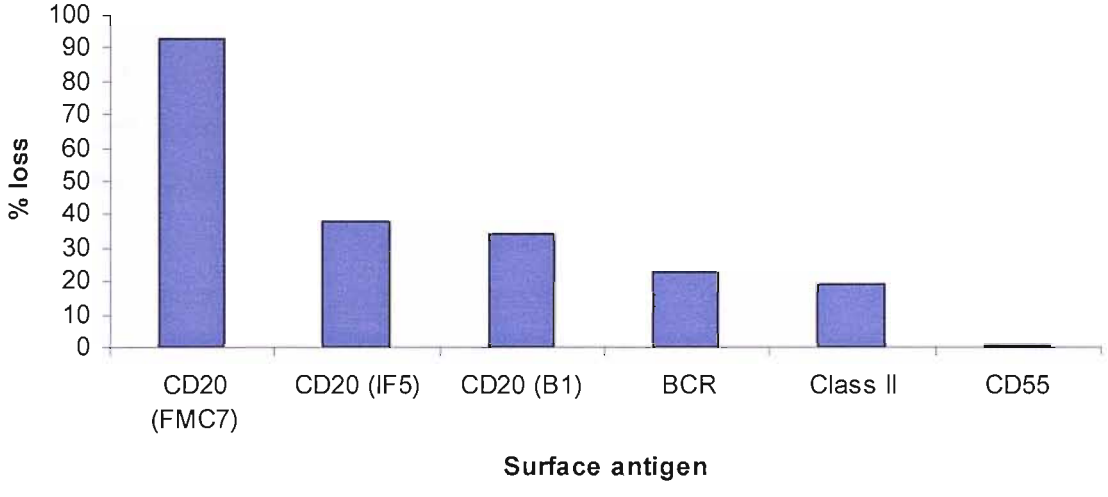

Figure 4.10: Other surface antigens are not as sensitive to cholesterol depletion. $0.1x10^6$ Daudi cells were treated or not with 10mM MCD before being incubated with 10 μg/ml FITC labelled Anti-CD20 (B1, IF5 and FMC7), BCR (M15/8), Class II (L243) and CD55 (Clone 26 Serotec) for 15 minutes at room temperature. Samples were washed and analyzed by flow cytometry. Values shown are the % loss which was calculated as % loss = $[1-(MFI_{sample}/MFI_{control})]x100$.

4.2.5.2 The effect of cholesterol depletion on TX-100 insolubility

We have already demonstrated in Section 4.2.3 that treatment of cells with MCD results in a loss of CD20 from TX-100 insoluble domains, when treated with ritux. To underpin our western blot results in Figure 4.7, the effect of cholesterol depletion on CD20 TX-100 insolubility induced by a panel of anti-CD20 mAb was assessed and whether any effects could be reversed by repleting the cells with cholesterol. To this end, SUDHL4 cells were either un-treated, pre-treated with 10mM MCD (depleted cells) or with 10mM MCD washed twice and then 12.5μg/ml cholesterol added for 1 hour (repleted cells). The samples were prepared for TX-100 analysis as outlined in materials and methods Section 2.7.2.

In agreement with our earlier results, it was evident the cholesterol depletion reduces the TX-100 insolubility conferred by type I anti-CD20 mAb like ritux and it had no effect on the type II mAb such as B1 and 11B8, treated cells. In SUDHL4 cells, only ritux and 1F5 redistributed CD20 into TX-100 insoluble domains (Figure 4.11A) with the 85% and 45% of CD20, respectively, insoluble to TX-100 treatment. The level of CD20 in these domains was reduced by cholesterol depletion to 55% and 10% respectively. This reduction was counteracted by the presence of cholesterol with ritux treated cells increasing to 65% and 1F5 treated cells to 30%. These results suggest that cholesterol is a critical component of TX-100 insoluble domains. This is possibly due to its ordered structure which allows tight packing of the membrane and hence resistance to solubilisation by detergents.

To ensure our results were not due to the high expression level of CD20 on SUDHL4 cells, we assessed the effect of MCD and cholesterol repletion on TX-100 insolubility in Ramos cells (figure 4.11B). These cells expressed a three fold lower level of CD20 than SUDHL4. We found the results mirrored those in SUDHL4 cells with both ritux and 1F5 mAb conferring 80% and 55% TX-100 insolubility of CD20 respectively. The level of insolubility was decreased upon treatment of MCD but again was counteracted by the repletion with cholesterol, showing the reversibility and specificity of MCD treatment. These results correlate well with our previous observations that some cell lines were more sensitive to cholesterol depletion than others (Figure 4.9A). From the mAb binding profiles it was evident that 1F5 binding

is reduced in MCD treated Ramos cells yet no effect was observed in SUDHL4 cells. Intriguingly, even though the binding is not affected, the level of TX-100 insolubility was decreased. Furthermore in SUDHL4 cells, mAb binding was increased in cells treated with MCD and then repleted with cholesterol compared to non-treated control cells yet the % insolubility remained lower. This suggests that the loss in insolubility was not simply due to loss of binding of the mAb but was a direct effect of disrupting TX-100 insoluble domains by cholesterol extraction.

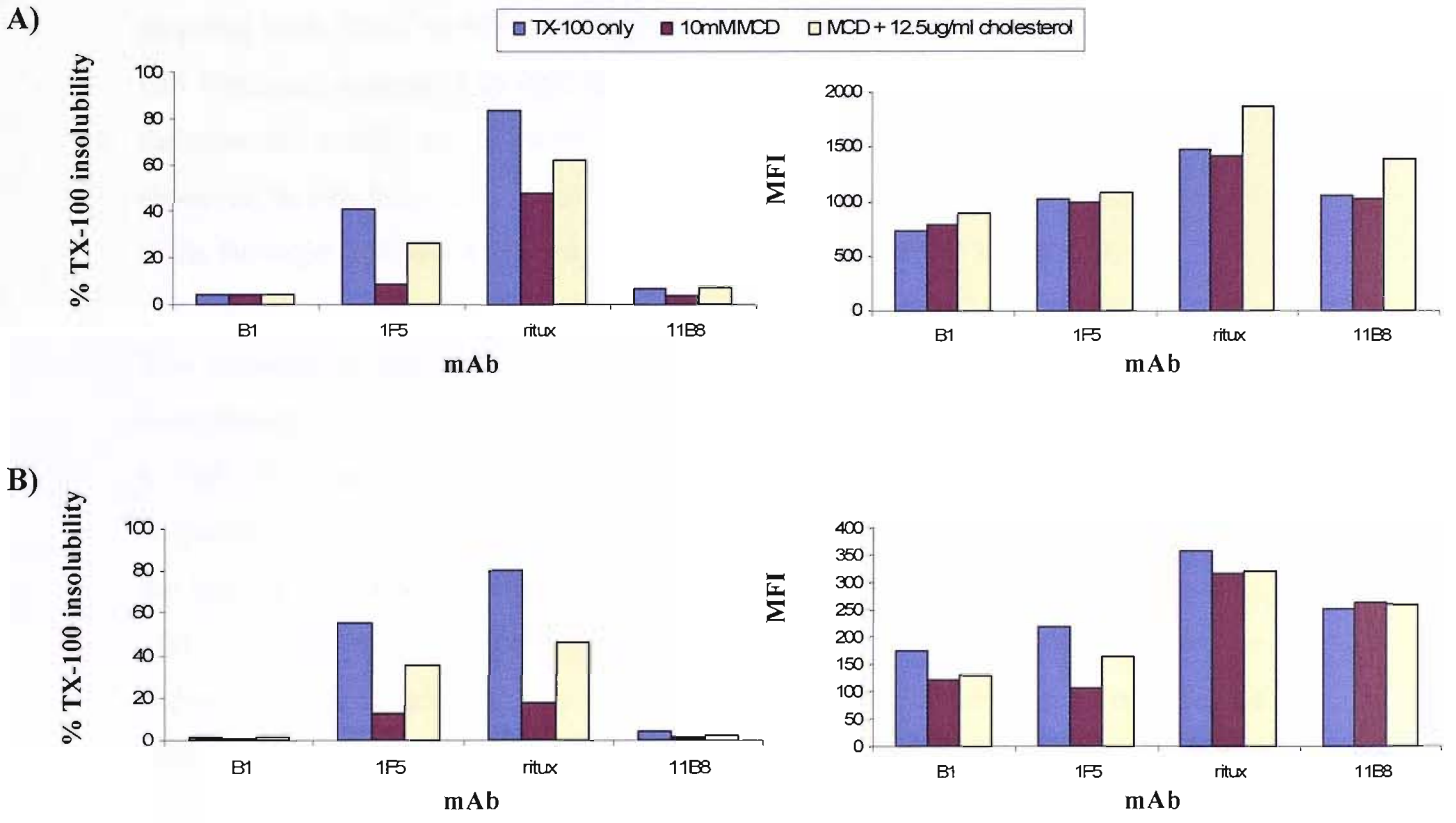

Figure 4.11: Effect of MCD on TX-100 insolubility. A) $1x10^5$ SUDHL4 cell were treated or not with 10mM MCD for 15 minutes at room temperature or 10mM MCD washed twice and 12.5µg/ml cholesterol for an hour at room temperature. Cell were then treated with 10µg/ml FITC labelled anti-CD20 mAb for 15 minutes at room temperature before being assessed for TX-100 insolubility as outlined in Section 2.7.2. The % insolubility is shown on the left hand side and the MFI of mAb binding in unlysed cells are shown on the right hand side. **B)** Ramos cells were treated as outlined in A

4.2.6 The ability of anti-CD20 mAb fragments to redistribute CD20

The ability of CD20 to redistribute into TX-100 insoluble domains is an unusual property [66, 72]. We wondered whether this redistribution involved a signalling pathway or was simply due to the cross-linking effect of the mAb. To investigate this, anti-CD20 Fab and $F(ab')_2$ fragments were assessed by flow cytometry and pellet/lysate assays for their ability to redistribute CD20 into rafts in Ramos cells. From Figure 4.12A it is apparent that Fab fragments of type I mAb such as ritux can confer TX-100 insolubility to CD20. As expected, B1 IgG or B1 Fab did not redistribute CD20. The level of insolubility induced by type I mAb ritux and 7D8 was decreased in Fab treated cell with ritux dropping from 80% to 40% and 7D8 dropping from 100% to 60%. An explanation for this is may be the lower avidity of Fab fragments compared to IgG mAb. Whole mAb molecules bind bivalently and therefore the avidity of the mAb will be the amassed affinity of both Fab "arms". However, in Fab fragments as the name suggest, only one "arm" of the original mAb binds the target and hence has only half the avidity compared to whole IgG.

This reduction in avidity is reflected in the binding profiles shown in Figure 4.12B. Even though more Fab fragments are added to the cells (25 μg/ml, 10mM) compared to IgG (10 μg/ml, 1.4mM), their binding is still lower than their IgG counterparts. Arguably this could be due to a difference in dye:protein ratio. However, aside from the binding differences, these results demonstrate that CD20 redistribution into TX-100 lipid rafts is not simply due to cross-linking by bivalent binding but can be induced by Fab fragments. To confirm our results we decided to investigate the redistribution seen by FACS analysis by pellet/lysate assay and western blot. The data in Figure 4.12C mirror those of the TX-100 flow cytometry assay. Ramos cells were treated with 10μg/ml IgG or $F(ab')_2$ or 25 μg/ml Fab for 15 minutes at room temperature before being lysed in 1% TX-100. The samples were prepared for pellet/lysate assay and western blot as outlined in Section 2.7.1

As seen earlier in Figure 4.7, CD20 does not constitutively reside in TX-100 insoluble domains in non-treated cells. CD20 is only detected in the soluble lysate (L) fraction. However, upon stimulation of CD20 with a type I mAb such as ritux, CD20 is found in the insoluble, pellet (P) fraction.

A)

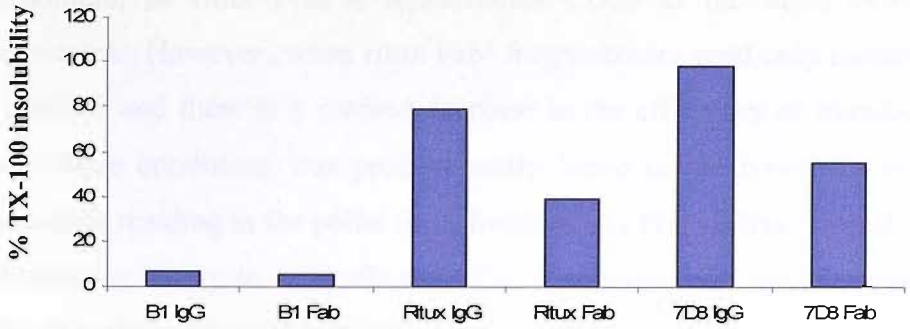

B)

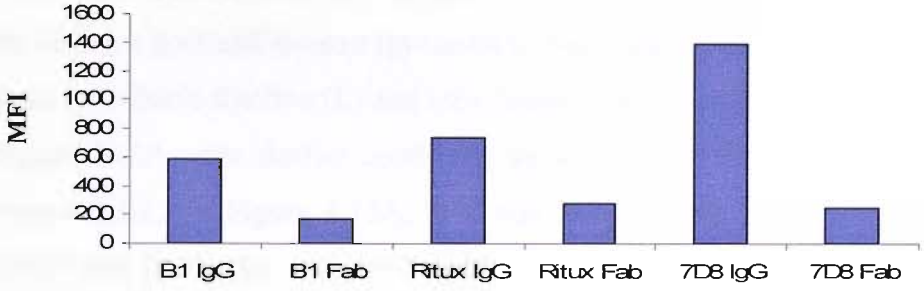

C)

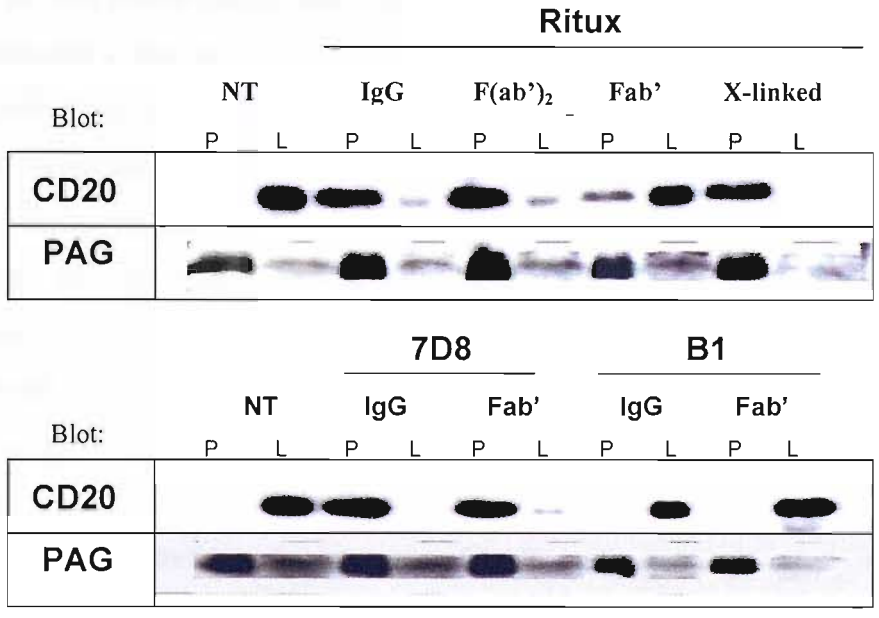

Figure 4.12: The ability of antibody fragments to redistribute CD20 into TX-100 insoluble rafts. **A)** $1x10^5$ Ramos cells were stimulated with either 10μg/ml IgG or 25μg/ml Fab' of different FITC labelled anti-CD20 mAb for 15 minutes at room temperature. Cells were prepared for TX-100 analysis as outlined in Section 2.4.7. **B)** IgG and Fab' binding was assessed by flow cytometry. The level of binding is depicted by MFI. **C)** $1x10^6$ Ramos cells were treated with 10μg/ml IgG, 10μg/ml $F(ab')_2$ or 25μg/ml Fab' for 15 minutes at room temperature before being lysed in 1% TX-100 and prepared for western blot analysis as outlined in Section 2.7.1. Membranes were blotted for CD20 with 7D1 then stripped and re-probed for PAG with MEM 255.

The ability of ritux to redistribute CD20 does not appear to be affected by loss of its Fc domain, as ritux $F(ab')_2$ redistributes CD20 to the same extent as its IgG counterpart. However, when ritux Fab' fragments are used only monovalent binding is possible and there is a marked decrease in the efficiency of translocation. CD20 under these conditions was predominantly found in the lysate fraction with a low percentage residing in the pellet (raft) fraction. As $F(ab')_2$ fragments do not show this reduction in ability to redistribute CD20, it supports our earlier suggestion that the reduction observed upon Fab' stimulation is due to the lower avidity of the fragment which also leads to less cross-linking of CD20. When CD20 was hyper cross-linked by adding a goat anti-human IgG mAb to ritux labelled cells, CD20 is completely lost from the soluble fraction (L) and only found in the pellet (P). The results with ritux in Figure 4.12A were further confirmed by analysis of 7D8 (type I) and B1 (type II) treated cells. In Figure 4.12A, 7D8 was seen to have potent ability to redistribute CD20 into lipid rafts with 100% of CD20 becoming insoluble to TX-100 treatment when bound by 7D8 IgG. In this pellet/lysate assay (Figure 4.12C), we found that the potency of 7D8 redistribution was comparable to cross-linked ritux with 100% of the CD20 detected in the raft fraction (P). Stimulation of CD20 with 7D8 Fab' fragment lead to a similarly high percentage of CD20 redistributing into the pellet fraction. The level of translocation appeared even higher than the 60% demonstrated in Figure 4.12A. However, the flow cytometry and pellet/lysate assays are very different techniques and the reason why a lower result was found in the flow cytometry technique may be due to the wash step after cell lysis which is absent in the pellet/lysate assay. When CD20 was stimulated with B1, a type II mAb, no translocation from the lysate to the pellet occurred in either IgG or Fab' treated samples. The distinction between the raft and non-raft fractions by pellet/lysate separation was validated by the presence of PAG predominating in the pellet (or raft) fraction (see Section 4.2.1).

As Fab fragments are unable to cross-link surface antigens, the ability of type I Fabs to redistribute CD20 into rafts suggest that this redistribution may involve a signalling pathway. In accordance with this suggestion previous work in our group has shown that mutation of residues in the cytoplasmic tail of CD20 led to loss of CD20 redistribution upon mAb binding [52]. To address this possibility, the involvement of early cell signalling events was assessed. Phosphorylation of Src family kinases are

reported to be one of the earliest events in BCR signalling [98]. To investigate their possible involvement in CD20 redistribution, Src kinases were inhibited by using a specific intracellular inhibitor PP2. However, we found this to have no effect on the redistribution of CD20 into TX-100 insoluble domains (data not shown). Furthermore, re-arrangement of the actin cytoskeleton is known to be an early signalling event for several signalling cascades. However, when actin rearrangement was hindered by the use of several specific inhibitors no effect was observed in the redistribution of CD20 into lipid rafts (see later in Section 6.2.5.1).

In summary, redistribution of CD20 into TX-100 insoluble domains can be induced by Fab' fragments of type I anti-CD20 mAb demonstrating that cross-linking of CD20 by mAb is not required for its redistribution. Further work is required to determine if the translocation of CD20 involves a signalling cascade or whether it is a physical phenomenon that CD20, once bound by type I mAb favours a certain area of the membrane and is therefore more of a conformational change after mAb binding.

4.2.7 Long term kinetics of CD20 redistribution

Previously in this chapter the ability of CD20 to redistribute into TX-100 insoluble domains was assessed over a relatively short 15-30 minute period as we found no difference in the redistribution between 15 minutes and 60 minutes (data not shown). However, to eliminate the possibility that type II mAb like B1 might show no redistribution of CD20 as they utilise slower kinetics we decided to assess the kinetics of this event over a longer time course. As such, Raji cells were labelled with FITC-labelled mAb and incubated over 24 hours. Cells were harvested at 15 minutes 6 hours and 24 hours and either assessed for mAb binding or lysed in 1% TX-100 for 15 minutes on ice before washing and assessment by flow cytometry. The data in Figure 4.13 demonstrates that CD20 redistribution mediated by type I mAb is a relatively rapid process, occurring over 15 minutes, and is maintained over a prolonged period of time.

The kinetics of CD20 redistribution appears to be similar for both type I mAb, ritux and 1F5. In Raji cells, at 15 minutes ritux redistributes 35% of CD20 into TX-100 insoluble domains. After 6 hours the insolubility increases to 45%. After this time,

there is a slight decline to 41%. Interestingly, neither type II mAb, B1 nor 11B8, effectively redistribute CD20 over 24 hours demonstrating that type II mAb do not redistribute CD20 with slower kinetics that would have been missed by previous experiments. A similar trend was observed in Ramos cells (Figure 4.13B). However, it is interesting to note that there are differences in the levels of redistribution between the cell lines. In ritux treated Ramos samples, 60% of the CD20 is insoluble after 15 minutes compared to 35% in Raji cells. This is possibly linked to the heterogeneity of the cell membrane. It was demonstrated earlier that TX-100 insolubility of CD20 was not affected by expression level (Section 4.2.2) but is affected by cholesterol content (Section 4.2.5.3). Therefore, the difference in % insolubility of CD20 between the two cell lines is possibly linked to different levels of cholesterol in the membrane.

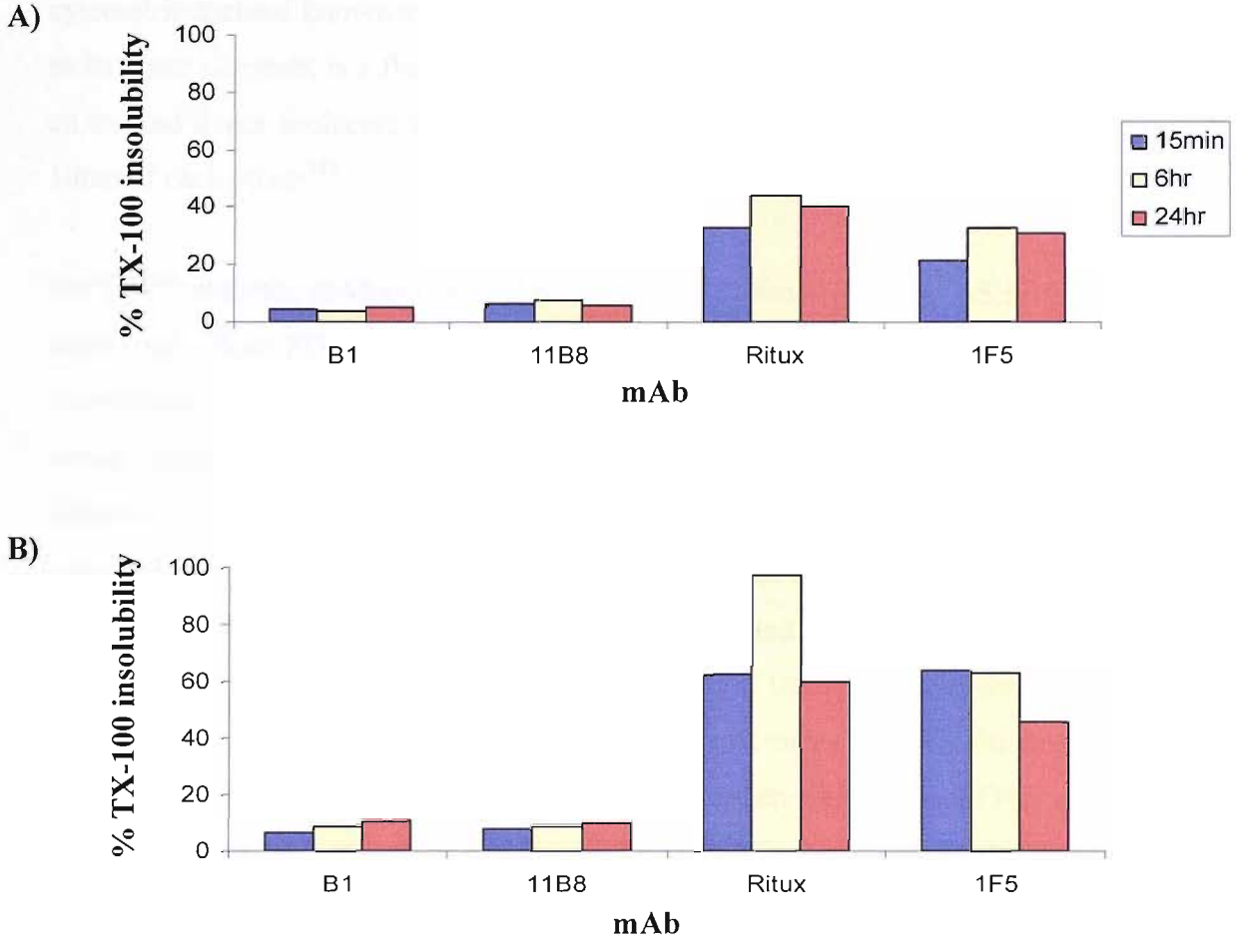

Figure 4.13: 24 hour kinetics of CD20 redistribution into TX-100 insoluble domains. A) $1x10^6$ Raji cells were treated with 10μg/ml FITC labelled anti-CD20 mAb. $1x10^5$ cells were harvested at the indicated time points and assessed for TX-100 insolubility as per materials and methods section 2.7.2. **B)** Ramos cells were treated as outlined in A

4.2.8 FRET analysis of CD20 clustering

The use of detergent to assess the distribution of CD20 is a very effective technique when coupled with SDS-PAGE and western blotting or using flow cytometry assays. However, there are limitations to this methodology; firstly, it can be argued that the results obtained could be artefacts of detergent treatment. Secondly, the technique is limited by the fact that in this system detergents only discriminate cellular contents based on their resistance to solubilisation. Therefore the association of two surface antigens with the insoluble fraction in detergent lysis does not necessarily mean that they are associated with each other or even in the same domain in the plasma membrane, in reality they could be in completely different and distinct insoluble domains. Because of these caveats, we decided to use another complementary flow cytometric method known as fluorescence resonance energy transfer (FRET). FRET, as its name suggests, is a fluorescence-based method where energy is transferred from an excited donor molecule to an acceptor molecule when the two are located within 10nm of each other [189].

For FRET analysis, mAb conjugated to Cy3 or FITC donor (D) and Cy5 acceptor (A) were used. Both FITC and Cy3 have been used by other investigators as the donor fluorophore in such experiments [190]. For our studies we decided to use FITC as the donor because we had an array of FITC labelled mAb readily available in the laboratory and it was also found that the ratio of FITC:protein labelling was more consistent than Cy3:protein. The basic principle of the assay is illustrated in Figure 4.14. The donor and acceptor mAb were incubated either on their own with equimolar unlabeled mAb or together in the absence of unlabeled mAb for 20 minutes at 37°C. The samples were then assessed by flow cytometry for their fluorescence in FL2 (FITC emissions), FL3 (emission from Cy5 when excited by FITC) and FL4 (emission from Cy5 when excited by FL4 laser). Essentially the FRET value is calculated from the signal generated when FITC and Cy5 labelled mAb are bound to cells simultaneously. If they are within 10nm of each other an increase in fluorescence in FL3 will be observed as shown in Figure 4.14. The MFI value representing this signal (FL3 (DA)) is then adjusted for background fluorescence using the formula, where DA is the fluorescence in the sample containing both the FITC (D) and Cy5 (A) labelled mAb.

FRET = FL3(DA) - [FL2(DA)*FL3(D)/FL2(D)] – [FL4(DA)*FL3(A)/FL2(A)]

Each value is adjusted for non-specific binding. Due to this adjustment, experiments that do not give FRET sometimes calculate out to a negative number. If this situation arises, the values are set to zero. A detailed account of how FRET values are calculated is outlined in the materials and methods (Section 2.7.3).

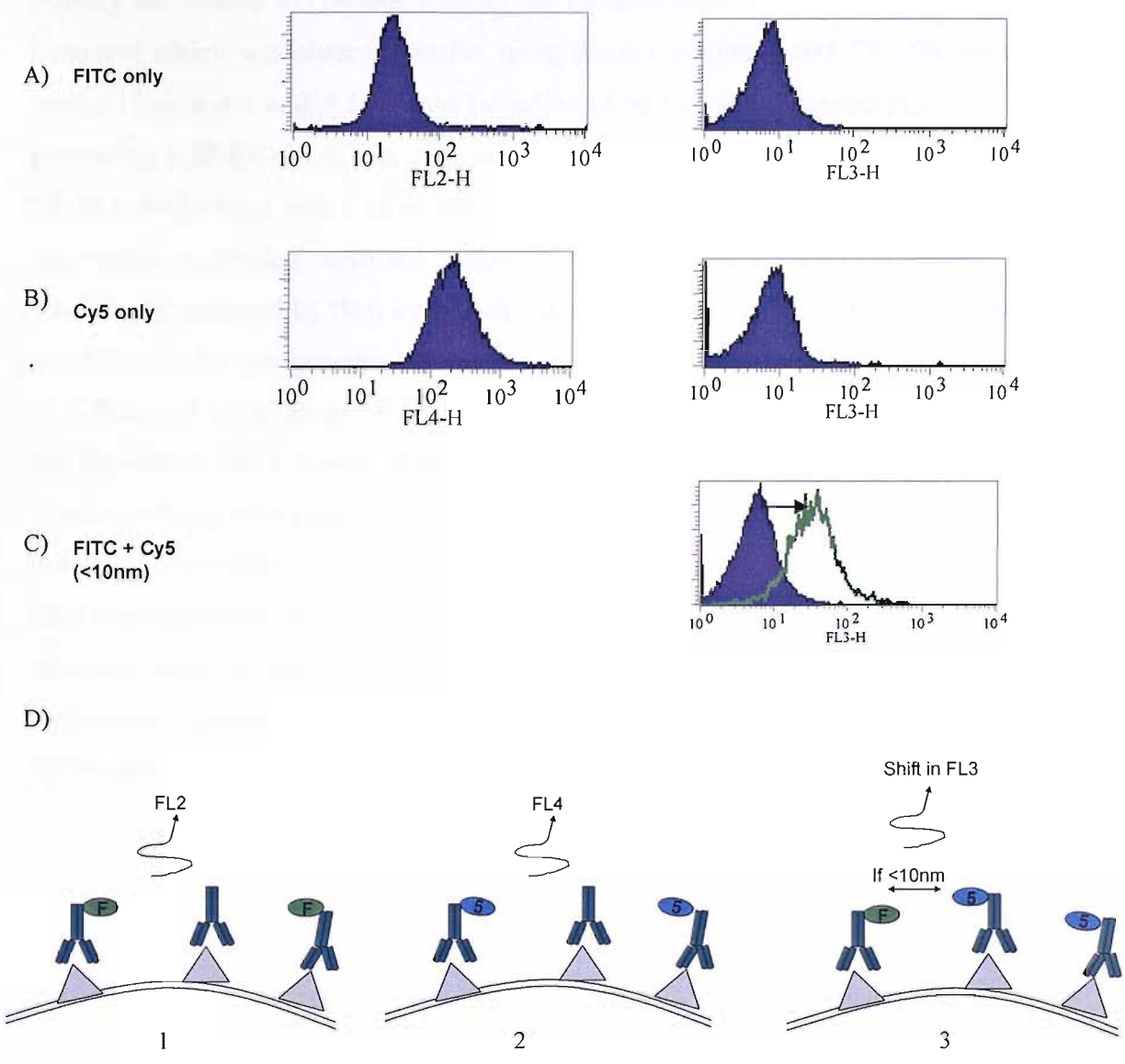

Figure 4.14: Illustration of FRET. $3x10^5$ Daudi cells are treated with either a) 10 μg/ml FITC labelled ritux + 10 μg/ml unlabeled ritux b) 10 μg/ml Cy5 labelled ritux + 10μg/ml unlabeled ritux c) 10 μg/ml FITC labelled ritux + 10 μg/ml Cy5 labelled ritux for 20 minutes at 37°C before being washed and analysed by flow cytometry. Sample **(A)** is analysed for FL2 as this is representative of the mAb binding level, and is also assessed for leakage into FL3. Sample **(B)** is assessed for fluorescence in FL4 to measure binding and FL3 for leakage. Sample **(C)** is assessed for fluorescence in FL2, FL3 and FL4. FRET is essentially the shift in FL3 observed in the cells incubated with FITC and Cy5 labelled mAb, depicted by the green line which is overlaid on the background FL3 fluorescence. **D)** Diagrammatic depiction of FRET generation. 1. Diagrammatic representation of sample A, FITC label is denoted by "F". 2. Diagrammatic depiction of sample B, Cy5 5 label is denoted by "5". 3. Visual interpretation of Sample C.

4.2.8.1 FRET generated by anti-CD20 mAb

Initially we wanted to confirm whether the redistribution of CD20 with type I mAb treatment which was observed earlier using density gradients and TX-100 detergent assays (Figure 4.3 and 4.5) would be reflected in the surface association of CD20 generating a FRET signal. In preliminary experiments in Daudi cells, various anti-CD20 mAb labelled with Cy5 or FITC were co-incubated at 10μg/ml (along with the appropriate unlabelled mAb see Figure 4.14) for 20 minutes at 37°C before being washed and analyzed by flow cytometry. It is evident from Figure 4.15 that different anti-CD20 mAb can generate varying levels of FRET where ritux is the highest at 21.5 followed by AT80 at 19.3 and in marked contrast, B1 which does not generate any detectable FRET signal. It may be suggested that as CD20 is believed to reside constitutively in rafts then B1 should also give a FRET signal. However, these mini-rafts/micro-domains may not be of sufficient size to permit several anti-CD20 mAb to bind simultaneously thereby generating a FRET signal. This suggests that the FRET observed with the type I mAb ritux and AT80 is due to the clustering of mini-rafts/micro-domains into larger raft structures confirming the results observed for TX-100 treated cells earlier in this chapter.

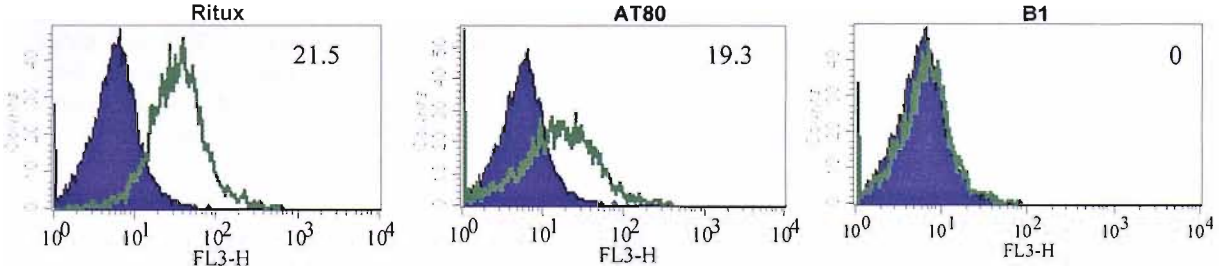

Figure 4.15: Different anti-CD20 mAb generate different levels of FRET. $3x10^5$ Daudi cells were incubated with 10 μg/ml Cy5 and FITC labelled mAb for 20 minutes at 37°C before being washed and analysed by flow cytometry. The open histogram represents the FRET generated. The value calculated for this FRET is shown in the top right hand corner of each histogram. These profiles are representative of three independent experiments

Our next line of investigation was to assess whether this was a general phenomenon and not cell line specific. The ability of type I and type II mAb to generate FRET was assessed on a range of B cell lines. To this end, several cell lines were treated with the archetypal type I and type II mAb, ritux and B1. It is evident from Table 4.1 that the difference between ritux and B1 to generate FRET is consistent on all cell lines, with ritux generating a higher level of FRET compared to B1. The only cell line where B1 generated a FRET signal was in the high CD20 expressing cell line, SUDHL4 and even then the signal is approximately 30 times lower compared to that generated by ritux (2 compared to 62.5). From the five cell lines assessed it is evident that ritux always generates a FRET signal whereas with the minor exception of SUDHL4, B1 does not generate FRET. However, the level of FRET generated by ritux is dependent on the cell line. Homo-association of ritux-bound CD20 on SUDHL4 cells results in a FRET of 62.5 compared to a FRET of 4.35 for BL41 cells. The reasons for this are discussed below.

Cell line	**B1**	**Ritux**
SUDHL4	2.1 ± 3.02	62.5 ± 3.7
Raji	0 ± 0	32.7 ± 2.1
Daudi	0 ± 0	15.06 ± 4.3
ARH77	0 ± 0	11.1 ± 3.2
BL41	0 ± 0	4.35 ± 6.1

Table 4.1: FRET is cell line dependent. $3x10^5$ cells were incubated with 10 μg/ml Cy5 and FITC labelled mAb for 20 minutes at 37°C before being washed and analysed by flow cytometry. The values shown are the FRET values calculated from the formula outlined earlier in Section 4.2.8 and are the mean ± standard deviation of three independent experiments

4.2.8.2 The dependence of FRET on expression level

In an attempt to explain why some cell lines generate more FRET than others, the most probable explanation is in the expression level of CD20 on the cells. Taking Table 4.1 and Figure 4.16 together, it is apparent that type I mAb induced FRET is dependent on CD20 expression level. Hence explaining the higher FRET observed in ritux stimulated SUDHL4 cells compared to ARH77 and BL41 cells. To directly

address the effect of CD20 expression level on FRET, we used NS/0 cells transfected to express various amounts of human CD20. These cells are murine cells and therefore normally lack expression of human CD20. Transfection of human CD20 into these cells allowed us to probe the importance of CD20 surface density for FRET. Three clones were selected which expressed CD20 at different levels – low in Clone 5 to high in Clone 2. The data in Table 4.2 confirms the dependence of FRET on expression level where FRET induced by homo-associated ritux, increased in correlation with the expression level. Interestingly, B1 also demonstrates FRET at high expression levels agreeing with data from high CD20-expressing SUDHL4 cells in the last section. It seems most probable that this is due to the expression level and not due to any difference in the redistribution of CD20 in these cell lines. At high expression levels, the probability of the CD20 surface antigen, and hence two mAb being bound sufficiently juxtaposed to generate FRET, is high. Therefore this low FRET signal is not dependent on redistribution. This will be further discussed in Section 4.2.8.5.

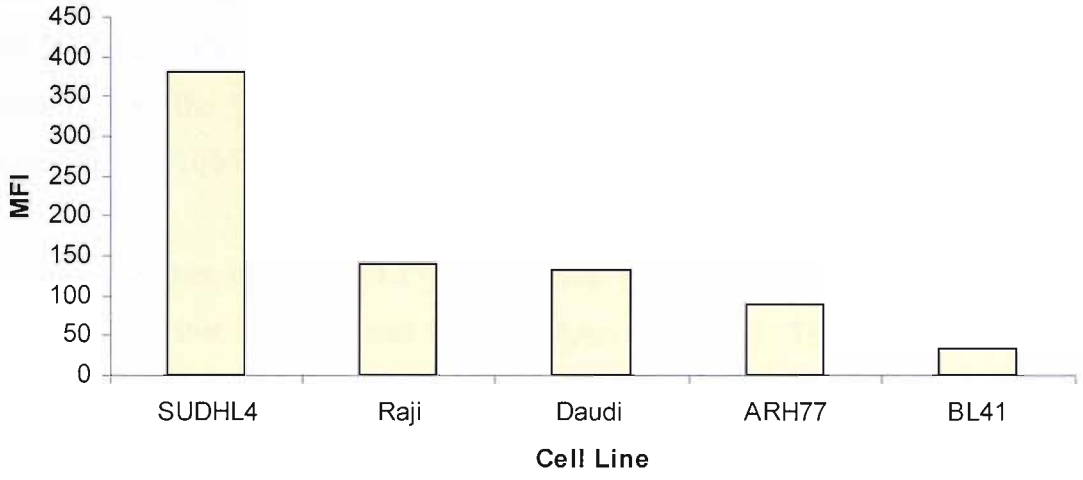

Figure 4.16: CD20 expression level of different cell lines. $1x10^5$ cells were incubated with 10 μg/ml ritux FITC labelled for 15 minutes at room temperature before being washed and analysed by flow cytometry.

	Clone 5 (90)	Clone 3 (280)	Clone 21 (540)
B1	0	10.1	66.9
Ritux	0	152.8	408

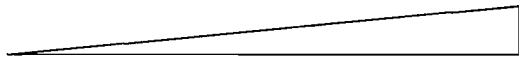

CD20 expression

Table 4.2: FRET is dependent on expression level. $0.3x10^5$ NS/0 cells of different clones were treated with 10 μg/ml of the appropriate mAb (FITC-, Cy5- and unlabelled-B1 and ritux, as outlined in Section 2.7.3) and incubated for 20 minutes at 37°C before being washed and assessed for FRET. The CD20 expression level (MFI) of the clones, as measured by ritux, are shown in brackets beside the clone no.

4.2.8.3 The effect of TX-100 lysis on FRET

Having established in Section 4.2.8.1 that the distinction between type I and type II mAb was the same using both TX-100 and the detergent-less FRET method, we decided to investigate whether the FRET observed reflected redistribution into TX-100 insoluble rafts or simply clustering of CD20. As such, SUDHL4 cells were assessed for FRET (as outlined previously in Section 2.7.3) for homo-associations of either B1 (10μg/ml), ritux (5 μg/ml) or F3.3 which detects MHC Class II (5 μg/ml). However, after the 15 minute incubation, the cell samples were split in two and assessed for TX-100 insolubility as outlined in Section 2.8.2.

The results shown in Figure 4.17 demonstrate that in SUDHL4 cells the FRET associated with ritux is not reduced following lysis in TX-100. This suggests that like the TX-100 insolubility assay, the FRET value obtained for ritux is representative of CD20 redistribution into TX-100 insoluble rafts as mAb binding is not lost in these domains and therefore FRET is still generated. Furthermore, in support of the observations with sucrose density gradients and TX-100 detergent assay analysis, B1 FRET is completely lost upon TX-100 treatment as is that for MHC class II, suggesting that these mAb do not redistribute their relevant antigens into TX-100 insoluble domains hence mAb binding is lost and no signal is generated. This data correlates with the mAb binding data shown in Figure 4.17B; retention of ritux binding is not adversely affected by the increasing presence of TX-100 whereas it is

evident that increasing concentration of detergent have a detrimental effect on the retention of B1 and F3.3 mAb binding. In summary, this data demonstrates that type I mAb redistribute CD20 into clusters on the membrane which are insoluble to 1% TX-100 detergent.

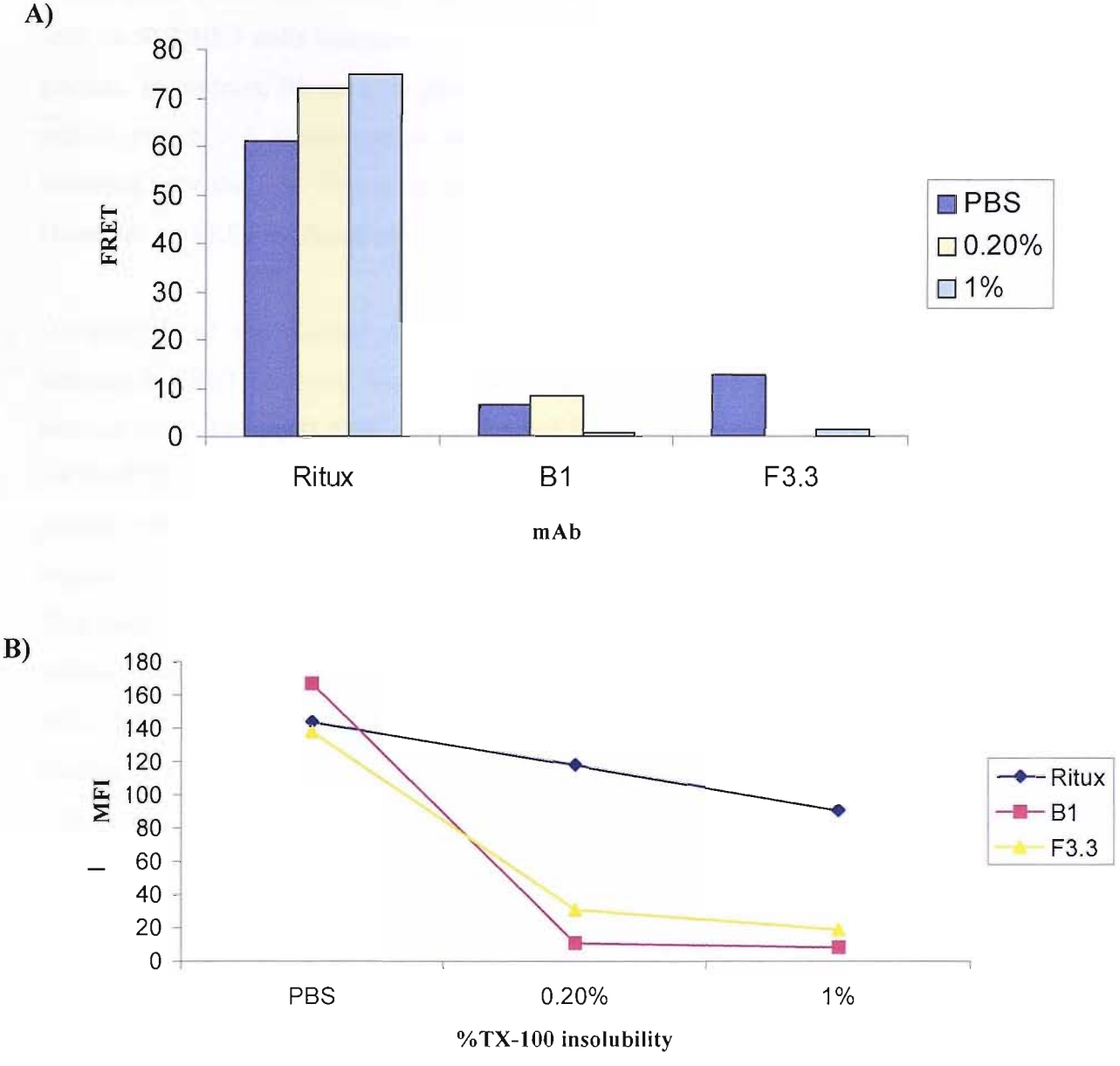

Figure 4.17: Effect of TX-100 lysis on FRET. $3x10^5$ SUDHL4 cells were incubated with Cy5 and FITC labelled B1 (10 μg/ml), ritux (5 μg/ml) and F3.3 (anti-Class II, 5 μg/ml) for 20 minutes at 37°C. Cells were washed and lysed in various concentrations of TX-100 for 15 minutes on ice before being washed and analysed by flow cytometry. The FRET values for each sample are shown in A. The binding level of the FITC mAb are depicted in B.

4.2.8.4 Kinetics of CD20 clustering

In order to extend our knowledge of CD20 redistribution upon mAb binding we decided to analyse the dynamics of anti-CD20 mAb induced FRET kinetically. The assay conditions were the same as previously used (Section 2.8.3) with B1 (10 μg/ml) and ritux (5 μg/ml) being incubated with cells at 37°C for various times. It is evident from Figure 3.18A that FRET is time dependent where the FRET associated with ritux in SUDHL4 cells increased steadily from 5 to 20 minutes and then reached a plateau. In contrast, B1 does not generate significant FRET at any point within the 40 minute period. A similar result is observed for Daudi cells where FRET again increases over the first 20 minutes of the assay when cells are incubated with ritux. However, no FRET is observed with the type II mAb B1.

On analysis of the binding profiles (right-hand profiles), it is apparent that the increase in FRET observed with ritux is not simply due to a progressive increase in binding level. First in SUDHL4 cells, B1 and ritux bind at similar levels to each other yet the FRET generated is very different. Second, the binding level of ritux and B1 plateau within the first 5 minutes and then gradually decrease over the remaining 30 minutes. However, the FRET generated by ritux increases for a 20 minute period. This result strongly suggests that the FRET associated with ritux binding is due to redistribution of CD20 into large clusters. A similar result was obtained for Daudi cells, the binding of B1 was lower yet based on previous experiments with ritux, the binding level would be sufficient to generate FRET if clustering was to occur (Table 4.3). Again ritux binds at a maximal level within the first 5 minutes and maintains this binding level for the remainder of the assay. However, the FRET increases between 5 minutes and 20 minutes before plateau further supporting the theory that the FRET generated by ritux is due to clustering of CD20.

A)

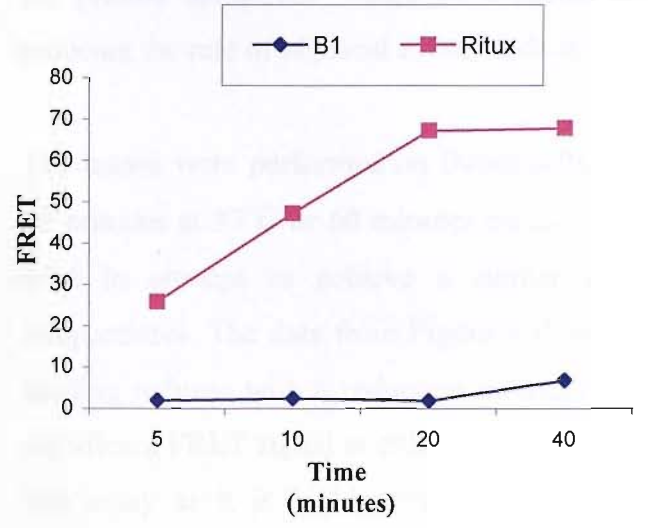

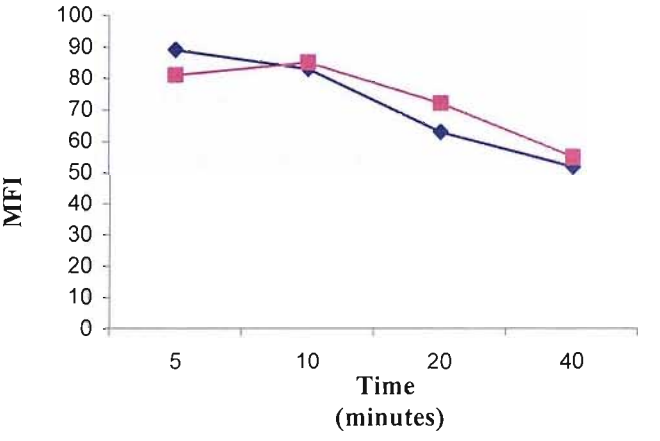

B)

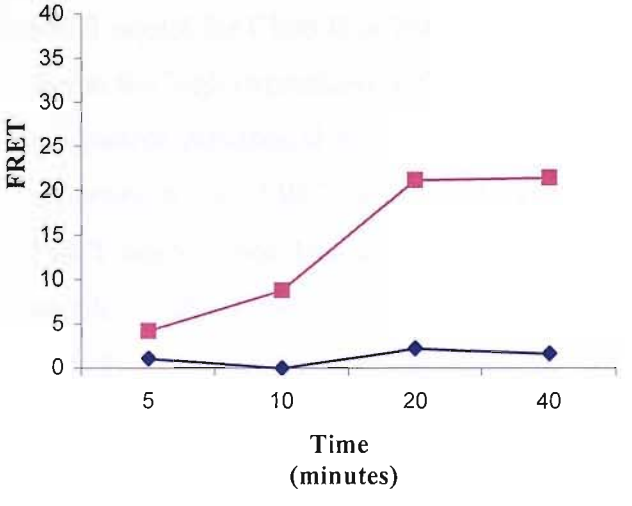

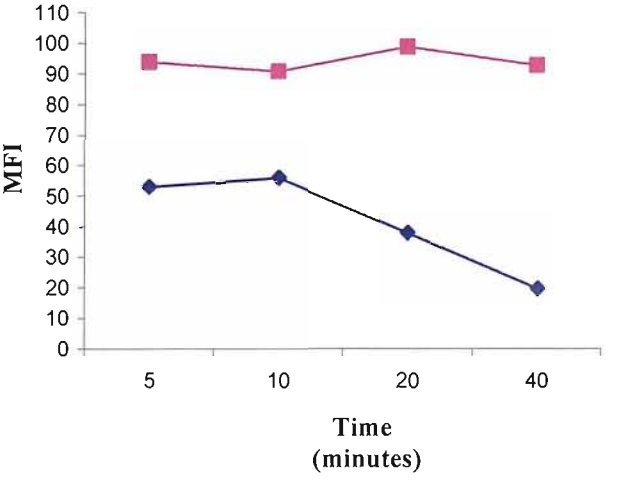

Figure 4.18: FRET is time dependent. A) 3 x 10^5 SUDHL4 cells were incubated with 10μg/ml B1 or 5 μg/ml ritux for 5, 10, 20 and 40 minutes at 37°C before being washed and analyzed by flow cytometry. The binding profiles of the Cy5 mAb are depicted in the graph on the corresponding right hand side. **B)** The same method was used as above for analysis of Daudi cells.

4.2.8.5 Effect of temperature on FRET generation

To further investigate the dynamics of CD20 clustering, we decided to assess the temperature dependence of CD20 redistribution. When cells are maintained at 4°C the plasma membrane would be expected to be less fluid and dynamic, thereby reducing the rate of physical events such as CD20 redistribution.

The assays were performed on Daudi cells, with 10 μg/ml mAb incubated for either 20 minutes at 37°C or 60 minutes on ice. The difference in incubation periods was used in attempt to achieve a similar level of mAb binding at the different temperatures. The data from Figure 4.19 demonstrates that FRET generated by ritux binding reduces with a reduction in temperature. As expected, B1 does not show a significant FRET signal at either temperature. MHC Class II was also investigated in this assay as it is highly expressed on B cells and is reported to be unable to redistribute into rafts upon mAb binding [72]. As is evident from the data, there was a FRET signal for Class II at both 4°C and 37°C. The FRET generated is thought to be due to the high expression of Class II where the probability that Cy5 and FITC being adequately juxtaposed to generate FRET is high. This theory is supported by the observation that FRET is not reduced when incubated on ice suggesting that the FRET signal is not dependent on redistribution. Interestingly, analysis of the binding profiles of B1 and F3.3 (anti MHC Class II) revealed that mAb binding was similar at both 37°C and 0°C, the MFI for the FITC mAb are shown above the histogram bars in Figure 4.19. However, ritux demonstrated a reduced level of binding after 60 minutes on ice from an MFI of 40 at 37°C to 26 at 0°C. This result suggests that redistribution of CD20 into clusters or rafts is required before maximal binding of ritux can occur.

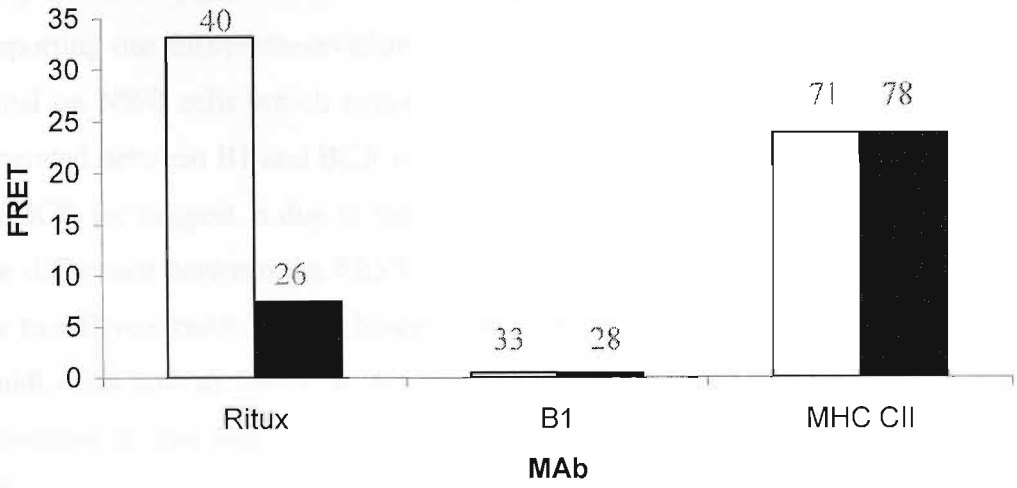

Figure 4.19: FRET is temperature dependent. $3x10^5$ Daudi cells were incubated with 10 μg/ml mAb either at 37°C for 20 minutes (open bars) or 0°C for 60 minutes (closed bars) before being washed and analyzed by flow cytometry. F3.3 was used to assess Class II. The MFI for FITC mAb binding is shown over the relevant histogram bar.

4.2.8.6 The association of CD20 with other surface antigens

One of the major advantages of FRET analysis is the ability to investigate associations between different surface antigens on viable cells. We decided to assess the association of CD20 with a variety of surface antigens which are important in cell signalling such as the BCR and MHC Class II which are key molecules in generating an immune response and CD59 which is a complement defence protein. Furthermore CD59 is a GPI-linked protein and constitutively present in lipid rafts, whereas the BCR and MHC Class II are not [47, 72]. The same basic procedure was used as outlined for the assessment of CD20 homo-associations except that the FITC and Cy5 mAb will be specific for different antigens.

From this analysis it was revealed that anti-CD20 mAb produce FRET with CD59, the BCR and Class II to varying degrees. This FRET of CD20 with CD59 and the BCR only occurs whit type I anti-CD20 mAb such as ritux (Table 4.4). However, both B1 and ritux induce FRET with MHC Class II, suggesting that this association is independent of CD20 redistribution and most likely due to high Class II expression supporting our earlier observation in Section 4.2.8.2 in that B1 can generate a FRET signal on NS/0 cells which express high levels of CD20. Similarly the low FRET generated between B1 and BCR in SUDHL4 cells compared to that between ritux and the BCR we suggest is due to the high expression of CD20 and BCR on these cells. The difference between the FRET values obtained for different cell lines is primarily due to different mAb binding levels. For example, CD59 mAb binding is very low on Daudi cells and as FRET is dependent on binding of both FITC and Cy5, if the expression is low then the mAb binding will be low and therefore the FRET value will be low.

In summary, type I anti-CD20 mAb can induce clustering of CD20 molecules. It appears that this clustering of CD20 can lead to the localisation of CD20 with other surface molecules such as the BCR and CD59. In direct contrast and in support of density gradient analysis and TX-100 flow cytometry experiments, type II anti-CD20 mAb do not appear to cluster CD20 in the membrane.

Hetero-associations	**Daudi**	**SUDHL4**
Ritux + CD59	0	23.55
Ritux + BCR	6.2	56.2
Ritux + MHC CII	12.02	16.60
B1 + CD59	0	0
B1 + BCR	ND	1.1
B1 + MHC CII	13.05	11.44

Table 4.3: The association of CD20 with other surface antigens. Anti-CD20 mAb were titrated to achieve similar binding levels i.e. 5 μg/ml Ritux and 10 μg/ml B1. The other mAb used, Class II (A9-1), CD59 (MEM43) and BCR (M15/8) were at 10 μg/ml. The assay conditions were the same as described in Section 2.7.3.

4.2.9 Electron microscopy analysis of CD20 clustering

Based on the density gradients (Section 4.2.1), TX-100 insolubility flow cytometry (Section 4.2.2) and FRET analysis (Section 4.2.8) it is evident that certain anti-CD20 mAb effectively redistribute CD20 into clusters which are TX-100 insoluble and cholesterol sensitive. In all three assays the results were in agreement; type I mAb such as ritux can effectively cluster CD20 whereas type II mAb like B1 cannot.

To gain a visual image at the sub-cellular level of what is happening at the cell surface when CD20 is bound by either type I or type II anti-CD20 mAb we decided to use electron microscopy (EM). The transmission electron microscope (TEM) operates on the same basic principles as the light microscope but uses electrons instead of light. Briefly, Ramos cells were treated with 10μg/ml ritux (type I), 11B8 (type II) or a negative control (anti-41BB, JG 13.5) for 45 minutes at 4°C to facilitate maximal binding and then for 15 minutes at 37°C to allow CD20 redistribution. Samples were washed twice at 4°C and incubated with 1:20 gold labelled mouse anti-human IgG (15nm) for the same incubation periods as used for the primary labelling. Cells were washed twice and fixed in 3% gluteraldehyde, 4% para-formaldehyde in 0.1M PIPES buffer. Fixed samples were given to the biomedical imaging department at Southampton General Hospital for processing into sections which were fixed to copper grids using an alginate matrix. Cell sections were then analysed using a transmission electron microscope, magnifying images up to 50,000X.

The images shown in Figure 4.20 support our previous results in that type I mAb (ritux) effectively cluster CD20 whereas type II mAb (11B8), shown in Figure 4.21, do not. As the cell is cross-sectioned, gold particles throughout (black dots indicated by the arrow in panel A) are only observed around the periphery of the cell. In ritux treated cells, gold beads can be seen in close proximity to each other. In contrast, 11B8 treated cells gold particles are seen to be more dispersed on the cell surface so only a few gold particles are seen. As the cells are cross-sectioned, each section is representative of only a five hundredth of the cell surface. Therefore for 11B8 and ritux, we assessed 10 different cell sections in two independent experiments using Ramos cells and the results are presented in graphical format to demonstrate the differences. Figure 4.22 demonstrates the difference in clustering ability of ritux

compared to 11B8 mAb. The difference between 11B8 and ritux becomes apparent as the cluster size increases above two but particularly from clusters of four and higher. In 11B8 treated cells 60% of the cells had beads in groups of two. After this point the number of cells with higher clusters declined with no cells demonstrating clusters larger than four beads. In contrast, in ritux treated samples over 80% of the cells had CD20 in clusters of four and five.

Furthermore, we found that the average number of beads differed between the two mAb treatments. In support of our observation that type I mAb have a higher saturation binding level than type II mAb, we found that ritux treated cells had an average of 42 beads on its surface compared to 23 beads for 11B8 treated cells (data not shown). However, this does not appear to be the direct cause for the difference in redistribution as when individual sections with the same amount of mAb bound (i.e. same number of gold beads) were directly compared, ritux treated cells still demonstrated clustering of CD20, with beads present in clusters of 4 or more whereas beads were predominantly found in isolation in 11B8 treated cells (data not shown). This data provides further direct evidence to support our previous findings that type I mAb such as ritux readily induce clusters of CD20 whereas type II mAb like 11B8 do not.

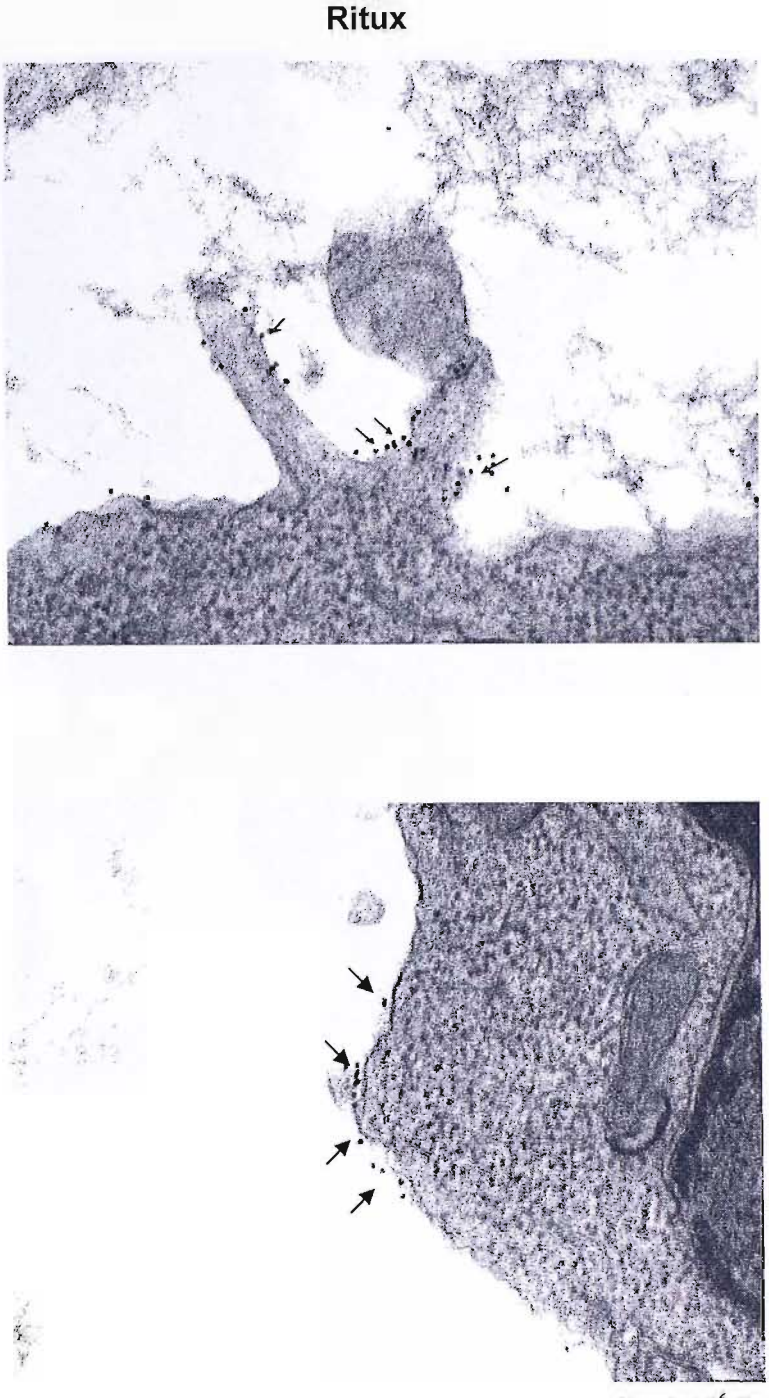

Figure 4.20: Electron microscopy images of type I mAb bound cells. $5x10^6$ Ramos cells were treated with 10μg/ml ritux (type I) for 45 minutes at 4°C followed by 15 minutes at 37°C before being washed twice and incubated with 1:20 gold labelled secondary mAb with the same incubation conditions. Cell sections were processed by the biomedical imaging unit and viewed using a Hitachi TEM. Both images are of ritux treated cells and are shown at 50,000X magnification. These images are representative of two independent experiments and a selection of gold particles are indicated by the arrows.

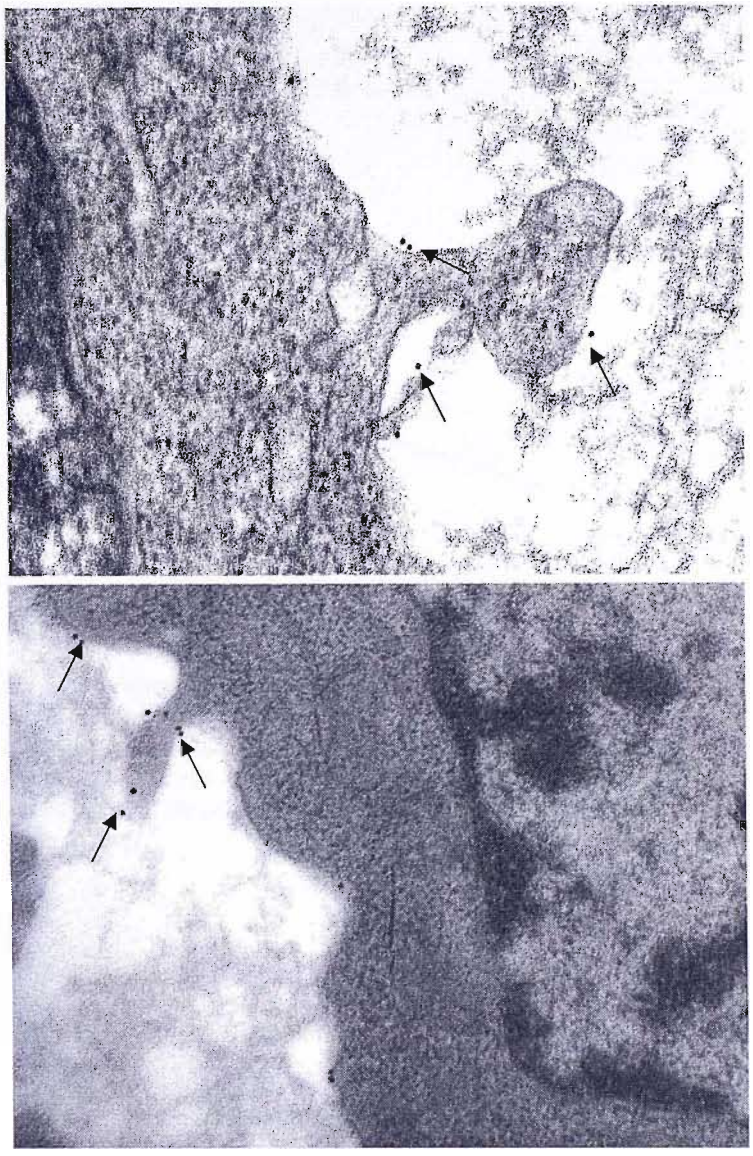

Figure 4.21: Electron microscopy images of type II mAb bound Ramos cells. $5x10^6$ cells were treated with 10μg/ml 11B8 (type II) for 45 minutes at 4°C followed by 15 minutes at 37°C before being washed twice and incubated with 1:20 gold labelled secondary mAb with the same incubation conditions. Cell sections were processed by the biomedical imaging unit and viewed using a Hitachi TEM. Both images are of ritux treated cells and are shown at 50,000X magnification. These images are representative of two independent experiments and a selection of gold particles are indicated by the arrows.

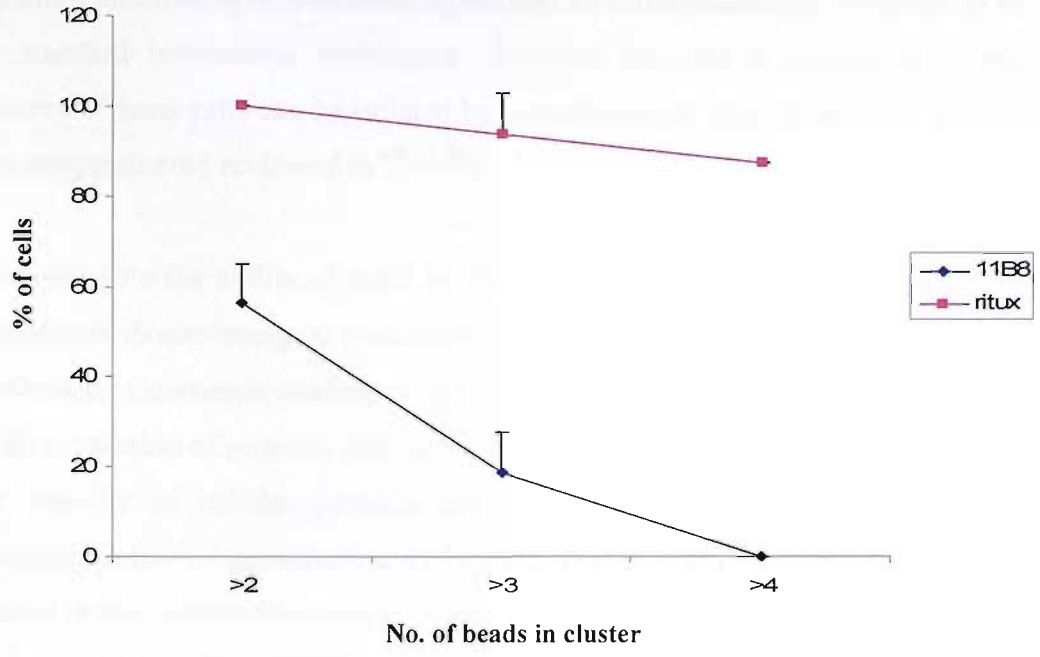

Figure 4.22: Graphical representation of electron microscopy results. The redistribution of 20 sections from two independent experiments was assessed for ritux and 11B8 treated cells. A total of forty sections were assessed for the number of beads on their surface and whether the beads were in clusters or on their own. **A)** Cells were assessed the presence of clusters. The % of positive cells is calculated based on the total of 20 cells (ritux of 11B8 treated) which were positive for the cluster size.

4.3 Discussion

In the last chapter we demonstrated that type I anti-CD20 mAb were potent inducers of complement lysis compared to type II mAb. The difference between the two types of anti-CD20 mAb was only partially explained by the difference in binding ability of the mAb. In this chapter, we explore whether this difference might be explained by the differential ability of the mAb to redistribute CD20 in the plasma membrane. The plasma membrane is a dynamic structure which is believed to contain micro-domains enriched in sphingolipid and cholesterol known as lipid rafts. As several important signalling molecules such as G proteins, Src family PTKs and adaptor proteins e.g. PAG, reside within these domains, rafts have been postulated to be important in signal transduction [69, 70, 79]. Furthermore, non-resident raft proteins such as receptors have been demonstrated to localise into rafts upon mAb cross-linking [72]. It has been suggested that this is an important step in some signal transduction pathways. Partitioning of receptors into rafts can result in a new microenvironment, facilitating modification of their phosphorylation state by localized kinases and phosphatases,

therefore modulating downstream signalling. As raft domains are too small to be seen by standard microscope techniques, detergent resistant microdomains containing clusters of many rafts can be isolated by extraction with TX-100 or other detergents at low temperatures (reviewed in [69, 71, 82])

To investigate the ability of mAb to redistribute CD20 into different domains of the plasma membrane detergent lysis followed by sucrose density gradient separation was performed. Coomassie staining of the ten resulting fractions demonstrated that only a small proportion of proteins were found in the raft fractions insoluble in TX-100, with the majority of cellular proteins detected in the soluble, high density fractions (fractions 7-10). In agreement with Deans and colleagues [66], it was found that CD20 resides in the soluble fractions in resting cells but upon stimulation with certain mAb such as ritux and 7D8, CD20 can translocate into the insoluble fractions. Intriguingly, such translocation was not observed with B1 or 11B8. These results were later confirmed using flow cytometric and pellet / lysate assays.

Interestingly then, the good inducers of CD20 translocation such as ritux and 7D8 were those classified in Chapter Three as type I mAb, the effective mediators of CDC. In contrast, those classified as type II mAb e.g. B1 and 11B8 which were poor inducers of CDC were shown here to be poor inducers of CD20 redistribution. Interestingly, this difference in redistribution was stable and was maintained over a 24 hour analysis. Together, this data indicates that CD20-mediated CDC redistribution may be dependent on CD20 redistribution into TX-100 insoluble rafts. However, it should be noted that redistribution of CD20 into TX-100 insoluble domains is not identical for all type I mAb with for example 7D8 appearing to be more potent than ritux. The potency of 7D8 to induce CD20 redistribution in the sucrose density assay is similarly reflected in the flow cytometry and pellet/lysate assays where in MHH Pre B-1 cells 65% of CD20 is found in the insoluble domain after TX-100 lysis compared to only 32% for ritux. This hierarchy seems to reflect the off-rate of the mAb. Elegant work by Teeling and colleagues [200] report that 7D8 has a much slower off rate than 7D8 or ritux suggesting that it is more stably bound to the cell. Therefore it is conceivable that 7D8 may stabilise CD20 clusters more effectively to confer greater resistance to TX-100 lysis compared to ritux treated cells.

In order to assess whether translocation into TX-100 insoluble rafts was a common phenomenon, other surface antigens were investigated. It was demonstrated that mAb ligation of CD37, which is similar in structure to CD20, did not induce redistribution into TX-100 rafts. Class II was also assessed and found that despite its high expression in B cells it did not gain TX-100 insolubility upon mAb binding. Together this data highlights the fact that the ability of surface antigens to redistribute into TX-100 insoluble domains upon mAb binding is not a common event, where CD20 was the only transmembrane protein tested here that redistributed. This is in agreement with a previous study that found that only 3 out of 24 antigens could redistribute into TX-100 insoluble domains after mAb binding [72]. This relatively unusual characteristic, allowing CD20 and the associated mAb to redistribute and cluster in a defined region of the plasma membrane may well explain why CD20 is such a potent inducer of CDC compared to other surface antigens with similar structures and expression levels which do not redistribute into rafts.

We have suggested that as TX-100 is a stringent detergent, it isolates larger rafts or clusters of mini-rafts which are stabilised by mAb binding. A recent publication by Li et al [48] investigated the association of CD20 with insoluble domains generated with a panel of detergents. They demonstrated that CD20 is associated with the insoluble fractions of less stringent detergents such as CHAPS and Brij 58 prior to mAb ligation, suggesting that CD20 is constitutively present in small lipid rafts or microdomains. We compared the effect of 0.5% TX-100 and 1% Brij 58 on the association of CD20 with the insoluble fraction (i.e. rafts) and found similar results. In contrast to TX-100 analysis, lysis of cells with Brij 58 showed that CD20 was constitutively resident in the insoluble fraction of non-stimulated cells. Cholesterol depletion with MCD resulted in the loss of CD20 from the insoluble fraction, supporting the idea that the association of CD20 with the insoluble fraction is representative of its association with lipid rafts. It has been reported that MCD treatment can cause the loss of surface antigens [201]. However in our experiments, the loss of CD20 from the insoluble raft fraction was accounted for by its appearance in the soluble fraction, indicating that this is not the case with CD20, at least within the sensitivity of the western blot assay. For TX-100 analysis, CD20 was only found in the raft fraction when ligated by type I mAb such as ritux. Again, this association was

lost upon treatment with MCD indicating that the presence of CD20 in the insoluble fraction was due to its association with lipid rafts.

Interestingly, with Brij 58 analysis, ligation of CD20 with ritux completely ablates the effect of cholesterol depletion on the association of CD20 with the raft fraction. The reason for this is not fully understood. However, it may be due to the strength of the detergent. When ritux binds CD20, it presumably cross-links the mini raft domains resulting in a larger, stabilised domain. This domain is destabilised by cholesterol extraction through MCD treatment. As TX-100 is a relatively stringent detergent, when MCD treated cells are lysed in TX-100 it causes complete loss of the raft and hence of the insoluble domain. However, when MCD treated cells are lysed by Brij 58, the detergent is not potent enough to cause complete destabilisation of the raft structure, therefore the insoluble domain remains.

In line with our suggestion that CD20 constitutively resides in lipid raft microdomains, it was recently revealed that the epitope on CD20 for mAb binding may be conformationally dependent, relying on cholesterol in the membrane. Polyak et al [85] reported that binding of anti-CD20 mAb, FMC7, was lost upon cholesterol depletion. We expanded this analysis to a range of different CD20 mAb and showed that even though FMC7 mAb binding is the most sensitive mAb to cholesterol depletion, the binding of most anti-CD20 mAb are affected by cholesterol depletion. Furthermore, the sensitivity to cholesterol depletion was cell line dependent where Daudi cells were the most sensitive, then Ramos, with SUDHL4 cells least sensitive. Further investigation is required to understand this difference in sensitivity. Moreover, the anti-CD20 mAb demonstrated a range of sensitivities to cholesterol depletion, where murine mAb appeared more sensitive than chimerised and human mAb. Again, the reason for this is unclear but it may due the binding kinetics of the mAb or possibly due to the secondary mAb used for detection. However, the much higher susceptibility of FMC7 to cholesterol depletion is most likely due to it being an IgM mAb rather than IgG mAb. As IgM are generally lower affinity than IgG and rely on avidity from their five binding arms (compared to two in IgG) to compensate, any disruption to the binding epitope would be expected to have a more pronounced effect on mAb binding The effects of cholesterol depletion on mAb binding can be reversed upon cholesterol repletion. Cholesterol is an important constituent of the plasma

membrane, particularly in lipid rafts and therefore the effect of cholesterol depletion was assessed on mAb binding to other surface antigens. It was demonstrated that CD20 is the most sensitive of those tested to cholesterol depletion. Monoclonal Ab binding to the BCR and Class II were mildly sensitive to depletion but anti-CD55 mAb binding was not affected. Interestingly, CD55 is GPI-linked and therefore believed to be a resident raft protein, however despite this it was not sensitive to cholesterol depletion. This may be due to the nature of its attachment to the membrane.

To summarise, the two classical features used to determine lipid raft domains is their insolubility at 4°C in detergent (usually TX-100) and their cholesterol content. We have demonstrated in this chapter that the domains which type I mAb translocate CD20 into have both of these characteristics. Surprisingly, it appears that cross-linking is not required for redistribution of CD20 into lipid rafts by type I mAb and that Fab fragments can redistribute CD20 into lipid raft domains. Although Fab fragments display a lower binding level than their IgG 'parent', Fab fragments from both ritux and 7D8 were able to translocate CD20 into TX-100 insoluble regions, whereas Fab fragments from B1 were not. These results highlight two points, firstly it is not simply cross-linking of CD20 which results in association with the raft domain,; and secondly, that it is not the bivalent nature of B1 which prevents it from redistributing CD20 .

Work by us and others [48, 52] have shown that residues 217-225 in the cytoplasmic tail of CD20 are important for its redistribution. The fact that the residues in the cytoplasmic tail contain three putative serine/threonine phosphorylation sites supports the suggestion that CD20 clustering is mediated through a signalling event. We investigated here whether early signalling events such as actin rearrangement or phosphorylation of Src family kinases was involved but found no effect on CD20 redistribution when either event was inhibited. Interestingly, it has been reported that ritux can activate acid sphingomyelinase in Daudi cells and a recent review highlighted the potential of this enzyme to induce raft formation [77, 78]. Acid sphingomyelinase hydrolyses sphingomyelin to release its hydrophobic ceramide moiety. These ceramides are then free to spontaneously associate to form ceramide rich microdomains. These domains also demonstrate TX-100 insolubility as the

ceramide associate with cholesterol to form tightly packed structures. Due to these similarities, it is possible that CD20 clustering by type I mAb involves a similar mechanism but this has yet to be demonstrated conclusively.

Detergent lysis is a common method utilised for the analysis of rafts and their contents. However, there are several downfalls to detergent analysis as outlined in numerous reviews [79-81]. Firstly, the contents of the lipid raft domains are highly dependent on the cell type and the detergent used. Secondly, this approach cannot determine whether the proteins under study are together in a raft or present in multiple separate rafts. Therefore, the identification of two proteins in the raft fraction only indicates that both are in raft domains but does not demonstrate that they are closely associated as they could be in different rafts. Furthermore, detergent lysis results in the loss of cell integrity and as a result cannot be used to detect rafts in living cells. In order to try and circumvent these problems, FRET analysis was employed. This method allows for analysis to be performed on live cells and indicates whether two proteins are associated within 10 nm of each other in the plasma membrane. This may occur if the target antigen is highly expressed on the cell surface where the probability that antigens will be within 10nm of each other without the need for redistribution would be high or if antigens are in some way induced to cluster together, for example following redistribution into rafts. On comparison of type I (ritux) and type II (B1) mAb to generate a FRET signal, it was found that type I mAb efficiently redistributed CD20 and generated a FRET signal. In stark contrast, B1 did not (except for a small signal in SUDHL4 cells which we suggest is due to high surface expression rather than a redistribution event). The FRET observed is in correlation with TX-100 analysis. Therefore, we suggest that the generation of FRET reflects the clustering of CD20 mini-rafts into larger raft domains stabilised by mAb binding. We previously showed that type I mAb bind at a higher level compared to type II mAb and so to ensure that the reason B1 (type II) stimulation resulted in no FRET compared to ritux (type I), ritux was titrated down to achieve a comparable binding level. We found that at this lower level of ritux binding a FRET signal was still generated, albeit lower than that observed at the usual concentration of 10μg/ml, yet no FRET was observed for B1 stimulated cells. It could be suggested that if CD20 was constitutively present in mini rafts, then FRET should be observed

irrespective of the anti-CD20 mAb used. However, it is not known what size these CD20 domains are ,for example, a mini-raft may compose of a single CD20 molecule.

The data from five different B-cell lines demonstrated that even though ritux consistently gave a FRET signal, the level of FRET measured was variable ranging from 8 in BL41 cells to 91.5 in SUDHL4 cells, correlating with the expression level of CD20. To address the importance of expression level more formally, NS/0 cells transfected with varying levels of human CD20 were used. It was found that CD20 expression level was indeed a determining factor in the level of FRET observed where the amount of FRET observed could be directly correlated to expression level. Again as for SUDHL4 cells which express high CD20, FRET was also observed for B1 in high CD20 expressing NS/0 clones 3 and 21. This we believe was due to the high expression level of CD20 in these cells and not due to redistribution of CD20, as discussed previously.

To relate the FRET results obtained directly to the previously used TX-100 assays, we addressed whether the FRET generated by ritux binding was representative of the redistribution of CD20 into TX-100 insoluble domains and so performed TX-100 assays on the FRET samples. These experiments demonstrated that the level of FRET with ritux was not reduced following treatment with TX-100, indicating clearly that ritux clusters CD20 in the intact plasma membrane, causing FRET and that this is synonymous with the TX-100 insoluble microdomains. Moreover, in correlation with earlier data, FRET induced by type II mAb (B1) or Class II (F3.3) homo-associations was lost upon lysis with TX-100, again indicating that the low level of FRET observed was due to high expression levels of these target antigens. To clarify that the FRET observed with ritux was due to CD20 clustering, the kinetics of CD20 binding and FRET was examined. These experiments showed that maximal binding of CD20 occurred much faster than the maximal level of FRET. As such, the maximal binding of ritux was achieved within the first 5 minutes in both SUDHL4 and Daudi cells. However, maximal FRET was not observed with ritux until 20 minutes clearly demonstrating that the FRET increase observed within this final 15 minutes is not due to increased mAb binding but to clustering of ligated CD20 mini rafts.

Further to these observations, the temperature dependence of CD20 clustering was assessed and compared to that of Class II. At low temperatures, the plasma membrane would be less fluid and therefore will hinder efficient membrane redistribution of surface antigens. As expected, the FRET induction of ritux was effected by temperature and was much lower at 4°C than 37°C. Therefore the dependence of ritux generated FRET on temperature supports the suggestion that redistribution in the membrane is occurring. In contrast, B1 did not generate significant FRET at either temperature. With class II mAb, the same level of FRET was observed at both temperatures, supporting the suggestion that class II associated FRET is due to expression level and not a redistribution event. It is conceivable that the reduction in FRET by ritux at 4°C may be due to the slightly reduced ritux binding at low temperature, although we think this unlikely Interestingly, this reduction in binding is not observed for B1 or Class II, and so may indicate that clustering of CD20 in the first five minutes (observed in the time course study) may be required for maximal binding of ritux.

CD20 has no known ligand. Therefore, it is highly probable that CD20 functions as a component of other receptor signalling pathways. To investigate this, we used FRET analysis to investigate the association of CD20 with other surface antigens such as CD59, the BCR and MHC Class II. CD59 is a GPI-linked protein and therefore is constitutively present in lipid rafts [79]. As expected, CD20 only localises with this transmembrane protein when redistributed into rafts by type I mAb stimulation. Similarly, we found that CD20 only associates with the BCR when stimulated by type I mAb. Our results are in agreement with other reports which demonstrate that CD20 and the BCR can co-localise when assessed by confocal microscopy [47, 65]. Furthermore, we found that CD20 can associate with MHC class II when stimulated with either type I or type II mAb, presumably indicating that this interaction occurs outside of lipid rafts. There are conflicting reports on the association of MHC class II with lipid rafts. Poloso and colleagues [202] reported that a proportion of MHC class II is constitutively present in TX-100 insoluble rafts in mouse and human B cells whereas other reports suggest that MHC class II resides outside of lipid rafts until required for antigen presentation [203]. Here we find that both types of CD20 mAb localize with MHC Class II irrespective of their raft association suggesting that CD20 and MHC class II are constitutively associated. This result is in agreement with

immunoprecipitation studies showing that CD20 and MHC class II are physically associated in Raji and Ramos cells [46]. These associations indicate a possible role for CD20 in other receptor signalling pathways and will be further investigated in the next chapter.

Finally, to investigate the ultra-structural features of anti-CD20 mAb binding, we used immuno-electron microscopy. In these experiments type I or type II mAb were bound to the cells, allowed to cluster at 37°C, then washed and bound Ab detected using gold-particle labelled secondary antibodies. These experiments revealed that when Ramos cells are stimulated with type I mAb ritux, CD20 can be found in clusters. Although not all CD20 appeared to form clusters, at least 50% of the beads were found in clusters of three or more. It should be noted however, that the cells are cross-sectioned for analysis and therefore only 2D images are formed so it is possible that when the cell is fully intact, the single beads were indeed clustered. In contrast to ritux, the CD20 distribution in type II treated cells (11B8) cells was more diffuse, where labelled CD20 was predominantly (75%) found on its own. The difference between ritux and 11B8 clustering became more pronounced as the cluster size increased where 60% of ritux treated cells possessed clusters of 4 or more labelled CD20 molecules compared to none for 11B8 treated cells. Furthermore, from the location of the gold beads on the surface in membrane protrusions, it is apparent that CD20 is found in microvilli. Microvilli are enigmatic structures that are thought to be involved in cell adhesion and motility. Therefore, this particular location may have some bearing on the function of CD20. Recently, Li and colleagues [68] provided support for this observation by demonstrating that CD20 is localised to microvilli when stimulated with anti- CD20 mAb 2H7.

In conclusion, we show here that CD20 is constitutively present in small lipid microdomains. These CD20-containing mini-rafts can cluster and be stabilised by type I anti-CD20 mAb binding resulting in insolubility to TX-100. Cholesterol plays an important part in these microdomains as extraction of cholesterol resulted in the reduction of anti-CD20 mAb binding and loss of TX-100 insolubility. The significance of CD20 redistribution into TX-100 insoluble domains is not fully understood. However, as only type I mAb such as ritux induce this redistribution and recent work in our group have demonstrated that type I but not type II mAb are

capable of binding high levels of C1q [67], it seems likely that raft redistribution by type I anti-CD20 mAb accounts for their high potency in evoking CDC. However, in addition to this advantageous clustering, lipid rafts are also postulated to be important signalling platforms. We have shown here that redistribution of CD20 into TX-100 insoluble rafts brings CD20 into close proximity with other important signalling molecules like the BCR. Hence, in the next chapter we investigated whether redistribution of CD20 into rafts is important for induction of intracellular signalling cascades

CHAPTER FIVE

5.0 Calcium Signalling

5.1 Introduction

CD20 can redistribute into lipid rafts upon mAb binding. In Chapter Four we demonstrated that only type I mAb like ritux, could translocate CD20 into these domains. The significance of this event is still unclear. These domains are highly ordered, tightly packed structures rich in cholesterol and sphingolipid [82]. They are estimated to contain <1% of membrane proteins but are postulated to be important signalling platforms where several intracellular signalling proteins such as G proteins and Src kinases constitutively reside [70, 82]. Hence, we wondered whether the difference in ability of type I and II mAb to redistribute CD20 into these domains could translate into a difference in signalling ability of CD20 when stimulated by the two types of mAb. To this end, we assess here the ability of type I and II anti-CD20 mAb to induce a calcium flux.

An increase in intracellular free Ca^{2+} concentration is a ubiquitous early signalling mechanism that regulates a broad spectrum of kinetically disparate processes ranging from exocytosis to cell growth and proliferation [204]. It is well established that stimulation of surface immunoglobulin (sIg) (part of the B cell receptor (BCR)) through mAb ligation of antigen binding leads to an increase in intracellular Ca^{2+} [17, 22]. The signalling pathway involved is outlined in Figure 5.1 and is discussed in detail in Section 1.3.2.1. It is evident from the diagram that a complex signalling cascade involving the interaction of intracellular kinases such as Lyn and Syk kinase and adapter molecules such as BLNK. This complex cascade culminates in the production of IP_3 which binds the IP_3 receptor in the endoplasmic reticulum (ER), signalling for the release of Ca^{2+}. Calcium flux generation in response to receptor stimulation in lymphocytes involves two closely coupled components: an initial rapid, transient release of Ca^{2+} stored in the ER followed by slowly developing extracellular Ca^{2+} entry for store repletion [17].

CD20 was first linked to calcium signalling by Bubien and colleagues in 1993 [45]. Since that initial observation, several groups have investigated the ability of anti-

CD20 mAb ligation to generate a change in cytosolic Ca^{2+} [48, 56, 62, 63]. Li and colleagues [48] reported that reduced expression of CD20 in Ramos cells by anti-sense probes resulted in a decrease in the Ca^{2+} flux induced by anti-CD20 mAb. Of more interest is that this knock down in CD20 expression also leads to a decrease in the BCR-mediated calcium flux. Conversely, CD20 negative cell lines like Jurkat cells transfected with CD20 demonstrated an increase in Ca^{2+} flux [45].

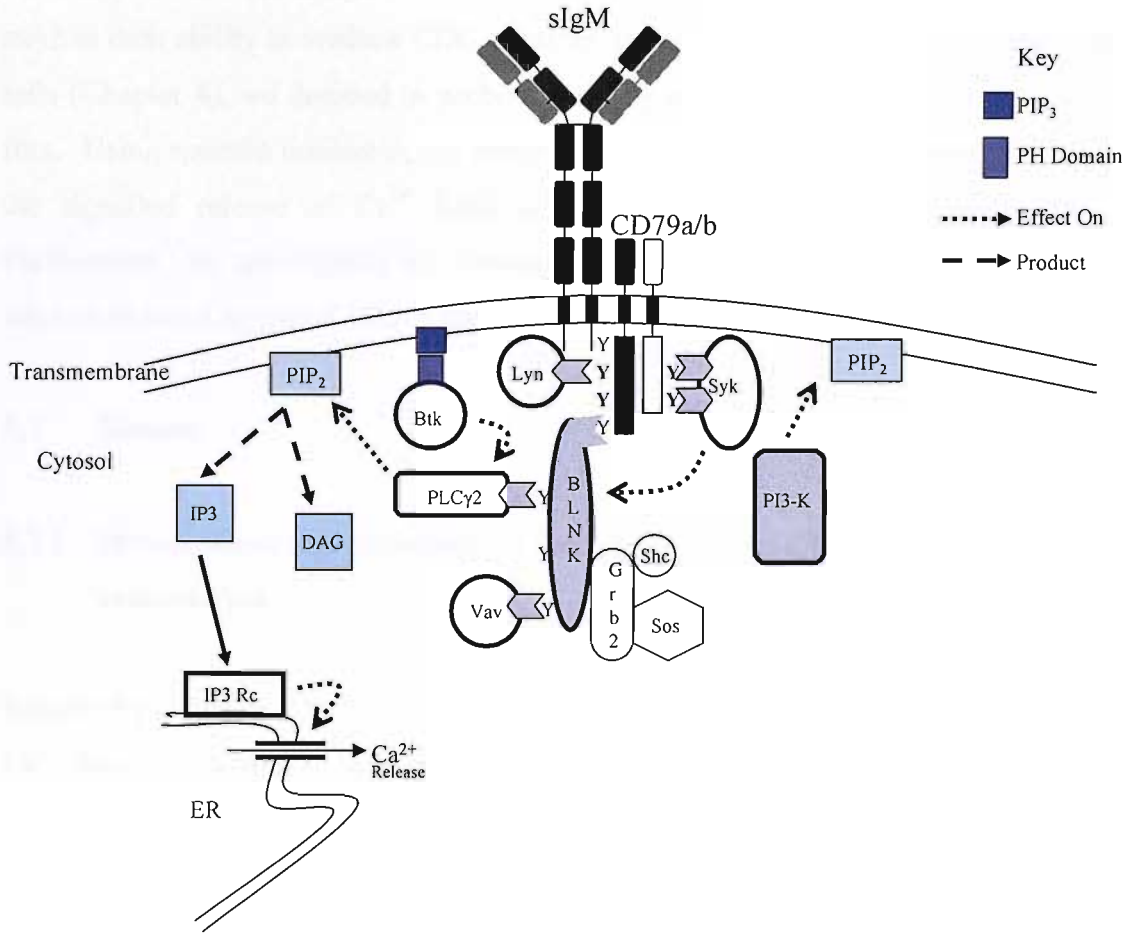

Figure 5.1 Overview of BCR induced calcium signalling. Cross-linking of the BCR on the surface of B cells in response to Ag or mAb can stimulate an increase in intracellular calcium. Calcium release from intracellular stores involves a complex signalling cascade culminating in the production of IP3 which binds the IP3 receptor in the endoplasmic reticulum (ER), signalling for the release of calcium.

It is still not clear whether CD20 plays a role in regulating a calcium entry pathway or actually forms an ion channel itself. There are several lines of evidence suggesting that the latter may be the case. Firstly, CD20 has several physical features of a typical ion channel; it is a tetra-span structure and is suggested to reside in oligomeric

complexes in the membrane [31, 98]. Secondly, when CD20 was ectopically expressed in different cells such as Chinese Hamster Ovary (CHO) cells or human T cells an increase in cytosolic Ca^{2+} concentration was observed [45, 48]. Finally, it is a members of the recently classified MS4a super-family which includes FcεRIβ chain, part of the high affinity receptor for IgE which is known to be involved in calcium conductance [34].

Building on our knowledge of the inherent differences between type I and type II mAb in their ability to mediate CDC (Chapter 3) and redistribution of CD20 into lipid rafts (Chapter 4), we decided to probe the ability of anti-CD20 mAb to induce Ca^{2+} flux. Using specific inhibitors, we reveal important signalling mediators involved in the signalled release of Ca^{2+} from intracellular stores upon CD20 stimulation. Furthermore, we investigated the downstream consequences of changes in cytosolic calcium induced by anti-CD20 mAb.

5.2 Results

5.2.1 Investigation into the ability of Type I and II anti-CD20 mAb to induce a calcium flux

Reports by other groups [62, 63, 68] have suggested that anti-CD20 mAb can induce a Ca^{2+} flux. These studies were primarily performed in the Burkitt's lymphoma B cell line Ramos. However to date, no report has focussed on a direct comparison of anti-CD20 mAb and their ability to induce a Ca^{2+} flux. Therefore, we decided to investigate the ability of a large panel of anti-CD20 mAb to induce a change in intracellular Ca^{2+}. Initial investigations were carried out using another Burkitt's lymphoma B cell line, SUDHL4. These cells were labelled with the intracellular calcium sensitive dye Indo-1, stimulated with mAb and assessed for changes in intracellular calcium using a FACS Vantage Flow cytometer (see Section 2.9). Indo-1 is a fluorescent dye which changes its fluorescence emission ratio depending on the level of free cytosolic calcium. Indo-1 fluoresces at approximately 400nm (detected in FL5) when Ca^{2+} is bound compared to approximately 480nm (detected in FL4) when the dye is unbound [205]. If the results are assessed based on the ratio of FL5 to

FL4, the FL5/FL4 ratio shifts up when the level of cytosolic calcium increases. The increase in Ca^{2+} detected could be due to the release of calcium from intracellular stores or through a calcium influx from the extra-cellular milieu or a combination of the two. As both these events occur in rapid succession, the calcium profile generated does not generally distinguish between release from intracellular stores and influx of calcium but depicts a composite of the two.

Here we demonstrate that not all anti-CD20 mAb generate a calcium response (Figure 5.2A). When Indo-1 labelled SUDHL4 cells were warmed to 37°C and treated with 10μg/ml anti-CD20 mAb ritux, 7D8, AT80 and LT20, a Ca^{2+} flux was observed. However, when samples were stimulated with 11B8 or B1 no Ca^{2+} flux was observed. Intriguingly, the anti-CD20 mAb which generate a Ca^{2+} flux are the type I mAb shown in Chapter Four to efficiently redistribute CD20 into lipid rafts. In direct contrast, mAb which poorly redistribute CD20 (type II mAb), 11B8 and B1, do not generate a Ca^{2+} response. From the calcium profiles in Figure 5.2, it is evident that only about 10-20% of cells show an increasing shift in the ratio of FL5/FL4 upon type I mAb stimulation. The reason for this is unclear, although it could be due to the limited sensitivity of the dye as a threshold level of free calcium must be surpassed before a notable change in the FL4/FL5 ratio is obtained. This threshold is certainly surpassed by stimulation with the positive control ionomycin, a calcium ionophore. Ionophores are compounds that increase the permeability of cellular membrane barriers to ions by functioning as mobile ion carriers or channel formers.

When cells are stimulated through the BCR which is a well established inducer of Ca^{2+} mobilisation (see Figure 5.1), although the flux is greater and more acute than that induced by type I mAb, still only about 20% of the sample displays a shift in FL5/FL4 ratio. Further to this, we investigated two other surface antigens, MHC class II which is highly expressed on SUDHL4 cells and the lowly expressed surface antigen CD52. MHC Class II is reported to induce a Ca flux in tonsillar B cells [206] whereas CD52, which is a successful target used in the immunotherapy of CLL (see Section 1.2), does not appear to mediate calcium conductance [207]. In SUDHL4 cells, we found that neither of these induced a calcium flux upon mAb binding (see Figure 5.2) indicating that the generation of a Ca^{2+} flux in SUDHL4 cells is dependent on the surface antigen.

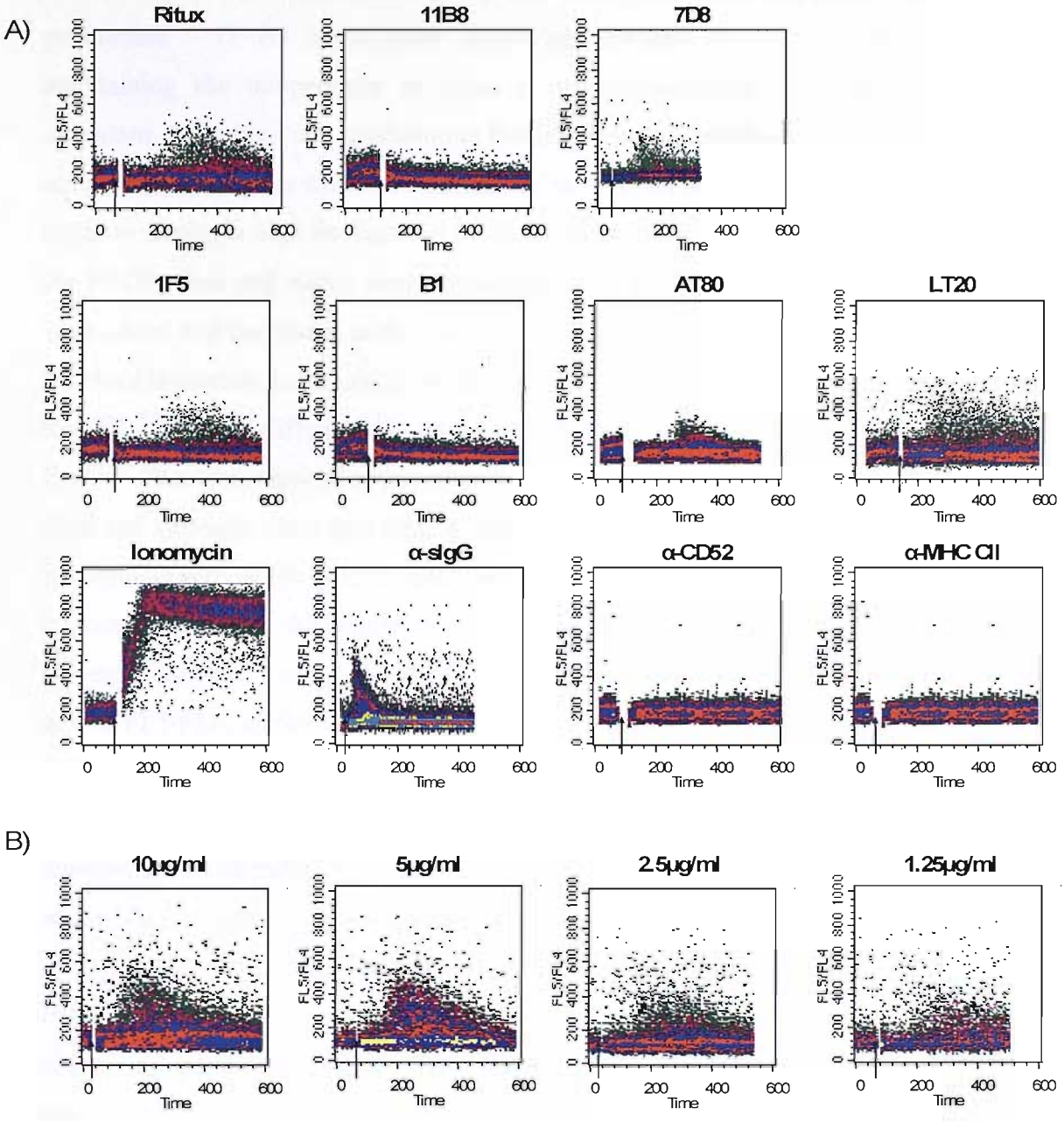

Figure 5.2: Type I anti-CD20 mAb can induce a calcium flux in SUDHL4 cells. **A)** $1x10^7$ SUDHL4 cells were labelled with the calcium sensitive dye INDO-1. After labelling, cells were resuspended in 5 mls RPMI (10% FBS) and left in the dark for 30 minutes at room temperature. To assess changes in the intracellular calcium level, 300µl of cells was added to 200µl of pre-warmed 10% RPMI and left at 37°C for 2 minutes. A basal level of intracellular Ca^{2+} was established before addition of 10µg/ml Type I anti–CD20 mAb (ritux, 7D8, 1F5, AT80 and LT20), type II mAb (B1 and 11B8), anti (α) -sIgG (SB2H2), α-CD52 (Campath-1H), α-MHC class II (L243) or 1µM ionomycin at a time point indicated by the arrow (time shown in seconds). A change in intracellular Ca^{2+} is depicted by a shift in the fluorescence ratio of FL5/FL4 Data shown is representative of three independent experiments. **B)** SUDHL4 cells were prepared as outlined in A and treated with various concentrations of ritux.

We found that Ca^{2+} flux induced by anti-CD20 mAb was dependent on several parameters. 1) As intracellular signalling cascades involve enzyme activity, maintaining the temperature as close to the physiological level as possible is important. However, one limitation to this is that indo-1 labelled cells are sensitive to temperature. Samples which are maintained at 37°C for any longer than three minutes begin to display a high background level due to dye leakage. As a compromise, both the FACS tubes and media were maintained at 37°C in a heat box and labelled cells were added and incubated in the heat box for 1 minute before use. 2) The affinity of the mAb is another factor which needs consideration, ritux and 7D8 are higher affinity than B1 [52, 200], this difference in affinity is reflected in the time delay and intensity of the Ca^{2+} flux generated after stimulation where 7D8 generated a faster response than ritux and similarly ritux generated a faster response compared to 1F5 (Figure 5.2A). 3) From Figure 5.2B, it is evident that the calcium flux was dependent on mAb concentration where the amplitude of the Ca^{2+} flux generated by ritux decreased in correspondence to a reduction in mAb concentration. At 10μg/ml the flux peak was at 600 FL5/FL4, as the concentration was decreased two fold, the flux decreased to 550, 420 and when at 1.25μg/ml the peak ratio was 380. 4) The time delay between addition of the mAb and the detected increase in FL5/FL4 increases with lower concentrations of mAb. The time delay is 60 seconds before a flux was detected when 10μg/ml ritux is added compared to 120 seconds when 1.25μg/ml was added. To ensure the difference between type I and type II mAb was not due to different levels of mAb bound to the surface (see section 3.2.3) ritux was titrated down to a level (1.25μg/ml) comparable to that of 11B8 binding at 10μg/ml and it was found that a Ca^{2+} flux was still generated by ritux but not by 11B8 (data not shown). In summary, the data in Figure 5.2 demonstrates that of the anti-CD20 mAb assessed only type I mAb can induce a Ca^{2+} flux. The kinetics of the flux are similar to that induced through BCR stimulation, however the magnitude of the flux is dependent on the stimulating mAb.

5.2.2 Investigation into the ability of Ramos cells to generate a Ca^{2+} flux through anti-CD20 mAb stimulation

To confirm the results we observed in stimulated SUDHL4 cells, the same panel of mAb were used to stimulate Ramos cells. We found that Ramos cells did not generate

a Ca^{2+} flux through stimulation with type I mAb unless the antibodies were cross-linked with a secondary mAb (data not shown). Therefore all human anti-CD20 mAb (ritux, 7D8 and 11B8) were cross-linked in these experiments with a mouse anti-human IgG (MAH) mAb SB2H2. Likewise, the murine anti-CD20 mAb (1F5, AT80 and B1) were cross-linked by the addition of goat anti-mouse IgG (GAM). Figure 5.3A demonstrates that as found in SUDHL4 cells, only anti-CD20 mAb which are classed as type I induce a Ca^{2+} flux. Upon cross-linking of Ritux, 7D8 and 1F5, 20% of the cell sample shows an increase in the FL5/FL4 ratio. The delay which was observed in SUDHL4 (Figure 5.2) has been eliminated. This may be due to the mAb's inherent ability to redistribute CD20 into lipid microdomains (discussed in Chapter Four), therefore when the secondary mAb is added only minimal grouping of CD20 clusters is required to induce a Ca^{2+} flux. Furthermore, because of the hyper cross-linking of CD20 required in Ramos cells the dependence of the Ca^{2+} flux on mAb affinity displayed by SUDHL4 cells is greatly reduced. This is demonstrated by the minimal difference in flux intensity with ritux compared to 1F5 shown in Figure 5.3A.

Ramos cells were also treated with positive controls, the calcium ionophore ionomycin and by mAb stimulation through the BCR (Figure 5.3A). In the case of Ramos and most B lymphoma cell lines, the surface immunoglobulin is IgM. The calcium profiles obtained (Figure 5.3A) are similar to that for SUDHL4 where ionomycin causes all cells to increase in intracellular calcium and hence 100% of the sample displays an elevated and pro-longed FL5/FL4. Again stimulation of the sIgM results in a larger calcium flux than that induced by type I mAb. Other surface antigens such as CD52 and MHC class II were assessed and even upon hyper cross-linking by the addition of secondary mAb, MAH and GAM respectively, no Ca^{2+} flux was observed.

Unlike SUDHL4 cells where the ritux-induced Ca^{2+} flux reduced out with decreasing concentrations of mAb, the need for hyper cross-linking in Ramos cells results in an apparent reduced dependency on ritux binding but more so on the concentration of the hyper cross-linking mAb. Data in Figure 5.3 B-C demonstrates that decreasing concentrations of ritux have minimal effect on the magnitude of the Ca^{2+} flux when cross-linked with the same amount of MAH. CD20 clustering by ritux or any type I

mAb is an important first step in the generation of a Ca^{2+} flux, but it appears for Ramos cells, that to surpass the critical point or threshold hyper cross-linking is required. This presumably groups the CD20 clusters into larger domains. Therefore it is reasonable to suggest that even at lower concentrations of ritux, sufficient clustering of CD20 occurs so that the hyper cross-linking effects of 20μg/ml MAH can still generate a maximal CD20-mediated Ca^{2+} flux. However, when CD20 is clustered using the same concentration of ritux (10μg/ml) and then hyper cross-linked by the addition of various concentrations of MAH, the flux decreases with decreasing MAH concentration (Figure 5.3C). At 10-20μg/ml MAH concentration, the resulting flux is at approximately 600 FL5/FL4 and does not return to a basal level before 300 seconds. Upon addition of 5μg/ml the flux is beginning to decrease, still maintaining a maxima of approximately 600 but the flux period is curtailed, returning to a basal level 220 seconds after stimulation. At 1μg/ml, the flux is reduced to 500 FL5/FL4 and returns to a basal level 200 seconds after stimulation.

The results shown in Figure 5.3A mirror the data in Figure 5.2A. Of the anti-CD20 mAb assessed only type I mAb could generate a Ca^{2+} flux. However, in contrast to SUDHL4 cells, the magnitude of the flux was not as dependent on the anti-CD20 mAb as cross-linking of the bound mAb was required to generate a flux, which appears to be the determining factor in the kinetics of the resultant flux.

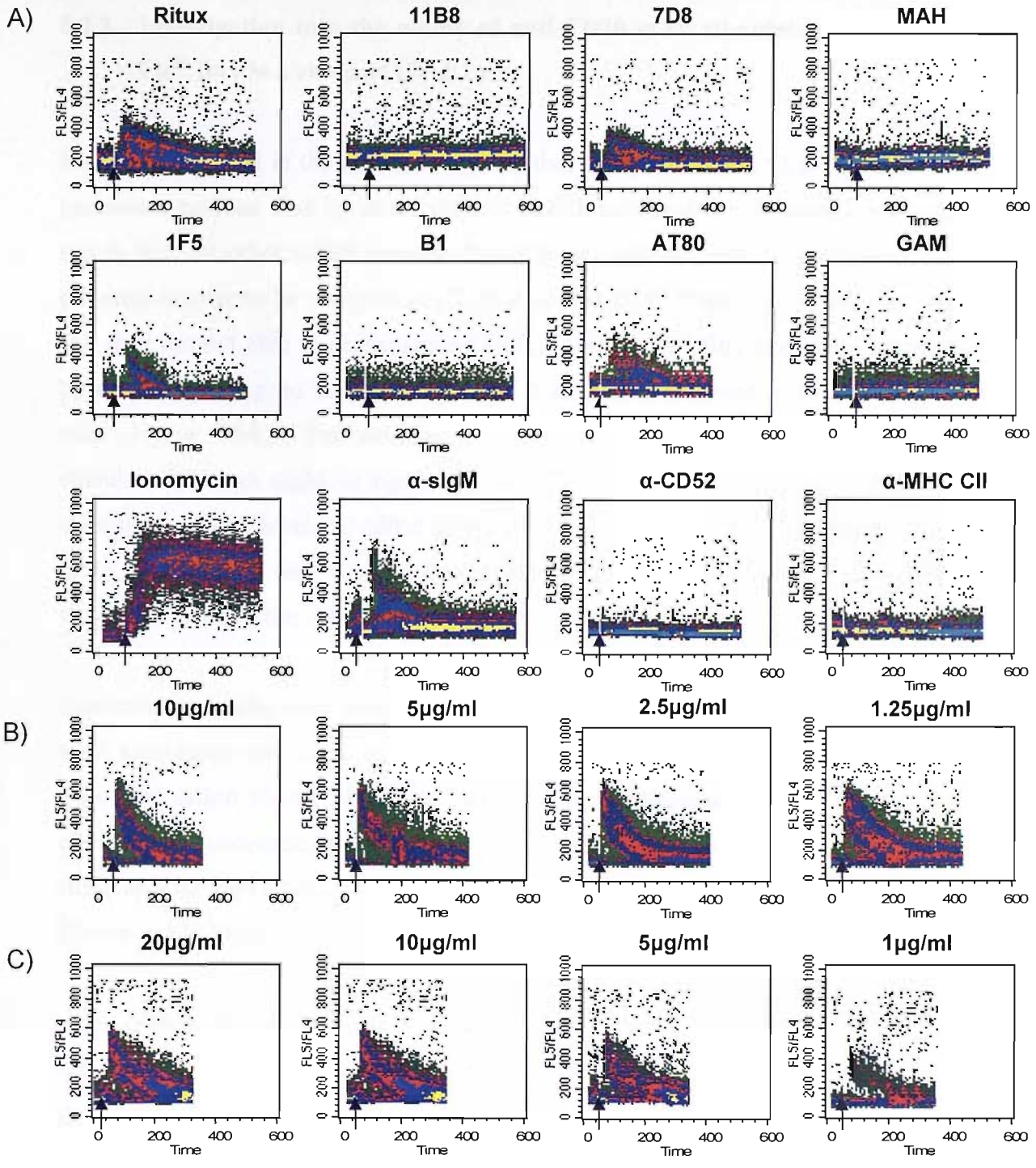

Figure 5.3: mAb stimulation of CD20 can induce a Ca^{2+} flux in Ramos B cell line . $1x10^7$ Ramos cells were labelled with Indo-1 as outlined in Materials and Methods Section 2.9. **A)** Samples were treated with 10μg/ml type I anti-CD20 mAb (ritux, 7D8, 1F5 and AT80), type II mAb (B1 and 11B8), α-CD52 (campath-1H) or α-MHC class II (L243) for 15 minutes at room temperature before being washed in RPMI and resuspended in 500μl pre-warmed 10% RPMI. Addition of a secondary mAb for hyper cross-linking is indicated by the arrow (time shown in seconds) and assessed by flow cytometry. Depending on the isotype either 20μg/ml mouse anti-human IgG (MAH, SB2H2) or goat anti-mouse IgG (GAM, Sigma UK) were added. Samples were also treated with 10μg/ml α-sIgM (M15/8), or 1μM ionomycin. Data shown is representative of three independent experiments. **B)** Ramos cells were treated with various concentrations of ritux for 15 minutes at room temperature before being washed and 20μg/ml MAH added at a time point indicated by the arrow. **C)** Ramos cell were treated with 10μg/ml ritux for 15 minutes at room temperature before being washed and various concentrations of MAH added at the time point indicated by the arrow.

5.2.3 Investigation into the ability of anti-CD20 mAb stimulation to induce a Ca^{2+} flux in a range of B cell lines

Having established in the previous sections that both Ramos and SUDHL4 cells can generate a calcium flux by stimulation of CD20, we decided to investigate whether this is true for other CD20 positive B cell lines. ARH77 cells were shown in the previous chapter to be sensitive to CD20-mediated CDC (Figure 3.4). Here we find that they are not able to demonstrate CD20-mediated Ca^{2+} flux even with extensive hyper cross-linking no shift in the FL5/FL4 ratio was observed in ritux stimulated cells (Figure 5.4A). Furthermore, no signal was observed when the cells were stimulated through sIgM or sIgG. As ARH77 cells have an unusually high MHC class II expression level, the effect of hyper cross-linking the HLA-DR specific mAb, L243, was assessed and was found to have no effect. The only increase in FL5/FL4 was obtained when the cells were stimulated with ionomycin.

Similarly, Raji cells were assessed for their ability to induce a calcium flux through mAb stimulation and found to generate a small but measurable flux upon sIgM and ritux stimulation shown in Figure 5.4B. Again, an increase in FL5/FL4 ratio is observed in ionomycin treated cells. The shift in FL4/FL5 in Raji cells when stimulated through sIgM or cross-linked ritux is not as large as previously observed in Ramos and SUDHL4 cells but is notable compared to the insensitive ARH77 cells.

Another Burkitt's lymphoma B-cell line, BL60 was assessed for its ability to induce a calcium flux through CD20 (Figure 5.5). Upon ionomycin stimulation these cells demonstrated a similar sensitivity to that of Ramos and SUDHL4 cells with 100% of the cells responding to treatment. The similarities between BL60 and Ramos continued as comparable profiles were obtained for the other mAb treatments. Like Ramos cells , treatment with type I anti-CD20 mAb (ritux and 1F5) on their own did not generate a Ca^{2+} signal (data not shown), however after washing and hyper cross-linking with MAH or GAM respectively, a Ca^{2+} flux was observed. The flux generated by ritux cross-linking was smaller in magnitude and demonstrated slightly different kinetics than that in Ramos cells. In BL60 cells the flux does not peak sharply and then fall off but rather maintains the maximum level for 1 minute and is slower to reduce back to a basal level (Figure 5.5). The flux induced by 1F5 cross-

linking is similar to that already observed in Ramos cells with a smaller peak than that induced by ritux but the peak is sharp and is relatively quick to return to a basal level. Similarly, stimulation through sIgM resulted in a quick Ca^{2+} flux, without the need for hyper cross-linking. Once again, stimulation with type II anti-CD20 mAb (11B8 and B1) did not result in the generation of a Ca^{2+} flux even upon hyper cross-linking. In summary, the data shown demonstrates that not all CD20-positive B cell lines can generate a Ca^{2+} flux through type I mAb stimulation but it appears to be cell line specific, with BL60 and Raji generating a response to type I mAb whereas no flux was observed in ARH77 stimulated cells.

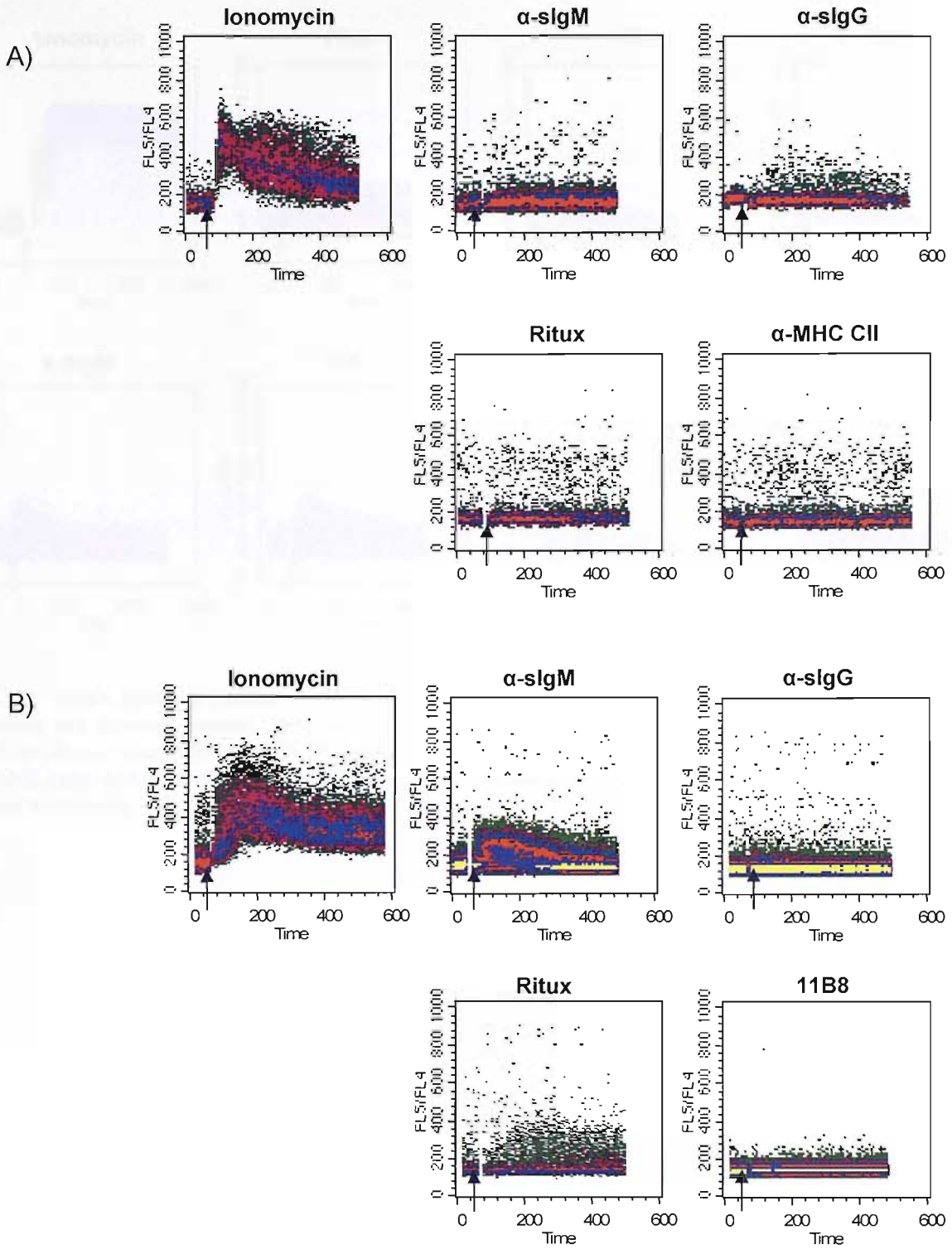

Figure 5.4: The sensitivity of other B cell lines to CD20-mediated Ca^{2+} flux. A) ARH77 cells were treated as outlined in Materials and Methods Section 2.9. Samples were either treated with 1μM ionomycin, 10μg/ml α-sIgM (M15/8), α-sIgG (SB2H2) or with 10μg/ml anti-CD20 mAb Ritux or anti- MHC class II (L243) for 15 minutes at room temperature before being washed in RPMI and treated with either 20μg/ml MAH (SB2H2) or GAM respectively. Time shown in seconds. **B)** Raji cells are treated as outlined in A except that instead of anti-MHC class II, cells were treated with the anti-CD20 mAb 11B8.

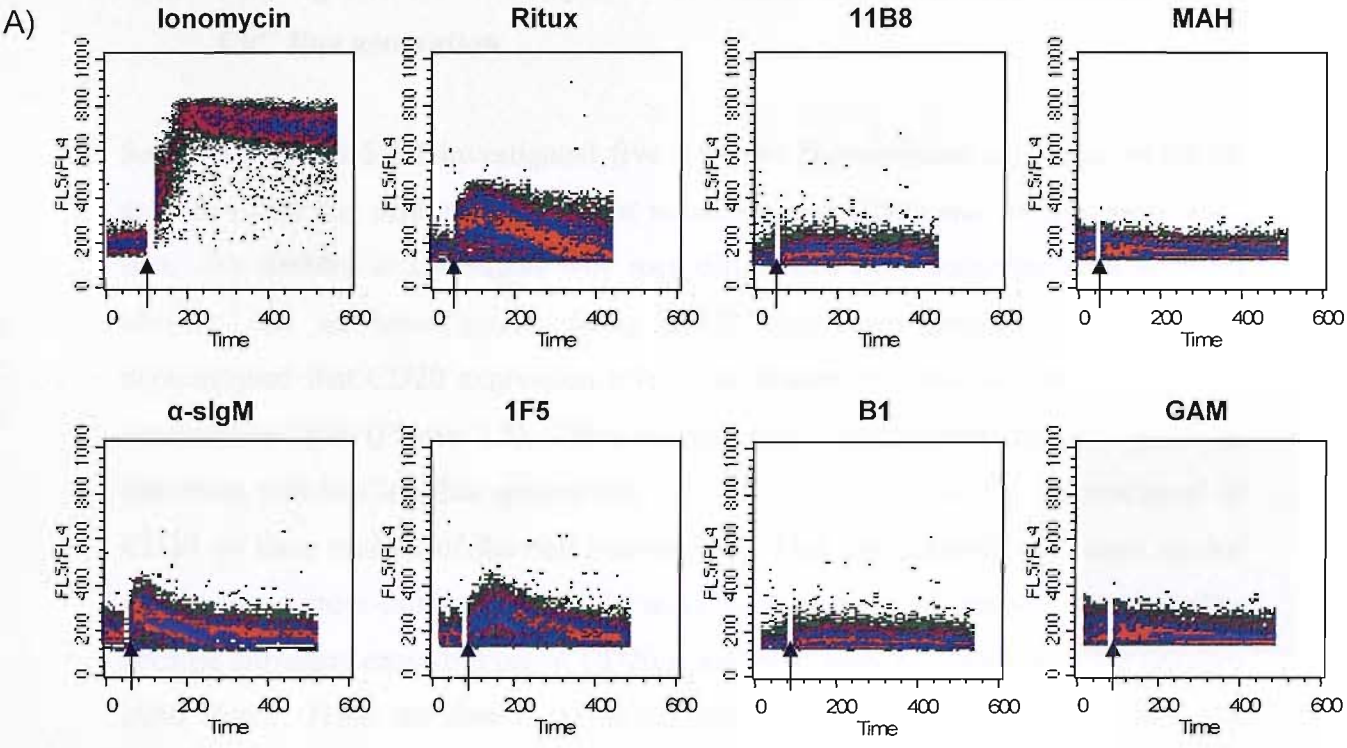

Figure 5.5: Type I mAb can induce a Ca^{2+} flux in BL60 cells. A) $1x10^7$ cells were labelled with Indo-1 as outlined in Materials and Methods Section 2.9. Samples were then treated with either 1μM ionomycin, 10μg/ml α-sIgM (M15/8), or 10μg/ml anti-CD20 mAb for 15 minutes at room temperature before being washed and 20μg/ml secondary mAb added, either MAH (SB2H2) or GAM (Sigma) as the time point indicated by the arrow. Profiles for the samples which are treated with secondary mAb only are also shown.

Cell line	CD20	BCR
SUDHL4	2730.7	596.2*
Ramos	774.6	539.9
BL60	416.8	367.9
Raji	286.9	55.8
ARH77	192.1	57.6

Table 5.1: CD20 and BCR expression levels. The expression level of CD20, sIgM and *sIgG (SUDHL4 only) was assessed in various cell lines. Briefly, $1x10^5$ cells were incubated with either 10μg/ml FITC-labelled ritux (CD20), M15/8 (IgM) or SB2H2 (IgG) respectively before being washed in PBS/BSA/Azide (PBA) and analysed by flow cytometry as outlined in Section 2.6. The values shown are the mean fluorescent intensity (MFI).

5.2.4 Investigation into the importance of CD20 and BCR expression levels for Ca^{2+} flux generation

Sections 5.2.1 to 5.2.3 investigated five different B-lymphoma cell lines which all express CD20 but demonstrate various sensitivities to CD20 and BCR-induced Ca^{2+} flux. We decided to investigate why such differences were occurring with the most obvious line of investigation being CD20 expression level. Chapter three demonstrated that CD20 expression level is an important factor for the induction of complement lysis (Figure 3.5). Here we find that CD20 expression level plays an important role in Ca^{2+} flux generation. SUDHL4 cells express the highest level of CD20 on their surface of the cell lines tested. This may explain why they do not require hyper cross-linking of CD20 by mAb to generate a Ca^{2+} response, presumably because sufficient cross-linking of CD20 is achieved with the addition of the primary mAb alone. From the data in Table 5.1, the hierarchy of CD20 expression is as follows;

SUDHL4 > Ramos > BL60 > Raji > ARH77

On direct comparison of the cell lines that required hyper cross-linking to generate a Ca^{2+} response through type I mAb stimulation (shown in Sections 5.2.2 and 5.2.3), it became apparent that Ramos generated the highest flux, followed by BL60 and Raji and no flux was observed in ARH77 cells. This hierarchy mirrors the hierarchy of CD20 expression shown above.

The same correlation was observed in BCR induced Ca^{2+} Flux. Interestingly, the hierarchy of BCR expression correlates with CD20 expression. SUDHL4 express the highest level of BCR, albeit sIgG, followed by the sIgM-expressing Ramos, BL60, ARH77 and Raji cells (Table 5.1). Again, the magnitude of the Ca^{2+} flux is reflected in the expression level with Ramos generating the greatest signal of the sIgM expressing cell lines, followed by BL60. Interestingly, even though Raji and ARH77 express a comparable level of sIgM, only the former demonstrates a Ca^{2+} flux upon CD20 stimulation. However is should be noted that, Raji cells express a higher level of CD20 supporting the suggestion the CD20 expression level is an important factor for effective flux generation. Together, the data suggests that the expression level of

the BCR and more so CD20, are important factors for the effective generation of a Ca^{2+} flux through type I mAb stimulation.

5.2.5 Effect of CD20 knockdown in SUDHL4 cells

Having established in the previous section that CD20 expression level is a critical parameter for effective Ca^{2+} signalling, we wanted to investigate whether the ability of SUDHL4 cells to generate a Ca^{2+} flux without the need for hyper cross-linking was due to the fact that it has a higher CD20 expression level rather than due to its expression of surface IgG instead of IgM. To this end, CD20 expression was reduced using siRNA targeting CD20 as previously published [48]. 24hrs after the cells were nucleofected™ (Ambion) with siRNA against CD20 (outlined in Section 2.10), the expression of CD20 was assessed by flow cytometry using FITC labelled ritux and was found to have reduced by more than 50% (see Figure 5.6A). Control cells i.e. cells which were transfected with a mock siRNA had an MFI of 1107 compared to 456 in CD20 siRNA treated cells. The specificity of the CD20 siRNA was demonstrated by the fact that the expression of sIgG was not affected by the CD20 siRNA (Figure 5.6A).

From Figure 5.6B, it would appear that CD20 expression is the determining factor with regard to the requirement for hyper cross-linking to generate a Ca^{2+} signal. In control SUDHL4 cells (mock transfected with siRNA) ritux can generate a Ca^{2+} signal without the need for hyper cross-linking. However, in CD20 siRNA treated cells the signal was ablated suggesting that as the CD20 expression level drops, hyper cross-linking is required to generate a signal. As SUDHL4 cells express sIgG instead of sIgM, cross-linking of ritux (a chimeric mAb of human IgG1 isotype) was unfeasible in these studies as addition of a MAH mAb would therefore also stimulate the BCR directly leading to a Ca^{2+} flux. Therefore, the murine type I anti-CD20 mAb AT80, was utilised. AT80 is also a type I anti-CD20 mAb which can generate a Ca^{2+} flux in SUDHL4 cells without the need for hyper cross-linking (see Figure 5.2A). As AT80, in contrast to ritux, is a murine mAb, the addition of a hyper cross-linking agent was possible. Figure 5.6B (panel iv) shows that AT80 can generate a Ca^{2+} flux in control cells without the need for cross-linking, however in siRNA treated cells, there is no Ca^{2+} signal generated by the addition of AT80 alone (panel v).

A)

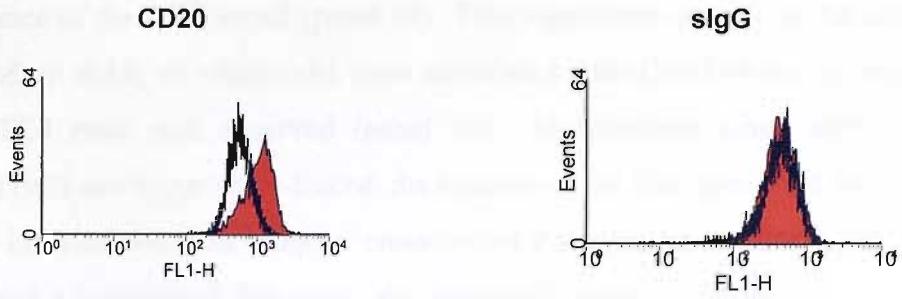

B)

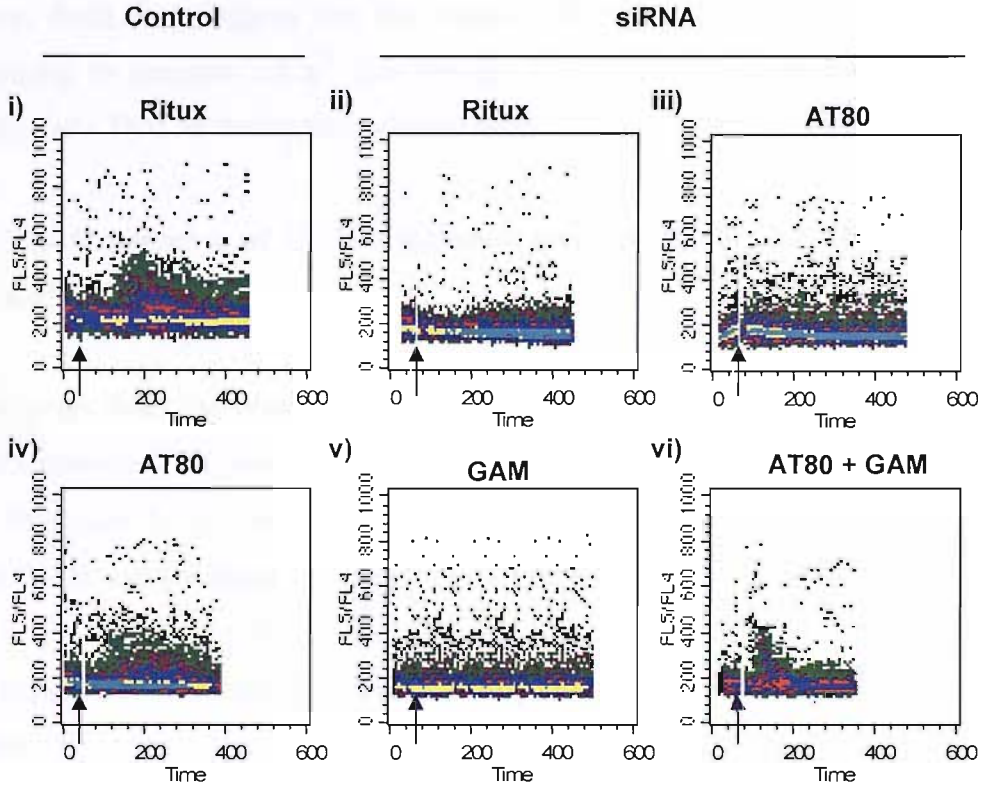

Figure 5.6: Knockdown of CD20 in SUDHL4 cells using siRNA. SUDHL4 cells were transfected as suggested by Amaxa Nucleofection™ guidelines outlined in materials and methods Section 2.10. Briefly, $2x10^6$ cells were incubated in 100µl solution T and nucleofected with 600nM siRNA primer against CD20 (CCACTCTTCAGGAGGATGT [48]) or 600nM negative control primer (on program setting G16). Samples were then resuspended in 1.5mls of pre-warmed 10% RPMI and kept in a 12-well plate at 37°C and 5% CO_2. **A)** After 24hrs, cells were harvested and the expression level of CD20 and sIgG were assessed by flow cytometry using FITC labelled ritux and SB2H2 respectively using the method outlined in Section 2.6. Control samples are shown in red and siRNA samples are overlaid in black. **B)** Cells were labelled with INDO-1 as outlined in Section 2.9. Samples were treated with 10µg/ml ritux, AT80 or 20µg/ml GAM in the absence of cross-linking or samples were pre-treated with 10µg/ml AT80 before being washed and 20µg/ml GAM added at the time point indicated by the arrow.

From the data, it is evident that hyper cross-linking of AT80 results in the reappearance of the Ca^{2+} signal (panel vi). This signal was not due to the addition of the secondary mAb, as when cells were stimulated with GAM alone, no increase in the FL5/FL4 ratio was observed (panel iii). Furthermore, when siRNA treated SUDHL4 cells are hyper cross-linked, the kinetics of the flux generated are similar to the rapid kinetics observed in hyper cross-linked Ramos cells (Figure 5.3A). Similar kinetics and a heightened flux were also observed when 1F5, a murine IgG2a mAb which does not give a large flux in SUDHL4 cells with mAb stimulation alone as shown in Figure 5.2, was cross-linked in normal SUDHL4 cells (data not shown). In summary, these data suggest that the reason SUDHL4 cells do not require hyper cross-linking to generate a Ca^{2+} flux through CD20 stimulation is due to the high expression of CD20 on the surface of these cells.

5.2.6 The importance of CD20 expression level for CD20 and BCR mediated Ca^{2+} flux

Following on from the observation that CD20 induced Ca^{2+} flux is dependent on CD20 expression level; we decided to look at a titration of CD20 siRNA in Ramos cells. In Figure 5.7A Ramos cells were treated with 400, 100 and 25nM siRNA against CD20 and the same concentration of negative control siRNA. As expected, CD20 surface expression decreased with increasing concentration of specific siRNA. CD20 expression level was measured by flow cytometry using FITC labelled ritux. The data in Figure 5.7A show that the MFI decreased from 756 (control) to 589 (25nM), 410 (100nM) and 346 (400nM). Again, the level of BCR expression was not altered, demonstrating the specificity of the siRNA.

The effect of CD20 expression knockdown is evident from the data shown in Figure 5.7B. Cross-linking of ritux by MAH mAb resulted in a large, rapid Ca^{2+} flux in control cells. This flux was reduced with increasing concentrations of siRNA where the FL5/FL4 peak went from 600 (control) to 590 (25nM), 500 (100nM) and 400 (400nM). The effect of CD20 expression level was also investigated in cells stimulated with 11B8 or via the BCR (Figure 5.7B).

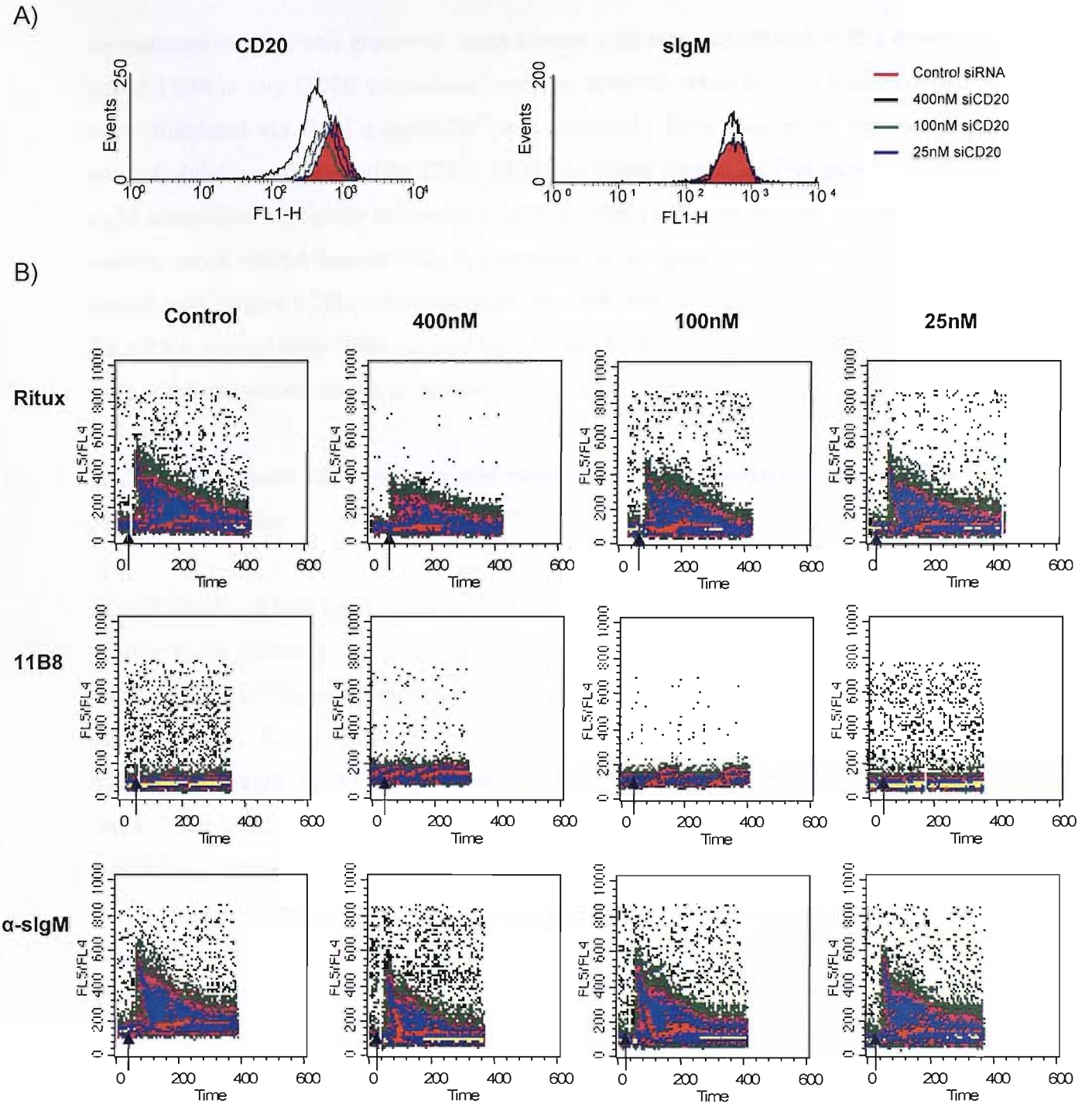

Figure 5.7: The effect of CD20 knockdown on CD20- and BCR-mediated calcium flux in Ramos cells. Ramos cells were treated as outlined in the previous figure except that different concentrations of CD20 siRNA were used as indicated, 400nM negative control siRNA was also used. **A)** After 24hrs the expression levels of CD20 and sIgM were assessed by flow cytometry using 10μg/ml ritux and M15/8 respectively. Expression levels of the control cells are shown in red and expression level of the siRNA treated cells are overlaid in the colours indicated. **B)** Cells were labelled for Ca^{2+} signalling analysis as outlined in Materials and Methods Section 2.9. Samples were either treated with 10μg/ml α-sIgM or pre-treated with 10μg/ml ritux or 11B8 for 15 minutes at room temperature before being washed. 20μg/ml MAH was added at time points indicated by the arrow and assessed by flow cytometry.

As expected no flux was generated when Ramos cells were stimulated with a cross-linked 11B8 at any CD20 expression level. In contrast, when control Ramos cells were stimulated via sIgM a rapid Ca^{2+} was observed. Even though the expression level of sIgM is not affected by CD20 siRNA as stated above, the flux generated by sIgM stimulation is slightly decreased in siRNA treated cells. If the flux generated in control, mock siRNA treated cells is compared to that generated in 400nM siRNA treated cells (Figure 5.7B), it is evident that the area underneath the curve is smaller in the siRNA treated cells. This reduced area reverts back to the profile seen in control cells as the amount of siRNA is decreased from 400 to 25nM.

5.2.7 Involvement of store operated channels in CD20-mediated calcium flux generation

In cells there are two main classifications of ion channels - voltage-gated and non-voltage gated channels. Lymphocytes are believed to mediate calcium flux via the latter [17]. One of the main categories of non-voltage gated channels is store operated channels. Ca^{2+} flux through store operated channels or capacitative Ca^{2+} entry was first demonstrated in 1992 by Penner and colleagues [208]. They showed that intracellular Ca^{2+} store depletion resulted in the activation of a Ca^{2+} selective current called I_{CRAC} (calcium release activated current) resulting in refilling of the stores with Ca^{2+} from the extracellular space. To investigate the possible involvement of these channels in CD20-mediated Ca^{2+} flux, we assessed the effect of extracellular calcium chelation by EGTA on the Ca^{2+} signal.

Generally, the initial release of Ca^{2+} from intracellular stores and the subsequent Ca^{2+} influx from the extracellular space is too rapid in succession to be distinguished experimentally and hence one composite flux is observed. Chelation of the extracellular calcium using EGTA, segregates the two fluxes as Ca^{2+} influx from the extracellular domain cannot occur. Therefore in EGTA treated cells, the flux observed is due to the release of Ca^{2+} from intracellular stores alone. Here in Figure 5.8 Ramos cells were stimulated through anti-sIgM mAb stimulation or by cross-linking ritux or 11B8-bound CD20. As demonstrated in Figure 5.9, both ritux and sIgM stimulated cells generate a Ca^{2+} flux to a FL5/FL4 peak of 600. To investigate the effect of extracellular calcium chelation, samples were pre-incubated in media

supplemented with 1.5mM EGTA (which binds Ca^{2+} at a molar ratio of 2:1). At this concentration, the EGTA is in 4 fold molar excess of the estimated free ion Ca^{2+} concentration in RPMI supplemented with 10% serum (0.37mM). Upon reintroduction of Ca^{2+} by the addition of 3mM $CaCl_2$, indicated by the red arrow in Figure 5.8B, another flux is generated which we believe to be calcium influx or I_{CRAC}, replenishing the intracellular stores.

A shift in the FL5/FL4 ratio is also observed in EGTA chelated non mAb-treated cells, this shift is probably due to the calcium 'tick-over' normally occurring in the cell. As a wide range of intracellular enzymes require Ca^{2+} to function, there is a constant low level of Ca^{2+} (116nM) maintained in lymphocytes [209]. As one of the major sources of free Ca^{2+} ions for this process is from the extracellular space, when this source is effectively removed by EGTA chelation the cell becomes Ca^{2+} 'starved'. This 'starvation' can be overcome when Ca^{2+} is reintroduced by the addition of extracellular $CaCl_2$, then Ca^{2+} ions enter the cell generating a flux in the absence of other external stimuli.

The calcium flux in SUDHL4 cells was also assessed for the involvement of store operated channels (Figure 5.8C and D) and found to mirror the results detailed above in Ramos cells. Figure 5.8C shows that stimulation of cells through either sIgG or CD20 (ritux) without hyper cross-linking resulted in a Ca^{2+} flux similar to that observed earlier in Figure 5.2. After chelation of the extracellular Ca^{2+} with EGTA, a division of the flux is visible into what we believe to be the release of Ca^{2+} from intracellular stores (first peak) and influx of Ca^{2+} from the extracellular domain (second peak). Again a slight increase in the FL5/FL4 ratio was observed in chelated, non mAb-treated cells which was attributed to calcium 'tick-over' in the cell. There are slight discrepancies between samples such as the FL5/FL4 peak in BCR stimulated Ramos cells in Figure 5.9A compared to the initial peak in BCR stimulated Ramos cells in B. These discrepancies are due to intra-assay variation such as temperature differences. In summary, these results demonstrate that the flux normally observed in cells stimulated through CD20 or the BCR is a composite of calcium being released from intracellular stores and calcium entering the cell from the extracellular domain. The main feature of a calcium store operated calcium entry is the depletion and subsequent repletion of Ca^{2+} in intracellular stores.

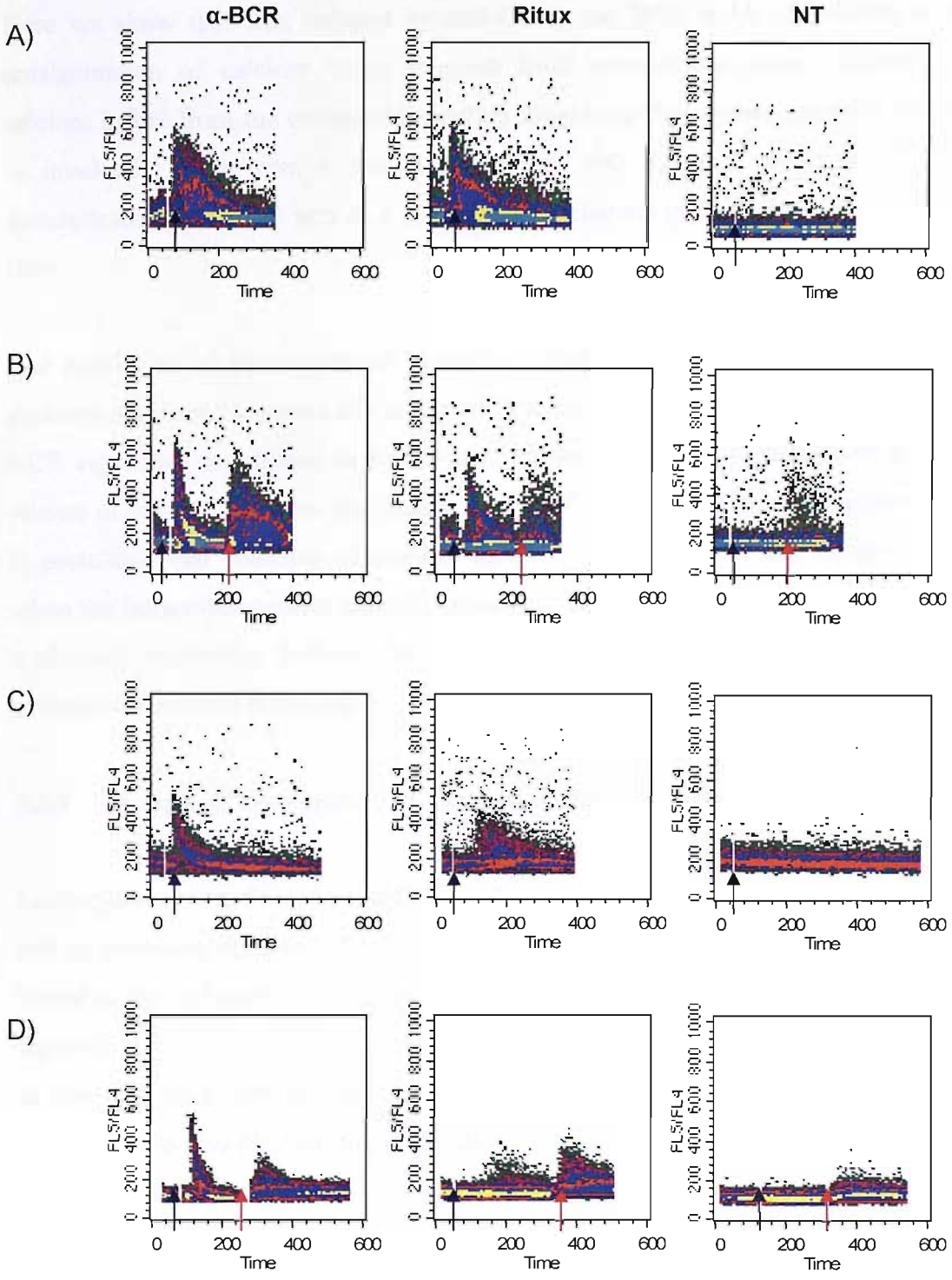

Figure 5.8: The effect of extracellular calcium chelation on the calcium flux induced by CD20 and BCR mAb stimulation. Ramos and SUDHL4 cells were labelled with Indo-1 as outlined in Materials and Methods Section 2.9. **A)** Ramos cells are treated with either 10μg/ml M15/8 or pre-treated with 10μg/ml ritux or not for 15 minutes at room temperature before being washed and stimulated with 20μg/ml MAH at the time indicated. **B)** Before mAb binding, samples are pre-treated with 1.5mM EGTA for 15 minutes at room temperature before addition of the 10μg/ml mAb at the indicated time point (black arrow). After approximately 2 minutes 3mM $CaCl_2$ was added to the sample, indicated by the red arrow. **C + D)** SUDHL4 cells were treated as outlined in A and B respectively except that samples did not require hyper cross-linking and were therefore directly stimulated be the addition of anti-CD20 mAb. Results shown are representative of two independent experiments.

Here we show that flux induced by anti-CD20 and BCR mAb stimulation is the amalgamation of calcium being released from intracellular stores, followed by calcium influx from the extracellular milieu suggesting that a store operated channel is involved. These results are in agreement with Li and colleagues [48] who demonstrated that CD20 acts as a store operated channel in Ramos and BJAB B cell lines.

The regulation of store operated channels is still not understood. The signalling pathway involved in release of Ca^{2+} from intracellular stores has been elucidated for BCR signalling as outlined in Figure 5.1. However, little is known about how the release of calcium activates ion channels for Ca^{2+} influx at the plasma membrane. It is postulated that cessation of calcium influx from the extracellular domain occurs when the intracellular stores are fully replenished [58]. However, whether this involves a physical interaction between the stores and the plasma membrane or whether a pathway is involved is unclear.

5.2.8 The role of Fc receptors in CD20 mediated Ca^{2+} flux

Leukocytes express four types of Fc receptor – stimulatory receptors RI, RIII and RIV and an inhibitory receptor RII. These receptors can bind the Fc domain of antibodies bound to the cell surface or aggregated Ig. The importance of Fc receptors has been reported in BCR-mediated Ca^{2+} signalling. Fc gamma RIIβ, an inhibitory Fc receptor, is reported to down-regulate BCR-mediated Ca^{2+} signalling [201]. To investigate whether FcRs also play an important role in CD20-mediated Ca^{2+} flux, we compared whole IgG and $F(ab')_2$ derivatives of ritux mAb in their ability to induce a Ca^{2+} signal. Because the absence of the Fc domain is the only difference between IgG and $F(ab')_2$, the binding affinity should not be affected (Dr R. French, Personal Communication). Furthermore, in Chapter Four, it was demonstrated that ritux IgG and $F(ab')_2$ could redistribute comparable amounts of CD20 into TX-100 insoluble rafts (Figure 4.12).

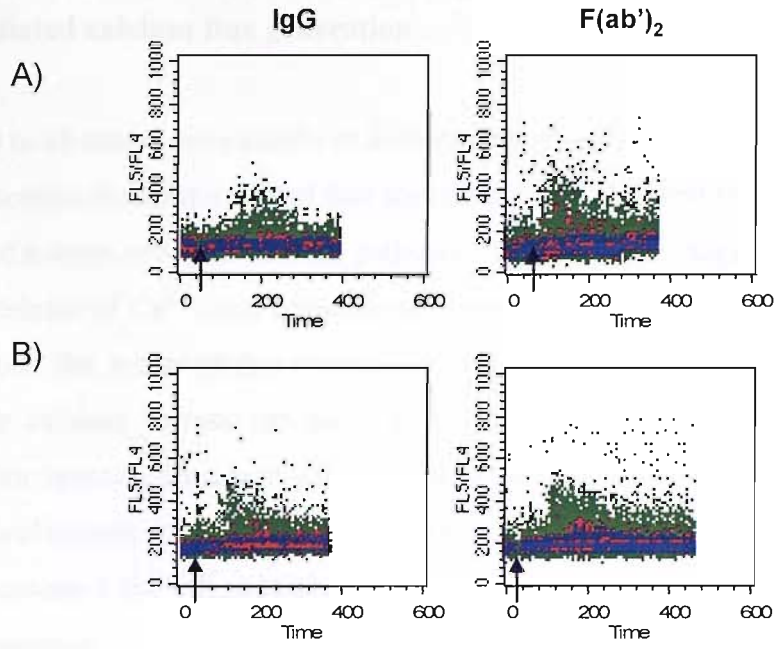

Figure 5.9: The ability of anti-CD20 mAb fragments to induce a Ca^{2+} flux. SUDHL4 cells were prepared for calcium signalling analysis as outlined in Materials and Method section 2.9. **A)** Cells were treated with either 10μg/ml ritux IgG or $F(ab')_2$ at the indicated time point. **B)** Cells were treated as outlined in A except the mAb used was 7D8.

The data shown in Figure 5.9 illustrates a comparison of SUDHL4 cells stimulated with ritux IgG and its $F(ab')_2$ counterpart and it can be seen that the Ca^{2+} flux increased when cells were treated with $F(ab')_2$ compared to whole IgG i.e. in the absence of Fc domains. This would suggest that binding of the whole IgG by the inhibitory FcRIIβ reduces the mAb ability to generate a Ca^{2+} flux. To confirm our findings another anti-CD20 type I mAb was investigated and it was found that the same result was obtained when cells were stimulated with 7D8. Figure 5.9 shows that 7D8 IgG and $F(ab')_2$ generated a Ca^{2+} flux in SUDHL4 cells without the need for cross-linking. However, in the absence of its Fc domain, the signal generated was greater in magnitude. Unfortunately Ramos cells could not be assessed due to the requirement for hyper cross-linking of CD20 to generate a flux, cross-linking was not possible due to the absence of an Fc domain on $F(ab')_2$ fragments. An attempt was made to cross-link the $F(ab')_2$ using an anti-kappa light chain mAb but this itself induced a flux through sIgM. Collectively, the data in Figure 5.8 demonstrates that like BCR-mediated calcium mobilisation, Fc receptor interactions are indeed important in CD20-mediated Ca^{2+} signalling.

5.2.9 Investigation into the involvement of a signalling pathway in CD20-mediated calcium flux generation

How CD20 mAb stimulation results in a change in cytosolic calcium remains unclear. In the last section we demonstrated that stimulation of CD20 and the BCR resulted in activation of a store operated calcium pathway. There are two stages in this pathway; the first is release of Ca^{2+} from intracellular stores followed by the influx of Ca^{2+} into the cell from the extracellular space. The pathway involved in BCR mediated intracellular calcium release has been well studied and is outlined in Figure 5.1. However, for reasons discussed earlier in Section 5.1, there is limited data on the possible involvement of a signalling pathway in CD20-induced Ca^{2+} flux. For this reason we assessed the effect of a range of kinase inhibitors on the flux induced by CD20 stimulation.

Several reports have suggested that there is a direct link between CD20 and the BCR signalling pathways [48, 91, 92]. The most convincing evidence comes from CD20 knockdown studies using siRNA which show a reduction in the Ca^{2+} flux induced through BCR stimulation [48]. We observed similar results to those reported (Figure 5.7). Therefore, we decided to target specific kinases which are reported to be important in BCR signalling pathways and assess their effect on CD20-mediated Ca^{2+} flux generation. One of the earliest kinases activated in BCR-mediated Ca^{2+} signalling is Syk (splenic tyrosine kinase). Syk is thought to interact with the ITAM motif in CD79β chain cytoplasmic domain [17]. When Ramos cells were pre-treated with a Syk inhibitor, the flux induced by hyper cross-linked ritux was completely ablated compared to the flux induced by ritux when hyper cross-linked on non pre-treated Ramos cells (Figure 5.10A). Furthermore, inhibition of Syk lead to the complete abrogation of the Ca^{2+} flux induced through sIgM stimulation (Figure 5.10B). The effect of phosphoinositide 3-kinase (PI3K) was assessed next by the use of the specific inhibitor LY294002 which inhibits ATP binding to the catalytic subunit of the kinase. PI3K phosphorylates phosphatidylinositol lipids at the plasma membrane which can then act as anchoring points for the recruitment of pleckstrin homology (PH)-domain containing signalling molecules such as the protein kinase Akt [210]. From Figure 5.10 it is evident that PI3K also appears to play a pivotal role in the induction of CD20-mediated calcium flux where inhibition through LY294002 results

in a dramatic reduction in both the peak and longevity of the flux induced by cross-linked ritux. Again, the same effect is observed in sIgM induced flux with a clear reduction in signal upon LY294002 treatment.

To probe kinases which are further upstream of PI3K and Syk kinase, we targeted the Src family kinases. After BCR cross-linking, phosphorylation of Src family kinases (Lyn, Lck, Fyn, Blk and Fgr) is believed to be the earliest event in BCR signalling [22]. Activity of Src kinases is inhibited by PP2 which competes with ATP for binding at the ATP site. Surprisingly, in marked contrast to the results seen in Syk and PI3K inhibition, inhibition of Src kinase led to elongation of the Ca^{2+} flux. The flux has a similar FL5/FL4 maximum to ritux treated control cells but the level of intracellular Ca^{2+} does not decrease over the 10 minutes assessed compared to a return to baseline after 3 minutes in control cells (Figure 5.10A). This effect was also observed in sIgM stimulated cells. The reason for this is currently unclear. As the flux plateaus at a maximum level similar to that for cells stimulated in the absence of inhibitors, it suggests that the first stage of the store operated calcium pathway is occurring i.e. release from intracellular stores, but that the subsequent stage i.e. influx of Ca^{2+} from the extracellular domain, is hindered. Researchers have postulated that once the intracellular stores have been replenished, calcium influx is terminated [58]. Therefore, the elongation in the flux might be due to either the hindered ability of intracellular stores to either take up calcium or to signal for the cessation of Ca^{2+} influx.

Src kinases, PI3K and Syk kinase are all involved in the early stages of BCR-signalling cascades (reviewed in [17]). Therefore, our next line of investigation was in the involvement of kinases activated at a later stage of BCR signalling such as members of the mitogen activated protein kinases (MAPK) family, extracellular-signal-regulated kinase (ERK) and P38. ERK activation in B cells has been associated with a variety of cellular responses as diverse as proliferation and apoptosis [173]. We assessed its involvement in Ca^{2+t} signalling by the use of the specific inhibitors PD980059 and U0126. The mode of inhibition of these inhibitors is still somewhat controversial, although it has been suggested that they work by allosteric inhibition, binding outside the ATP binding site making ERK unable to become activated by upstream kinases [211].

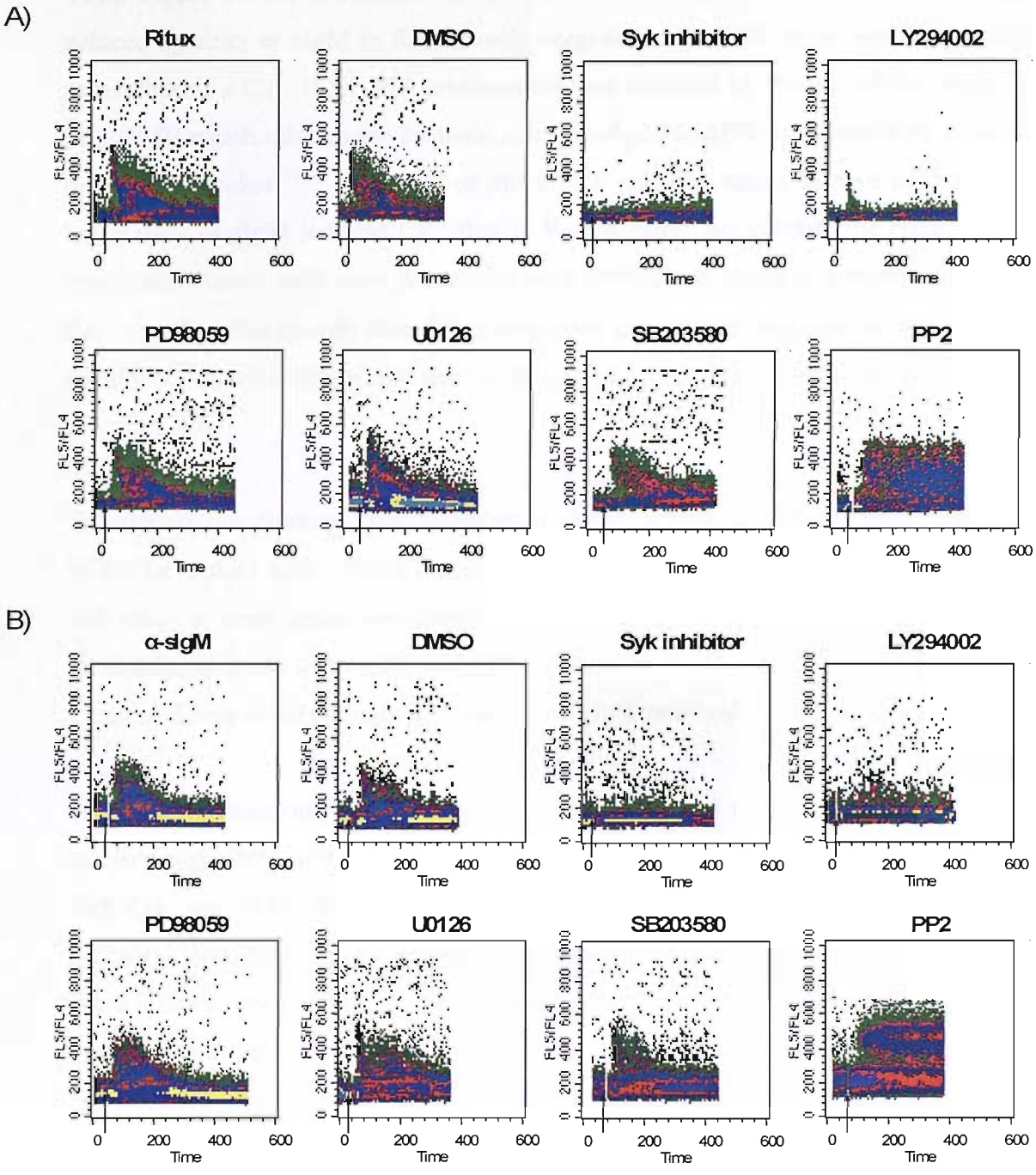

Figure 5.10: The involvement of intracellular kinases in Ca^{2+} flux generation in Ramos cells. $1x10^7$ Ramos cells were treated as outlined in Materials and Methods Section 2.9. **A)** Samples were treated or not with 10μM Syk inhibitor, LY294002 (PI-3 kinase inhibitor), PD98059 (MEK inhibitor), UO126 (ERK 1/2 inhibitor), SB203580 (p38 inhibitor), PP2 (Src kinase inhibitor) or 1% DMSO. After 20 minutes at room temperature 10μg/ml ritux was added for 15 minutes at room temperature before being washed and 20μg/ml MAH added at the time point indicated by the arrow. **B)** Samples were treated as outlined in A except that instead of ritux, 10μg/ml α-sIgM M15/8 was added. The results in A and B are representative of two independent experiments.

From Figure 5.10 it is evident that neither inhibitor had an effect on the Ca^{2+} flux induced by ritux or sIgM in Ramos cells suggesting that ERK is not involved in the generation of a Ca^{2+} flux. P38 involvement was assessed by the use of the inhibitor SB203580 which inhibits the catalytic activity of p38 MAPK by competitive binding in the ATP pocket [212]. Inhibition of this kinase was also found to have no effect on either ritux or sIgM induced Ca^{2+} flux in Ramos cells. To validate the effect of the inhibitors, control cells were pre-treated with DMSO and found to generate the same Ca^{2+} signal as that in cells stimulated with mAb only confirming that the effect of the inhibitors was specific and not due to the solvent the inhibitors were reconstituted in (Figure 5.10).

To support our findings, we investigated if the inhibitors had the same effect in SUDHL4 treated cells. From Figure 5.11, it is clear that the flux generated by sIgG and ritux is once again completely ablated by Syk inhibition, reduced by PI3K inhibition, unhindered by ERK and P38 inhibition and prolonged by inhibition of Src kinases. These results mirror our observations in Ramos cells.

Here, we demonstrate for the first time that CD20 and the BCR utilise the same calcium signalling pathway. From the results in Figure 5.10 and 5.11, it is evident that Syk and PI3K are involved in the first stage of the store operated calcium pathway, signalling for the release of Ca^{2+} from intracellular stores as inhibition of these kinases results in no flux. In contrast, inhibition of Src family kinases results in an elongated Ca^{2+} flux. This suggests that it is distal to the release of Ca^{2+} from intracellular stores and is possibly involved in signalling for shutdown of Ca^{2+} influx from the extracellular space.

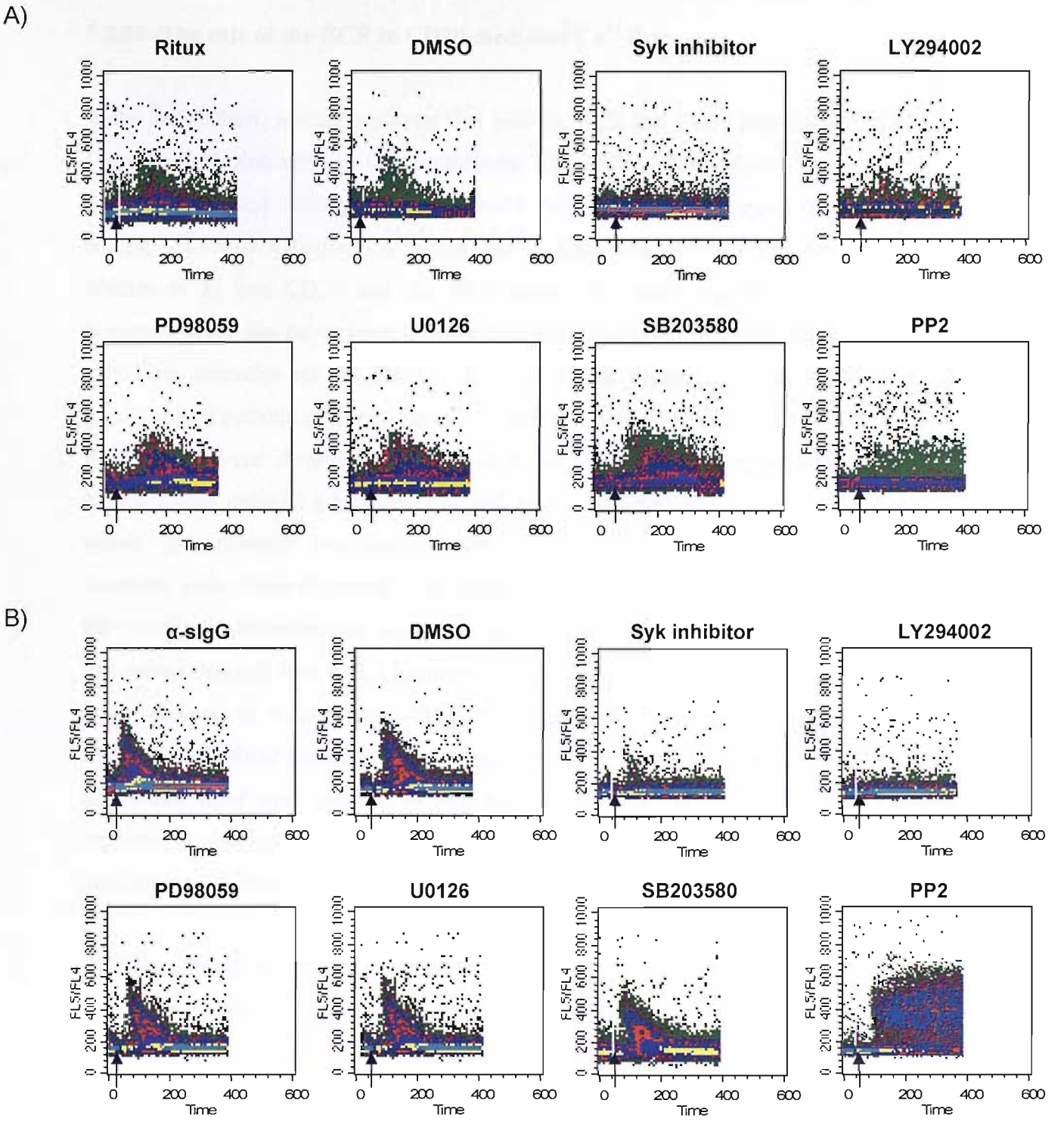

Figure 5.11: Involvement of intracellular kinases in the generation of a Ca^{2+} flux in SUDHL4 cells. $1x10^7$ SUDHL4 cells were treated as outlined previously in Materials and Methods section 2.9. **A)** Samples were treated or not with 10μM Syk inhibitor, LY294002 (PI-3 kinase inhibitor), PD98059 (MEK inhibitor), UO126 (ERK 1/2 inhibitor), SB203580 (p38 inhibitor), PP2 (Src kinase inhibitor) or 1% DMSO for 20 minutes before addition of 10μg/ml ritux for 15 minutes at room temperature after which, samples were washed and 20μg/ml MAH added at the time point indicated by the arrow. **B)** Samples were treated as outlined in A except that instead of ritux, 10μg/ml α-sIgG SB2H2 was added.

5.2.10 The role of the BCR in CD20-mediated Ca^{2+} flux

In the last section, we demonstrated that both the BCR and CD20 signalling pathways show marked similarity in the intracellular kinases that they employ to generate a Ca^{2+} flux. Li and colleagues have recently published data to suggest that the BCR requires CD20 for effective Ca^{2+} signalling [48]. Furthermore, it has been suggested by Mathas et al that CD20 and the BCR share cell death signalling pathways [91]. However, there has never been a direct link made between the dependence of CD20 signalling cascades on the BCR. We decided to probe this possibility by the generation of a stable derivative of the Ramos cell line which does not express sIgM. Ramos cells were chronically stimulated through sIgM by treatment with the mAb M15/8 which induced a high level of cell death. However, the surviving population which 'grew through' expressed a lower level of BCR on their surface compared to untreated cells. After chronically stimulating the cells a further two times, only 3% of the resulting cells expressed sIgM and did not increase over time (data not shown). We called this cell line Rx3. Extensive phenotyping of the cell line was performed and compared to Ramos cells (refer to Appendix I). Of the 11 surface antigens assessed, only three demonstrated a major difference between Ramos and Rx3 cells. CD79 and sIgM were reduced to near background level in Rx3 cells whilst CD19 expression was increased above wild type Ramos CD19 expression. The FACS profiles for CD20 and sIgM expression are shown in Figure 5.12A.

To demonstrate that these cells maintained normal signalling pathways, we firstly looked at the ability of CD20 to redistribute into TX-100 insoluble domains by the method outline in Section 2.8.2. Data in Figure 5.12A demonstrates that Rx3 cells can redistribute CD20 into TX-100 insoluble domains to the same extent as wild type Ramos cells. As seen in the previous chapter (Figure 4.11) type I mAb effectively redistribute CD20 with ritux being more efficient than 1F5 whereas virtually no insolubility is observed in cells treated with type II mAb, B1 or 11B8. We also looked at the ability of the cells to signal for cell death through CD20 stimulation. This is further discussed in Section 6.2.9 but we found that Rx3 cells were sensitive to anti-CD20 mAb-mediated cell death. The level of cell death was comparable to Ramos cells (Figure 6.18).

Comparison of the calcium profiles generated by Ramos and Rx3 cells, suggested that CD20 requires the BCR to generate a Ca^{2+} flux. As seen earlier in Figure 5.2 and demonstrated in Figure 5.12C, Ramos cells are highly sensitive to ionomycin treatment with 100% of the cells responding. Stimulation through sIgM and CD20 by hyper cross-linking ritux also resulted in generation of a Ca^{2+} flux (Figure 5.12C). However, even though Rx3 cells displayed high sensitivity to ionomycin, their ability to generate a Ca^{2+} flux through sIgM or CD20 stimulation was ablated with no increase being observed in the ratio of FL5/FL4 (Figure 5.12D). These data imply that the BCR is pivotal to CD20 calcium signalling. Even though the level of CD20 expressed on the surface is slightly reduced in Rx3 cells, based on data shown in Figure 5.3B where 1.25 μg/ml of ritux could generate a Ca^{2+} flux, this reduction in expression alone would not be sufficient to ablate the Ca^{2+} flux. This result is in conflict with reports that CD20 ectopically expressed in transfected cell lines such as human T cells and CHO cells [45, 48] can induce a Ca^{2+} flux through anti-CD20 mAb stimulation as these cells do not express the BCR. We investigated the ability of murine NS/0 cells transfected with CD20. These cells were shown in chapter three, Figure 3.5, to express a high level of CD20 on the surface. However, NS/0 clone 2 cells failed to induce a Ca^{2+} flux when stimulated with up to 50 μg/ml ritux or when hyper cross-linked with MAH (data not shown). The difference between our results and other reports is not clear. It is possible in transfected T cells that CD20 could associate with the T cell receptor for calcium signalling. There is no clear explanation as to why a flux was observed in transfected CHO cells and not NS/0 cells, however the method and dye used to assess the Ca^{2+} flux was different and therefore there could be a difference in the sensitivity of the assays.

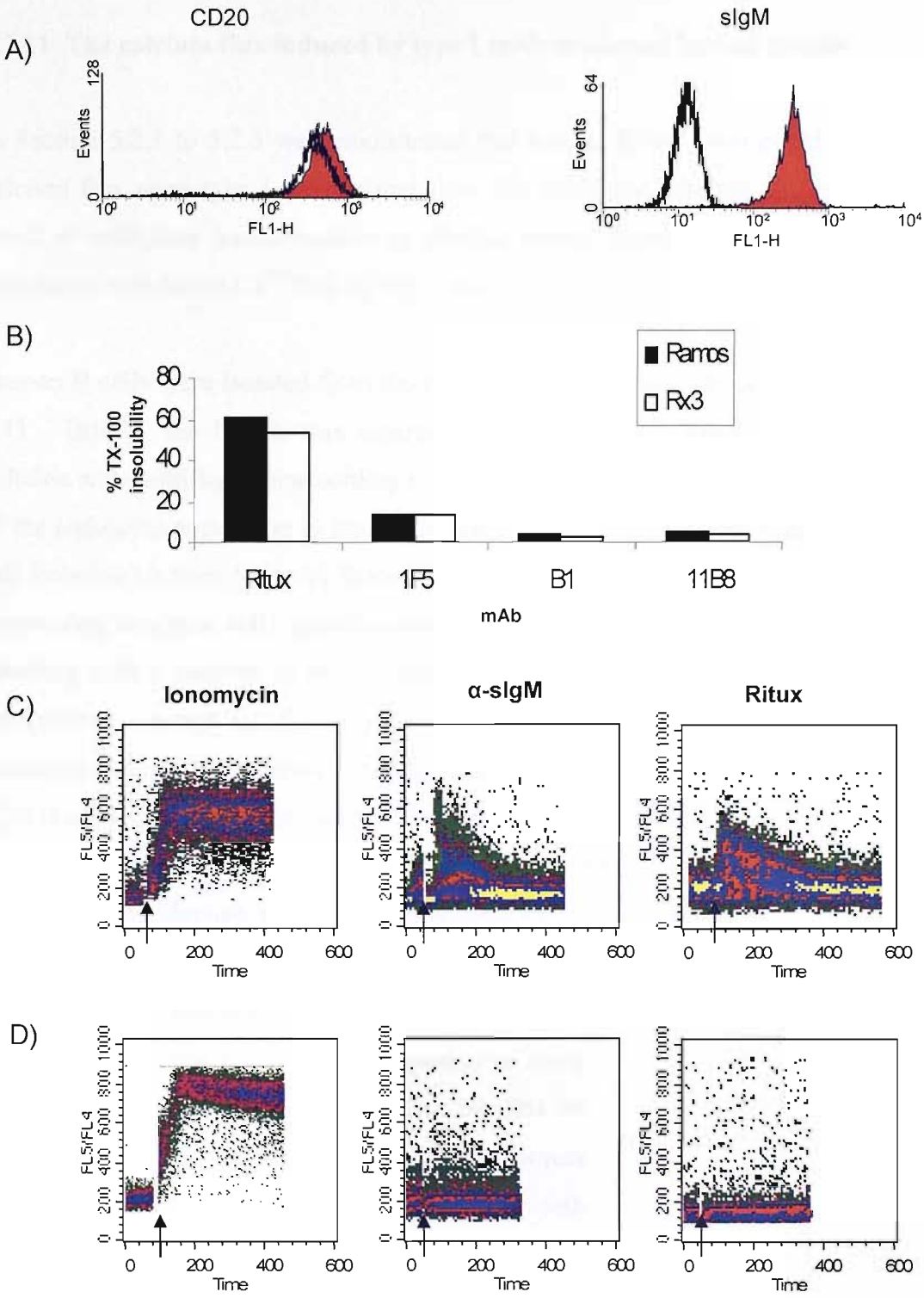

Figure 5.12: The BCR is required for CD20-mediated calcium flux generation. Ramos cells were chronically treated with α-sIgM and BCR-negative cells were selected to generate a stable derivative of Ramos cells which lack BCR expression known as Rx3 cells. **A)** Expression levels of CD20 and sIgM was measured on Ramos and Rx3 cells as outlined in Section 2.6. Briefly, $1x10^5$ cells were incubated with 10μg/ml FITC-labelled ritux or m15/8 for 15 minutes at room temperature before being washed and analysed by flow cytometry. The expression level in Ramos is shown in red and the expression level of Rx3 is overlaid in black. **B)** Rx3 cells can still redistribute CD20 into TX-100 insoluble domains. The method used is outlined in materials and methods section 2.8.2. **C)** Ramos cells were prepared for analysis of calcium signalling as outlined in Section 2.9. Samples were treated with either 1μM ionomycin or 10μg/ml α-sIgM (M15/8) or ritux. **D)** Rx3 cells were treated as outlined in C.

5.2.11 The calcium flux induced by type I mAb in normal human B cells

In Section 5.2.1 to 5.2.3 we demonstrated that human B cell lines could generate a calcium flux upon type I mAb stimulation. We wondered whether this event was a result of malignant transformation or whether normal human B cells could also be stimulated to induce a Ca^{2+} flux by type I mAb.

Human B cells were isolated from the blood of healthy donors as outlined in Section 2.11. Briefly, the lymph was separated from the plasma using a lymphoprep™ solution and centrifugation according to manufacturer's instructions. As only 10-15% of the leukocyte population in human peripheral blood is B cells we used a MACS B cell isolation kit from Miltenyi Biotech to further purify the B cells. T cells, NK cells, monocytes, dendritic cells, granulocytes, platelets and erythroid cells are removed by labelling with a cocktail of biotinylated CD2 (adhesion receptor on T cells), CD14 (macrophage receptor), CD16 (low affinity IgG receptor on NK cells and granulocytes), CD36 (receptor expressed on platlet cells), CD43 (T cell marker) and CD235a (Glycophorin A expressed on erythrocytes) antibodies which are subsequently removed by labelling with anti-biotin 'MicroBeads'. After passing the B cell solution through the separation column twice, the B cells were 85% pure as measured by CD20 positivity. The expression level of CD20 (MFI of 480) and sIgM (MFI 440) was assessed by flow cytometry using FITC labelled ritux and M15/8 respectively. These levels were comparable to the expression level in the Ramos B cell line (see Table 5.1). The cells were labelled with Indo-1 and assessed for their ability to induce a Ca^{2+} flux through CD20 stimulation as outlined in Section 2.8. From Figure 5.13 it is evident that normal B cells can induce a Ca^{2+} flux upon stimulation of CD20 or sIgM. Hyper cross-linking of CD20 was required to generate the flux. This requirement is in accordance with our earlier observations in Section 5.2.2 that B cell lymphoma lines which express lower levels of CD20 need hyper cross-linking of CD20 to generate a Ca^{2+} signal where both normal human B cells and Ramos cells express comparable levels of CD20.

It is important to note that the isolated B cell samples used in these experiments still contained 15% non B cells most likely made up of macrophages, NK cells and T cells which are all known to express Fc receptors [213, 214].

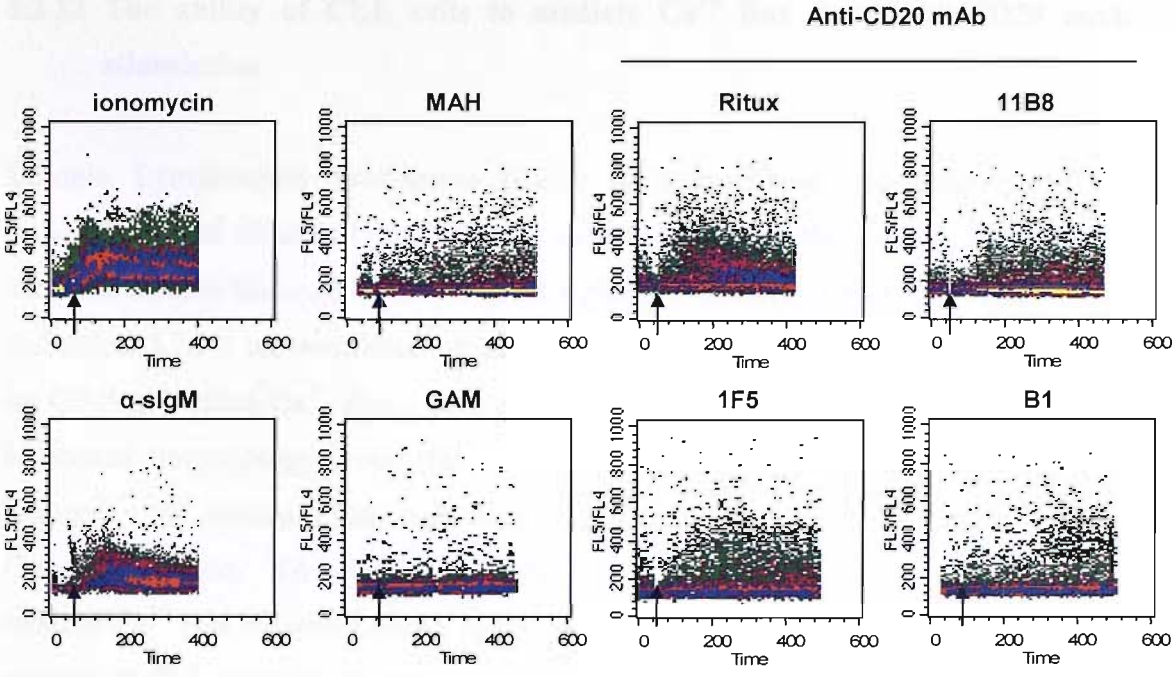

Figure 5.13: The ability of normal human B cells to generate a Ca^{2+} flux. Normal human B cells were isolated from donors blood as per manufacturer guidelines of the MACS B cell isolation kit (Miltenyi Biotech) outlined in Section 2.11. $5x10^6$ of the isolated B cells labelled with INDO-1 as outlined in Materials and Methods Section 2.9. Samples were stimulated with either 1μM ionomycin, 10μg/ml α-sIgM or were pre-treated with 10μg/ml anti-CD20 mAb (ritux, 11B8, 1F5 and B1) for 15 minutes before being washed and 20μg/ml of the relevant secondary mAb added. Profiles for samples treated with 20μg/ml secondary mAb only are also shown.

Therefore, the cross-linking mAb used in these experiments were commercial $F(ab')_2$'s in an attempt to minimise the effect of mAb Fc-FcR interactions which have been reported to induce calcium signalling [215]. However, it is evident from the profiles generated by the type II mAb B1 and 11B8 in Figure 5.13 that not all the non-specific effects were eliminated. In all our previous work, type II mAb were unable to generate a Ca^{2+} flux. We believe that this non-specific effect is due to the Fc domain of the anti-CD20 mAb interacting with Fc receptors in the 15% of contaminating non-B cells. As 11B8 generated a larger signal compared to B1, it suggests that it may be due to 11B8 being a humanised mAb (IgG1) compared to the murine B1 mAb, thus the human Fc domain of 11B8 would be expected to interact more effectively with the 15% non specific population of human cells. On comparison of the type I and type II stimulated cells in Figure 5.13, it is clear that hyper cross-linking of type I mAb generate a large and rapid response whereas hyper cross-linking of type II mAb results in a slow, smaller and we would suggest non-specific response. In line with data from B-cell lines, stimulation through sIgM by the addition of M15/8 stimulates a Ca^{2+} flux without the need for hyper cross-linking.

5.2.12 The ability of CLL cells to mediate Ca^{2+} flux upon anti-CD20 mAb stimulation

Chronic Lymphocytic Leukaemia (CLL) is a condition characterised by an accumulation of abnormal lymphocytes in the blood and the bone marrow. One common disease feature is a low level of sIgM [216]. Given our previous observations in Section 5.2.10, we wondered whether this reduction in sIgM would have an effect on CD20-mediated Ca^{2+} flux. Primary CLL samples were kindly provided by the Molecular Immunology group (formerly the HIT group), Cancer Sciences Division, University of Southampton and were utilised under approval from the Ethical Committee Board. To investigate whether the sensitivity of CLL samples to CD20-induced Ca^{2+} flux is compromised by the lack of IgM expression we decided to assess a range of CLL samples of varying CD20 expression level. The expression level of CD20, sIgM and sIgD were measured by direct staining and flow cytometry as detailed in Section 2.6. The data in Table 5.2 demonstrate that even though CLL cells lack sIgM expression, they can express normal levels of CD20.

Patient A, B and C were assessed for their ability to induce a Ca^{2+} flux through sIgM, sIgD or hyper cross-linked CD20 stimulation (Figure 5.14A). We found that aside from their ability to induce an increase in the FL5/FL4 ratio with ionomycin treatment, the cells were only able to generate a signal through sIgD stimulation in our experiments. To ensure that the reason why CD20 did not generate to Ca^{2+} signal in these cells was not due to an inability to cluster CD20, a TX-100 assay was performed as outlined previously in Section 2.8.2. The data in Figure 5.14A demonstrates that samples from Patients A, B and C could all generate the same CD20 redistribution pattern as Ramos cells. In accordance with earlier TX-100 studies (see Figure 4.11), we found that in CLL samples, ritux treatment conferred the highest level of TX-100 insolubility followed by 1F5 and then B1. The ability of B1 to translocate CD20 into these insoluble domains was increased in CLL samples compared to the Ramos B cell line. The reason for this is unclear although it could be related to differences in the plasma membrane composition of the cells.

Based on the expression level data shown in Table 5.2, sIgM in these cells is expressed at approximately the same level as sIgD. Thus, it may be surprising that

sIgD can generate a Ca^{2+} signal whereas sIgM stimulation cannot. However, it should be noted that the stimulation of these two surface receptors in these studies is not directly comparable due to the use of a polyclonal anti-sIgD mAb compared to a monoclonal anti-sIgM mAb. In section 5.2.2 we suggested that hyper cross-linking of CD20 was required in lower CD20 expressing cell lines as a threshold of cross-linking needed to be overcome before a Ca^{2+} flux was observed. Hence, sIgD is most likely cross-linked to a greater extent than sIgM and therefore more likely to overcome the threshold required to generate an increase in the FL5/FL4 ratio.

To assess whether hyper cross-linking of sIgM could over come this threshold we hyper cross-linked sIgM bound mAb (M15/8) by the addition of a goat anti-mouse IgG (GAM). Patient D demonstrated a high expression level of CD20 and a comparably low expression of both sIgM and sIgD (Table 5.2). From the profiles depicted in Figure 5.15 it is clear that hyper cross-linking of sIgM is necessary to generate a Ca^{2+} flux in low IgM expressing CLL cells. When the cells from Patient D were stimulated with polyclonal anti-sIgD a Ca^{2+} flux was generated. In contrast, stimulation with monoclonal anti-IgM resulted in no flux being generated. However, when α-sIgM mAb were hyper cross-linked by the addition of GAM (α-sIgM+GAM), a large increase in the FL5/FL4 ratio was observed which was not observed in cells treated with GAM alone, indicating that greater cross-linking of sIgM is required to surpass the threshold and generate a Ca^{2+} response. In addition, we decided to query whether the use of a polyclonal antibody to hyper cross-link ritux-bound CD20 could achieve a similar result. To this end, 20 μg/ml goat $F(ab')_2$ anti-human IgG was added to ritux treated cells but in this case it was found to make no difference as no increase in FL5/FL4 ratio was observed.

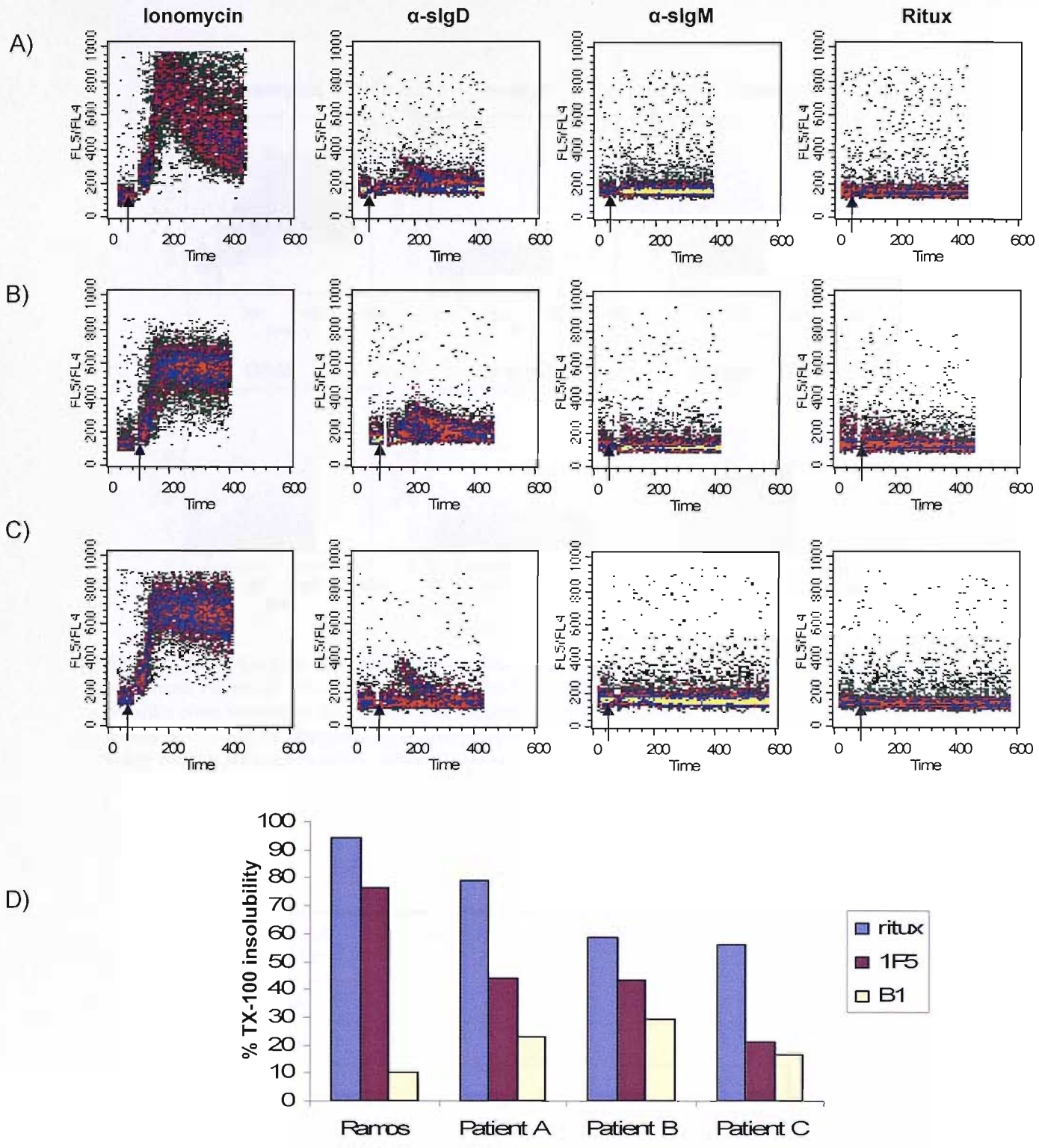

Figure 5.14: CLL cells do not generate a CD20 calcium signal. A) $1x10^7$ primary CLL cells from Patient A were labelled with Indo-1 as outlined in Materials and Methods Section 2.9. Samples were stimulated with either 1μM ionomycin, 10μg/ml α-sIgM (M15/8) or α-sIgD (goat $F(ab')_2$ anti-human IgD, Southern Biotech) or samples were pre-treated with 10μg/ml ritux for 15 minutes before being washed and 20μg/ml MAH added at a time point indicated by the arrow. **B + C)** Primary CLL samples from 2 other patients (Patients B and C respectively) were treated as outlined in A. **D)** The ability of anti-CD20 mAb to redistribute CD20 into TX-100 insoluble domains was assessed by flow cytometry as outlined in Section 2.8.2. Briefly, cells were treated with 10μg/ml FITC labelled mAb, either ritux, 1F5 or B1 for 15 minutes at 37°C before washing and dividing into 2. One half was maintained on ice in PBS, whilst the other half was treated with 1 % TX-100 for 15 minutes on ice. Samples were washed and assessed by flow cytometry.

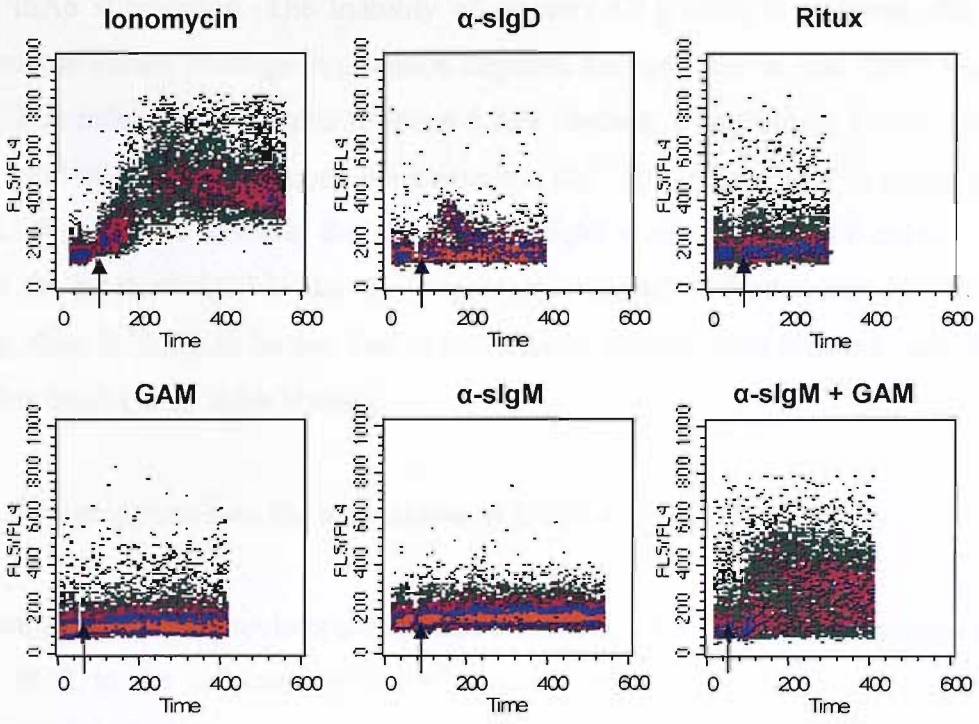

Figure 5.15: CLL cells can generate a calcium flux through sIgM with hyper cross-linking. CLL cells from Patient D were labelled with Indo1-1 as outlined in Materials and Methods Section 2.9. Samples were stimulated with either 1μM ionomycin, 10μg/ml α-sIgM or α-sIgD or samples were pre-treated with 10μg/ml ritux or α-sIgM before being washed and 20μg/ml of either GAH (SIGMA) or GAM were added respectively. Sample treated with 20μg/ml GAM only is also shown.

Patient/ cell line	CD20	sIgM	sIgD
A	622.8	49.6	15.44
B	474.4	18.24	21.12
C	122.28	21.6	22.36
D	458.1	23.7	20.26
Ramos	746.2	402.9	10.62

Table 5.2: Phenotype of CLL samples. $1x10^5$ cells were labelled with 10μg/ml of either FITC labelled ritux (CD20), M15/8 (sIgM) or mouse anti- human IgD (Pharmingen) for 15 minutes at room temperature before being washed and analysed by flow cytometry.

In summary these data show that CLL cells are unable to generate a Ca^{2+} flux through CD20 mAb stimulation. The inability of primary CLL cells to generate this flux supports our earlier findings in the BCR negative Rx3 cell line in that CD20 requires the BCR to induce a Ca^{2+} signal (Section 5.2.9). Indeed, it appears CLL cells, despite a low level of sIgM expression, can generate a Ca^{2+} flux when sIgM is hyper cross-linked. We propose however that the level of sIgM is critical to CD20 induced Ca^{2+} flux, if the level of sIgM is too low to generate a signal without the need for cross-linking, then it likely to be too low to sufficiently interact with CD20 to generate a Ca^{2+} flux upon CD20 mAb binding.

5.2.13 Investigation into the association of CD20 with the BCR

The data shown in the previous section and Section 5.2.9 demonstrate the requirement of the BCR in the induction of a Ca^{2+} flux through CD20 stimulation. To assess whether the dependence of CD20 on the BCR was due to association of CD20 with the BCR, FRET was utilised. In Section 4.2.8 we discussed how FRET could be used to depict the proximity of surface antigens, with a FRET signal only being generated when the mAb bound to antigens were less than 10 nm apart. In section 4.2.8.1 and in Figure 5.16A a FRET signal of 19.2 is generated when CD20 is ligated with ritux (ritux + ritux) but no signal in Ramos cells was observed when CD20 was bound by type II mAb, 11B8. For reasons discussed in Section 4.2.8.1 and 4.2.8.4, we suggest that this FRET is a reflection of CD20 redistributing into rafts. Interestingly, there was a high FRET signal of 51.6 when cells were assessed for sIgM homo-association (M15/8 + M15/8). Here the data in Figure 5.16A suggests however, that in Ramos cells sIgM only associates with CD20 when CD20 is bound by a type I mAb. A FRET signal of 20.1 is observed when cells were co-ligated with ritux and anti-sIgM mAb compared to 0 when cells were co-ligated with 11B8 and anti-sIgM. This data implies that CD20 and the BCR only associate when CD20 is redistributed into rafts by type I mAb.

We have shown previously in this chapter that Ramos cells require hyper cross-linking to generate a Ca^{2+} signal through CD20 (Section 5.2.2). To reflect this, we added the hyper cross-linking mAb MAH to the FRET samples to investigate if there was any effect on the interaction between CD20 and sIgM. As ritux is a chimeric

mAb and M15/8 is murine, the addition of MAH only hyper cross-linked CD20. Intriguingly we found that CD20 and the BCR actually dissociated upon CD20 hyper cross-linking as shown in Figure 5.16B. It is evident from the data that this dissociation was a time dependent event which began almost immediately after mAb addition; after two minutes, the FRET was decreased 50% compared to the original FRET (i.e. before addition of MAH), beyond this point the decrease was less rapid with a further 10% decrease after 5 minutes. At 20 minutes there was an 80% decrease in the FRET signal initially observed. CD20 and BCR homo-association (ritux + ritux and M15/8 + M15/8 respectively) were not affected by the addition of MAH. In addition, dissociation of BCR and CD20 as detected by FRET, did not occur over time in the absence of hyper cross-linking (data not shown). To ensure that this was not a cell line specific phenomena, we investigated whether the same dissociation occurred in other cell lines. Unfortunately as SUDHL4 cells induce a Ca^{2+} flux through CD20 without the need for hyper cross-linking we could not use these cells for this study. Therefore, we investigated if the dissociation occurred in Raji cells which like Ramos cells can generate a Ca^{2+} flux upon CD20 hyper cross-linking (Figure 5.4B). Even though the dissociation is reduced compared to that seen in Ramos cells, the kinetics data shown in Figure 5.16C suggests that the dissociation of CD20 and BCR over time is not a cell line dependent event as it also occurs in Raji cells.

Our results are in agreement with a report by Deans and colleagues [47] who demonstrated by fluorescent microscopy that CD20 and the BCR can associate in Ramos cells upon CD20 stimulation. However, they found that this association was transient where rapid dissociation of the BCR from CD20 occurred after BCR mAb stimulation but not CD20 mAb stimulation. In contrast, our FRET experiments involved CD20 and sIgM mAb ligation for 15 minutes prior to flow cytometry analysis and an association was still observed. Furthermore we found that dissociation of CD20 and the BCR only occurred upon hyper cross-linking of CD20.

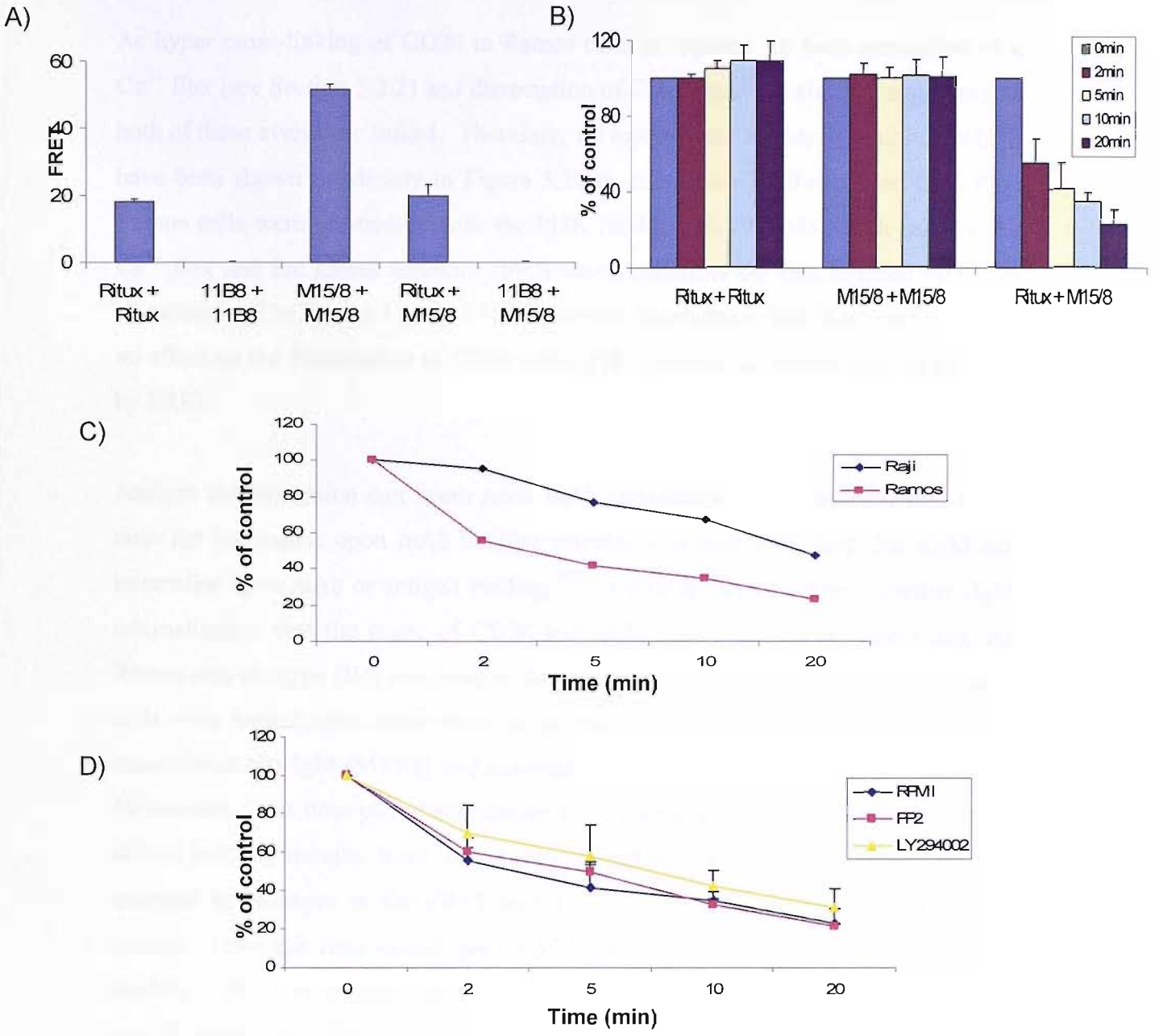

Figure 5.15: CD20 and sIgM associate upon Type I mAb binding and dissociate upon hyper cross-linking. **A)** FRET analysis was performed as outlined in Materials and Methods Section 2.8.3. Briefly, Ramos cells were labelled with a either 10μg/ml unlabelled, FITC or CY5 labelled Ritux, 11B8 or M15/8 for 15 minutes at room temperature before being washed and analysed by flow cytometry. The FRET value was calculated using the formula outlined in section 2.8.3.2. Data shown are mean and standard error of two independent experiments **B)** For the kinetics study, samples were analysed after washing (0 minutes), followed by the addition of 20μg/ml MAH (SB2H2) and analysed at the indicated time points. Values shown are calculated as a % of the FRET at the initial time point (0 Minutes=100%). Values shown are the mean and standard deviation of at least three independent experiments. **C)** Ramos and Raji cells were assessed for the association and dissociation between ritux-bound CD20 and sIgM (M15/8) as measured by FRET. Values shown are calculated as a % of the FRET as measured at the initial time point. **D)** The effect of inhibitors on the association/dissociation of ritux-bound CD20 and m15/8-bound sIgM was assessed. Briefly, samples were pre-treated or not for 30 minutes at room temperature with either 10μM PP2 (Src kinases inhibitor) or LY294002 (PI-3 kinase inhibitor) before addition of mAb as outlined in A. After washing, samples were analysed before and after addition of 20μg/ml SB2H2. Values shown are calculated as a % of the FRET measured at the initial time point. Data shown is the mean and standard error of two independent experiments.

As hyper cross-linking of CD20 in Ramos cells is required for both generation of a Ca^{2+} flux (see Section 5.2.2) and dissociation of CD20 from the sIgM, it suggests that both of these events are linked. Therefore, we assessed the effects of inhibitors which have been shown previously in Figure 5.10 to affect the CD20-mediated Ca^{2+} flux. Ramos cells were pre-treated with the PI3K inhibitor (LY29004) which reduces the Ca^{2+} flux and Src kinase inhibitor (PP2) which enhances the flux induced by CD20 stimulation. The data in Figure 5.16D however demonstrate that these inhibitors had no effect on the dissociation of CD20 and sIgM compared to control cells as detected by FRET.

Antigen internalisation can occur upon mAb stimulation. It is reported that CD20 does not internalise upon mAb binding whereas it is well published that sIgM can internalise upon mAb or antigen binding [217]. Therefore we wondered whether sIgM internalisation was the cause of CD20 and sIgM dissociation. To assess this, the Ramos anti-idiotype (ID) was used to detect sIgM expression. In Figure 5.17 Ramos cells were treated with either ritux, polyclonal anti-IgM (Goat anti-human IgM) or monoclonal anti-IgM (M15/8) and assessed for sIgM internalisation over a period of 60 minutes. This time period was chosen to be comparable to the FRET assay which allows mAb to initially bind for 15 minutes before the cells are washed and then assessed for changes in the FRET signal over 20 minutes for the effect of cross-linking. Over this time period, poly-IgM induced a 60% loss of anti-idiotype mAb binding. This was presumably due to internalisation of sIgM. Similarly, the mAb M15/8 internalised 20% of sIgM but the anti-CD20 mAb ritux had no effect on sIgM expression. In order to block the internalisation of sIgM a method previously published to stop endocytosis of cell-bound mAb using 2-deoxyglucose (DOG) and sodium azide was utilised [192]. From Figure 5.17B it is evident that when Ramos cells were pre-treated with DOG/azide the internalisation induced by poly-IgM mAb was completely blocked compared to non-treated cells. Moreover, we found that internalisation of sIgM was not the cause for the apparent dissociation of CD20 and the BCR as this event (depicted by a decrease in FRET in Figure 5.17C) was not affected by the presence of DOG/azide.

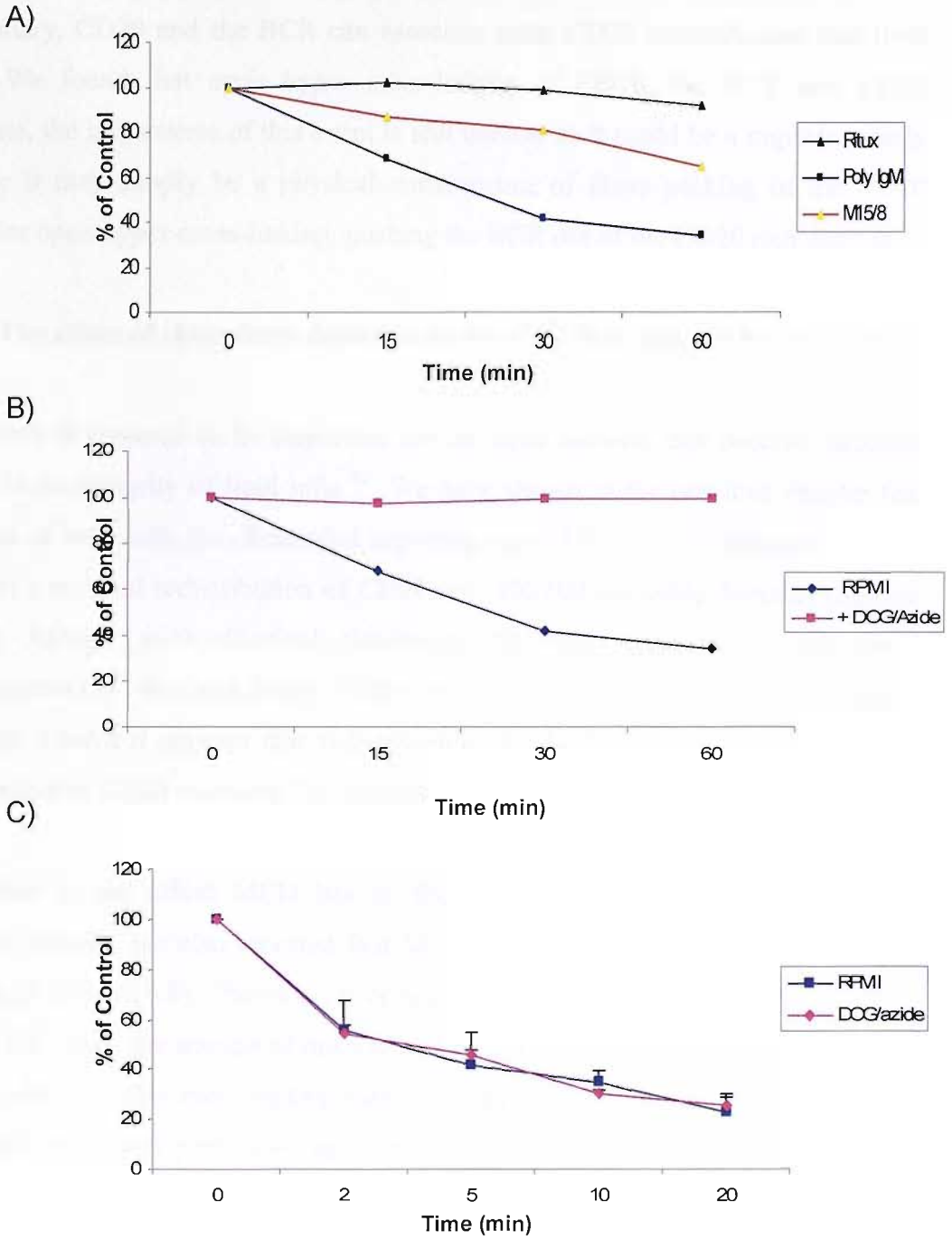

Figure 5.17: The dissociation of the sIgM from CD20 is not due to internalisation. A) $1x10^6$ Ramos cells were treated as outlined in Materials and Methods Section 2.12. Briefly cells were stimulated with either 10μg/ml α-sIgM (M15/8) or goat anti-sIgM (Jackson Immunoresearch) or were pre-bound with 10μg/ml ritux for 15 minutes at room temperature before being washed and 20μg/ml MAH added. All samples were maintained at 37°C. Aliquots were removed at the indicated time point and 10μg/ml FITC-labelled anti-Ramos idiotype mAb (ZL16/1) was added for 15 minutes before being washed and analysed by flow cytometry. Data shown is represented as % of initial MFI at time point 0. **B)** Ramos cells were treated with Goat anti-human IgM for the indicated time points in the presence and absence of 50mM 2-deoxyglucose and 15mM sodium azide. After harvesting cells were treated with 10μg/ml ZL16/1 for 15 minutes at room temperature before being washed and analysed. Data shown is represented as % of initial MFI at 0 Minutes **C)** Samples were pre-treated or not with 2-deoxyglucose/ sodium azide and assessed for the effect of dissociation of ritux-bound CD20 and M15/8-bound sIgM as measured by FRET. Data shown is mean and standard error of two independent experiments where the values are calculated as % of FRET at the initial time point 0 which was set at 100%.

In summary, CD20 and the BCR can associate upon CD20 redistribution into lipid rafts. We found that upon hyper cross-linking of CD20, the BCR and CD20 dissociate, the importance of this event is still unclear as it could be a important early event or it may simply be a physical consequence of close packing of the CD20 molecules upon hyper cross-linking, pushing the BCR out of the CD20 rich domain.

5.2.14 The effect of cholesterol depletion on the Ca^{2+} flux induced by type I mAb

Cholesterol is reported to be important for the tight packing and ordered structure pivotal to the integrity of lipid rafts [82]. We have shown in the previous chapter that treatment of cells with the cholesterol depleting agent Methyl-β-cyclodextrin (MCD) results in a reduced redistribution of CD20 into TX-100 insoluble domains (Section 4.2.5.3). As type I mAb effectively translocate CD20 into rafts, secondly only type I mAb induce a Ca^{2+} flux and thirdly, CD20 only associates with the BCR when ligated by a type I mAb it appears that redistribution of CD20 into rafts appears to be a pivotal event in CD20 mediated Ca^{2+} signalling.

In addition to the effect MCD has on the redistribution of CD20 into TX-100 insoluble domain, we also reported that MCD can lower the binding level of anti-CD20 mAb (Figure 4.8). Therefore, to accurately assess the effects of MCD on CD20 induced Ca^{2+} flux, the amount of mAb bound should be the same in control and MCD treated cells. To this end, binding curves of ritux, M15/8 (anti-sIgM) and SB2H2 (anti-sIgG) mAb was performed on both Ramos and SUDHL4 cells to establish a concentration of mAb which produced comparable levels of binding in control cells to 10 μg/ml ritux, M15/8 or SB2H2 in MCD treated cells. We found that after MCD treatment of SUDHL4 cells 10 μg/ml ritux had a comparable binding level to approximately 4.5 μg/ml ritux in control cells, and 10 μg/ml SB2H2 (anti-BCR) had a comparable binding level to 5 μg/ml SB2H2 in control cells. Furthermore, in Ramos cells we found that for both BCR and CD20, the binding level of 10 μg/ml mAb after MCD treatment was comparable to 5 μg/ml mAb in control cells (data not shown).

Utilising this binding data to ensure a comparable level of mAb binding was achieved, the effect of MCD treatment on Ca^{2+} flux generation was assessed. When SUDHL4 cells were pre-treated with 10mM MCD, there was a notable reduction in the Ca^{2+}

flux observed (Figure 5.18). This data is in accord with previous reports that suggest raft integrity is required for BCR-mediated Ca^{2+} influx [47]. We found that the reduction in flux occurred in both CD20 (ritux) and BCR (SB2H2) stimulated cells. The kinetics of the flux in ritux stimulated SUDHL4 cells shown in Figure 5.18A appears to be similar for both MCD treated and non-treated cells with the difference lying in the maximum FL5/FL4 value suggesting that the difference might be due to a reduced initial release of Ca^{2+} from intracellular stores and therefore a lower secondary Ca^{2+} influx to replete the stores. When SUDHL4 cells are treated with MCD and a Ca^{2+} flux is induced through BCR (SB2H2) stimulation, only the initial release from intracellular stores is observed as in conditions of extracellular calcium chelation shown in Figure 5.8. These results were mirrored in Ramos cells where again an overall reduction in BCR-mediated Ca^{2+} flux was observed upon MCD treatment (Figure 5.18B). Furthermore the flux generated by stimulation through the BCR with M15/8 was decreased in MCD treated cells to a flux similar to that observed in cells pre-treated with EGTA. The reduction in ritux-mediated flux in MCD treated Ramos cells is much more pronounced than that observed in SUDHL4 cells with the FL5/FL4 signal being almost completely lost upon treatment possibly reflecting the sensitivity of the cells to cholesterol depletion as demonstrated previously in Figure 4.9. From this data we suggest that cholesterol content and therefore raft integrity is a pivotal requirement for a maximal Ca^{2+} flux induced through CD20 and BCR stimulation.

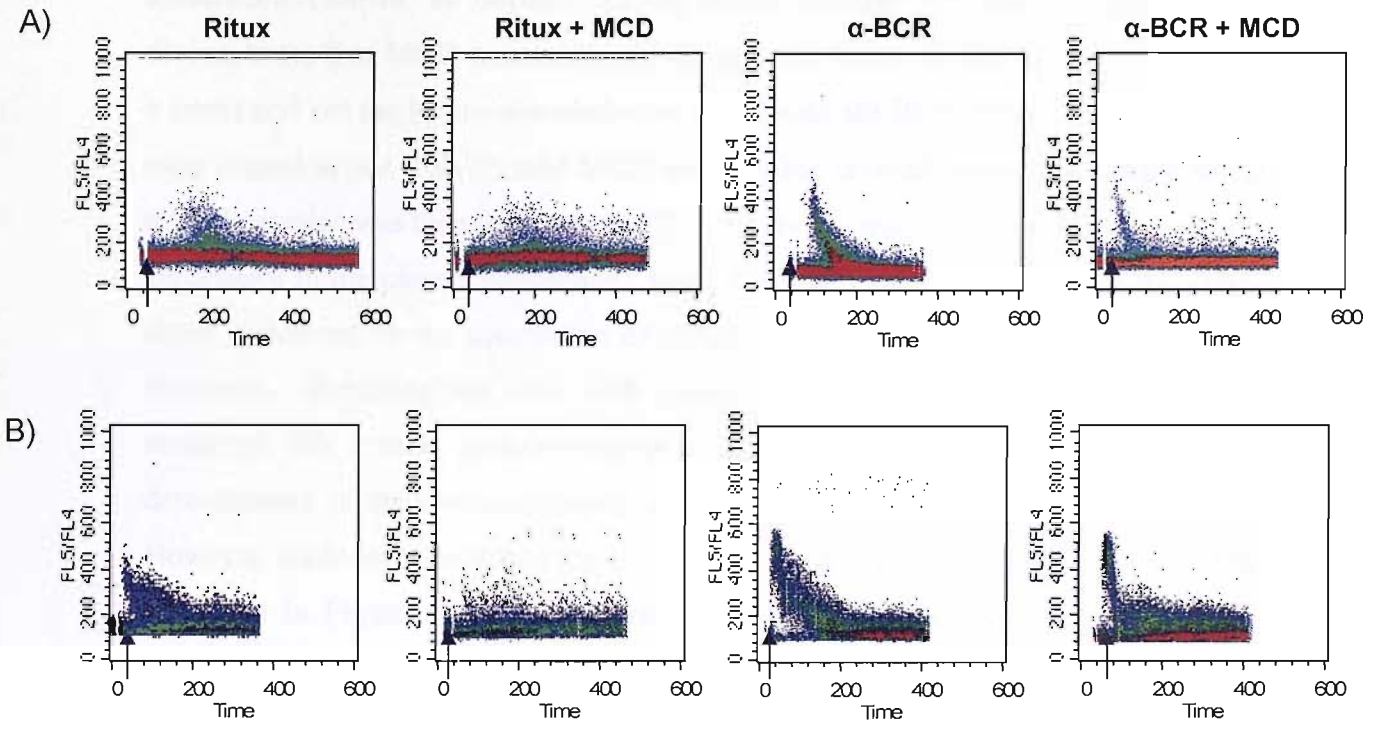

Figure 5.17: Cholesterol depletion reduces the calcium flux. **A)** SUDHL4 cells were prepared as outlined in Materials and Methods Section 2.9. Samples were pre-treated or not with 10mM MCD for 15 minutes at room temperature before washing twice and stimulating with either 4μg/ml ritux or 5μg/ml α-sIgG (SB2H2) for non-treated samples or 10μg/ml of each for MCD treated samples. mAb were added at the time point indicated by the arrow. Data shown is representative of two independent experiments. **B)** Ramos cells were treated as outlined in A with minor modifications. For ritux treated samples, cells were washed after the addition of 5μg/ml ritux and 20μg/ml MAH was added at the arrow. Also, for stimulation through the BCR, 5μg/ml α-sIgM (M15/8) was used. Again for MCD treated samples, 10μg/ml of each mAb was used. Data shown is representative of two independent experiments.

5.2.14 The effect of cholesterol depletion on the association of CD20 and the BCR

Treatment of cells with MCD resulted in a reduction in the Ca^{2+} flux induced by ritux stimulation (see above). We then investigated whether the reduced BCR and CD20 association (shown in Section 5.2.13) might account for this. Figure 5.19A demonstrates that MCD treatment only disrupts the homo-association of CD20 (ritux + ritux) and not the hetero-association of CD20 with the BCR (ritux + M15/8). Cells were treated or not with 10 mM MCD before being washed twice. One of the MCD treated samples was then treated with 12 μg/ml cholesterol for 60 minutes to replenish cholesterol in the plasma membrane. From Figure 5.19A it is evident that the FRET signal generated by the association of CD20 and the BCR is not hindered by MCD treatment. Repleting the cells with cholesterol led to an increase in the FRET measured, this is most probably due to a slight increase in ritux binding which, as demonstrated in the previous chapter, can occur in excess cholesterol (Figure 4.11). However, cholesterol depletion has a notable effect on the homo-association of CD20, as shown in Figure 5.19. MCD treatment reduces the homo-association of CD20 induced by Type I mAb with a FRET value of 20 in control cells which is reduced to 4.3 with MCD treatment. This difference in signal is not attributable to lower binding levels as the concentration of mAb used was the same as used in the previous MCD experiment (Figure 5.18). Once again, upon cholesterol repletion, the FRET was increased slightly above normal levels (from 20 to 23) which can again be attributed to increased ritux binding. Having established that the reduction in Ca^{2+} flux by MCD treatment is not due to a reduced association of CD20 and BCR we probed the possibility that MCD treatment could disrupt the dissociation of CD20 and the BCR (discussed in the previous section). From Figure 5.19B it is evident that this is not the case; whether Ramos cells are treated or not with MCD, the dissociation of CD20 and the BCR as measured by a reduction in FRET signal was still observed.

Overall, this data suggests that cholesterol depletion causes a reduction in the Ca^{2+} flux induced by ritux stimulation due to the reduced ability of CD20 to cluster in the cell membrane. This result correlates with the observation that a certain level of CD20 cross-linking is required to generate a Ca^{2+} flux through CD20 mAb stimulation. Here we have shown that MCD hinders the ability of type I mAb to

cluster CD20, therefore the cross-linking effect on CD20 is presumably reduced thereby lowering the resultant Ca^{2+} flux.

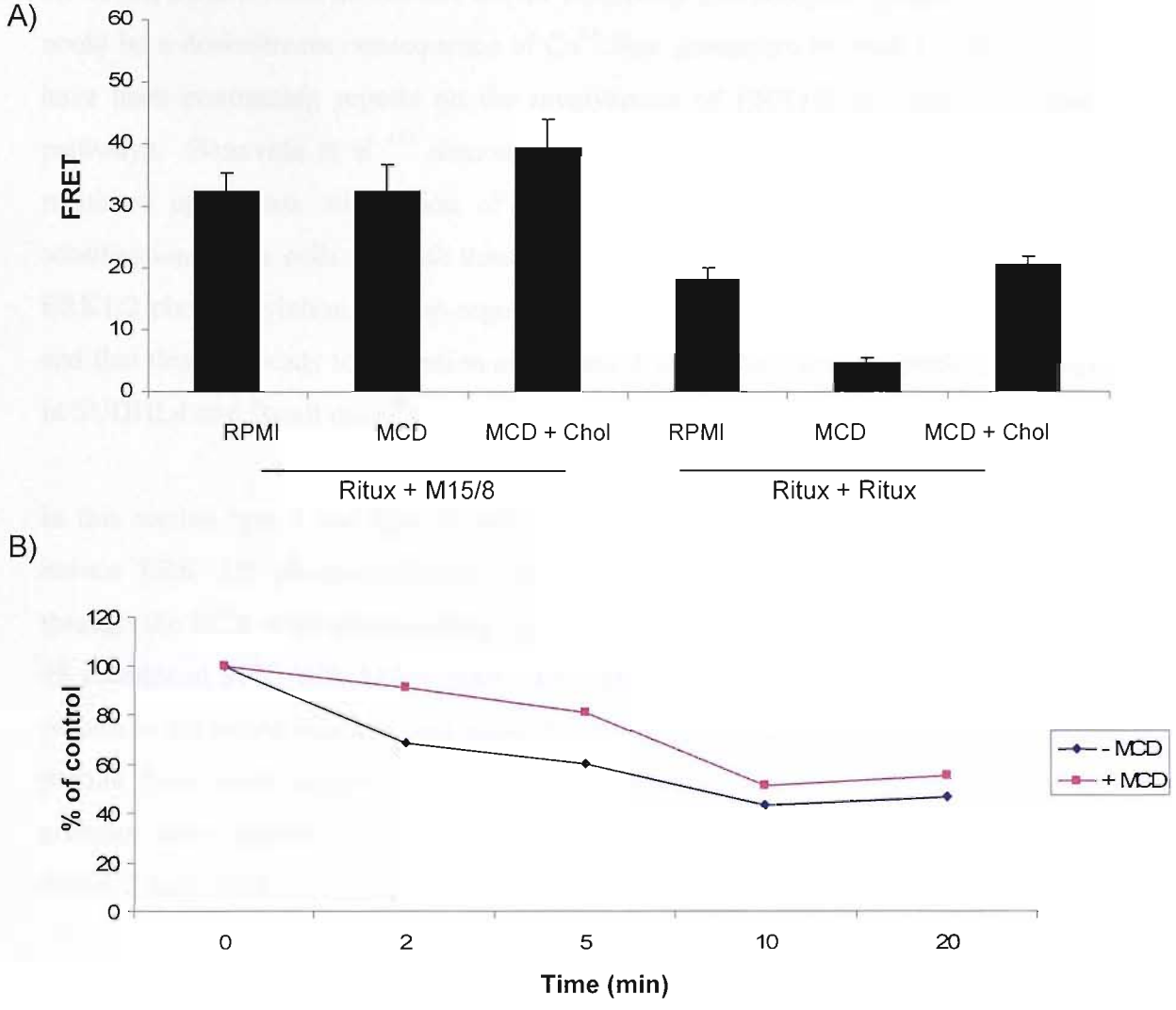

Figure 5.19: The effect of MCD on the association/dissociation of CD20 and BCR. A) Ramos cells were pre-treated or not with 10mM MCD for 15 minutes at room temperature, MCD + Chol samples are treated for a further 60 minutes with 12μg/ml cholesterol (SIGMA) before being washed and assessed for FRET generated by either CD20 and BCR association (ritux + M15/8) or CD20 homo-association (ritux + ritux). mAb concentrations used were the same as outlined in Figure 5.18 i.e. 4μg/ml ritux and 5μg/ml M15/8 for non-treated samples and 10μg/ml of each for MCD treated samples. Samples treated with cholesterol were stimulated with the same mAb concentration as untreated (RPMI) samples. The samples were assessed for FRET by flow cytometry as outlined in Materials and Methods Section 2.8.3. The values shown are mean and standard error of two independent experiments. **B)** Ramos cells were treated or not with MCD and assessed for FRET generated by ritux + M15/8 as outlined in A. After analysis at 0 minutes, 20μg/ml MAH (SB2H2) was added to the samples and assessed at the indicated time points. Data shown is calculated as a percentage based on the FRET value obtained at the initial time point (100%).

5.2.16 ERK Phosphorylation induced by anti-CD20 mAb

It was demonstrated earlier by inhibitor studies discussed in Section 5.2.9 that ERK 1/2 does not play a role in the induction of a Ca^{2+} flux induced by CD20 stimulation. However, these studies do not rule out the possibility that phosphorylation of ERK 1/2 could be a downstream consequence of Ca^{2+} flux generation by type I mAb. There have been contrasting reports on the involvement of ERK1/2 in CD20 signalling pathways. Bonavida et al [131] demonstrated that ERK1/2 phosphorylation is down-regulated upon ritux stimulation of Ramos and Daudi cells, which leads to the sensitisation of the cells to death through Bcl-$_{xL}$ down-regulation. In another report, ERK1/2 phosphorylation was up-regulated in cells stimulated with cross-linked ritux and that this also leads to activation of caspase 3 and subsequent apoptotic cell death in SUDHL4 and Daudi cells [91].

In this section type I and type II anti-CD20 mAb were assessed for their ability to induce ERK 1/2 phosphorylation. Briefly, Ramos cells were stimulated either through the BCR or by cross-linking type I (ritux) or type II (11B8) bound CD20 for 15 minutes at 37°C with MAH mAb. The cells were then lysed and the amount of protein in the lysate was assessed using the bicinchoninic acid (BCA) assay. 30μg of protein from each sample was loaded and separated by SDS-PAGE. Separated proteins were transferred to a nitrocellulose membrane and blotted for phospho-ERK1/2, total ERK or β-actin as a loading control.

The ERK1/2 complex is made up of two proteins, at 44 and 42 kDa respectively. Figure 5.20A demonstrates that in Ramos cells, of the two anti-CD20 mAb assessed only the type I mAb ritux induced ERK phosphorylation compared to the type II mAb 11B8 which did not change from background level. Furthermore we demonstrate that sIgM stimulation can also lead to ERK 1/2 phosphorylation. The kinetics of ERK phosphorylation appears to be similar for both sIgM and ritux stimulated cells where there is no notable increase in band intensity between 2 and 60 minutes. However, the extent of phosphorylation is markedly different in sIgM stimulated cells compared to ritux stimulated cells with the latter inducing a lower level of phosphorylation. Furthermore, ERK2 is phosphorylated to a greater extent than ERK1 (Figure 5.20A). To assess the levels of total ERK1/2, the membranes were stripped using a solution of

2-mercaptoethanol (2-ME) and SDS for 30 minutes at 50°C (see materials and methods Section 2.13.1). After several washes of the membrane with TBS-Tween, it was re-probed for ERK1/2. In Figure 5.20A the intensity of the dual bands corresponding to ERK1/2 does not change with mAb treatment compared to control cells, demonstrating that change observed in the phosphorylation of ERK1/2 is not due to expression levels. Indeed for cells stimulated with sIgM a lower amount of total ERK2 is apparent, however this reduction may be explained by the large amount of phosphorylated ERK2 in the sample possibly hindering mAb binding. To ensure that equal loading and transfer to the membrane was achieved, the level of β-actin was assessed for all samples. β-actin is commonly used as a loading control as it is constitutively and ubiquitously expressed in cells. From Figure 5.20, it is clear that equal loading and transfer was obtained as the level of β-actin appears similar in all samples. As a further control we wanted to ensure that phospho-ERK1/2 was specifically being detected. To this end, the effects of ERK1/2 inhibitor PD98059 were assessed on the level of phospho-ERK1/2 detected. From Figure 5.20B it is evident that the band observed at 44/42 kDa was phospho-ERK1/2 as in the presence of this inhibitor no band was detected in contrast to NT and DMSO treated cells. Furthermore, the use of PD98059 had no effect on the level of total ERK1/2 in the cell as no major differences were observed between control and treated cells.

To assess whether ERK1/2 phosphorylation was cell line dependent we extended our analysis to SUDHL4 cells. We demonstrated in Section 5.2.1 that SUDHL4 cells do not require hyper cross-linking to induce a Ca^{2+} flux through CD20. Remaining consistent with this, the western blot in Figure 5.20B shows cells that were stimulated with type I (ritux) or type II (11B8) alone. ERK2 appears to be constitutively phosphorylated in SUDHL4 cells as a band is detected in the non-treated control cells. However, ERK2 phosphorylation does appear to further increase upon mAb addition with ritux and SB2H2 (anti-BCR) increasing the level to a greater extent than 11B8. More interestingly, is the appearance of a weak upper ERK1 phosphorylation band. From Figure 5.20B it is evident that this band only appears in samples stimulated with ritux (primarily at 2 minutes) and sIgG (at 2-60 minutes). This result correlates with the mAb which could induce a Ca^{2+} flux shown in Figure 5.2. Both the total ERK and β-actin loading controls suggest that this is not due to unequal loading of the gel as no difference was observed between 11B8, ritux or sIgM stimulated samples.

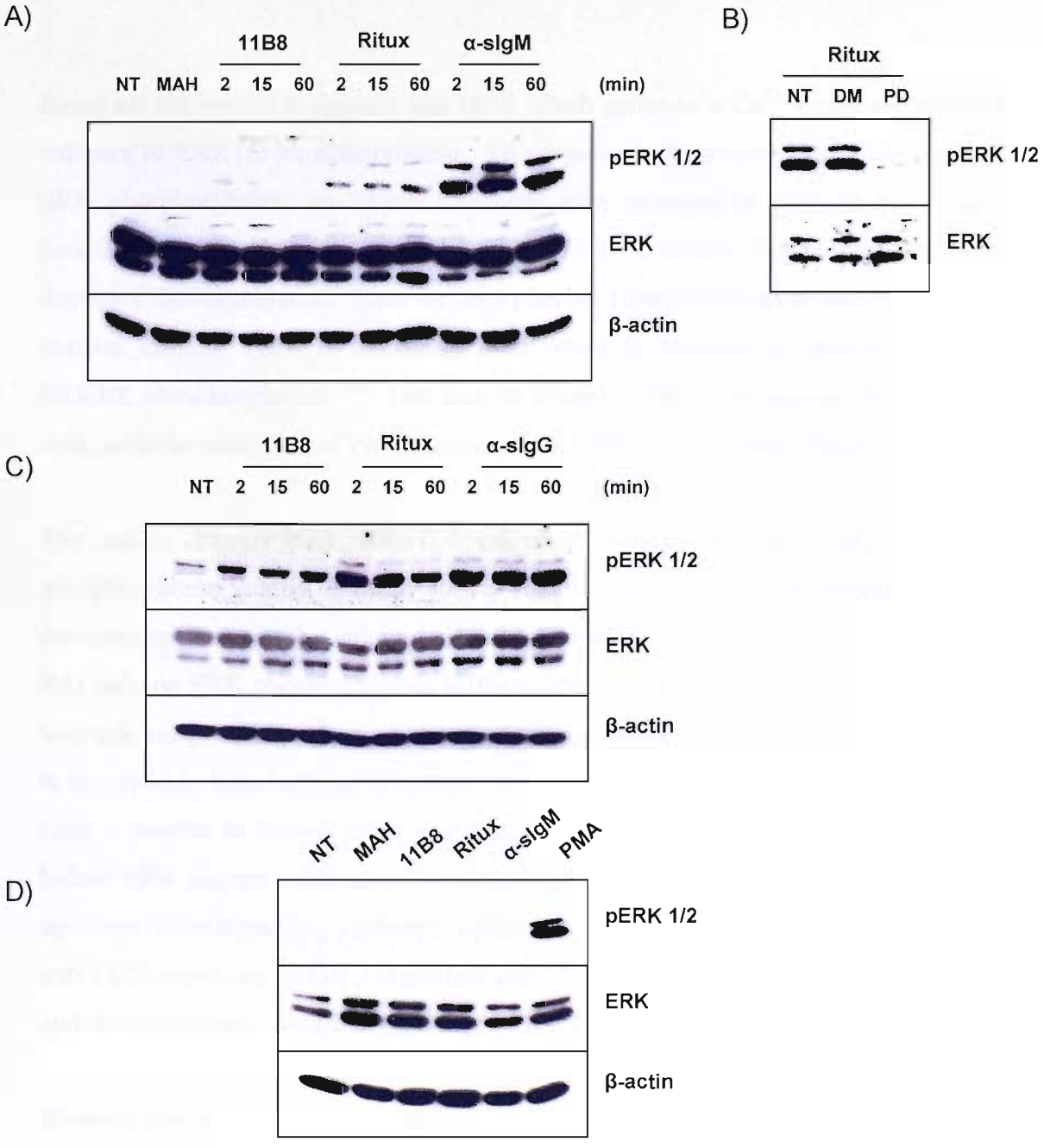

Figure 5.20: ERK phosphorylation can be induced by type I anti-CD20 mAb. A) Ramos cells were assessed for ERK phosphorylation as outlined in Section 2.13.1. Briefly, $1x10^7$ cells were pre-treated or not with 10μg/ml ritux or 11B8 for 15 minutes at room temperature. Either 10μg/ml α-sIgM (M15/8) or 20μg/ml MAH (SB2H2) was added to non-pre-treated samples and 20μg/ml MAH was added as a cross-linking agent to ritux and 11B8 treated samples. Samples were incubated at 37°C until being harvested at the indicated time points (60 minutes for NT and MAH) and lysed on ice in 0.5% NP40 solution containing phosphatase inhibitors. After lysis, samples were centrifuged and 30μg of protein was loaded into each well of a 10% SDS-PAGE gel and was western blotted for pERK (Cell signalling Technology). Membranes were stripped and re-probed for ERK and β-Actin. Data shown is representative of three independent experiments. **B)** Ramos cells were pre-treated or not with either 10μM PD (PD98059, ERK 1/2 inhibitor) or 1% DMSO for 30 minutes at room temperature before addition of 10μg/ml ritux for 15 minutes at room temperature. Samples were washed, stimulated with 20μg/ml MAH for 15 minutes and treated as outlined in A. **C)** SUDHL4 cells were treated as outlined in A except that no cross-linking of ritux and 11B8 was performed. **D)** Rx3 cells were treated as outlined in A with the addition of a sample treated with 20ng/ml PMA. The time point shown is 15 minutes.

Based on our results it appears that mAb which generate a Ca^{2+} signal are efficient inducers of ERK1/2 phosphorylation. To support the observation that Ca^{2+} flux and ERK phosphorylation are linked Rx3 cells were assessed as they do not possess functional sIgM and were shown in Figure 5.12 to be unable to generate a Ca^{2+} flux through CD20 stimulation. Here we used phorbol 12-myristate 13-acetate (PMA) as a positive control. PMA is a phorbal ester which is reported to directly stimulate ERK1/2 phosphorylation [218]. The data in Figure 5.20D demonstrates that the Rx3 cells, with the exception of PMA, cannot induce ERK1/2 phosphorylation.

The earlier Ramos and SUDHL4 inhibitor studies (Section 5.2.9) and ERK phosphorylation studies detailed above, suggest that ERK1/2 phosphorylation is a downstream event in the calcium signalling pathway. It would be expected that in Rx3 cells no ERK phosphorylation is observed in sIgM stimulated cells as these cells lack that antigen. Importantly however, in Figure 5.20D no ERK1/2 phosphorylation is observed in type I (ritux) stimulated cells either. As the level of ERK1/2 in Rx3 cells is similar to Ramos cells, it suggests that the inability of anti-CD20 mAb to induce ERK phosphorylation is linked to their inability to induce a Ca^{2+} flux further upstream in the signalling pathway. Collectively this data presents the idea that type I anti-CD20 mAb can induce a signalling cascade which results in Ca^{2+} flux generation and the downstream phosphorylation of ERK1/2.

Western blot is an effective method to assess ERK phosphorylation. However, the results displayed in a western blot are an amalgamation of the results from approximately 5 million cells and reflect the population as a whole. To assess the cells on a more individual basis, a flow cytometry assay was employed. For this assay cells were stimulated with the desired mAb for 15 minutes at 37°C before being fixed in 2% paraformaldehyde. Samples were then permeabilised in 90% methanol and labelled for phospho-ERK1/2 using the Alexa-fluor-488 conjugated mAb (Promega), an increase in FL1 fluorescence was correlated to an increase in phospho-ERK1/2.

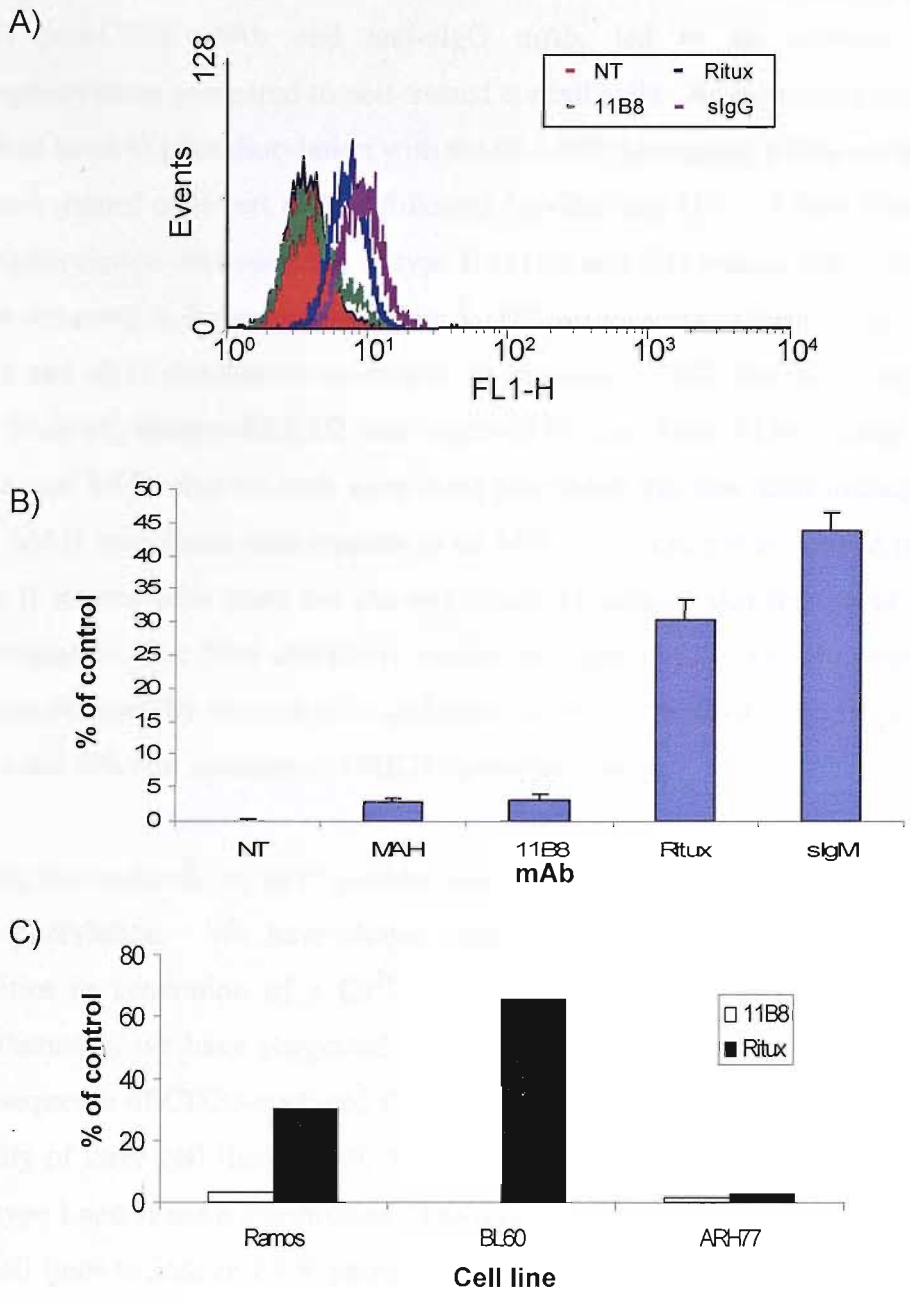

Figure 5.21: Investigation of ERK phosphorylation by flow cytometry. A) SUDHL4 cells were assessed for ERK phosphorylation by flow cytometry as outlined in Section 2.13.2. Briefly, $1x10^6$ cells were treated or not (filled in red) with 10μg/ml type I anti-CD20 mAb (ritux, blue overlay) or type II (11B8, green overlay) or α-sIgG (SB2H2, purple overlay) for 15minutes at 37°C before fixing in 2% paraformaldehyde for 10 minutes at 37°C. Samples were centrifuged and re-suspended in 90% ice cold methanol for 30 minutes on ice before being washed twice and 10μl Alexa-Fluor-488 conjugated anti-phospho-ERK 1/2 (BD Bioscience), for 60 minutes at room temperature. Samples were washed and analysed by flow cytometry. Data shown is representative of two independent experiments. **B)** Ramos cell were treated as outlined in A except that after the addition of anti-CD20 mAb, samples were washed and treated with 20μg/ml MAH (SB2H2) for 15 minutes at 37°C. Also M15/8 was used to stimulate cells through sIgM. The values shown are the mean and standard error of two independent experiments. **C)** Ramos, BL60 and ARH77 cells were treated as outlined in A except anti-CD20 mAb were cross-linked by the addition of MAH. All values shown are calculated based on the MFI of NT samples using the following formula; % of control =[$(MFI_{sample} - MFI_{NT})/MFI_{NT}]x100$

In Figure 5.21A it is shown that stimulation of SUDHL4 cells with type I (ritux and 1F5) anti-CD20 mAb and anti-sIgG mAb, led to an increase in ERK1/2 phosphorylation compared to non-treated control cells. As expected sIgG induced the highest level of phosphorylation with the FL1 MFI increasing 110% compared to non-treated control cells (set at 0%) followed by ritux and 1F5. A low level of ERK1/2 phosphorylation also occurred in type II (11B8 and B1) treated cells. Similar results were observed in Ramos cells (Figure 5.21B) where cross-linking of type I anti-CD20 mAb and sIgM stimulation resulted in an increase in ERK phosphorylation. Again a low level of phospho-ERK1/2 was observed in type II and MAH treated cells. When the actual MFI value for each sample are compared, this low level induction in type II and MAH stimulated cells equates to an MFI shift from 5.0 in control cells to 5.5 in type II treated cells (data not shown) hence we suggest that this event is of no real consequence. The flow cytometry results in Figure 5.21A and B correlate with the results obtained by western blot, and demonstrate that anti-BCR and type I anti-CD20 mAb are efficient inducers of ERK1/2 phosphorylation.

Using this method, we next assessed the ability of other B cell lines to induce ERK phosphorylation. We have shown earlier that B cell lines demonstrate different abilities in generation of a Ca^{2+} flux through CD20 stimulation (Figure 5.2-5.5). Furthermore, we have suggested above that ERK phosphorylation is a downstream consequence of CD20-mediated Ca^{2+} flux. To directly link the two we compared the ability of three cell lines BL60, ARH77 and Ramos to induce ERK phosphorylation by type I and II mAb stimulation. The data in Figure 5.21C shows that the ability of B cell lines to induce ERK phosphorylation correlates with their ability to induce a Ca^{2+} flux upon type I mAb stimulation. Ramos and BL60 were able to generate a Ca^{2+} flux through ritux stimulation (Figure 5.3 and 5.5) and similarly it is shown here that they can induce ERK phosphorylation through ERK stimulation. In contrast, ARH77 cells were unable to generate a Ca^{2+} signal when ritux was cross-linked (Figure 5.4) and similarly are unable to induce ERK phosphorylation.

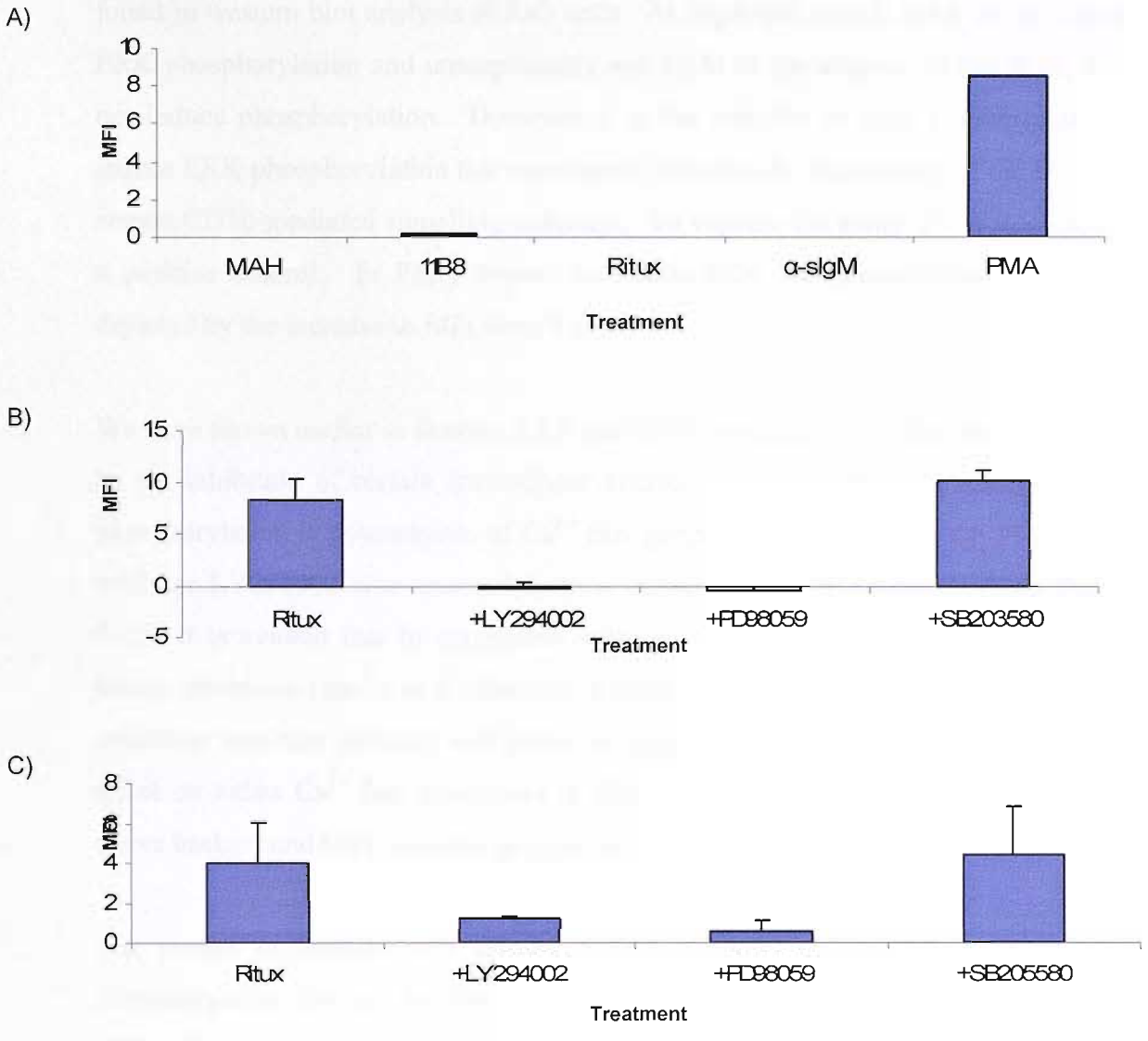

Figure 5.21: Effect of kinase inhibitors on ERK phosphorylation. Cells were labelled with anti-phospho-ERK 1/2 as outlined in Materials and Methods Section 2.13.2 **A)** Rx3 cells were stimulated for 15 minutes at 37°C with either 10μg/ml α-sIgM (M15/8), 50ng/ml PMA or 20μg/ml MAH or samples were pre-treated with 10μg/ml 11B8 or ritux for 15 minutes at room temperature before being washed and stimulated with 20μg/ml MAH for 15 minutes at 37°C and assessed by flow cytometry. **B)** SUDHL4 were pre-treated or not with either 10μM LY294002 (PI-3 kinase inhibitor), PD98059 (ERK 1/2 inhibitor) or SB203580 (P38 inhibitor) for 30 minutes at room temperature before being stimulated or not with 10μg/ml ritux for 15 minutes at room temperature and assessed by flow cytometry. The values shown are the mean and standard error of two independent experiments. **C)** Ramos cells were treated as outlined in B except that ritux treated samples were washed and hyper cross-linked by the addition of 20μg/ml MAH for 15 minutes at 37°C. All data shown has the is adjusted for background by the subtraction of NT. The values shown are the mean and standard error of two independent experiments.

This observation is further supported by the finding that type I induced ERK phosphorylation does not occur in Rx3 cells. Figure 5.22A mirrors the results we found in western blot analysis of Rx3 cells. As expected, type II mAb do not induce ERK phosphorylation and unsurprisingly anti-sIgM in the absence of the BCR, does not induce phosphorylation. However, it is the inability of type I mAb (ritux) to induce ERK phosphorylation that once again indicates the importance of the BCR for certain CD20-mediated signalling pathways. To validate the assay, PMA was used as a positive control. In PMA treated Rx3 cells ERK phosphorylation occurred as depicted by the increase in MFI from 0 to 10.

We have shown earlier in Section 5.2.9 that CD20 mediated Ca^{2+} flux can be reduced by the inhibition of certain intracellular kinases. To test our hypothesis that ERK phosphorylation is downstream of Ca^{2+} flux generation, the effect of the PI-3 kinase inhibitor LY294002 was assessed in ritux stimulated SUDHL4 cells. From Figure 5.22B it is evident that in correlation with the Ca^{2+} flux data in Figure 5.12, PI-3 kinase inhibition results in a reduction in ERK phosphorylation. The effect of P38 inhibition was also assessed and found to mirror the Ca^{2+} flux data in that it had no effect on either Ca^{2+} flux generation or ERK phosphorylation. As expected no shift above background MFI occurred in cells pre-treated with the ERK inhibitor PD98059.

The results in Ramos cells (Figure 5.22C) support the SUDHL4 data. ERK phosphorylation induced by ritux was again reduced by inhibition of PI-3 kinase but P38 inhibition had no effect. Furthermore, other work from our laboratory has shown that in SUDHL4 cells BAPTA-AM, an intra and extracellular calcium chelator, also reduces the pERK induced by ritux back to background level (M Cragg, personal communication). Together, this data provides strong evidence to support our theory that type I anti-CD20 mAb induce a signalling cascade which involves PI3 kinase activation followed by Ca^{2+} flux generation and the downstream phosphorylation of ERK1/2.

5.2.17 The effect of anti-CD20 mAb stimulation on NFκB activity

The nuclear factor kappa B (NFκB) family of transcription factors plays a major role in inflammation, immune and stress responses and has more recently been linked to

oncogenesis [219]. It has been reported that ritux sensitises patients to chemotherapy by inducing a down-regulation in NFκB activity [131] (see Section 1.6.5) and therefore we investigated whether NFκB activity was altered by either type I or II anti-CD20 mAb stimulation in Ramos cells.

In most resting cells, NF-κB is sequestered in the cytoplasm in an inactive form associated with IκB inhibitory molecules such as IκBα, IκBβ, IκBε, p105, and p100. Activation of NFkB is achieved through the action of a family of serine/threonine kinases (IKK) which phosphorylate IkB proteins. This phosphorylation event separates NFκB from IκB leaving it free to migrate to the nucleus to initiate transcription [219, 220]. Phosphorylation of IκBα is commonly used as a measure of NFκB activity [220, 221]. We used western blot analysis and a rabbit anti-phospho IκBα antibody from Cell Signalling Technology to detect this phosphorylation event.

Because NFκB activation typically occurs in the latter stages of signalling pathways we extended the time point of our assays to 12 hours. From the data in Figure 5.23 it is evident that NFκB is constitutively active in Ramos cells with phospho-IκBα being detected in non-treated cells. The level of phospho-IκBα was not affected by type I (ritux) or type II (11B8) anti-CD20 mAb. There was however, an apparent reduction in the level of phospho-IκBα in sIgM stimulated cells after 12 hours which appeared to be a real event based on the equal loading depicted by the β-actin loading control. In this experiment, ERK phosphorylation was also assessed and it was found that at 1 hour the results were similar to that reported earlier (Figure 5.20) where both ritux and sIgM stimulated cells demonstrated ERK phosphorylation. However, no ERK phosphorylation was found at 12 hours in either ritux or sIgM stimulated samples which is in agreement with Mathas et al [91] who demonstrated that in BL60 cells ERK phosphorylation is induced by ritux mAb within 30 minutes of stimulation but decreases over time with less than 50% of the initial induction remaining after 8 hours (longest time point assessed).

These results are in contrast to those published by Jazirehi and colleagues [187] who demonstrated that NFκB activity was decreased upon ritux stimulation of Ramos cells. However the discrepancy in results may be attributable to the use of ritux alone

as a stimulating agent in their assays compared to cross-linked ritux in our experiments.

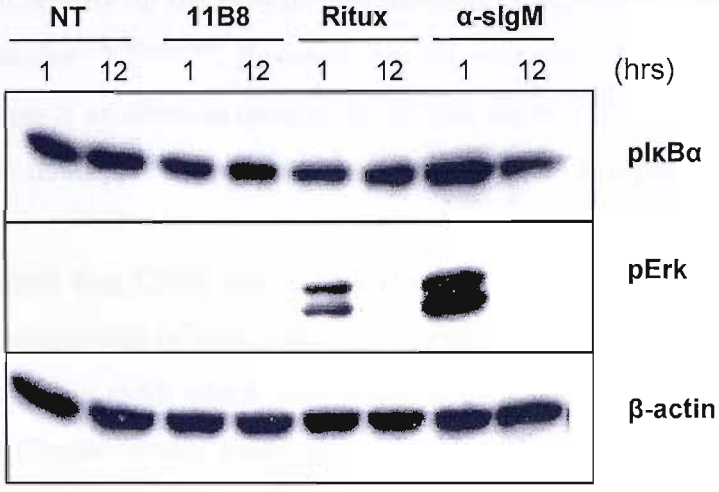

Figure 5.23: NFκB activity is not affected by anti-CD20 mAb. $1x10^7$ Ramos cells were treated or not with 10μg/ml 11B8 or ritux for 15 minutes at room temperature before being washed. Samples were then stimulated or not with either 10μg/ml α-sIgM or 20μg/ml MAH (to 11B8 and ritux treated samples). Cells were maintained at 37°C/5% CO_2 and after the indicated time points, samples were harvested and treated as outlined in Materials and Methods Section 2.13.1. Briefly, samples were lysed in 0.5% NP40, resolved on SDS-PAGE and western blotted for phospho-IκBα (Cell Signalling Tech.). Membranes were stripped and re-probed for pERK and β-actin.

5.3 Discussion

The ability of CD20 to deplete B cells upon mAb stimulation has made it a highly successful target for the treatment of NHL and other B cell malignancies. There have been a plethora of reports on the effector mechanisms employed by anti-CD20 mAb, rituximab in particular [56, 62, 63, 68]. However, not all patients respond to ritux therapy [129]. Therefore, there is an obvious need to dissect the signalling pathways induced by anti-CD20 mAb to maximise the potential of CD20-directed therapies.

Here we demonstrate that CD20 can induce changes in cytosolic [Ca^{2+}] upon mAb stimulation. On assessment of eight anti-CD20 mAb in SUDHL4 and Ramos B cell lines we found that only mAb which were found to efficiently redistribute CD20 into TX-100 rafts (see Chapter Four), could generate a Ca^{2+} flux. In agreement with other reports we found that hyper cross-linking of CD20 was required to generate a flux in Ramos cells [56, 63]. However, hyper cross-linking was not required in SUDHL4 cells for flux generation. We found that the reason for the difference in dependency of hyper cross-linking was shown to be due to the high level of CD20 expressed on the surface of SUDHL4 cells compared to Ramos cells. When the level of CD20 was reduced on SUDHL4 cells by silencer RNA, the cells became dependent on hyper cross-linking, like Ramos cells, to generate a response with anti-CD20 mAb. Furthermore, on analysis of three other $CD20^+$ B cell lines BL60, Raji and ARH77 it was apparent that the level of Ca^{2+} flux induced was dependent on the level of CD20 expressed on the surface of the cells as the flux decreased with decreasing expression level. This data supports an early observation by Bubien and colleagues [45] who transfected CD20 into five $CD20^-$ cell lines and found that the level of calcium mobilisation correlated with the level of CD20 expressed on the surface. From this observation, and the belief that CD20 resides in the membrane in oligomers [45, 98], it was suggested that CD20 itself may act as the ion channel.

Our data and reports by others [48] have suggested that CD20 mediates Ca^{2+} flux through store operated channels (SOC). These ion channels mobilise calcium in two phases; the first phase is the release of Ca^{2+} from intracellular stores followed by Ca^{2+} influx from the extracellular domain to replenish the stores. In Ramos and SUDHL4 cells, we demonstrated that the Ca^{2+} flux observed by flow cytometry upon CD20 and

the BCR stimulation was the composite of the two phases – the first flux from the release of Ca^{2+} from intracellular stores (as in EGTA chelation conditions) and the other from the influx of Ca^{2+} into the cell from the extracellular domain (as observed upon the re-introduction of Ca^{2+} by $CaCl_2$).

In BCR-mediated calcium signalling the cascade of events involved in the release of Ca^{2+} from intracellular stores upon BCR stimulation has been elucidated (reviewed in [17]). However, as it was thought that CD20 may itself act as the ion channel, little work has been afforded to the investigation of a pathway involved in CD20-mediated flux. It has been reported that several phosphorylation events occur upon CD20 stimulation with Src family kinases, PKC and PLCγ2 all being reported to be phosphorylated upon CD20 mAb stimulation [97, 98]. Furthermore phosphorylation of CD20 itself is up-regulated upon mAb stimulation [61, 65]. Therefore it is feasible that phosphorylation may play a role in the regulation of CD20-mediated calcium mobilisation.

Here for the first time we demonstrate that CD20 and the BCR utilise the same signalling pathway for Ca^{2+} flux generation. In Ramos cells we found that inhibition of Syk resulted in complete ablation of the flux induced by type I anti-CD20 mAb. Furthermore there was a notable reduction in the CD20-mediated flux with PI-3 kinase inhibition. The same result was observed in SUDHL4 cells. More importantly, the effect of kinase inhibition was the mirrored in BCR-stimulated cells with both Syk and PI3K inhibitors notably reducing the flux. As inhibition of Syk and PI3K resulted in a diminished Ca^{2+} flux it implies that the kinases are involved in the generation of the flux i.e. in the signalling cascade linking the membrane events (mAb binding) to the release of Ca^{2+} from the endoplasmic reticulum. Furthermore, we demonstrated that inhibition of Src family kinases (SFK) with the specific inhibitor PP2, resulted in an elongation of the flux induced by anti-CD20 and -BCR mAb. This result is in contrast with reports by other who demonstrate that PP2 ablates the flux induced by anti-CD20 mAb ritux and 2H7 in Ramos cells [56, 65]. The reason for this discrepancy is unclear. We found that PP2 (from two different suppliers) had the same effect in Ramos and SUDHL4 cells and in both CD20 and BCR-mediated Ca^{2+} flux. As the initial Ca^{2+} flux can occur, resulting from the release of Ca^{+} from intracellular stores, and the FL5/FL4 maximum was not affected by PP2

we propose that in CD20-mediated Ca^{2+} mobilisation, SFK is involved in regulation of the shutdown of Ca^{2+} influx which occurs after activation of SOC at the membrane. The involvement of Syk in the CD20-mediated signalling pathway was somewhat surprising. The intracellular domain of CD20 has no ITAM motifs and contains no tyrosine residues [31]. Syk has only been reported to reside within the BCR signalling complex via interaction of its SH2 domains [222]. Furthermore, immuno-precipitation studies of CD20 have demonstrated that CD20 is linked to members of the SFKs by PAG [98]. However, no association has ever been reported with Syk. This dependence of CD20 on Syk for calcium mobilisation suggests that CD20 may be dependent on BCR-mediated signalling pathways to generate a flux. Furthermore, the calcium signal initiated upon BCR cross-linking with mAb has been demonstrated to be down-regulated by Fc receptors [201]. Here we demonstrate that the same effect is observed in CD20-mediated calcium mobilisation where in Ramos cells, the absence of the Fc domain of the stimulating mAb resulted in an increase in the Ca^{2+} flux observed.

Several investigators have linked CD20 and the BCR. In 1993, Bourget et al [92] demonstrated that B1 decreases the expression of IgM at the surface on normal human B cells and B cell lines. In agreement with this we found that ritux and B1 reduced sIgM and CD38 expression after 24 hours whereas class II, CD37, Fas and CD52 were not affected on Daudi cells (data not shown). In contrast, we found that stimulation of cells with anti-sIgM mAb resulted in an increase in expression of CD20 (data not shown). Another investigation reported that anti-CD20 and –BCR mAb induce similar cell death pathways in SUDHL4 and BL60 cells [91] (which was contradicted by a different study in Ramos cells [160]). Li and colleagues [48] directly linked CD20 and the BCR by the demonstration that Ca^{2+} flux induced by BCR stimulation was decreased in correspondence with a decrease in CD20 expression. Here we investigated the inverse of this relationship and found that CD20-mediated Ca^{2+} flux was actually dependent on BCR expression.

The first solid indication that CD20 was dependent on the BCR to induce a Ca^{2+} flux was from investigation of Rx3 cells. We generated these cells by chronic stimulation of the BCR in Ramos cells leading to the outgrowth of BCR negative cells with minimal effect on the expression level of CD20. These Rx3 cells were unable to generate a Ca^{2+} flux through CD20 stimulation. It could be argued that these cells lost

their signalling ability due to chronic stimulation however, they were found to maintain normal CD20 signalling events such as redistribution of CD20 into rafts and induction of programmed cell death. To gain a more conclusive result we attempted to reduce BCR expression using silencer RNA in a range of B cell lines using two different primer sequences targeting CD79b but failed to achieve a significant reduction in BCR expression (data not shown).

Using a different approach, we investigated four different primary CLL samples. CLL is a low grade NHL which typically has dim BCR expression as depicted by the phenotyping shown in Table 5.2. Firstly, we demonstrated that normal B cells isolated from peripheral blood could mediate calcium mobilisation upon CD20 mAb stimulation. The analysis was hindered by the 15% of non-B cell in the sample which we found to interact with the Fc domain of both the primary and secondary antibodies inducing a non-specific response. Despite this, it is evident from the data in Figure 5.13 that type I CD20 mAb can generate a Ca^{2+} flux above non-specific, background level. On assessment of the 4 primary CLL cells, we found that even though CD20 was expressed at a sufficient level to induce a Ca^{2+} flux, calcium mobilisation did not occur upon cross-linking of type I mAb bound to CD20. Furthermore no Ca^{2+} flux was observed when sIgM was stimulated. However by hyper cross-linking sIgM in Patient D cells, we found that a Ca^{2+} flux could be generated. Like CD20, it appears that the BCR requires a certain threshold of BCR re-arrangement and clustering for calcium mobilisation to occur, therefore in low expressing cells hyper cross-linking is required to surpass this threshold. Together these data support our findings in Rx3 cells – CD20 is dependent on BCR expression for generation of a Ca^{2+} flux.

CD20 can be redistributed into lipid rafts upon type I mAb ligation (see Chapter Four). The significance of this event is unclear although we have suggested that this redistribution is important for effective CDC activation and lysis by anti-CD20 mAb [67]. Using fluorescent microscopy Deans and colleagues [47] demonstrated that CD20 can constitutively associate with the BCR in lipid rafts but upon BCR stimulation, the two surface antigens dissociate to allow the BCR to become internalised. We used FRET to assess the association in real time on live cells. The data presents a different scenario to what Deans et al [47] reported. We found that in Ramos cells, CD20 and the BCR only associate upon CD20 ligation with type I mAb ritux. This association is

stable for over the 30 minutes assessed. However, upon hyper cross-linking of CD20, CD20 and the BCR dissociate. Hyper cross-linking of CD20 had no effect on the level of CD20 homo-association or BCR homo-association. This dissociation was not due to internalisation of the BCR and did not appear to involve intracellular kinases SFK and PI3K which were shown to mediate Ca^{2+} flux generation. Until this event can be inhibited, the significance of this dissociation remains elusive; it may play an important role in regulation of the signalling pathway or it may simply be a physical consequence of tight packing of the CD20 molecules by hyper cross-linking, pushing the BCR out of the domain.

CD20 only generates a flux when stimulated by type I mAb, furthermore CD20 only associates with the BCR when ligated with type I mAb. We demonstrated in the previous chapter that type I mAb effectively redistribute CD20 into TX-100 insoluble lipid rafts. Taking all of this together, it implies that redistribution of CD20 into lipid rafts plays an important role in the generation of a Ca^{2+} flux. Other groups have demonstrated the dependence of CD20-mediated Ca^{2+} flux on raft integrity by the use of the cholesterol extracting drug MCD [48, 62, 65]. However, these studies failed to address the possibility that anti-CD20 mAb binding could be lost upon MCD treatment. In the previous chapter, we demonstrated that MCD treatment can result in loss of mAb binding (Section 4.2.4) and therefore it is feasible that the observed reduction in Ca^{2+} flux could be directly attributed to this. To allow for this, we performed a binding curve analysis to achieve comparable levels of binding of ritux in control and MCD treated Ramos cells. We found that with comparable mAb binding levels in control and MCD treated Ramos cells, the Ca^{2+} flux induced by CD20 and the BCR was visibly reduced in the latter cells. The extent of inhibition with MCD was different for both CD20 and BCR-mediated Ca^{2+} flux. In BCR stimulated samples, MCD treatment resulted in a flux similar to that observed in calcium chelation conditions with EGTA (See Figure 5.8 and 5.17). This suggests that raft integrity is only required for the Ca^{2+} influx as in extracellular Ca^{2+} chelation conditions, changes in cytosolic Ca^{2+} can only result from release of Ca^{2+} from intracellular stores. However, in CD20 stimulated cells, MCD treatment caused a clear reduction in the overall Ca^{2+} flux in SUDHL4 cells and in Ramos cells treatment lead to an almost complete ablation of the flux. Taking this data together it indicates

that the BCR is dependent on rafts primarily for Ca^{2+} influx whereas CD20-mediated Ca^{2+} flux requires raft integrity for the initial release of Ca^{2+} from intracellular stores.

The effect of MCD on CD20 association with itself and with the BCR was investigated by FRET analysis. We demonstrated in the previous chapter that cholesterol depletion had a detrimental effect on the association of type I-bound CD20 with TX-100 insoluble domains (Figure 4.11). Here we show a similar effect by FRET analysis with the CD20 homo-association decreasing from a FRET value of 30 in control cells to 5 in MCD treated cells. The effect of MCD was negated by the presence of cholesterol, demonstrating the specificity of the assay. Interestingly however, the association of CD20 and the BCR was not affected by MCD treatment. Moreover, CD20 and the BCR still dissociated in the presence of MCD. Therefore we suggest that the reduction in CD20-mediated Ca^{2+} flux is not due to a disruption in the association of CD20 and the BCR but due to a hindered ability of CD20 to cluster together. As CD20 and the BCR are shown to only associate when CD20 redistributes into lipid rafts by type I mAb binding, it is surprising that MCD treatment does not disrupt the association. However, it is possible that MCD disrupts large rafts breaking them up into smaller domains, depending on the distribution pattern of the surface antigens and of cholesterol this may have a notable effect on CD20 homo-associations but the effect may be minimal on CD20 and the BCR association.

From the study of the Rx3 cells, primary CLL cells and FRET analysis we propose that CD20 requires the BCR to generate a Ca^{2+} flux. The exact details of the relationship are not understood. We propose that CD20 is redistributed upon type I mAb binding into lipid rafts, this redistribution event leads to the association of CD20 with the BCR possibly by entrapping the BCR in the domain. What remains unclear is which surface antigen signals for the Ca^{2+} flux. As the BCR and CD20-mediated calcium signalling cascade are, from what we observed, virtually identical it is feasible that the flux generated upon anti-CD20 mAb binding is actually the calcium signalling pathway induced by the BCR. We postulate that upon type I mAb binding of CD20, CD20 and the BCR (and its associated molecules e.g. CD79α/β and intracellular kinases like Syk and SFKs) associate (see Figure 5.24) . When CD20 is hyper cross-linked, the BCR signalling complexes are brought into close proximity

mimicking the effect of cross-linking BCR by specific anti-IgM mAb, therefore the BCR complex transduces a signal resulting in release of Ca^{2+} from intracellular stores. It is feasible that the slight difference in the kinetics of the flux observed when the BCR is directly stimulated by mAb could be due to a reduced efficiency of BCR clustering when induced CD20 mAb. In SUDHL4 cells it is likely that hyper cross-linking of CD20 is not required as CD20 is expressed at such a high level that addition of the anti-CD20 type I mAb alone is sufficient to effectively cross-link the BCR for the induction of a signalling cascade.

As calcium mobilisation is a relatively early event in cell signalling cascades we investigated downstream kinases for activity. There have been contrasting reports on the activation of ERK by ritux. One group show that ERK was down-regulated upon ritux hyper cross-linking in ARL cells [130] whereas another group demonstrate that ERK was up-regulated in SUDHL4 and BL60 cells when stimulated with ritux alone or cross-linked [91]. Our results are in agreement with the latter report. Over a 60 minute time period we found that cross-linked ritux and BCR (M15/8) stimulated Ramos cells led to a notable increase in the level of phospho-ERK. The level of phosphorylation remained relatively consistent from 2 to 60 minutes in ritux treated cells whereas in BCR treated cells, the extent of phosphorylation was greater compared to ritux stimulated cells and the kinetics were slightly different with a maximum phosphorylation occurring at 15 minutes. The anti-CD20 type II mAb 11B8 did not induce phosphorylation of ERK in Ramos cells. A similar result was observed in SUDHL4 cells except that ERK2 appeared to be constitutively phosphorylated. Therefore, up-regulation in phosphorylation was only apparent in ERK1 where again cross-linked ritux and BCR (SB2H2) stimulation lead to an induction in phosphorylation and 11B8 had no notable effect. The extent of phosphorylation was notably reduced in SUDHL4 cells possibly owing to the inherent difference between cell lines.

ERK inhibition had no effect on the Ca^{2+} flux induced through CD20 or BCR mAb stimulation. However from analysis of Rx3 cells, it became apparent that ERK phosphorylation is a downstream event in the CD20 calcium signalling pathway. Rx3 cells failed to induce a Ca^{2+} flux upon anti-CD20 mAb stimulation similarly these cells did not induce ERK phosphorylation upon mAb stimulation. In agreement with

this, ERK phosphorylation studies using intracellular staining and flow cytometry demonstrated that the level of ERK phosphorylation corresponds to the intensity of the Ca^{2+} flux induced by type I mAb. Of the three cell lines assessed, Ramos and BL60 generate a similar Ca^{2+} flux and no flux is observed in ARH77 cells when ligated with ritux and cross-linked. Reflecting these results, Ramos and BL60 induce ERK phosphorylation through type I mAb stimulation whereas no phosphorylation was observed in ARH77 cells. In addition, when Ramos and SUDHL4 cells were pre-treated with PI3 kinase which was shown previously to diminish the Ca^{2+} flux induced by anti-CD20 mAb, the level of ERK phosphorylation was notably decreased. Furthermore, other preliminary work in our laboratory demonstrated that BAPTA-AM chelation resulted in a decrease in the ERK signal (data not shown). Taken together this data demonstrates that ERK phosphorylation is a downstream event of Ca^{2+} flux generation however, further work is required to establish whether this is a result of release of Ca^{2+} from intracellular stores or from influx of Ca^{2+} from the extracellular domain.

We demonstrate that P38 inhibition had no effect on ERK phosphorylation. P38 is a member of the MAP kinase family and has been reported to be involved in the down-regulation of IL-10 induced by ritux stimulation [186]. We found that P38 was not involved in the calcium signalling cascade induced by type I anti-CD20 mAb as P38 inhibition had no effect on the generation of a Ca^{2+} flux or on the ERK phosphorylation induced by type I mAb. Furthermore we found that P38 itself was not phosphorylated upon Type I mAb stimulation (data not shown). We also investigated the involvement of NFκB activity in the calcium signalling cascade. Jazirehi and colleagues [131] reported that ritux acts as a chemosensitising agent by the down-regulation of NFκB activity making cells susceptible to programmed cell death. We used the phosphorylation of the inhibitory IκBα as a measure of NFκB activity but found no difference in ritux or 11B8 (cross-linked) treated cells when compared to the non-treated control. There was a reduction in the phosphorylation when Ramos cells were stimulated through sIgM for 12 hours. It is interesting to note that ERK phosphorylation induced by ritux which was present at 1 hour was reduced to background level by 12 hours indicating a relatively short time span for the signalling cascade.

A summary of these results are shown below in Figure 5.24. We propose that type I anti-CD20 mAb like ritux redistribute CD20 into TX-100 insoluble lipid rafts. This clustering of CD20 entraps the BCR which upon hyper cross-linking of CD20, initiates a signalling cascade analogous to the signalling pathway utilised upon BCR stimulation, involving Syk and PI3 kinase culminating in the release of Ca^{2+} from intracellular stores. This release of Ca^{2+} results in activation of I_{CRAC} and opening of store operated channels allowing Ca^{2+} influx into the cells to replenish the intracellular stores. This second phase of Ca^{2+} mobilisation appears to be regulated by Src family kinases. ERK phosphorylation occurs downstream of calcium mobilisation. Further work is required to assign a functional role to this signalling cascade, some groups have shown that ERK phosphorylation leads to decreased AP-1 binding and a subsequent decrease in Bcl-$_{XL}$ expression resulting in sensitisation of cells to apoptosis [91, 221]. We performed preliminary cell death cell death studies in Ramos cells and found no difference in the cell death induced by cross-linked ritux after 24 hours in the presence or absence of ERK inhibitor PD98059 (data not shown).

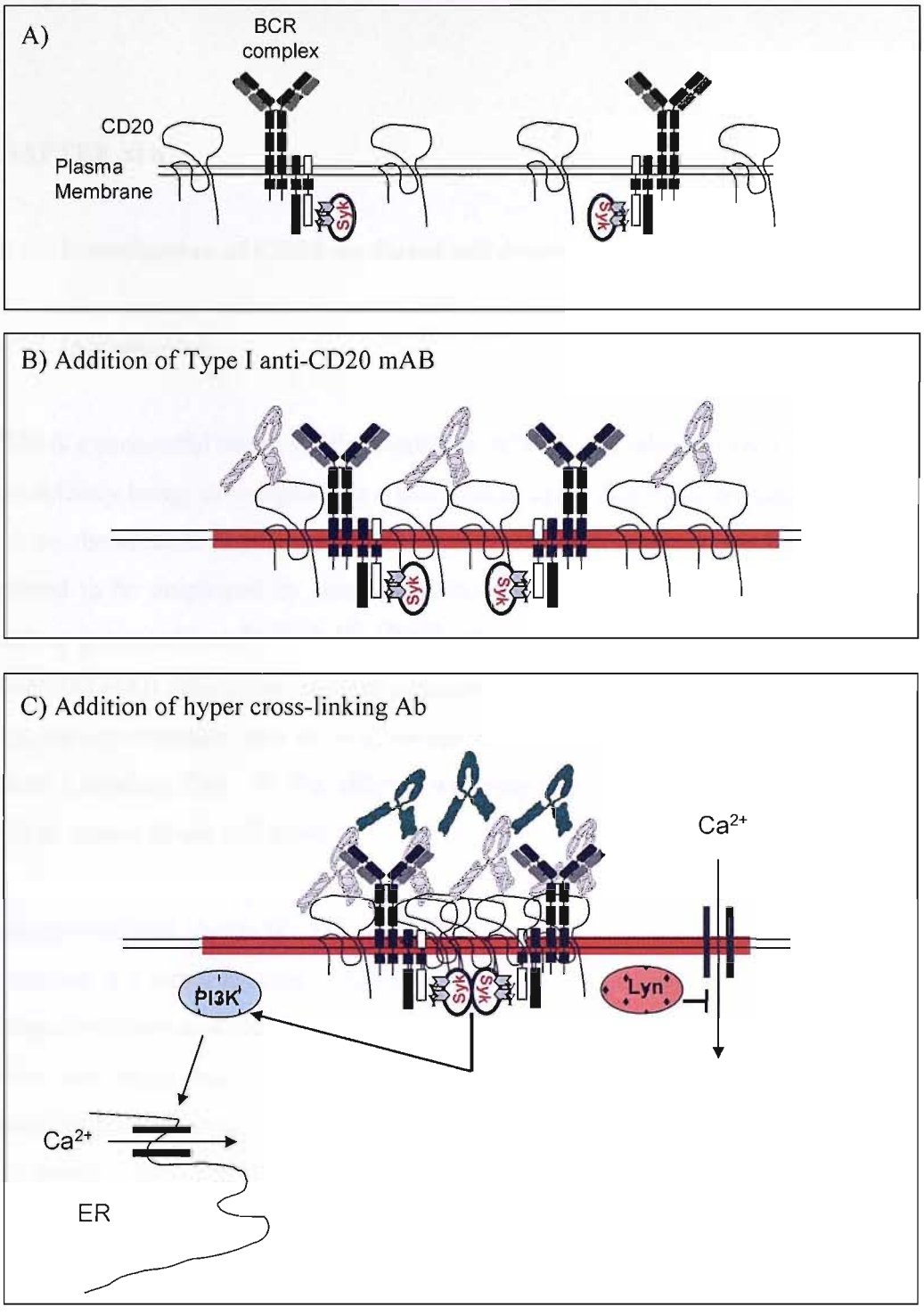

Figure 5.24: The signalling cascade induced by type I anti-CD20 mAb. **A)** CD20 and the BCR reside in the membrane in a non-clustered formation. **B)** Upon type I mAb binding like ritux, CD20 is clustered into TX-100 insoluble rafts on the plasma membrane (red), localising with the BCR on the membrane. **C)** We propose that cross-linking of type I bound mAb brings the ITAMS of BCR complexes associated with CD20 in close enough proximity to initiate signalling through Syk and PI3 kinase. The resultant Ca^{2+} flux is biphasic in nature. Firstly, Ca^{2+} is released from intracellular stores like the endoplasmic reticulum (ER) which results in the activation of store operated channels (SOC) (second phase of the flux) allowing Ca^{2+} influx into the cell and subsequent ERK phosphorylation. The Ca^{2+} influx appears to be negatively regulated by Src family kinases such as Lyn.

CHAPTER SIX

6.0 Investigation of CD20-mediated cell death

6.1 Introduction

CD20 is a successful target for the treatment of NHL and other B cell malignancies and is now actively being investigated as a therapeutic agent in a range of autoimmune diseases such as rheumatoid arthritis and SLE [223, 224]. Several effector mechanisms have been reported to be employed by ritux including; CDC, ADCC and direct induction of cell death or growth arrest [56, 67, 78, 118, 129, 149]. We have shown in Chapter Three that type I anti-CD20 mAb efficiently mediate complement lysis. Furthermore in Chapter Four and Five, we demonstrated that these mAb can readily redistribute CD20 into lipid rafts and induce a calcium flux. In this chapter we assess the ability of type I and II anti-CD20 mAb to induce direct cell death.

Programmed cell death (PCD) was until recently held synonymous with apoptosis. Apoptosis is a death process defined by morphological changes including condensation of the cytoplasm and chromatin, exposure of cell surface markers such as phosphatidyl serine and fragmentation of DNA (see Section 1.6.3). Importantly, apoptosis is a controlled cellular death program leading to minimal inflammation. Conversely, the other well known type of cell death, necrosis is not controlled and characterised by cellular edema and disruption of the plasma membrane, leading to the release of cellular components and subsequent inflammation [171]. Although apoptosis and necrosis are the two most studied cell death pathways, it is now becoming apparent that these two cell death processes are at polar ends of an array of cell death pathways which can occur in the cell. These PCD processes are often intermediates between apoptosis and necrosis and are distinct from apoptosis by their lack of clearly defined morphological changes, where cellular events such as chromatin condensation, nuclear fragmentation and exposure of PS may or may not occur (see Section 1.6.4 and reviewed in [175]).

Several groups have suggested that upon CD20 ligation with mAb, PCD can be induced [52, 56, 63, 91, 129, 159]. However, there are conflicting reports on the involvement of caspases, the induction of nuclear fragmentation and the involvement of mitochondrial regulation making the type of cell death pathway induced by CD20 unclear. In addition, these studies are limited in that generally only one anti-CD20 mAb, namely ritux, is assessed and a small number of B cell lines examined.

Therefore, we decided to investigate the ability of a large panel of anti-CD20 mAb to induce cell death in a range of B cell lines. This panel of mAb allowed us to probe the characteristics of anti-CD20 mAb which are important for the induction of cell death. In addition, the involvement of the actin cytoskeleton, caspases, mitochondrial regulation, intracellular kinases and other signalling molecules such as the BCR were investigated in an attempt to ascertain the cell death pathway engaged by anti-CD20 mAb.

6.2 Results

6.2.1 The ability of anti-CD20 mAb to induce programmed cell death

Initially, we assessed the ability of a panel of anti-CD20 mAb to induce PCD in an array of B cell lines over 24 hours. To ensure that the cell death observed was due to PCD and not CDC, the serum used in the media was heat inactivated preventing complement lysis from occurring (see Section 3.2.1). PCD was analysed by flow cytometry on the basis of Annexin V-FITC (FL1) and propidium iodide (PI) (FL2) positivity. Annexin V binds to phosphatidyl serine (PS) on the cell surface which undergoes membrane flipping, becoming exposed when the cell has entered the cell death pathway. PI is used to identify non-viable and secondary necrotic cells based on their membrane permeability where cells only become PI positive when their plasma membrane integrity is compromised.

The flow cytometry dot plots in Figure 6.1A demonstrate the difference in Annexin V and PI staining between non-treated (NT) Daudi B cells and Daudi cells treated with the anti-CD20 mAb B1. After 24 hours, 6% of NT cells are positive for Annexin V

compared to 38% in B1 stimulated cells. These values are also reflected in the FL1 histogram, with the Annexin V positive cells gated by M1. PI positivity predominantly occurs in cells with high levels of Annexin V binding. In Figure 6.1A, can be seen that as the Annexin V/PI negative population found in the lower left hand corner spreads across in B1 treated cells, the cells only begin to become PI positive when the Annexin V level is higher than an MFI of 100. This sequence of events is expected as PS flipping is an early event in PCD pathways whereas loss of membrane integrity and hence PI positivity occurs at a later stage.

It is evident from Figure 6.1B that anti-CD20 mAb can induce death of Daudi cells but the extent depends on the mAb. Treatment with B1 and AT80 result in a high level of cell death (42% and 35% respectively) compared to ritux (17%) or IF5 (13%). The differences in potency cannot be explained by the mAb isotype as both B1 and 1F5 are murine IgG2a.

To assess whether the ability of anti-CD20 mAb to induce different levels of cell death was specific to Daudi cells or could be induced in other cell lines, we extended our investigation to Raji cells. It is apparent from Figure 6.2A that the hierarchy of potency remains the same, with B1 and AT80 being the most efficient inducers of cell death compared to Ritux and 1F5. Next, we extended the investigation to assess whether mAb potency differs with other B cell lines. To this end, an array of B cell lines were assessed for their sensitivity to CD20-mediated cell death (Figure 6.2B). From this analysis, it transpired that the cell lines assessed could be categorised into three distinct groups based on their sensitivity to CD20-induced cell death; Firstly, highly sensitivity cell lines such as Raji and Daudi demonstrated the mAb potency hierarchy of B1>AT80>ritux. Secondly, moderately sensitive cells SUDHL4 and EHRB, in which AT80 induces a higher level of PCD than B1, and finally cell lines which are insensitive to CD20-induced death such as MHH Pre B-1 and Tanoue.

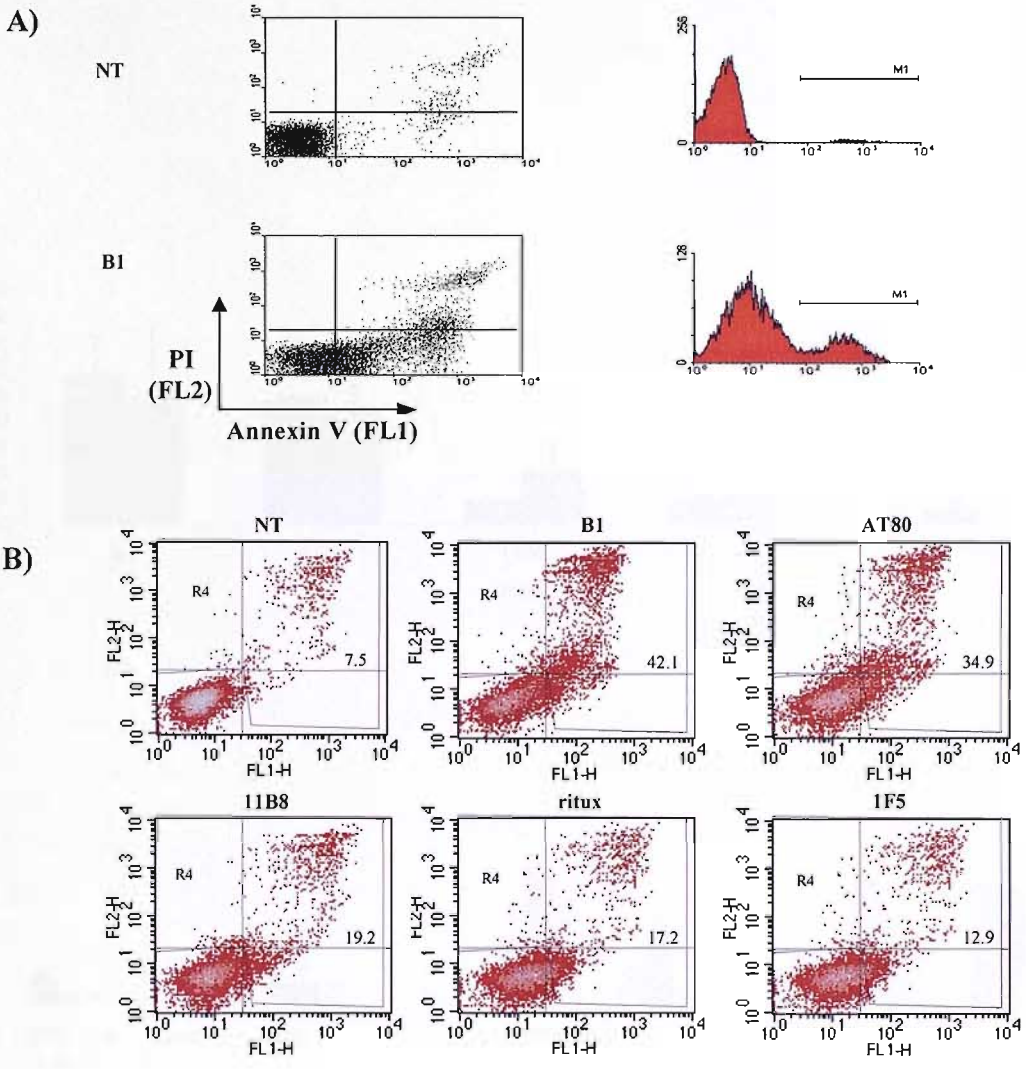

Figure 6.1: CD20 mAb induce varying levels of cell death. A) Illustration of Annexin V/PI method for measuring the level of cell death. Daudi cells were incubated or not (NT) with 10 μg/ml B1 for 24 hours at 37°C, 5% CO_2 before being washed and stained with Annexin V/PI for 15 minutes at room temperature in the dark. Samples were then analysed by flow cytometry. The scatter plots depict the level of cell death where viable cells were found in the lower left quadrant that is Annexin V/PI negative. As cells begin to die they became positive for Annexin V (shown by the spreading of the viable cell population into the lower right quadrant when treated with B1). Cells that became secondary necrotic and non-viable were both PI and Annexin V positive (top right quadrant). The corresponding histograms show the Annexin V positive population, essentially the cells in the top and bottom right hand quadrants. These cells are expressed as a percentage of the total population to calculate the % cell death **B)** $2.5x10^5$ Daudi cells were incubated, or not, with 10 μg/ml mAb for 24 hours at 37°C, 5%CO_2 and then analysed for cell death using the Annexin V/PI assay. The value shown in the scatter plot was the % of cells gated by R4, this was taken as % cell death.

A)

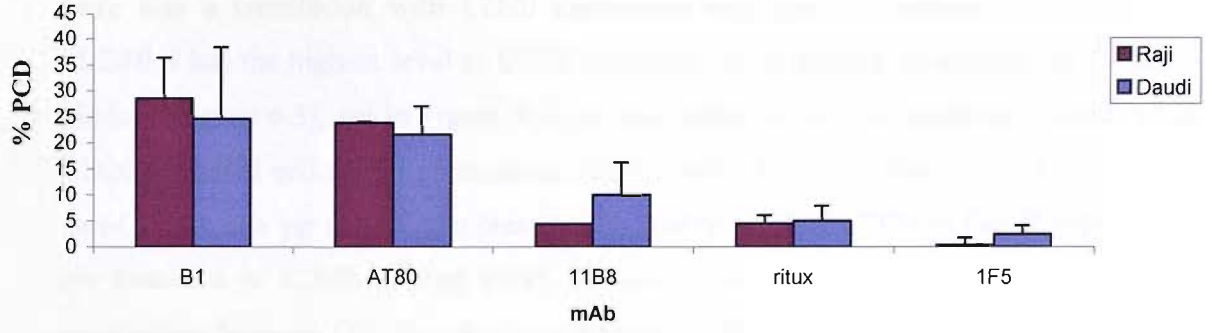

B)

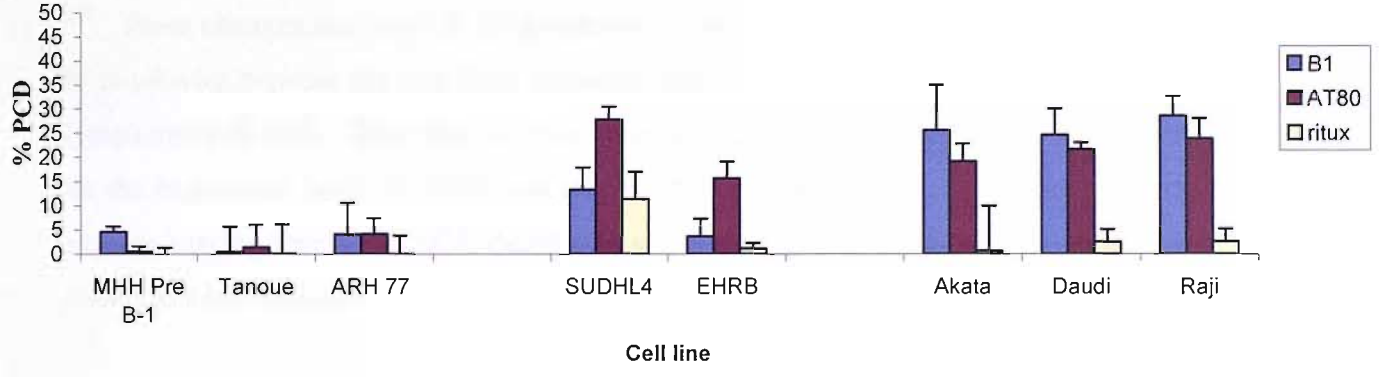

Figure 6.2 CD20 induced cell death is cell line dependent: **A)** $2.5x10^5$ Daudi and Raji cells were incubated, or not, with 10 μg/ml mAb for 24 hours at 37°C, 5% CO_2 and then analysed for cell death by Annexin V/PI assay. The data shown above have the background cell death (NT) subtracted. The values are the mean and standard deviation of three independent experiments. **B)** The same method was used as outlined in Materials and Methods Section 2.14.1. The values shown are the mean and standard deviation of three independent experiments.

6.2.2 The importance of CD20 expression level on the induction of cell death

The data shown in the last section demonstrated that not all B cell lines are sensitive to CD20 induced PCD. One of the more plausible explanations for this is the differences in the expression level of CD20 between the cell lines. Therefore, we assessed whether there was a correlation with CD20 expression level and the potency of cell death. SUDHL4 has the highest level of CD20 expressed on its surface as detected by B1 mAb binding (Figure 6.3), yet in Figure 6.2B it was shown to be only moderately sensitive to CD20-mediated cell death. Meanwhile, ARH77 cells are insensitive to PCD induced by anti-CD20 mAb yet the cells express a comparable level of CD20 to Daudi cells which are sensitive to CD20-induced PCD. As such, there is clearly not a straightforward relationship between CD20 expression and sensitivity to PCD in the cell lines. There are a number of mechanisms by which cells can undergo malignant transformation such as chromosomal translocation of Myc or Bcl-2, infection by EBV or P53 mutations [105, 225, 226]. These changes can result in the protection of the cell from PCD and so the difference in sensitivity between the cell lines probably relates to inherent differences between the lymphoma cell lines. Therefore to more formally examine the dependence of cell death on the expression level of CD20, we utilised the panel of NS/0 cell line clones which express varying levels of CD20, detailed in section 3.2.2. The CD20 expression level of these clones is depicted in Figure 6.3B.

The data shown in Figure 6.3B and C suggest that there is a correlation between CD20 expression level and the amount of cell death induced. Cell death is absent in the low expressing clones 8 and 5 and then becomes apparent from clone 3 and sustains a relatively similar level of cell death for clones 26 and 21. Even though the expression level of CD20 increases linearly from clone 8 to 21, the level of cell death does not appear to follow the same pattern with no real cell death occurring until clone 3. From this we suggest that there is a minimum threshold of expression required for cell death to be induced through CD20 and once this is reached, the level of death becomes independent of expression level. Furthermore, it is interesting to note that in contrast to in the complement assays where B1, a poor inducer of CDC, became effective at

inducing lysis at higher CD20 expression levels such as in SUDHL4 cells and NS/0 Clone 21 (Chapter 3, Figure 3.4 and 3.5 respectively), ritux does not appear to generate a significant level of cell death whatever the concentrations of CD20 on the cell surface.

A)

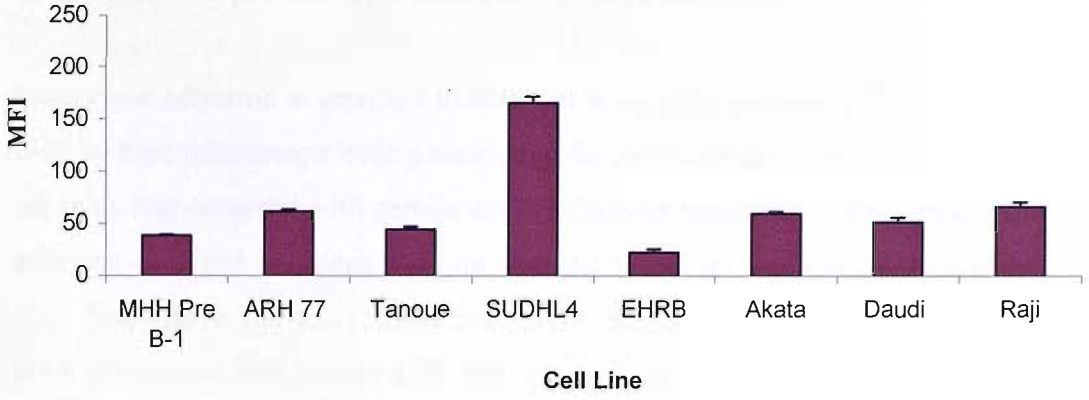

B)

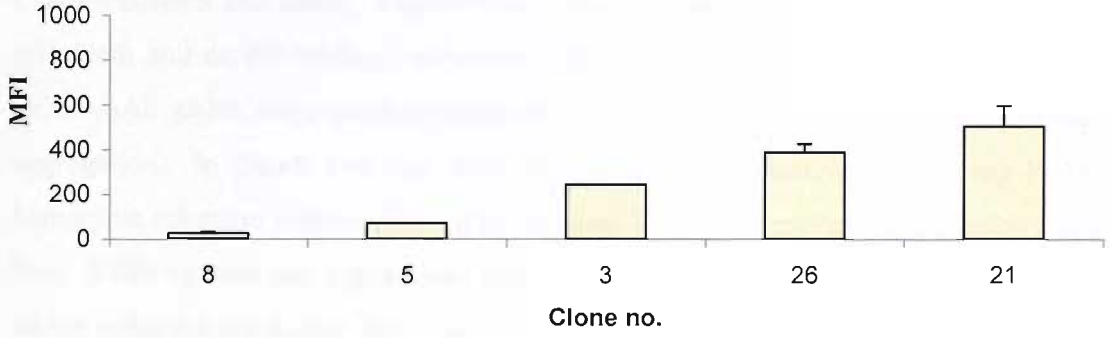

C)

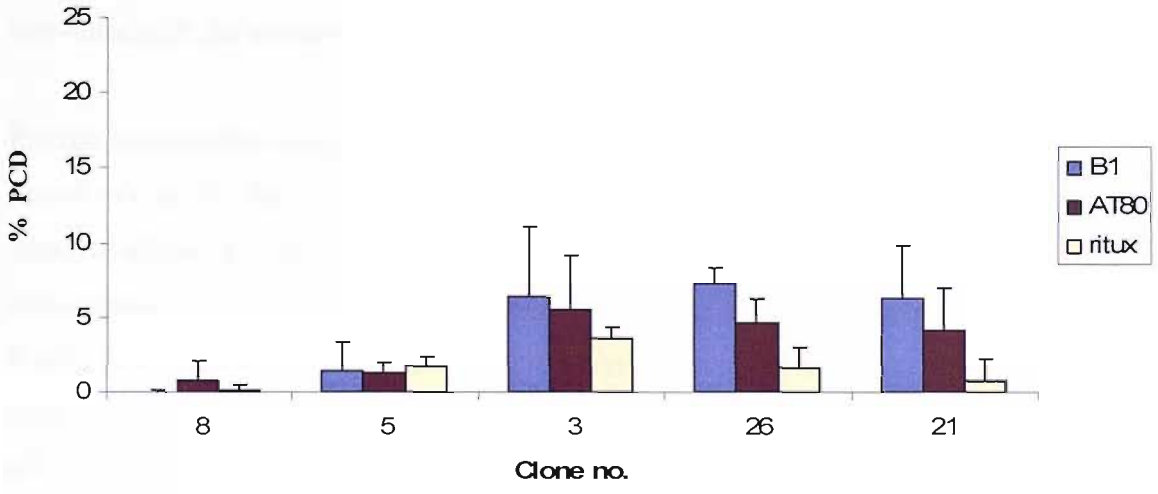

Figure 6.3: CD20 expression level is a determining factor in the level of cell death induced. A) Expression level of CD20 was determined by indirect labelling. Briefly, $1x10^5$ cells were incubated with 10 μg/ml B1 mAb, at room temperature for 15 minutes. Samples were then washed twice and incubated with 50μl 1:40 GAM for 15 minutes at room temperature before being washed and analysed by flow cytometry. **B)** $1x10^5$ NS/0 cells were incubated with 10 μg/ml B1 FITC for 15 minutes at room temperature before being washed and analysed by flow cytometry. Data shown for A and B is the mean and standard error or two independent experiments. **C)** $2.5x10^5$ NS/0 cells were incubated with 10 μg/ml mAb for 24 hours at 37°C and then analysed for cell death using the Annexin V/PI assay by flow cytometry. Values shown are the % cell death induced by the specific mAb minus control (cells incubated without mAb) and the mean and standard deviation of three independent experiments.

6.2.3 The role of homotypic adhesion in CD20-mediated cell death

Homotypic adhesion is reported to occur in some PCD pathways [227, 228]. Observation of cells by light microscope before harvesting for cell death analysis showed that homotypic adhesion had occurred with certain anti-CD20 mAb treatments. The extent to which this adhesion occurred was dependent on both the mAb used and the cell line treated (Table 6.1). The data in Table 6.1 shows that Daudi and Raji cells readily aggregate upon CD20 mAb stimulation and Figure 6.2B demonstrates that they are the most sensitive cells to CD20-mediated cell death. Furthermore, Tanoue cells are insensitive to CD20-induced cell death and do not undergo adhesion. When focussing on single cell lines, the anti-CD20 mAb which were good inducers of cell death are the most potent at inducing cell aggregation. In Daudi and Raji cells, B1 is the most effective at inducing PCD and homotypic adhesion followed by AT80 and then Ritux. Moreover, the adhesion resulting from AT80 ligation was higher than that for B1 in the moderate cell lines such as EHRB which reflected the higher level of cell death induced with AT80 in these cells (Figure 6.2B). From these observations it appears that the propensity of cells to undergo adhesion correlates with the sensitivity of the cells to CD20-induced cell death.

Further investigation was required to determine if homotypic adhesion actually plays an active role in the induction of cell death through stimulation with anti-CD20 mAb, or whether adhesion is an epiphenomenon that occurs independently of cell death or as a consequence of it. It has previously been suggested that CD20 mAb stimulation may induce LFA-1 adhesion [46]. LFA-1 is an integrin which is expressed on all leukocytes. It interacts with intracellular adhesion molecules such as ICAM-1 and is involved in both adhesion and migration of leukocytes [229]. Therefore, the expression of LFA-1 was assessed on a panel of B cell lines using the anti-LFA-1 mAb HB202. It can be seen from Figure 6.4 that Raji cells are the only cell line positive for LFA-1 out of the cell lines assessed. Further to this, we attempted to block adhesion on Raji cells using mAb directed to LFA-1 and found that even though a reduction in adhesion was observed in cells co-incubated with B1 and HB202 (anti-LFA-1) mAb after 6 hours, the level of cell death was not reduced (data not shown). These results suggest that homotypic adhesion

does not play a pivotal role in the induction of PCD. Furthermore, as is evident from Figure 6.4 the level of LFA-1 on the surface of Raji cells is low and indeed is absent on most other B cell lines tested suggesting that homotypic adhesion induced by anti-CD20 mAb may be mediated through a different set of integrins.

		Cell line			
	Isotype	**Tanoue**	**EHRB**	**Daudi**	**Raji**
NT	-	-	-	-	+
AT80	IgG1	+	+++/++	++	++
B1	IgG2a	+	++	+++	+++
1F5	IgG2a	-	-	+	++
ritux	Hu IgG1	+/-	+	+	++
11B8	Hu IgG1	-	++/+	++/+	++/+

Anti-CD20 mAb

Table 6.1: Homotypic cellular adhesion occurs upon CD20 mAb stimulation. To assess adhesion, $2.5x10^5$ cells were analysed under a light microscope at low power (4X). Results are representative of three independent experiments. Adhesion was assessed by the extent and size of cellular aggregates and is designated with an increasing number of +. Scoring increment on typical number of cells per aggregate; - =0-2, + =3-6, ++ =6-10, +++ =10-15, ++++ =>15

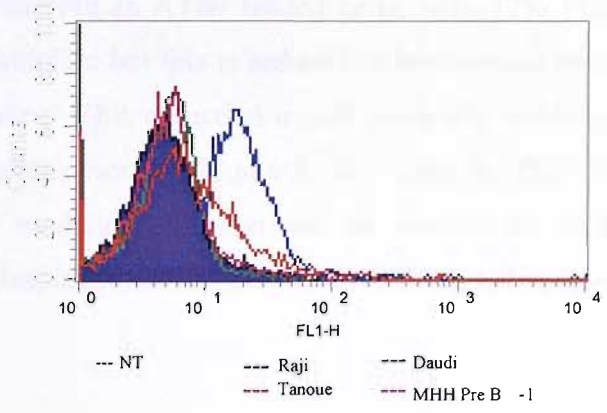

Figure 6.4: The expression level of LFA-1 on B cell lines. $1x10^5$ cells were incubated with 10 μg/ml HB202 FITC for 15 minutes at room temperature before being washed and analyzed by flow cytometry.

6.2.4 Effect of disruption of actin polymerization on CD20-induced programmed cell death

The actin cytoskeleton has been implicated in adhesion and cell death [230, 231]. Therefore we assessed whether adhesion and cell death induced by anti-CD20 mAb are effected by agents which interfere with actin physiology. Polymerisation of actin occurs when monomeric globular actin (G) is converted to filamentous (F) actin. This process can be disrupted by the use of Jasplakinolide which is a naturally occurring cyclic peptide from the marine sponge, *Jaspis johnstoni*. The mode of inhibition is unusual in that it appears to enhance actin polymerization and stabilization and therefore inhibit depolymerisation [232]. We found Jasplakinolide to be toxic at 24 hours in Daudi and SUDHL4 cells at concentrations over 10ng/ml (see appendix II). The reason for this is unclear but is probably due to disruption of normal cellular processes that require actin polymerization such as cell division. Therefore, we decided to harvest the cells after 6 hours when its toxic effects at higher concentrations of 50 and 100ng/ml are minimal.

The data in Figure 6.5A shows that in Daudi cells stimulated with B1, 21% of cells undergo PCD however, in the presence of Jasplakinolide the level of death reduces to 16% with 10 ng/ml of inhibitor to baseline levels in the presence of 50 or 100ng/ml. A

similar trend is observed in AT80 treated cells, with 12% PCD being induced in the absence of Jasplakinolide but this is reduced to background levels when treated with 50 or 100ng/ml inhibitor. This reduction in cell death was reflected in the reduction in the level of cell adhesion observed (Figure 6.5B). Like the PCD data in Figure 6.5A, B1, AT80 and Ritux mediated adhesion are all reduced to background after 6 hours incubation with a Jasplakinolide concentration of 50 ng/ml or higher.

A)

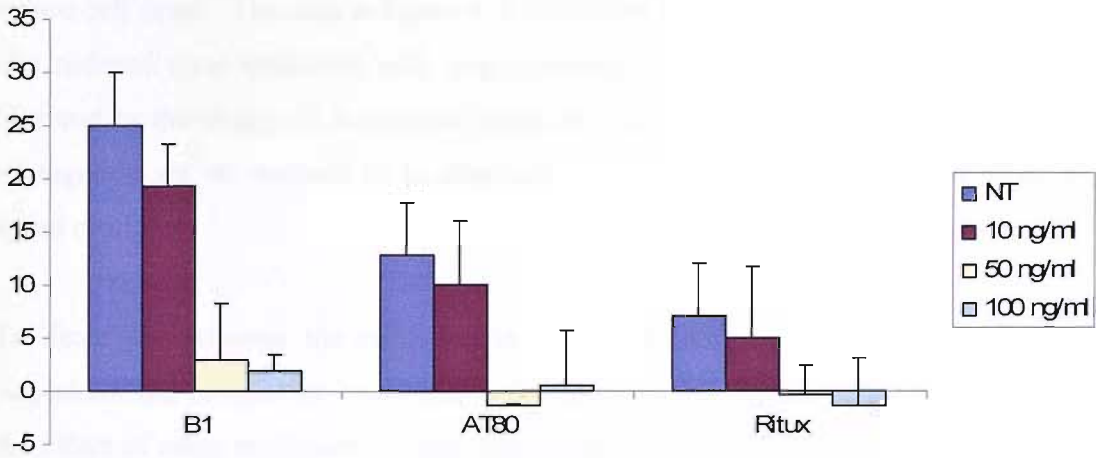

B)

Daudi	B1	AT80	Ritux
MAb only	++	+	++
10ng/ml	+/-	+	+
50ng/ml	-	-	-
100ng/ml	-	-	-

Figure 6.5: Effect of Jasplakinolide on CD20-mediated cell death. A) $2.5x10^5$ Daudi cells were treated with 10, 50 and 100 ng/ml Jasplakinolide for 30 minutes before addition of 10 µg/ml anti-CD20 mAb. Cells were harvested after 6 hours and assayed for cell death by Annexin V/PI assay as outlined in Section 2.14.1. Values shown are the % cell death induced by the specific mAb minus control (cells in medium only). **B)** Cell adhesion was scored under a light microscope at low power before harvesting the cells for A. The degree of aggregation is outlined in Table 6.1. Data is representative of two independent experiments.

Our analysis of the involvement of actin polmerisation was extended to other cell lines. Figure 6.6 shows that in SUDHL4 cells, the level of PCD induced by B1, AT80 and Ritux is notably reduced with 50 ng/ml and 100 ng/ml of Jasplakinolide but 10 ng/ml has little or no effect. The reduction in cell death was broadly reflected by reduced adhesion where B1, AT80 and Ritux showed no adhesion after 6 hours when actin polymerization was disrupted by the presence of Jasplakinolide. However, even though 10 ng/ml can marginally reduce the cell adhesion induced by anti-CD20 mAb, it failed to effectively reduce cell death. The data in Figure 6.6 shows that CD20 mediated death of Raji cells is also reduced upon treatment with Jasplakinolide. Again the reduction in cell death is mirrored by the change in homotypic adhesion where B1, AT80 and Ritux mediated cell aggregation are all reduced to background level with an inhibitor concentration of 50 ng/ml or higher.

To determine whether the reduction in cell death was specific to the inhibition by Jasplakinolide, or whether it was due to disruption of microfilament assembly in general, the effect of other inhibitors of actin polymerization, Latrunculin A and Cytochalasin D on CD20-induced PCD were investigated. Cytochalasin D inhibits actin polymerization by binding to and blocking specific sites at the point of monomer addition on actin filaments [233]. Latrunculin A is isolated from the sponge *Negombata magnifica* and also binds to actin monomers sequestering them and hence preventing polymerization [234]. The data in Figure 6.7A demonstrates that after 6 hours, the ability of B1 and AT80 mAb to induce PCD in SUDHL4 cells was ablated upon treatment with either Jasplakinolide (0.1 μg/ml), Cytochalasin D (1 μM) or Latrunculin A (1 μM). With ritux there was an increase (<10%) in PCD with Latrunculin A. The reduction in PCD in Daudi cells is mirrored by the reduction in homotypic adhesion shown in the corresponding table in Figure 6.7A where a low level of adhesion is observed after 6 hours but is completely abrogated upon actin inhibition. The same results were obtained for Raji cells shown in Figure 6.7B. Anti-CD20 mAb induced cell death and similarly homotypic aggregation was reduced to almost baseline when cells are treated with any of the actin inhibitors. Therefore, we believe that the reduction of CD20-induced cell death is due to disruption of actin polymerization in general and not due to specific effects of Jasplakinolide.

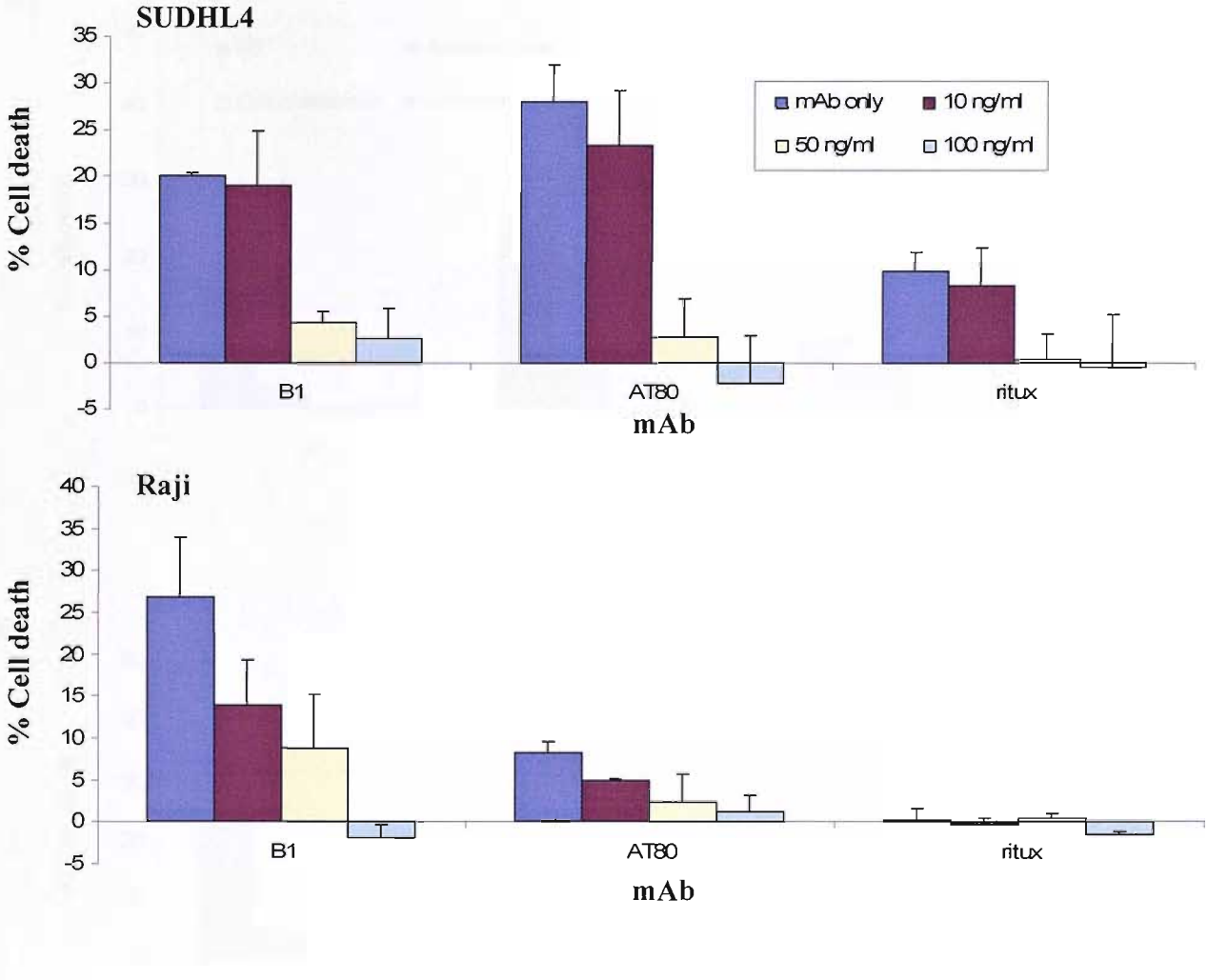

Figure 6.6: Effect of Jasplakinolide on SUDHL4 and Raji cells. $2x10^5$ cells were incubated with 10, 50 or 100 ng/ml Jasplakinolide for 30 minutes before addition of 10 μg/ml anti-CD20 mAb. After 6 hours the cells were harvested for AnnexinV/PI analysis as outlined in Section 2.14.1. Values shown are the % cell death induced by the specific mAb minus control (cells incubated without mAb) which are the mean and standard deviation of three independent experiments.

A)

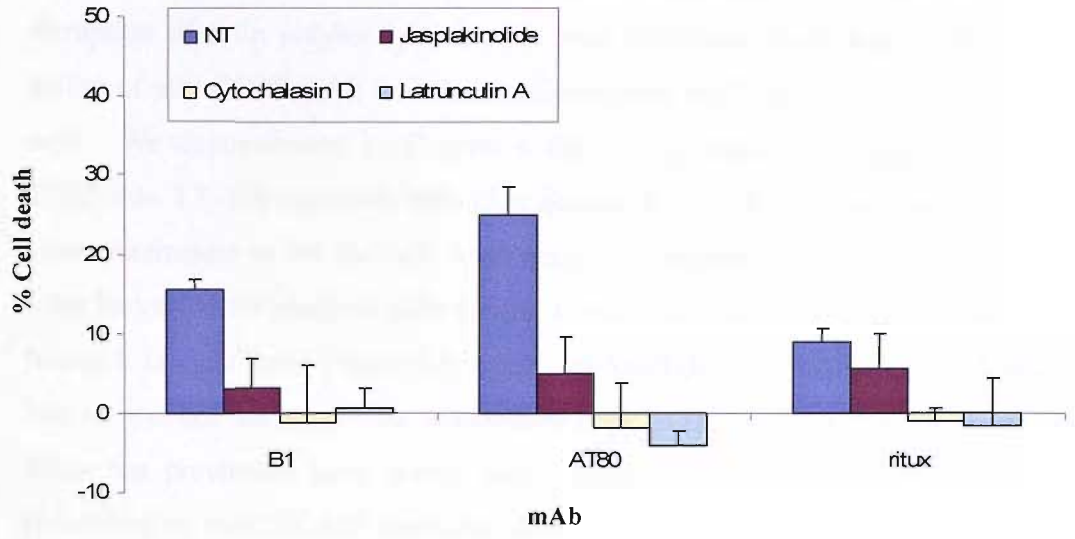

B)

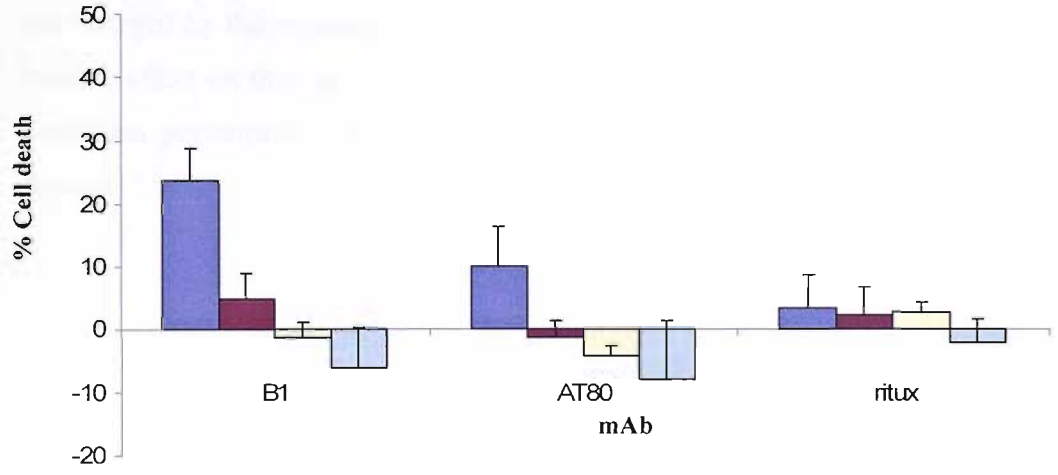

Figure 6.7: The effect of actin inhibitors on CD20-mediated cell death. A) $2.5x10^5$ SUDHL4cells were treated or not with 0.1 μg/ml Jasplakinolide, 1μM Cytochalasin D or 1μM Latrunculin A for 30 minutes prior to addition of anti-CD20 mAb (10 μg/ml). After 6 hours cells were assessed for cell death by Annexin V/PI assay as outlined in Section 2.14.1. Values shown are the % cell death induced by the specific mAb minus control (cells incubated without mAb). **B)** Raji cells were treated as outlined in A.

6.2.4.1 Effect of inhibition of actin polymerisation on the association of CD20 with TX-100 insoluble domains

As microfilaments associate with the plasma membrane, we decided to investigate if disruption of actin polymerization with these inhibitors could lead to disruption in the ability of anti-CD20 mAb to induce redistribution of CD20 into TX-100 insoluble lipid rafts. We demonstrated in Chapter 4 that certain anti-CD20 mAb could redistribute CD20 into TX-100 insoluble rafts (See Section 4.2.2). Raji cells were treated using the same parameters as for the cell death assays as described in Section 6.2.4 but the cells were harvested for analysis after the 30 minutes incubation with mAb instead of after 6 hours. It is clear from Figure 6.8, that Jasplakinolide, Cytochalasin D or Latrunculin A had no marked effect on the redistribution of CD20 into TX-100 insoluble domains. Ritux has previously been shown (see Section 4.2.2) to be a good inducer of CD20 redistribution into TX-100 insoluble domains. As shown in Figure 6.8, the ability of ritux to redistribute CD20 is not affected by the disruption of actin polymerisation. Similarly, the inability of B1 to redistribute CD20 into rafts, as seen in Section 4.2.2, is not changed by the presence of actin inhibitors. Furthermore, the actin inhibitors had no notable effect on the binding of anti-CD20 mAb (data not shown). These experiments were also performed in SUDHL4 cells and the same results were obtained (data not shown).

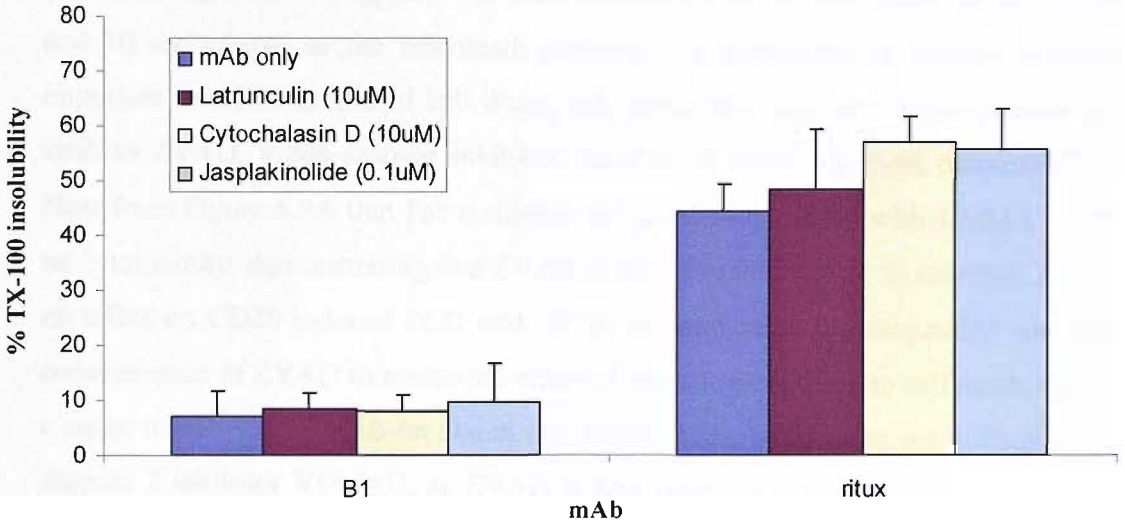

Figure 6.8: Actin inhibitors do not affect the association of CD20 with TX-100 insoluble rafts. $2.5x10^6$ Raji cells were treated with 0.1 μg/ml Jasplakinolide, 1μM Cytochalasin D or 1μM Latrunculin A for 30 minutes at 37°C. 10 μg/ml FITC labelled anti-CD20 mAb (B1 or ritux) were then added for 15 minutes at 37°C before washing and dividing the sample in half. One half was maintained on ice in PBS whilst the other was treated with 0.5% TX-100 for 15 minutes on ice. Cells were washed once, resuspended and assessed by flow cytometry as outlined in Section 2.8.2. Raji data is the mean and standard error of two independent experiments.

6.2.5 The importance of mitochondrial regulation and caspase activity in CD20-induced programmed cell death

Programmed Cell death processes such as apoptosis are mediated through a highly regulated cascade of events. Activation of cysteine proteases known as caspases is often a pivotal step in the induction of classical apoptotic pathways such as engaged by the Fas (CD95) antigen or TNF alpha ([154] and see Section 1.6.3). In these cases initiator caspase 8 and 10 are critical to the cell death pathway. To investigate if caspase activation is important in CD20-mediated cell death, cell permeable caspase inhibitors were utilized such as ZVAD, a pan-caspase inhibitor, capable of inhibiting most caspases [235]. It is clear from Figure 6.9A that Fas mediated cell death is inhibited with 10μM ZVAD with no cytotoxicity, demonstrating that ZVAD is active in these cells. In contrast, ZVAD had no affect on CD20 induced PCD with AT80 in these cells. Subsequently, we used this concentration of ZVAD to assess the effect of caspase inhibition on cell death induced by a range of anti-CD20 mAb on Daudi and EHRB cells. In addition we utilised a specific caspase 2 inhibitor VDVAD, as ZVAD is less potent in inhibiting caspase-2 compared with other caspases. Figures 6.9B and C demonstrate that the induction of cell death with anti-CD20 mAb is not dependent on the activation of caspases, neither inhibitor having a detrimental effect on PCD induced by B1, AT80 or ritux. In Raji cells shown in Figure 6.9B, the same trend in mAb potency as before (Figure 6.2A) with B1 and AT80 mAb inducing higher levels of PCD than ritux and 1F5. There was no detrimental effect observed by the presence of either caspase inhibitor. Once again, the assay was validated by the reduction of Fas mediated cell death from 40 to 6% in the presence of ZVAD. From this data it seems clear that CD20 does not induce a classical apoptotic pathway as caspase activation is not required for the induction of cell death.

Mitochondrial proteins are another important mediator in several cell death pathways. These proteins can be both pro-apoptotic such as Bim, Bad and Bax or anti-apoptotic such Bcl-2 and Bcl-x_L, the balance between these two groups is believed to be central to whether cell death is induced or not (reviewed in [157]) . To assess whether mitochondrial regulation is important in CD20-induced cell death, cytoplasts were generated.

Cytoplasts were formed by treating cells with Cytochalasin B followed by high speed centrifugation though a Ficol gradient to remove the mitochondria and nucleus from the cells (See Materials and Methods Section 2.14.2.2). To ensure that the cytoplasts lack mitochondria, DiOC6, an intracellular dye which detects the mitochondrial membranes, was used to determine the loss of mitochondria. The data in Figure 6.10A demonstrates that Cytochalasin B treated cells lost DiOC6 staining. These cytoplasts were then assessed for their ability to undergo cell death when ligated with anti-CD20 mAb. Figure 6.12B-C shows that removal of the mitochondria reduced the level of cell death occurring in Daudi and Raji cells. In Raji cells, B1 induced PCD was reduced by 15% from 48% to 33%. A similar result was observed in Daudi cells with B1 and AT80-mediated death being reduced (data not shown). However, although a slight reduction in PCD levels occurred, it appears that mitochondrial regulation is not crucial to CD20-mediated cell death.

A)

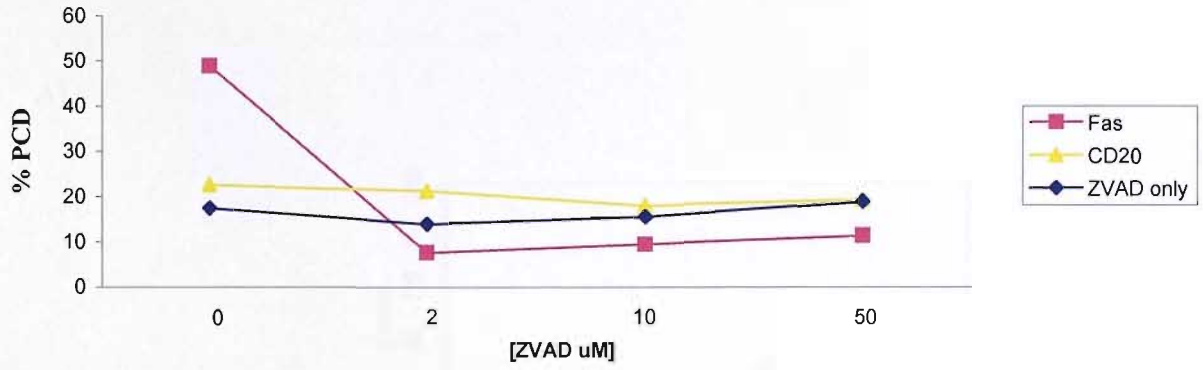

B)

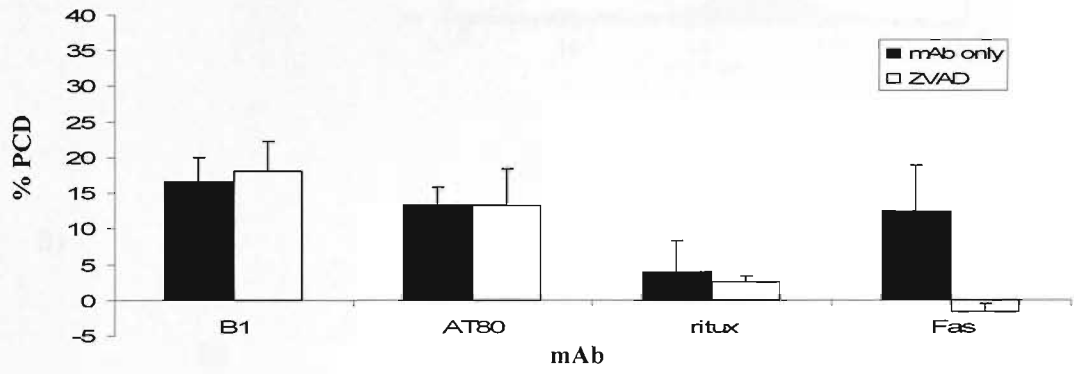

C)

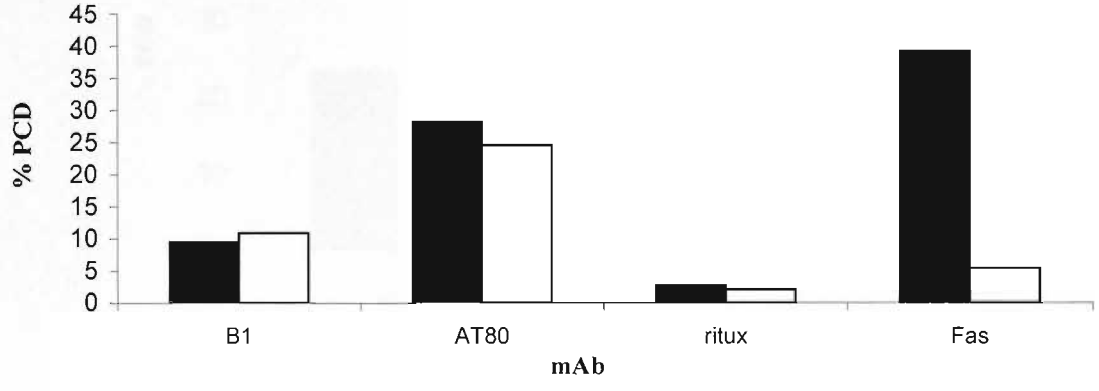

Figure 6.9: CD20 mediated cell death is independent of caspase activity. **A)** EHRB cells were incubated with various concentrations of ZVAD for 30 minutes at 37^{0}C before incubation or not with 10μg/ml anti-CD20 (AT80) or Fas (LOB3/11) for 24 hours. Cells were then washed and analysed for cell death by AnnexinV/PI assay. **B)** 1x10^5 Raji cells were treated with ZVAD-FMK and VDVAD (10μM each) for 1hr before 10μg/ml anti-CD20 mAb were added. Cell samples were harvested after 24 hours and analysed for cell death via Annexin V/PI assay as outlined in Section 2.14.2. Values shown are the % cell death induced by the specific mAb minus control (cells incubated with inhibitor in the absence of mAb). **C)** EHRB cells are treated and assessed as outlined in B.

A)

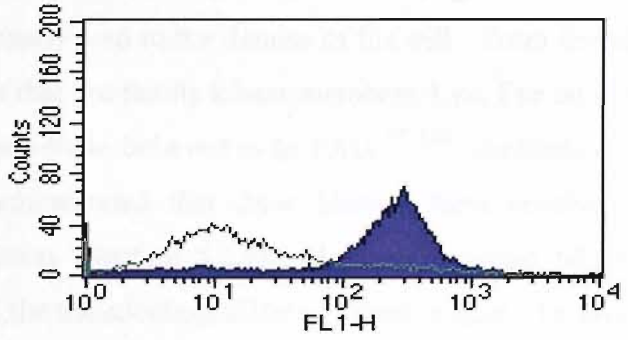

B)

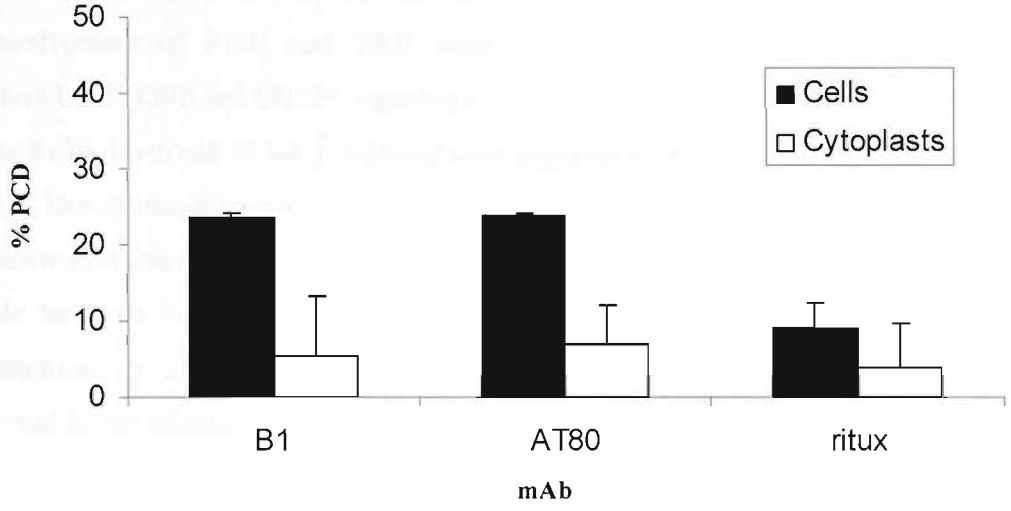

Figure 6.10: Removal of mitochondria influences CD20-induced cell death. A) 10nM DiOC6 was added to 150µl Raji cytoplasts (open) and control Raji cells (shaded) (both at $4x10^6$ cells/ml) for 15 minutes at 37°C before being washed and analysed by flow cytometry. **B)** Raji cells were treated as outlined above. Cells and cytoplasts were resuspended $5x10^7$ cells/ml and treated with 10 µg/ml anti-CD20 mAb for 18hrs before being harvested and analysed for cell death by Annexin V staining as outlined in Section 2.14.1. Values shown have the background (NT) subtracted and are the mean and standard error of two independent experiments.

6.2.6 The involvement of intracellular kinases in CD20-mediated cell death

In CD20-mediated PCD, death is initiated by the binding of mAb to a cell surface receptor which can ultimately lead to the demise of the cell. From immunoprecipitation studies it has been shown that Src family kinase members, Lyn, Fyn and Lck are linked to CD20 through an adaptor protein believed to be PAG [97, 159] (see Section 1.4.6.1). In the previous chapter we demonstrated that these kinases were involved in the CD20-mediated Ca^{2+} flux pathway (Section 5.2.9). Here we assessed whether intracellular kinases were involved in the transduction of the cell death signal. To investigate whether Src family kinases play a role in CD20-mediated programmed cell death, specific inhibitors, PP1 and PP2 and a mock inhibitor, PP3 were employed. PP1 and PP2 are of similar structure and potently inhibit Src-family tyrosine kinases with high-selectivity through competitive binding with ATP for its binding site [236]. PP3 is structurally very similar to PP1 and PP2 but does not have an inhibitory effect on Src PTKs. Furthermore, the involvement of PI3K and ERK were investigated through the use of specific inhibitors LY294002 and U0126 respectively. These kinases were shown in the previous chapter to be involved in the CD20-induced signalling pathway (see Section 5.2.9 and 5.2.16). The cytotoxicity curves of PP2 and LY294002 inhibitors in Daudi and Raji cells are shown in Appendix II. From the data, we decided that a concentration of 10μM was suitable for each inhibitor as that concentration was not highly toxic to the cells. A concentration of 20μM U0126 was recommended from other cytotoxicity studies performed in our laboratory (A. Ivanov, personal communication).

In Daudi treated cells shown in Figure 6.11A, the level of PCD induced by anti-CD20 mAb was similar to the levels shown before in Figure 6.2. Both B1 and AT80 mAb induced approximately 30% PCD with ritux only inducing 10% PCD. When the cells were pre-treated with ERK inhibitor U0126, there was no effect on B1 stimulated cells however in AT80 and ritux stimulated cells there was a minimal increase of 7% and 4% respectively. When Src kinase activity was inhibited by the action of PP2 again a minimal response was observed. The results obtained were conflicting with an increase of 7% in B1-mediated cell death and a decrease of 6% in AT80 mediated PCD. In

contrast, Src kinase inhibition had no effect on ritux induced PCD. Even though the effect of the Src kinase inhibitor is small, the results were found to be repeatable. Furthermore, the Src kinase mock inhibitor PP3 had no effect. The effect of PI3 kinase inhibition on PCD is also shown in Figure 6.11A. Treatment of Daudi cells with 10μM LY294002 resulted in a notable reduction in the level of PCD induced by B1 and AT80. When PI3K activity was inhibited, B1 induced cell death was reduced from 30% to 15% and AT80-mediated cell death was reduced from 29% to 13%. No effect was observed in ritux-induced PCD. As a control, the effect of the solvent DMSO was also assessed and found to have no effect on the cell death induced by anti-CD20 mAb demonstrating that the effect of the inhibitors on the PCD was due to the inhibitor alone and not the solvent they were reconstituted in.

Raji cells were also assessed for the importance of intracellular kinases in CD20-induced programmed cell death. The results shown in Figure 6.11B are similar to those observed in Daudi cells. ERK kinase inhibition by U0126 had no effect on the cell death induced by B1 but it increased the level of PCD induced by AT80 and Ritux by 5% and 10% respectively. The effect of Src kinase inhibition was different to the results obtained in Daudi cells seen in Figure 6.11A. In Raji cells treated with PP2, the level of PCD induced by both B1 and AT80 is reduced with a reduction of 9% and 7.2% respectively. The effect on ritux-induced PCD was minimal. Similar to Daudi cells, PI3 kinase inhibition by LY294002 in Raji cells resulted in an approximate 50% decrease in the cell death induced by B1 and AT80. Again, no effect was observed in ritux-induced PCD. Furthermore, no effect was observed when cells were treated with the control, DMSO. In summary these results demonstrate that certain intracellular kinases like Src kinases and PI3 kinase are important in CD20-induced PCD. The importance of Src kinases does not appear to be universal in CD20-induced PCD as in Daudi cells inhibition of Src kinase activity had contrasting effects in B1 and AT80 mAb induced cell death but in Raji cells, the PCD induced by both B1 and AT80 mAb was reduced. However, PI3 kinase appears to be important in both Raji and Daudi cells where the cell death induced by B1 and AT80 mAb was reduced by 50% in the presence of the PI3 kinase inhibitor LY294002.

A)

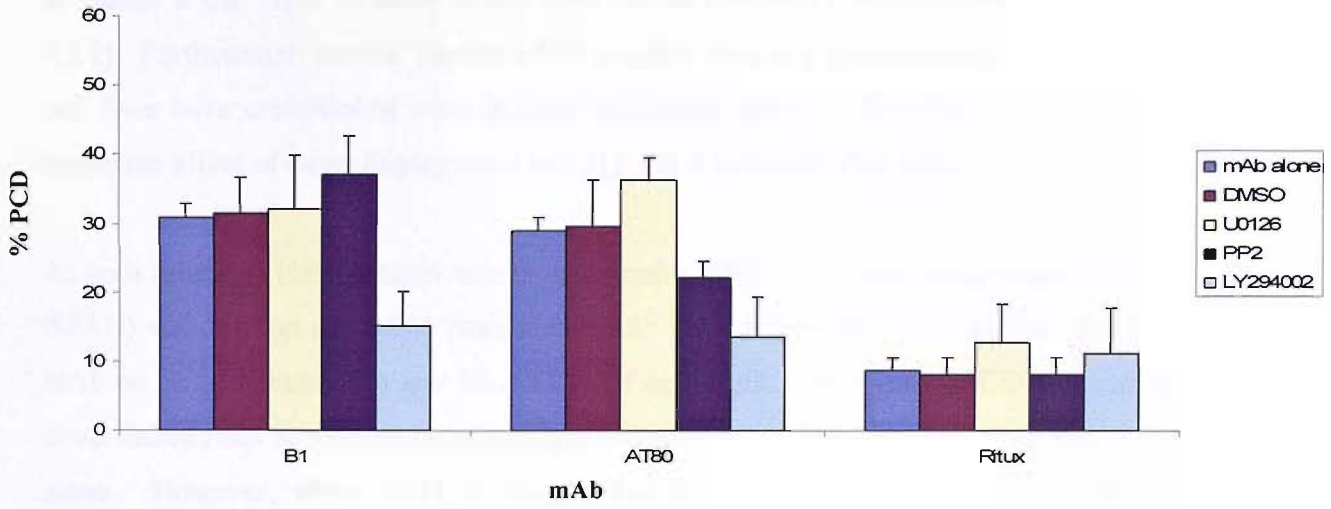

B)

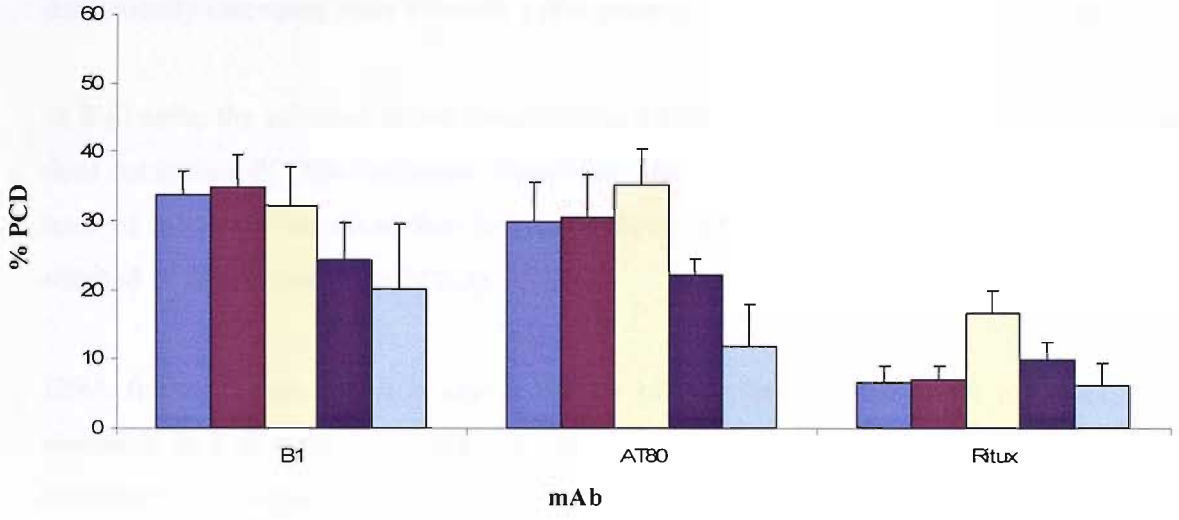

Figure 6.11: **The effect of kinase inhibitors on CD20-induced PCD.** $1x10^5$ Daudi **(A)** and Raji **(B)** cells were treated or not with 0.5% DMS0, 20μM U0126 (ERK inhibitor), 10μM PP2 (Src kinase inhibitor) or 10μM LY294002 (PI3K inhibitor) for 30 minutes at 37°C before addition of B1, AT80 or Ritux at 10 μg/ml. After 24 hours, cells were harvested and analysed for cell death via Annexin V/PI staining as outlined in Section 2.14.1. Values shown have the background cell death subtracted (% cell death induced by the inhibitor in the absence of mAb). Values are the mean and standard deviation based on three independent experiments

6.2.7 The effect of hyper cross-linking on CD20-induced cell death

We demonstrated in Chapter Five that ritux and other type I anti-CD20 mAb were unable to induce a Ca^{2+} flux in most B cell lines unless they were cross-linked (See Section 5.2.2). Furthermore, several reports which suggest ritux is a good mediator of PCD in B cell lines have cross-linked ritux in their cell death assays. Therefore, we decided to assess the effect of cross-linking ritux and 11B8 in Ramos and Raji cells.

As both ritux and 11B8 contain human Fc domains, SB2H2 a mouse anti-human Fc mAb (MAH) was used to cross-link ritux and 11B8. From Figure 6.12 it is evident that this mAb on its own induces a low level (3%) of cell death. The level of PCD induced by cross-linked ritux appears to be an additive effect of the PCD induced by ritux and MAH alone. However, when 11B8 is cross-linked in Ramos cells, the level of PCD is dramatically increased from 6% with 11B8 alone to 22% when cross-linked with SB2H2.

In Raji cells, the effect of hyper cross-linking CD20 is more pronounced. SB2H2 alone does not induce PCD in Raji cells. However, when ritux is cross-linked with SB2H2, the level of cell death increased four fold from 4% to 16%. Similarly, cross-linking of 11B8 resulted in an increase from 21% to 37%.

DNA fragmentation which is also a marker of programmed cell death induction was assessed. In Raji cells, B1, 11B8 and ritux induced minimal fragmentation on their own. However upon hyper cross-linking of 11B8 and ritux with MAH, the level of DNA fragmentation was notably increased from 17 to 40% and 16 to 60% respectively. In Ramos cells the level of DNA fragmentation occurring was lower. This correlates with the sensitivity of these cells to CD20-induced PCD as seen in Section 6.2.1 with Ramos cells being less sensitive than Raji cells.

Interestingly, we found that B1 alone was as effective at inducing PCD compared to cross-linked 11B8 and ritux samples (data not shown). However, minimal DNA

fragmentation occurs in Raji or Ramos cells with B1 indicating that the PCD induced by mAb cross-linking is mediated through a different pathway compared to mAb alone.

In Chapter Five we demonstrated that hyper cross-linking of CD20 was required in Ramos and Raji cells for generation of a Ca^{2+} flux (Section 5.2.2 and 5.2.3). Here we have shown that hyper cross-linking enhances cell death induced by ritux therefore we decided to investigate in the next section whether these two events were directly linked.

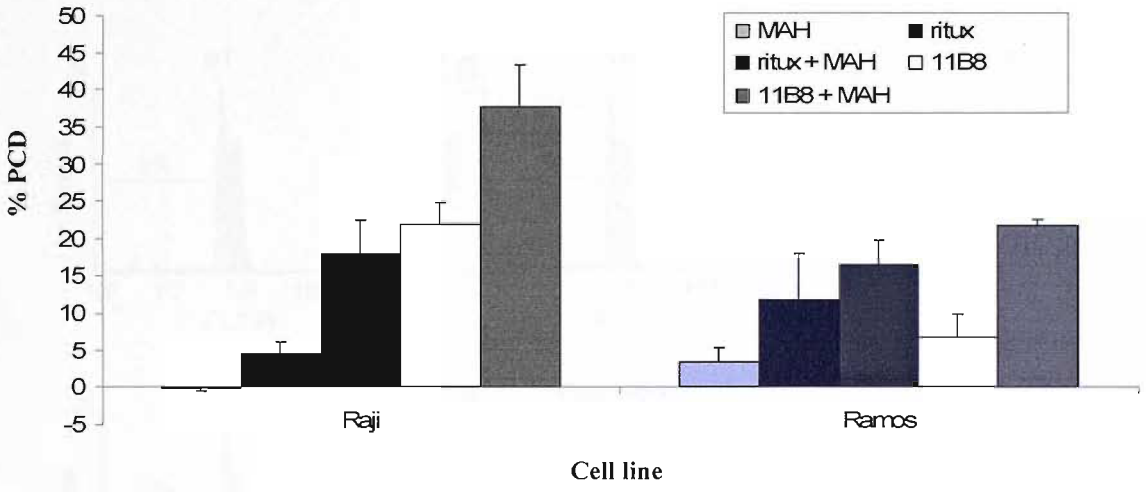

Figure 6.12: The effect of hyper cross-linking on CD20-induced cell death. A) $1x10^5$ Raji or Ramos cells were stimulated with 5μg/ml ritux or 11B8 for 30 minutes at 37^0C before the addition of 25μg/ml mouse anti-human IgG (MAH). MAH treated cells were treated with 25μg/ml MAH alone. All samples were harvested after 24 hours and analysed for cell death via Annexin V/PI staining as outlined in Section 2.14.1. Data shown have the background cell death subtracted. Values are the mean and standard deviation based on three independent experiments.

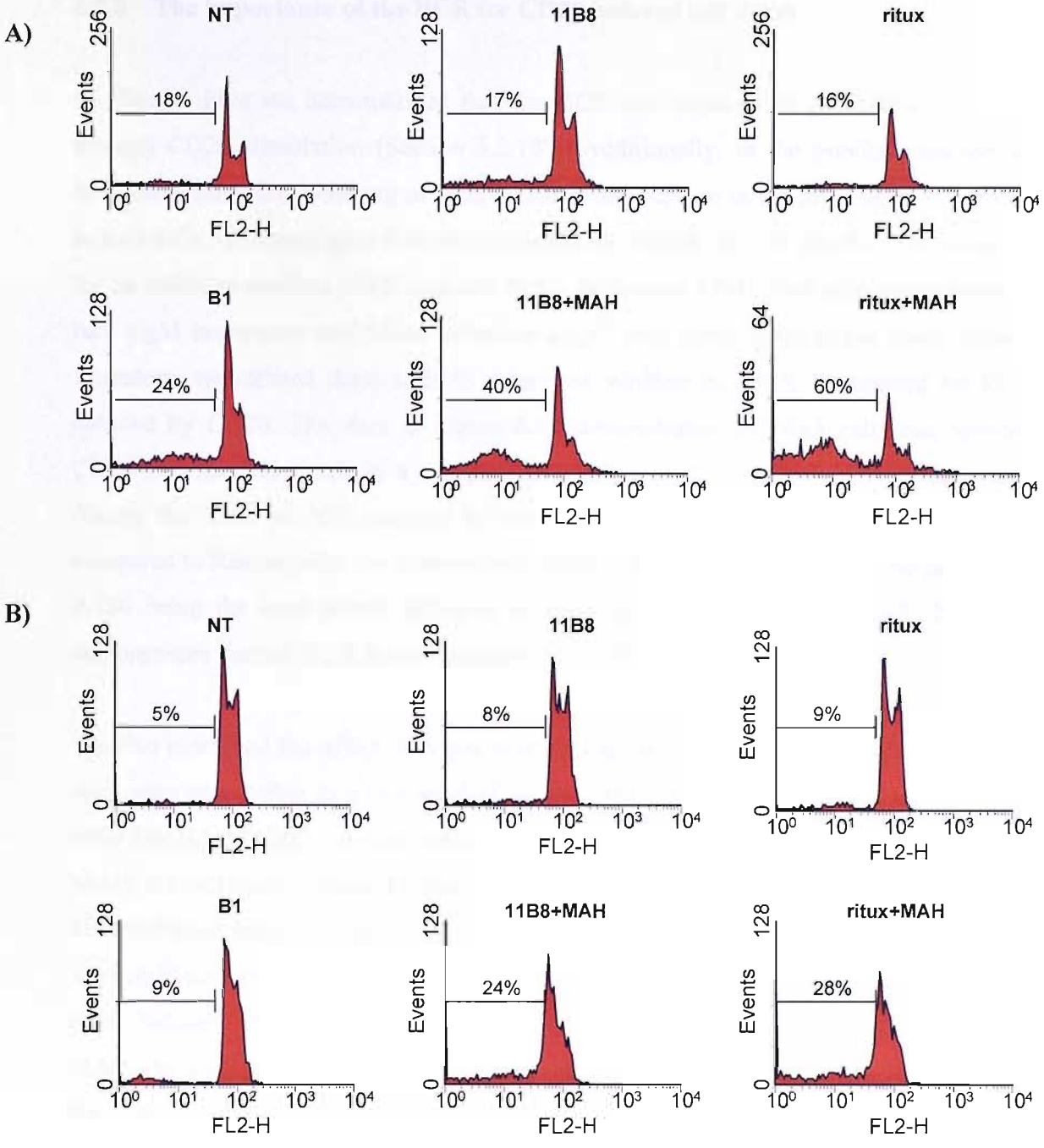

Figure 6.13: Effect of hyper cross-linking on DNA fragmentation: $1x10^5$ cells Raji (A) or Ramos (B) cells were treated with 10μg/ml B1, 11B8 or ritux or 25μg/ml MAH. For hyper cross-linked samples, cells were treated with 5μg/ml mAb for 30 minutes at 37°C before addition of 25μg/ml MAH. After 24 hours cells were harvested and assessed for DNA fragmentation by hypo PI staining as outlined in Materials and Methods section 2.14.1.3. Values shown are the percentage of cells which have undergone DNA fragmentation. Data shown is representative of two independent experiments.

6.2.8 The importance of the BCR for CD20-induced cell death

In Chapter Five we demonstrated that the BCR was required to generate a Ca^{2+} flux through CD20 stimulation (Section 5.2.10). Additionally, in the previous section we have shown that cross-linking of ritux results in an increase in the level of PCD induced in Raji cells. To investigate if these two events are linked, the cell line Rx3 was assessed for its ability to mediate CD20-induced PCD. In Section 5.2.10 Rx3 cells were shown to lack sIgM expression and failed to induce a Ca^{2+} flux upon CD20 hyper cross-linking. Therefore, we utilised these cells to determine whether the BCR is required for PCD induced by CD20. The data in Figure 6.14 demonstrates that Rx3 cells can mediate CD20-induced cell death in a comparable manner to the parent Ramos cells. Even though the level of PCD induced by anti-CD20 mAb is slightly lower in Rx3 cells compared to Ramos cells, the hierarchy of potency in anti-CD20 mAb was the same with AT80 being the most potent followed by ritux, B1, 11B8 and finally 1F5. This data demonstrates that the BCR is not necessary for CD20 PCD.

We also examined the effect of hyper cross-linking in these cells. Both Rx3 and Ramos cells were susceptible to a low level of death (<7% ± SD) induced by the cross-linking mAb SB2H2 (MAH). A cumulative effect was observed in cells treated with ritux and MAH; the cell death induced by the mAb alone was 7% and 3% respectively compared to 10% cell death when Rx3 cells were stimulated with 11B8 and MAH together. However, a synergistic effect was observed in Rx3 cells treated with cross-linked 11B8. 11B8 mAb alone induced approximately 3% PCD in Rx3 cells however when cross-linked with MAH, the level of PCD increased to 11%. The defining difference between Ramos and Rx3 cells is that Rx3 cells lack sIgM expression. Therefore as a positive control, the ability of anti-sIgM mAb to induce cell death in Ramos and Rx3 cell was compared. The data in Figure 6.14 show that stimulation of sIgM can induce cell death in Ramos cells however as expected, Rx3 cells are insensitive to anti-sIgM mAb stimulation. As Rx3 cells display a lower sensitivity to CD20-induced cell death compared to Ramos cells, it implies that the BCR is involved in CD20-mediated PCD. However, from the data in Figure 6.14 it is evident that anti-CD20 mAb maintained the ability to induce PCD in the

absence of the BCR suggesting that the BCR does not play a pivotal role in the induction of PCD but may augment the level of PCD induced by anti-CD20 mAb. Furthermore, as hyper cross-linking ritux in Ramos cells, which can induce a Ca^{2+} flux (Section 5.2.2), does not augment PCD and a similar result was obtained in Rx3 cells, we suggest that Ca^{2+} flux does not play an important role in CD20-mediated programmed cell death. As Rx3 cells have undergone chronic stimulation it is therefore feasible that the normal signaling cascades could be altered. Furthermore, as these cells have been chronically treated with sIgM, a potent death stimulus, it is possible that the Rx3 cells have become more resistant to PCD through selection of resistant clones.

Figure 6.14: The BCR is not crucial for CD20-induced cell death. $1x10^5$ Ramos or Rx3 cells were stimulated with 10 μg/ml anti-CD20 mAb B1, 11B8, AT80, ritux or IF5 or for hyper cross-linked samples (+ MAH), cells were treated with 5 μg/ml ritux for 30 minutes at 37^0C and 5% CO_2 before the addition of 25 μg/ml mouse anti-human IgG (MAH). MAH treated cells were treated with 25 μg/ml MAH alone. All samples were harvested after 24 hours and analysed for cell death via Annexin V/PI staining as outlined in Section 2.14.1. Data shown have the background cell death subtracted and are the mean and standard deviation based on three independent experiments

mAb

6.3 Discussion

Accumulating evidence from in vitro studies [51, 52, 63, 128], animal tumour models [141] and early clinical trials [129] have suggested that PCD plays an important role in the therapeutic efficacy of CD20-directed immunotherapy. One of the most convincing studies to date was performed using a mouse xenograft model in which $F(ab')_2$ fragments of the anti-CD20 mAb B1 (therefore lacking an Fc domain to activate ADCC or CDC) evoked an effective therapeutic response [141]. However, several unanswered questions regarding anti-CD20 mAb therapy remain open for investigation. Firstly, why are certain patients with $CD20^+$ malignancies resistant to ritux therapy and secondly what format of programmed cell death is evoked by anti-CD20 mAb.

Here we demonstrate that not only do cells lines from different haematopoietic origins have different sensitivities to CD20-mediated PCD but that some anti-CD20 mAb are more effective inducers of PCD than others. From analysis of the potency of anti-CD20 mAb to induce cell death after 24 hours, it emerged that mAb could be grouped into either high (for example B1) or low inducers of death (such as 1F5 and ritux). In the previous three chapters type I anti-CD20 mAb, like ritux and 1F5, were demonstrated to be good inducers of CDC, redistribution of CD20 into lipid rafts and generators of Ca^{2+} flux whereas their isotype-matched type II mAb 11B8 and B1 were the antithesis. However, although B1 and 11B8 are unable to redistribute CD20 into lipid rafts or generate a Ca^{2+} flux, they are good inducers of programmed cell death in contrast to isotype-matched type I mAb 1F5 and ritux, respectively. These data indirectly indicate that calcium flux generation and redistribution into lipid rafts is not important for cell death induction through CD20 ligation. Although it should be noted that these characteristics of B1 and 11B8 do not appear to be why type II mAb are such good mediators of PCD as based on AT80's ability to redistribute CD20 into TX-100 insoluble rafts (see Figure 4.5) we classified this mIgG1 mAb as a type I mAb however it is a good inducer of PCD. Intriguingly, AT80, a type I mAb based upon its ability to redistribute into rafts was unexpectedly potent at evoking PCD. These data indicate that some ill-defined property of anti-CD20 mAb confers the ability to evoke PCD.

We demonstrated here that from analysis of eight B cell lines, cell lines could be divided into three groups based on their sensitivity to CD20-induced cell death; low sensitivity cell lines such as ARH77 and MHH pre-B-1, moderately sensitive cell lines SUDHL4 and EHRB, and highly sensitivity ones such as Daudi and Raji cells. The reason for the differences in sensitivity of cell lines to CD20-induced PCD remains unclear. One of the suggested factors in resistance of CLL patients to ritux therapy is due to their low expression of CD20 [105]. On comparison of CD20 expression level in the eight cell lines tested, SUDHL4 had the highest CD20 expression level, yet was only classed as a moderately sensitive cell line. Daudi and Raji cells, which express less than half the level of CD20 present on SUDHL4 cells, were highly sensitive to CD20-induced PCD. From analysis of transfected NS/0 cells it appears that a critical CD20 expression level is required for efficient PCD induction. Clones 8 and 5 express very low levels of CD20 and are not sensitive to CD20-induced cell death. In Clone 3 cell death is induced by anti-CD20 mAb. Even though the CD20 expression level increases linearly from Clone 3 to 21, the level of cell death occurring remains almost constant. This suggests that there is not a linear relationship between CD20 expression level and sensitivity to CD20-induced death but that a threshold expression level must be reached. Once the minimum threshold is overcome, the level of cell death for that particular cell line will depend on the inherent characteristics of the cells. The B cell lines assessed were from different haematopoietic origins (see Table 2.1). Studies by our group and others have shown that expression level of Bcl-2 is not an important factor in CD20-mediated PCD [52, 56]. However, there are a range of other molecular alterations that can occur in a cell upon malignant transformation such as *myc* up regulation, p50 deregulation and EBV infection which can all impact on the sensitivity of cells to programmed cell death [103, 105, 225]. Hence we suggest that the difference in sensitivity between the cell lines is probably due to the inherent differences between the lymphoma cell lines.

A close correlation was found to exist between the sensitivity of cell lines to CD20-mediated cell death and the extent to which cells aggregated. From analysis of four cell lines, it was apparent that Tanoue cells undergo the lowest level of cell-cell adhesion.

This level of aggregation was increased in EHRB cells and higher again in Daudi and Raji cells. The trend of increasing homotypic adhesion was reflected in the sensitivity of the cell lines to CD20-induced cell death where Tanoue cells were the least sensitive and Raji were the most sensitive. Not only did the cell lines vary in the extent to which they aggregated but anti-CD20 mAb also differed in the level of homotypic aggregation that they induced. The level of adhesion induced was directly correlated to the PCD potency of the mAb. B1 and AT80 are the most potent inducers of cell death and were found to induce the highest levels of aggregation compared to poor inducers such as ritux and 1F5. As B cells can express Fc receptors, it may be postulated that the extent of aggregation would be related to the mAb isotype. However, this is not the case as both B1 and 1F5 are mIgG2a yet clearly demonstrate different potencies of homotypic aggregation and programmed cell death.

Integrins are the main family of proteins involved in homotypic adhesion [237]. Integrins are non-covalently associated αβ heterodimeric cell surface receptors which can bind to counter-receptors on adjacent cells [238]. LFA-1 dependent adhesion has previously been linked to CD20 stimulation [46], therefore we assessed whether the blockade of this receptor with mAb would affect CD20 mediated cell death. Of the 4 cell lines analysed, only Raji cells were positive for LFA-1. Co-incubation of Raji cells with anti-CD20 mAb and anti-LFA-1 mAb resulted in a reduction in homotypic adhesion occurring over 6 hours compared to cells stimulated with anti-CD20 mAb alone. However no difference in the level of cell death induced by B1 mAb was observed (data not shown). Hence, we suggest that homotypic aggregation does not have an active role in PCD induction but is rather a reflection of the level of cell death occurring.

Cytoskeleton remodelling is known to play an important part in lymphocyte activation and signalling [239]. We have revealed in this chapter that actin polymerisation plays a central role in the induction of CD20-mediated cell death. The disruption of actin polymerisation with three different inhibitors significantly reduced the PCD induced by anti-CD20 mAb. In Daudi and Raji cells, inhibition of actin polymerisation resulted in the reduction of B1 and AT80-induced cell death to a baseline level. In agreement with a

recent publication by Li et al [68], we found that inhibition of actin polymerisation did not affect anti-CD20 mAb binding to their target or of their ability to redistribute CD20 into TX-100 insoluble rafts. Furthermore, we found that the inhibition of actin polymerisation by Latrunculin A did not affect Ca^{2+} flux induction by ritux stimulation in Ramos and SUDHL4 cells (data not shown). Together with the observation that type II mAb like B1 are the most potent inducers of PCD and the least potent generators of a calcium signal and CD20 redistribution (Section 5.2.1 and 4.2.2 respectively) suggests that CD20-mediated Ca^{2+} flux generation and CD20-induced PCD are mediated by independent signalling pathways. The Ca^{2+} signalling pathway is induced by type I mAb such as ritux, dependent on CD20 redistribution into rafts and independent of actin rearrangement. In contrast, type II mAb like B1 are potent inducers of PCD. This pathway is independent of CD20 redistribution into rafts but dependent on cytoskeleton rearrangement.

The type of programmed cell death pathway induced by anti-CD20 mAb remains unclear. One of the defining characteristics in what is termed 'classical' apoptosis is the involvement of caspases [154, 175]. These cysteine proteases have been reported to be involved in CD20-induced cell death in Ramos and BL60 cells [56, 63, 91]. However, we found that inhibition of caspase activation by chemical inhibitors ZVAD and VDVAD, had no effect on the level of PCD induced by B1 or AT80 mAb in EHRB and Raji cells at a concentration sufficient to induce a notable reduction in the level of Fas-induced cell death. The reason for the conflicting results between us and those published in the literature is most likely due to the use of different mAb treatment conditions. For our assays, cells were treated with anti-CD20 mAb alone. In the other reports, anti-CD20 mAb were cross-linked with a suitable secondary mAb or FcR-expressing cells for 24 hours. In Chapter Five, cross-linking of type I mAb like ritux, as required to generate a calcium flux in Ramos and BL60 cell lines (Section 5.2.2 and 5.2.3). From the reports and results shown in this chapter (Figure 6.15), it is evident that ritux alone is not sufficient to induce high levels of PCD but that cross-linking of the mAb can generate an effective response.

Another key event in PCD is its regulation by mitochondrial proteins where a balance between pro- and anti-apoptotic Bcl-2 family members can determine the fate of the cell [157]. Like caspase activation, the involvement of mitochondria in CD20 stimulated cell death is still debatable. Van der Kolk et al [160] demonstrated that even though mitochondrial regulation and caspase activation are involved in the CD20 death pathway, they are not pivotal to the execution of cells by anti-CD20 mAb. Another group reported that in a clinical trial ritux therapy in combination with Bcl_2 anti-sense siRNA, achieves a higher overall response than ritux on its own [167, 240]. However, we and other groups have found that Bcl_2 expression does not effect the sensitivity of cells to CD20-mediated PCD [52, 56]. In this chapter we assessed the role of mitochondria by comparing the CD20-induced cell death in normal cells to cells which had their mitochondria removed, known as cytoplasts. It was demonstrated that the removal of mitochondria resulted in a minor decrease in the level of programmed cell death occurring in Daudi and Raji cells when stimulated with B1 or AT80. However, due to the small extent of the decrease it is suggests that mitochondria do not play a central role in CD20 induced cell death. Furthermore, during the generation of cytoplasts along with mitochondrial removal, the nucleus is also removed. As only a minor difference was observed in the cell death induced in normal cells compared to cytoplasts, it suggests that the death pathway is also independent of gene transcription

As neither caspases nor mitochondrial regulation appears to play a major role in PCD induced by anti-CD20 mAb alone, we suggest that a non "classical" apoptotic pathway is involved in CD20 mediated killing. The theory that anti-CD20 mAb alone do not induce a classical apoptosis pathway is in agreement with reports that nuclear fragmentation often does not occur during CD20-induced death [51, 52, 241]. The exact cell death pathway employed by CD20 has yet to be defined. However, on the basis of Jaattalias [175] classification of different PCD pathways, CD20-meditated cell death pathway is probably a type of apoptosis-like PCD rather than necrotic pathway due to the similarities it shares with the classical apoptosis pathway. As such, cells undergoing CD20-mediated PCD can demonstrate phosphatidyl serine flipping (as shown by Annexin V positivity) and mitochondrial involvement (as demonstrated by the cytoplasts).

In receptor mediated cell death pathways, activation of intracellular kinases is often required e.g. Src kinases in BCR receptor signalling [14]. The signalling pathways associated with CD20 are still not clearly defined. Upon stimulation of CD20 with certain mAb, it has been reported that CD20 itself can become phosphorylated as well as a range of cellular proteins such as phospholipase Cγ1 and PKC [45, 61, 63]. The tyrosine kinase activity associated with CD20 is primarily mediated through Lyn kinase, a member of the Src family protein tyrosine kinases, which is linked to CD20 via an adaptor protein believed to be PAG [98, 159]. To assess the role of such kinase activity in CD20 mediated cell death, the intracellular inhibitors PP2 was utilised. In Raji cells, both B1 and AT80 mediated cell death was reduced by the inhibition. However in Daudi cells, PP2 treatment did not affect B1-induced PCD and only had a minor effect on AT80-induced killing. Due to the incomplete abrogation with PP2 and the difference between cell lines, it indicates that Src family kinases may play a role but are not pivotal to effective induction of CD20-induced PCD. These results are in contrast to other reports which demonstrated a clear reduction in the level of PCD occurring in Ramos cells however, they studied the effects on cross-linked mAb rather than mAb alone [56, 63].

Further to the involvement of Src kinases we demonstrated that PI3 kinase also plays a role in the promotion of CD20-induced PCD. There was a notable reduction, over 50% in most cases, in the cell death induced by B1 and AT80 mAb in both Raji and Daudi cells with PI3 kinase inhibition. However, of the three kinases assessed in this chapter only ERK kinase appeared to play a possible protective role in AT80 and ritux mediated cell death. Inhibition of this kinase resulted in a slight increase in the level of PCD occurring in both Raji and Daudi cells. However no effect was observed in B1-mediated PCD. The involvement of ERK kinase has been reported by Mathas and colleagues [91] who compared the cell death signalling pathways induced by CD20 (hyper cross-linked) and the BCR. They found that in BL60 cells CD20 and BCR induced PCD showed similar characteristics with up-regulation of the pro-apoptotic protein Bax, caspase activation, c-myc down-regulation and ERK phosphorylation. A lot of these characteristics are in contrast to our findings. However, once again the mAb treatment

conditions were different, in their report they utilised immobilised anti-CD20 mAb (IDEC-C2B8, the murine parent of ritux) which essentially results in a cross-linking effect. Interestingly, in one of their assays soluble and immobilised IDEC-C2B8 were compared and it was found that in contrast to the result with immobilised mAb, with the soluble form no down-regulation of c-myc occurred. There has been much dispute over the effect of cross-linking anti-CD20 mAb on PCD induction. Our group and others have reported that cross-linking of B1 has no effect on the level of PCD [52, 162]. However, Shan and colleagues [51] demonstrated that B1 cross-linking in Ramos cells resulted in a notable increase in the level of PCD.

We suggest that an explanation for why our results differ from most of the published data on CD20-mediated PCD is that we investigated the ability of mAb alone to induce cell death whereas others have used anti-CD20 mAb cross-linked with either a polyclonal antibody or Fc expressing cells [51]. We found that if ritux and 11B8 mAb were cross-linked with a mouse anti-human Fc mAb, the level of PCD induced in Raji cells was notably increased (with only 11B8 being increased in Ramos cells). Furthermore we found that cross-linking resulted in DNA fragmentation where minimal fragmentation was observed in cells treated with mAb alone. As Ramos and Raji cells require hyper cross-linking for the generation of a Ca^{2+} flux (see Section 5.2.2 and 5.2.3) it would seem an obvious suggestion that the increase in PCD is somehow linked to Ca^{2+} flux generation. There are several reports to support this claim; firstly, PLCγ2 which is involved in calcium signalling has been reported to be involved in CD20-induced PCD [63], secondly, DNA fragmentation has been reported by some groups who use cross-linked ritux [51] and thirdly, caspase activation has also been reported to occur in assays using hyper cross-linked CD20 [56, 63, 91]. Finally, It has been reported that rapid influx of Ca^{2+} into the cell can lead to caspase cleavage [242]. Together, these results suggest that the PCD induced by cross-linked anti-CD20 mAb could be more like classical apoptosis. In contrast, we found that in B1-mediated cell death minimal DNA fragmentation occurred and caspase activation was not important. To formally address the question of the importance of Ca^{2+} flux generation we used Rx3 cells. In the previous chapter we demonstrated that these cells lack sIgM expression and fail to generate a Ca^{2+} upon type I

anti-CD20 mAb stimulation (Section 5.2.10). In contrast to the inability of anti-CD20 mAb to generate a Ca^{2+} flux in these cells, we found that anti-CD20 mAb maintained their ability to induce PCD, albeit at a lower level than Ramos cells. This reduction may be due to the chronic stimulation of these cells to achieve a sIgM negative cell line and therefore selecting a more PCD-resistant clone or it could indicate that the BCR is important in enhancing CD20-mediated PCD. However, it is clear that unlike CD20-induced Ca^{2+} signalling, CD20-induced PCD is not entirely dependent on the presence of the BCR thereby suggesting that these events are mediated through distinct pathways. In support of this, the type II anti-CD20 mAb B1 is one of the most potent inducers of PCD yet we have reported in the previous chapter that it did not induce a Ca^{2+} flux. However it should be noted that it appears likely that different PCD pathways can be evoked through CD20 stimulation. From conflicting reports in the literature and our results regarding caspase involvement, DNA fragmentation and mitochondrial regulation, it is becoming apparent that the PCD induced by anti-CD20 mAb alone and that induced by cross-linked anti-CD20 mAb may be mediated through two distinct pathways.

In conclusion, anti-CD20 mAb can induce an apoptosis-like PCD in B cell lines. The extent of PCD depends on the anti-CD20 mAb used and the inherent sensitivity of the cell line. We demonstrated that the signalling pathway involved was not synonymous with classical apoptosis as the PCD induced by anti-CD20 mAb was independent of caspase activation and had minimal dependence on mitochondrial regulation. Dissection of the signalling pathway involved in the cell's demise revealed that arrangement of the actin cytoskeleton, PI3 kinase activation and to a lesser extent, Src kinase and ERK kinase activity are all involved. Further investigation into the possibility that a para-apoptotic cell death pathway is utilised in B1 and AT80 mediated cell death, in contrast to the more classical apoptotic pathway used in cross-linked mAb mediated death is currently under investigation in our laboratory.

CHAPTER SEVEN

7.0 Final discussion and further work

CD20 is a 33-37kDa phosphoprotein which is the target for the highly successful monoclonal antibody drug, Rituximab (ritux). Ritux has been used in the clinic to treat over half a million patients with NHL and other B cell malignancies and is actively being investigated for therapeutic effects in other B cell disorders such as SLE and Rheumatoid Arthritis [223, 224]. The ability of ritux to deplete B cells in vivo is undisputed but the effector mechanisms employed are still being debated. Our knowledge of the molecular and cellular mechanisms by which anti-CD20 mAb deplete B cells has recently been extended by the generation of anti-mouse CD20 mAb allowing for the study of murine models [57]. Tedder and colleagues have demonstrated that the effector mechanism employed is dependent on the microenvironment where B cells in circulation are more rapidly cleared by ADCC compared to B cells within tissues such as the spleen where depletion is slower and more dependent on CDC [144, 148]. However, several questions remain to be addressed such as how the dynamics of B cell depletion change in the presence of tumour and whether Fc independent mechanisms such as apoptosis are involved. Furthermore, as ritux and other anti-human CD20 mAb do not recognise mouse CD20, transgenic mice expressing human CD20 must be generated to study the effects of the anti-CD20 mAb used in the clinic. Importantly, a recent report by Gong and colleagues [120] support Tedder's observations in the dynamics of B cell depletion by ritux and 2H7 mAb in tumour free mice. Again it will be interesting to see how the dynamics change in tumour bearing mice.

In this project we assessed a panel of anti-human CD20 mAb for their ability to evoke different effector mechanisms in B cell lymphoma cell lines. Our first line of investigation was to assess a panel of anti-CD20 mAb for their ability to induce complement lysis. We found that even though all the mAb bound the same target antigen, they were not all effective at evoking complement lysis. The classical complement cascade is activated by the binding of C1q to the Fc domains of two or more juxtaposed surface bound mAb and known to be isotype dependent [12, 199]. We found that anti-CD20 mAb could be divided into two groups; Type I mAb such as

ritux and 1F5 which were good inducers of complement and poor inducers of complement lysis such as 11B8 and B1 which were classed as Type II mAb. Importantly, although isotype was a factor in determining the efficacy of the mAb to give complement lysis, the type of mAb was more critical.

The extent of complement lysis induced by anti-CD20 mAb was found to be dependent on several other factors. In agreement with Golay and colleagues [118] we demonstrated that the expression level of CD20 and of complement defence molecules CD55 and CD59 all regulate the level of CDC. This finding was not unexpected as firstly, as C1q requires two juxtaposed Fc domains for binding and activation, the higher the expression level of CD20, the greater the probability of effective C1q binding. Secondly, both CD55 and CD59 are complement defence proteins which interject at pivotal points in the complement cascade to hinder lysis. Therefore, with lower expression levels of CD55 and CD59 higher complement lysis is achieved by anti-CD20 mAb. These findings however did not explain why anti-CD20 mAb of the same isotype can mediate such different effects. To further probe these unexpected observations, we assessed the binding properties of the two types of mAb. We found that at saturating concentrations, Type I mAb like ritux and 1F5 bound at twice the level compared to their Type II isotype-counterparts, 11B8 and B1, respectively. The reason for this is currently unclear but may possibly be explained by the binding mode of the mAb and we are currently exploring this phenomenon. Interestingly, even when the Type and isotype of mAb are considered, differences in CDC potency are still evident and so other factors may also serve to regulate CDC. Other work in our laboratory has shown that 7D8 is more potent than ritux and suggested that this difference is due to the slower off-rate of 7D8 [200]. It is speculated that this results in 7D8 interacting more stably with C1q for effective induction of the complement cascade. However, it is clear that the type and isotype are the two most critical parameters that largely define the ability of the anti-CD20 mAb to induce potent CDC. In Chapter Four we potentially provide the explanation for this marked difference in CDC efficacy between the Type I and Type II mAb; essentially their differential ability to effectively redistribute and cluster CD20 into TX-100 insoluble rafts in the cell membrane.

Lipid rafts are believed to be small micro-domains in the membrane that contain important signalling molecules such as G proteins and Src family kinases [69, 71]. Partition of receptors in and out of these domains is thought to be important in the initiation and regulation of some cell signalling cascades [70]. Here we demonstrate by sucrose density gradients, detergent fractionation and a flow cytometric assay that Type I mAb (ritux and 1F5) can effectively redistribute CD20 into TX-100 insoluble domains whereas Type II mAb (B1 and 11B8) can not. Furthermore, in line with other reports [72] we found that of five surface antigens assessed, CD20 was the only protein to redistribute into TX-100 insoluble rafts after the addition of mAb alone. Like CDC potency, we found that within the Type I mAb the extent of distribution differed slightly where the level of 7D8-mediated redistribution of CD20 into rafts was higher than other Type I mAb ritux and 1F5. This we suggest relates to the off rate of the mAb, as 7D8 has a slower off rate compared to the other two mAb and so may stabilise the raft domain more effectively hence conferring greater overall resistance to TX-100 solubilisation.

TX-100 is a relatively stringent detergent. A recent report by Li and colleagues [68] suggest that cells which were treated with 'weaker' detergents like CHAPS or Brij 58, found CD20 to be constitutively associated with the insoluble raft domain. Our results support this observation. In untreated cells lysed in Brij 58, CD20 is found in the detergent insoluble raft domain. Importantly, CD20 is also found in the raft domain after Type II mAb treatment suggesting that Type II mAb are not redistributing CD20 out of rafts. Cholesterol is an important constituent of cell membranes which is found intercalated between phospholipids. It is believed that cholesterol plays a pivotal role in the tight-packing of raft micro-domains [82]. In further support of the theory that CD20 constitutively resides in mini-rafts, we found that cholesterol disruption with MCD resulted in loss of CD20 from the raft domains in untreated cells lysed in Brij 58. We also showed that cholesterol extraction leads to a reduction in anti-CD20 mAb binding. The extent of the reduction was dependent on the mAb and the cell line. CD20 is a tetra-span molecule and therefore has two extracellular domains however it is believed only one loop is available for binding and within this loop an alanine-x-proline epitope was crucial for the binding of all anti-CD20 mAb assessed [32]. As MCD affects the binding of all anti-CD20 mAb, we suggest that this epitope is also conformation dependent with the stringency of

cholesterol holding the CD20 in the optimal orientation in the membrane for mAb binding. Why some cell lines are more sensitive to cholesterol depletion is unknown although it possibly relates to the amount of cholesterol already present in the membrane where cells with high cholesterol may not be as severely affected by MCD treatment compared to those with lower cholesterol content. Further work is required to investigate this.

As CD20 (untreated and ligated with Type II mAb) is associated with rafts when assessed by Brij58 but not when assessed with TX-100, we suggest that the distinction between Type I and II mAb to redistribute CD20 into TX-100 insoluble domains is reflective of the ability of Type I mAb to cluster these Brij-58 insoluble mini-rafts into a stable 'macro-domain' which is insoluble to TX-100. On further investigation into this clustering event we revealed that bivalent binding of mAb to CD20 is not required for redistribution where ritux and 7D8 Fab fragments effectively translocated CD20 into TX-100 insoluble domains and importantly bivalent binding was not hindering the ability of Type II mAb to redistribute CD20. Early cell signalling events like Src kinase phosphorylation and actin cytoskeleton rearrangement were not involved in this redistribution event perhaps indicating that Type I mAb induce a conformational change in CD20 in the plasma membrane which somehow favours cholesterol rich domains. Alternatively, it is still feasible that a signalling cascade is involved in this redistribution. Recently it has been suggested that small microdomains are converted into lipid rafts by the action of acid sphingomyelinase which hydrolyses sphingomyelin to ceramide [77]. These ceramide moieties can then spontaneously associate to form large raft domains. Interestingly, Bezombes et al [78] reported that cross-linked ritux generates activated acid sphingomyelinase providing a possible explanation for the association of Type I bound CD20 with TX-100 insoluble rafts. However, as redistribution still occurs at 4°C, which is likely to be prohibitive for an enzymatic reaction and is reversible (M Cragg, personal communication) we favour the conformational change hypothesis.

In all of our assays Type II mAb were unable to perform this redistribution event effectively. Furthermore, to rule out the possibility that Type II mAb were redistributing CD20 but at a slower rate as to avoid detection within the normal 15-30 minutes assessed, we assessed the cells over a 24 hour period. We found that no

redistribution of CD20 was observed upon Type II mAb stimulation yet Type I mAb redistributed CD20 within 15 minutes and held CD20 in the TX-100 insoluble domain for the 24 hour period.

The existence, size, nature and importance of lipid rafts remains controversial [71, 82]. Therefore we used a flow cytometric FRET technique to demonstrate that it is not necessarily the association of CD20 with lipid rafts which distinguishes Type I from Type II mAb but the clustering of CD20 together. The FRET assay detects whether proteins are within 10 nm of each other. This technique has the advantage over the sucrose density gradients and the TX-100 flow cytometry assay in that analysis can be performed in real time on live cells and it does not require detergent. From our FRET analysis it was found that Type I mAb clustered CD20 molecules within 10 nm of each other whereas Type II mAb did not. The level of the FRET signal was dependent on the expression level of CD20 however even in SUDHL4 cells which express three fold higher levels of CD20 compared to most B-cell lines, B1 could only generate a low level FRET signal. Furthermore, we suggest this low level FRET is due to the high expression level of CD20 on the SUDHL4 cells increasing the probability of CD20 molecules being sufficiently close to generate a signal without the need for redistribution.

Clustering of CD20 by Type I mAb was a time and temperature dependent event. Furthermore, by performing TX-100 lysis and MCD treatments we demonstrated that this clustering of CD20 by Type I mAb was reflective of the ability of these mAb to redistribute CD20 into TX-100 rafts.

To support the results obtained from density gradients, TX-100 flow cytometry assay and FRET we used immuno-electron microscopy to create a more visual image of this redistribution event at the cell surface upon Type I and II mAb ligation. The Type I mAb ritux produced a staining pattern indicating that CD20 (and the bound mAb) became clustered into groups of 5 or more whereas the Type II mAb 11B8 generated a staining pattern indicating that CD20 molecules were primarily found alone or in groups of two. These results confirm our findings with FRET and detergent assays that Type I anti-CD20 mAb like ritux and 7D8 can effectively cluster CD20 into domains which are TX-100 insoluble whereas Type II mAb like B1 and 11B8 fail to

effectively cluster CD20 in the membrane. The significance of CD20 translocating into clusters is still unclear. We have reported that clustering of CD20 by Type I mAb may explain its unexpectedly high ability to mediate complement lysis compared to other surface antigens [67]. However, lipid rafts are also believed to act as signalling platforms therefore it is feasible that CD20 redistribution into these domains is also important for initiation of intracellular signalling cascades.

Further to this suggestion, the FRET analysis suggested that upon redistribution with Type I mAb, CD20 localises with important signalling molecules such as the BCR and CD59. This localisation was not found when CD20 was ligated with Type II mAb. The association with CD59 upon Type I mAb ligation would be somewhat expected considering CD59 is GPI-linked protein and therefore is constitutively associated with rafts [79], however the BCR is not believed to be constitutively associated with lipid rafts possibly suggesting that this association is not simply a raft co-localisation event but may have important signalling consequences. In 1993, Bubien et al [45] demonstrated that CD20 could mediate calcium conductance. They demonstrated by patch-clamp analysis that different non B-cell lines transfected with CD20 showed a notable increase in transmembrane Ca^{2+} conductance. Recent work by Li and colleagues [48] demonstrated that CD20 is important for BCR-mediated calcium flux where it operates as part of a SOC channel response. However, it is still unknown whether CD20 itself is the SOC channel or whether it regulates one. Furthermore, limited work has been reported on the ability of anti-CD20 mAb to actually induce a Ca^{2+} flux [62, 63, 65, 221]. For this reason, we investigated the ability of Type I and II mAb to induce caclium flux.

We demonstrated that only Type I mAb could generate a Ca^{2+} flux. In Ramos cells the calcium flux required enhanced cross-linking and further investigation of other B cell lines revealed that the level of Ca^{2+} flux and requirement for cross-linking was dependent on the expression level of CD20. At very high expression levels of CD20 like in SUDHL4 cells no hyper cross-linking was required to generate a flux but as the expression level decreased, cells required hyper cross-linking to generate a flux and the size of the flux correlated to the expression level of CD20. Interestingly, we found that when murine NS/0 cells expressing human CD20 (at a higher level than SUDHL4 cells) were stimulated with Type I mAb no Ca^{2+} flux was observed,

suggesting that some component required for caclium flux is lacking in the murine cells. In turn this suggestion implies that CD20 does not act as a simple ion channel opening after ligation and indicates that CD20 calcium flux requires a signaling cascade.

Store operated channels (SOC) are thought to be one of the main ion channels in operation in non excitable cells such as lymphocytes [58]. These channels open upon the intracellular store release of Ca^{2+} which allows calcium entry from the extracellular space to enter the cell and replenish the stores. We demonstrated that SOC were involved in both CD20 and BCR mediated Ca^{2+} flux. This finding is in support of a recent publication by Li and colleagues [48] who reported that CD20 acts as a SOC for BCR-mediated Ca^{2+} flux in Ramos cells. Little is known about the regulation of these channels and what the exact signal is required for the opening and closing of the channel. It appears the level of free Ca^{2+} in intracellular stores is the deciding factor where the ion channels are open when the intracellular stores are depleted and closed when the stores are full. One reported regulator in the BCR-mediated calcium signalling pathway is Fc receptors where FcγRIIB has been shown to negatively regulate the flux [215]. These receptors are expressed on haemopoietic cell lineages including B lymphocytes. In SUDHL4 cells, we found that Type I mAb fragments which lack the Fc domain ($F(ab')_2$) generated a higher flux compared to Fc-bearing mAb suggesting that Fc receptors also negatively regulate the CD20-mediated Ca^{2+} flux.

It has been a common theory that CD20 may act as an ion channel based on its tetra-span structure and ability to oligomerise in the membrane. For this reason little work has been afforded to the possibility of CD20 mediating Ca^{2+} flux through a signalling cascade. As CD20 and the BCR calcium signalling pathways showed striking similarities in their involvement of SOCs and regulation by Fc receptors, we decided to target important signalling mediators in the BCR-mediated pathway and assess their effect on CD20-mediated Ca^{2+} flux. Our findings demonstrate that in both SUDHL4 and Ramos B cell lines, the Ca^{2+} flux induced by Type I mAb is mediated by an intracellular signalling pathway synonymous to that of the BCR calcium signalling cascade. We demonstrate for the first time that Syk and PI3 kinase are involved in the generation of a CD20-mediated Ca^{2+} flux and the Src family kinases

appear to negatively regulate the flux where MAPK, ERK and P38 kinases were not found to play a role. The involvement of Syk kinase in the signalling pathway is somewhat surprising considering the intracellular domain of CD20 has no ITAM motifs and the only kinases reported to be associated with CD20 are Src family kinases which are linked via an adaptor protein [98]. In BCR signalling Syk associates with the BCR signalling complex via tyrosine motifs in the ITAMs of CD79. Several reports [243, 244] suggest that Syk is the main kinase necessary for generation of a Ca^{2+} flux generated through sIgM stimulation and as there is no known direct or indirect association of CD20 with Syk, we suggest that CD20 and the BCR calcium signalling cascades are linked.

A number of lines of evidence support the hypothesis that CD20-mediated Ca^{2+} flux is linked to its interaction with the BCR. Firstly, both CD20 and BCR signalling pathways involved the use of SOCs and appeared to be regulated by Fc receptors. Secondly, we demonstrated by FRET that CD20 localises with the BCR upon Type I mAb stimulation and not with Type II mAb. Thirdly, the calcium signalling pathways induced by CD20 and BCR stimulation appear to be virtually identical as judged by inhibitor analysis. Hence, we decided to formally address the importance of the BCR in CD20-mediated Ca^{2+} flux by generating a BCR negative derivative of the Ramos cell line called Rx3. We found that these cells retained normal CD20 signalling ability in that Type I mAb could redistribute CD20 and anti-CD20 mAb could induce PCD to a comparable level to that observed in normal Ramos B cells. However, the one clear effect of the BCR absence was the inability of these cells to generate a Ca^{2+} flux through Type I mAb stimulation. To support our theory, primary CLL cells from a selection of patients were assessed for their ability to mediate Ca^{2+} flux generation by CD20 and BCR mAb stimulation. One common phenotype of this disease is the dim expression of sIgM [216]. Like the Rx3 cells, these cells failed to induce a Ca^{2+} flux upon CD20 stimulation or through sIgM stimulation. Interestingly, we found that like Ramos cells and cell lines expressing lower levels of CD20, if sIgM was hyper cross-linked by the addition of a secondary mAb then a Ca^{2+} flux could be generated. This result leds us to postulate that CD20 requires a threshold level of sIgM to generate a Ca^{2+} flux with type I mAb stimulation. Above this threshold, there is sufficient sIgM on the surface to be 'trapped' in the cluster formed by the ligation of type I anti-CD20

mAb which upon hyper cross-linking bring the 'trapped' BCR complexes in close enough proximity to signal through their ITAMs.

We also looked at the effect of cholesterol extraction by MCD on the flux generated through CD20 and BCR stimulation. Previously, we demonstrated that MCD treatment resulted in the loss of CD20 from the TX-100 insoluble domain. Recent reports have suggested that CD20 requires raft integrity to generate a Ca^{2+} flux [62, 65]. Here we found that MCD treatment resulted in a reduced Ca^{2+} flux induced by CD20. This reduction in flux was not due to a reduced association of CD20 and the BCR but more so on the ability of Type I mAb to cluster CD20 together. We also found that upon CD20 hyper cross-linking in Ramos cells, CD20 and the BCR dissociated. This dissociation was not due to internalisation of the BCR and could not be inhibited by blocking the Ca^{2+} flux using intracellular inhibitors. Interestingly, Petrie et al [47] reported that in Ramos cells, CD20 and the BCR localise together in the membrane and upon BCR stimulation they dissociate. They reported no dissociation upon anti-CD20 mAb addition. However, it is noteworthy that the addition of anti-sIgM mAb alone would be sufficient for Ca^{2+} flux generation but for CD20-mediated Ca^{2+} flux, a secondary mAb (as we have shown by FRET analysis) would have been required to observe the dissociation. As blocking the Ca^{2+} flux has no effect, the significance of this event is unclear and may simply be a physical consequence of tight packing of the CD20 microdomains upon the addition of the secondary mAb.

In summary, we believe that Type I mAb cluster CD20 microdomains in the membrane leading to close localisation or entrapment of BCR complexes within the clustered domains. Upon hyper cross-linking with a secondary mAb, these clustered domains are compacted even further, bringing the localised BCR complexes closer together (possibly mimicking anti-BCR mAb stimulation) allowing for initiation of a Ca^{2+} signalling cascade at which point the BCR complexes and CD20 dissociate (Walshe et al, in preparation).

An intracellular change in Ca^{2+} is a relatively early event in most cell signalling cascades. We looked for downstream effects of this pathway in the activation of MAP kinases ERK1/2 and P38 and changes in NFκB activity. We found that in Ramos cells ERK1/2 were phosphorylated upon Type I mAb stimulation. This

phosphorylation was not observed with Type II mAb stimulation. Furthermore, we found that in the presence of calcium chelators, or kinase inhibitors which reduced (PI3K) or ablated (Syk) the CD20 mediated flux, the level of ERK1/2 phosphorylation was reduced and in Rx3 cells which are unable to mediate a CD20 Ca^{2+} flux, no ERK1/2 phosphorylation occurs. From these results we suggest that ERK1/2 phosphorylation is a downstream event in the CD20 mediated Ca^{2+} signalling pathway although more work is required to establish if it is a result of release of Ca^{2+} from intracellular stores or Ca^{2+} influx from the extracellular domain. In addition, more work is required to find a downstream consequence of this pathway possibly activation of AP-1 [91] or TNF-α [127].

Anti-CD20 mAb, in particular ritux, are being extensively used in the clinic to treat a variety of diseases due to their effective depletion of B cells [104, 105, 223]. We have already demonstrated that Type I mAb are efficient mediators of complement lysis. It is believed that programmed cell death is another mechanism utilised by anti-CD20 mAb in the destruction of B cells [51, 52, 63]. Once again, we found a distinction between Type I and II mAb except this time it was the Type II mAb B1 and 11B8 that performed more efficiently than their Type I counterparts. The level of cell death induced by the mAb was dependent on the inherent sensitivity of the cell line. As cell lines are derived from lymphomas which by their nature are highly heterogeneous in their mechanism of tumourogenesis, evasion of immune surveillance etc., the sensitivity of the cell line could depend on a host of factors such as the EBV status, P53 mutations or chromosomal translocations such as Bcl-2 or Myc[165, 225, 226].

Rearrangement of the actin cytoskeleton is an important early event in many signalling cascades [245]. We found that inhibition of actin polymerisation in three different cell lines resulted in a significant reduction in CD20-induced PCD. This was found to be independent of the cell line or mAb used with B1, AT80 and ritux induced cell death being reduced to background level. Inhibition of polymerisation however did not affect the ability of Type I mAb to redistribute CD20 into TX-100 insoluble rafts. Furthermore, inhibition of actin polymerisation had no effect on the Ca^{2+} flux induced by Type I mAb (data not shown). This together with the fact that Type II mAb (poor redistributors of CD20) are more effective at inducing PCD

suggests that the signalling cascade involved in PCD induction is distinct from that involved in the redistribution of CD20 and Ca^{2+} flux generation.

The 'classical' apoptotic pathway involves caspase activation and regulation by Bcl-2 family of mitochondrial proteins [171]. However, the cell death pathway induced by B1 did not show the characteristic signs of classical apoptosis. Firstly we demonstrated that caspase activation is not required for effective cell death in Daudi or EHRB cells. This is in accordance with reports by us [52] and others [160, 180] who found that even though caspase-3 and other caspases can be cleaved during CD20-mediated PCD they do not play an critical role in the demise of the cell. Furthermore, by the generation of cytoplasts (mitochondrial-free cells) we found that the involvement of mitochondria regulation was minimal in CD20-induced PCD. This supports other work by us and others who have demonstrated that Bcl-2 over-expression has no effect on the level of PCD induced by anti-CD20 mAb [52, 160].

The involvement of a signalling cascade in CD20-mediated PCD has been investigated by several groups. Two groups [56, 63] have suggested that Src kinases and calcium signalling may play a role in the PCD induced in Ramos cells. Other reports have suggested that MAPK kinases are involved in the PCD induced by ritux [91, 246]. We investigated the effect of ERK, Src kinases and PI3 kinase inhibitors on the cell death induced by anti-CD20 mAb B1, AT80 and ritux. We found that inhibition of Src kinases and PI3 kinase reduced the level of PCD occurring with B1 and AT80 stimulation. The extent of Src kinases involvement in B1-mediated cell death appeared to be cell line dependent and only reduced cell death by 20-30% whereas the effect of PI3 kinase inhibition was observed in both cell lines assessed and reduced B1 and AT80-mediated PCD by 50% or more. No major effect of PI3 kinase inhibitors was noted in ritux-mediated cell death. However, it appears that ritux is only effective in PCD induction when cross-linked using a secondary antibody or Fc-bearing accessory cells. To consolidate our findings with that of others we compared the effect of cross-linking on 11B8 and ritux-mediated PCD. We demonstrated that the level of PCD induced by ritux in Raji cells is notably increased by the presence of a cross-linking mAb. This effect was also found with 11B8. This result explains some reports suggesting that ritux (cross-linked) is a good mediator of PCD [51, 62, 63] compared to results by us and others who assessed ritux alone and found that the level

of PCD is minimal [52, 78, 162]. Furthermore, we found that cross-linking ritux lead to the induction of DNA fragmentation where no fragmentation was observed in Raji or Ramos cells stimulated with ritux or B1 alone. More work is required to establish whether the cell death pathway engaged upon cross-linking anti-CD20 mAb is similar to that employed with mAb alone although the conflicting reports on the involvement of caspases and our DNA fragmentation results implies that the pathways are different.

As cross-linking was also required for the induction of a Ca^{2+} flux in Ramos and Raji cells and reports have shown that calcium chelation reduces the PCD induced by ritux [56, 63] we assessed the sensitivity of Rx3 cells to PCD. These cells are a derivative of Ramos cells which were incapable of inducing a Ca^{2+} flux upon cross-linking of Type I mAb. Despite the apparent inability of these cells to induce a Ca^{2+} flux through Type I mAb, they maintained their sensitivity to CD20 induced PCD. Furthermore, these cells have virtually no sIgM suggesting, like others [91, 160], that CD20-induced PCD is not entirely dependent on the BCR. As a small reduction in the sensitivity to CD20-induced PCD was observed in Rx3 cells compared to Ramos, it is not clear whether this is attributable to a dependency of the PCD pathway on the BCR or whether it is due to the chronic stimulation of the cells to achieve a BCR negative cell line and thereby selecting a more PCD-resistant clone. Further work is required to establish this possibly by the use of siRNA to reduce sIgM expression. The data from the Rx3 cells together with the fact that Type II mAb like B1 induce actin rearrangement but not redistribution of CD20 into lipid rafts suggests that CD20-directed PCD and calcium signalling are two distinct and separate pathways.

CD20 has no known natural ligand and disappointingly, CD20 knockout mice showed at best, only a marginal calcium flux defect, with no clear phenotype. Therefore the physiological importance of this molecule is not clear. However, the success of CD20 as a target for immunotherapy is undisputed with the anti-CD20 mAb, Rituximab, being used to treat a wide variety of malignancies and stemming from this success is actively being investigated in the treatment of auto-immune diseases and other B cell disorders. Since the identification of CD20 in 1980 a large panel of anti-CD20 mAb have been generated. This project was focussed on elucidating the different signalling pathways induced by anti-CD20 mAb and understanding why some patients are

resistant to ritux therapy. From our studies in B cell lines, we demonstrated that anti-CD20 mAb could be divided into two groups depending on their ability to redistribute CD20 into TX-100 insoluble rafts (see Figure 7.1).

On the one hand, Type I anti-CD20 mAb like ritux effectively redistributed CD20 in the membrane. The significance of this event is not fully understood but we believe it is a pivotal step in the effective activation of the classical complement cascade. Investigation into the sensitivity of cell lines to complement lysis revealed that the expression level of CD20 and complement defence molecules CD55 and CD59 determined the inherent sensitivity of the cells to anti-CD20 mAb induce lysis. Moreover, we demonstrated that redistribution of CD20 was pivotal for the association of CD20 with the BCR which lead to the generation of a Ca^{2+} flux. It appears that CD20 and the BCR-mediated Ca^{2+} flux are linked as Type I mAb are unable to generate a flux in Rx3 cells which lack sIgM or interestingly in primary CLL cells which have low sIgM expression. We demonstrated that ERK phosphorylation is a downstream event in this pathway although further work is required to identify the importance of this signalling cascade.

On the other hand, Type II anti-CD20 mAb like B1 do not effectively redistribute CD20 into TX-100 insoluble rafts and therefore do not generate a Ca^{2+} flux or mediate effective complement lysis. However, they are effective inducers of PCD, an event which appears to be dependent on re-arrangement of the actin cytoskeleton (actin re-arrangement is not required for redistribution of CD20 into rafts) and on PI3 kinase activation. This cell death pathway is not synonymous with 'classical' apoptosis as it was found to be caspase independent and does not involve DNA fragmentation. Interestingly, Type I mAb on their own are poor inducers of PCD yet in the presence of a cross-linking mAb they become effective inducers of PCD. Preliminary work based on DNA fragmentation suggests that the PCD induced by cross-linked Type I mAb and the PCD induced by Type II mAb alone is different, this theory is currently under investigation in our laboratory.

7.1 Further Work

From this thesis it is apparent that anti-CD20 mAb can induce different signalling cascades. However, due to time constraints there were several aspects of the project

which arose that I was unable to finish. The most pressing of was is the downstream significance of Type I-mediated Ca^{2+} flux. As NFκB was assessed and eliminated, based on reports by others the two other factors that could be assessed are activation of the transcription factor AP-1 [91] and the production of TNFα [247]. Microarray studies are currently being performed in the laboratory to assess this. In addition, further work is required to establish whether ERK phosphorylation is a consequence of release of Ca^{2+} from intracellular stores or due to the influx of Ca^{2+} from the extracellular space. This could be answered by the use of calcium chelators to segregate the two pathways. Another unfinished area was the inhibitor studies. To prove that PI3 kinase and Syk kinase are involved in the signalling cascade western blots should be performed to identify that phosphorylation (and activation) of these kinases were occurring. Further work is also required to study the association of CD20 with the BCR. Firstly, it would have been ideal to perform immuno-precipitation of the BCR before and after CD20 hyper cross-linking to answer whether the BCR is becoming activated by this cross-linking. Furthermore, to directly address the requirement of the BCR in CD20 calcium flux, it would be ideal to knockdown the sIgM using silencer RNA. This was attempted using siRNA specific to CD79b but was not effective. We are currently taking another approach which is to knock down sIgM by inducing internalisation with a polyclonal anti-IgM. As this process should take less than two hours and does not affect the CD20 level, it should provide further support that sIgM is necessary for CD20-mediated Ca^{2+} flux.

One area that requires further work is the suggestion that cross-linked Type I mAb may induce a more 'classical' apoptotic pathway. Ideally, the investigations into whether anti-CD20 mAb alone utilised caspases, mitochondrial regulation or kinase signalling inhibitor should be repeated with cross-linked mAb to determine if there is a difference in cell death pathway. Finally, we demonstrated quite comprehensively that Type I mAb like ritux effectively redistribute CD20 into TX-100 insoluble rafts. However, it is not understood how CD20 redistributes, whether a signalling cascade such as ceramide formation is involved or whether it is a conformational change which occurs in CD20 upon mAb ligation. Investigation into this may also explain why Type I mAb have twice the saturation binding level of Type II mAb.

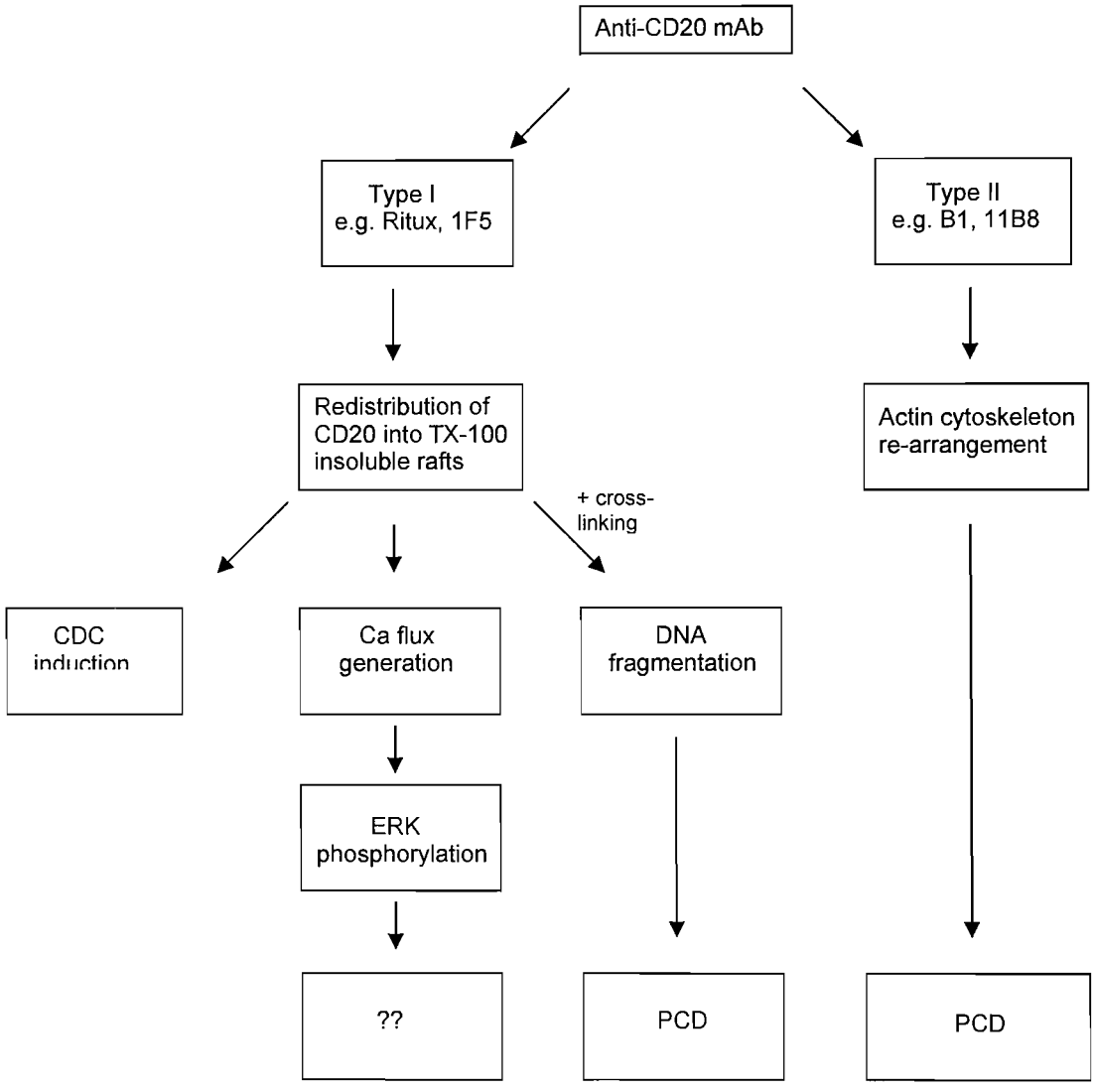

Figure 7.1: Differential signalling cascades of Type I and Type II anti-CD20 mAb. Anti-CD20 mAb can be divided into two groups depending on their ability to redistribute CD20 into TX-100 insoluble rafts. Type II mAb do not redistribute CD20 but do induce actin re-arrangement and lead to programmed cell death. Type I mAb induce redistribution of CD20 into rafts which we believe is pivotal to effective complement lysis and induction of a calcium signalling cascade which leads to ERK phosphorylation. Furthermore, it appears that cross-linking of Type I mAb leads to DNA fragmentation and PCD.

APPENDIX I

1.1 Phenotype of B cell lines

	CD20					
Cell line	**B1**	**1F5**	**11B8**	**Ritux**	**Class II**	**BCR**
Daudi	704.5	1441.1	808.2	1353.4	2210.0	1457.6[#]
EHRB	250.4	582.8	259.1	338.9	946.22	836.8[#]
MHH Pre B-1	464.6	893.3	379.9	593.3	1555.6	469.4[#]
Raji	492.3	865.7	435.5	711.7	2616.8	296.3[#]
Ramos	379.5	717.8	218.6	465.7	1061.4	705.2[#]
SUDHL4	425.3	1039.3	623.6*	1469.1*	900.8	530.7[$]*
Tanoue	174.9	521.1	195.7	343.3	373.2	463.5[#]

Table 1.1: Phenotype of B cell lines used in this project: Cells were phenotyped by indirect labelling as outlined in Materials and Methods Section 2.6. Briefly, $1x10^5$ cells were incubated with 10ug/ml mAb for 15 minutes at room temperature and washed X2 in PBA. Samples were treated with the relevant secondary mAb - GAM for B1, 1F5, Class II and BCR([#]sIgM, [$]sIgG) of MAH for 11B8 and ritux. Samples were analysed by flow cytometry. * FITC labelled mAb used instead of indirect, secondary labelled mAb.

1.2 Phenotype of Rx3 compared to Ramos

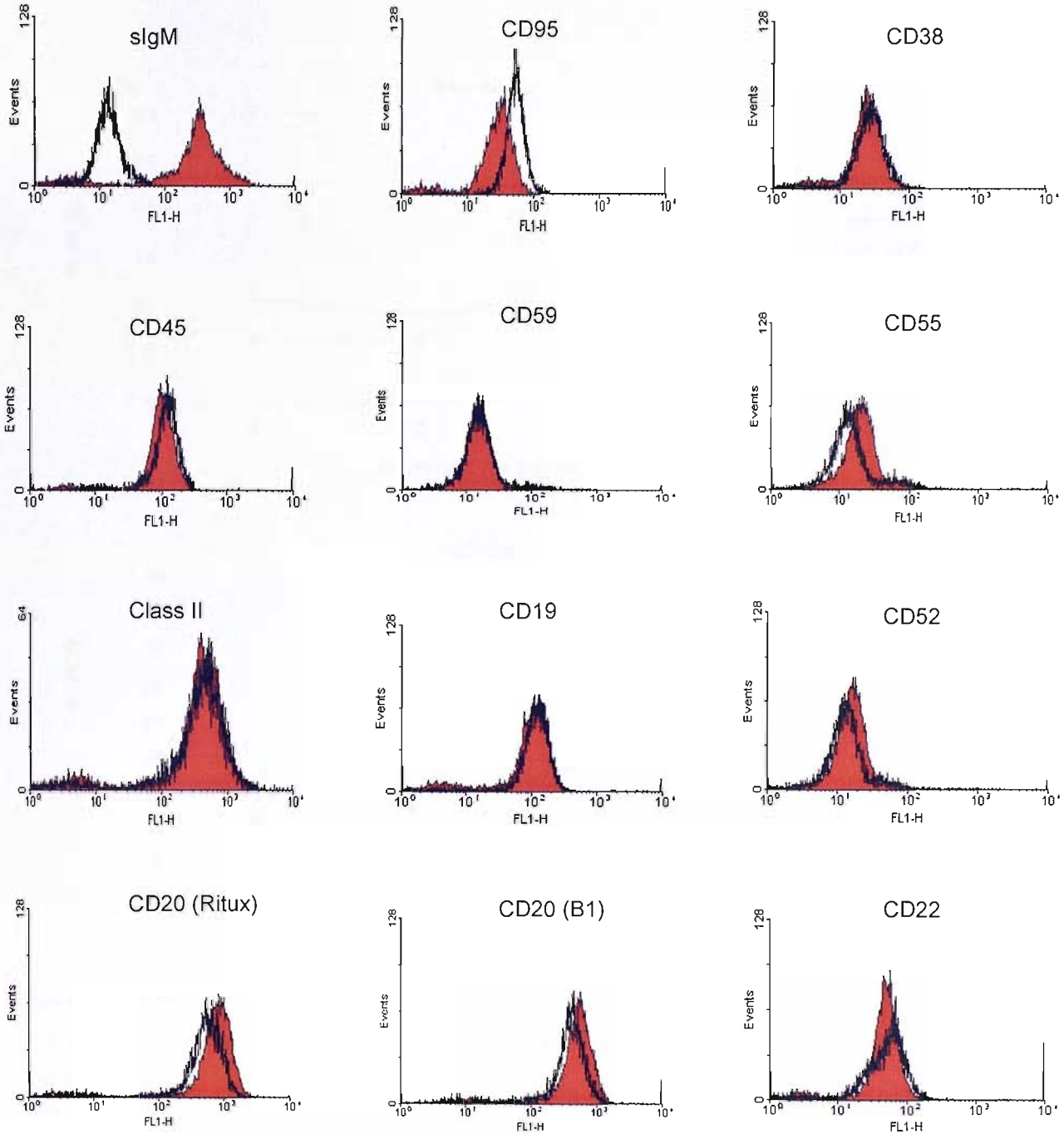

Figure 2: Phenotype of Rx3 cells compared to Ramos. $1x10^5$ Rx3 (clear) or Ramos (red) cells were labelled with 10ug/ml of the relevant FITC-labelled mAb for 15 minutes at room temperature before being washed and assessed by flow cytometry.

APPENDIX II

2.1 Cytotoxicity curve of Jasplakinolide

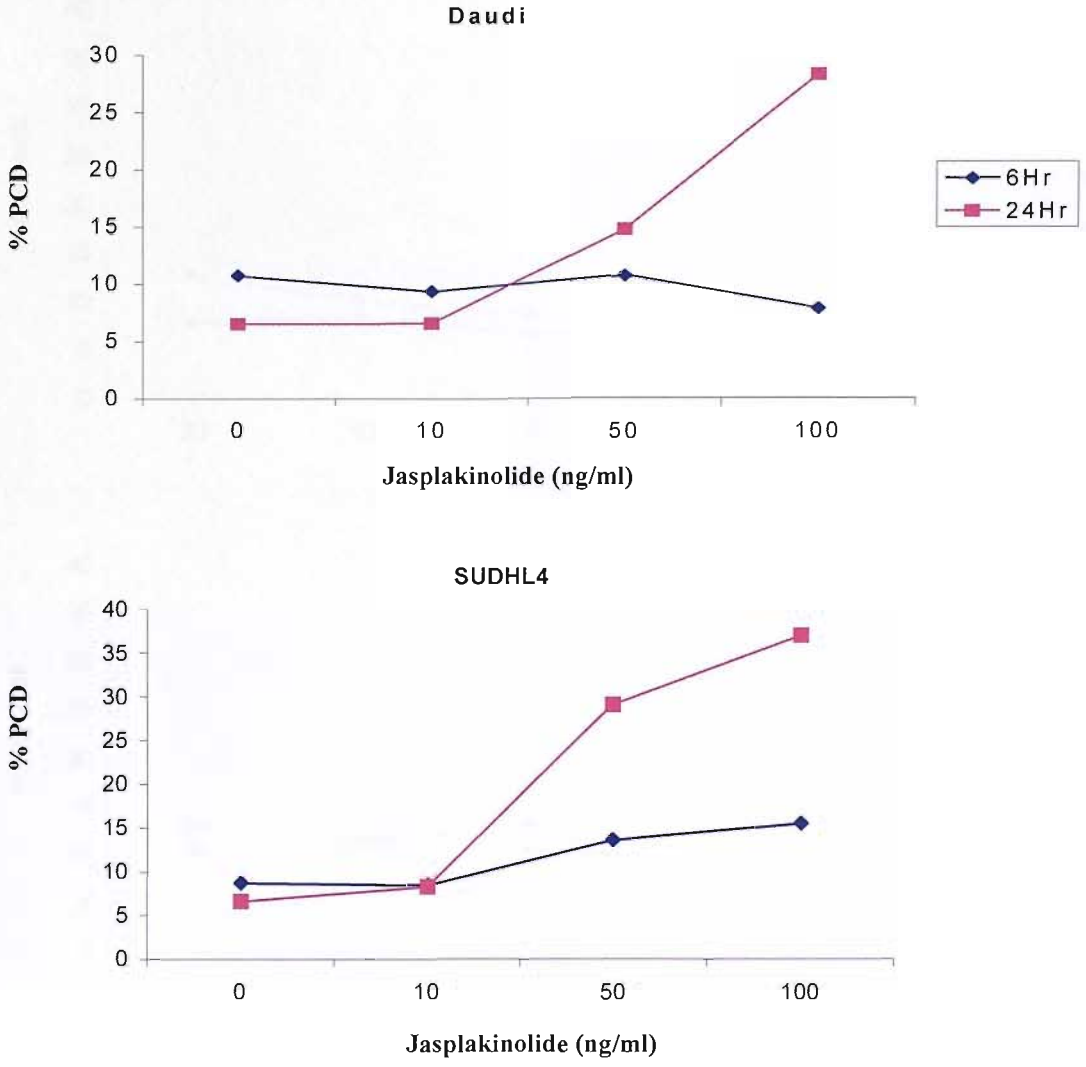

Figure 1: Cytotoxicity of Jasplakinolide. $2.5x10^5$ Daudi or SUDHL4 cells were treated with 10, 50 and 100 ng/ml Jasplakinolide for 30 minutes before addition of 10 μg/ml anti-CD20 mAb. Cells were harvested after 6 or 24 hours and assayed for cell death by Annexin V/PI assay as outlined in Section 2.14.1.

2.2 Cytotoxicity curve of the PI3 kinase inhibitor LY294002

A)

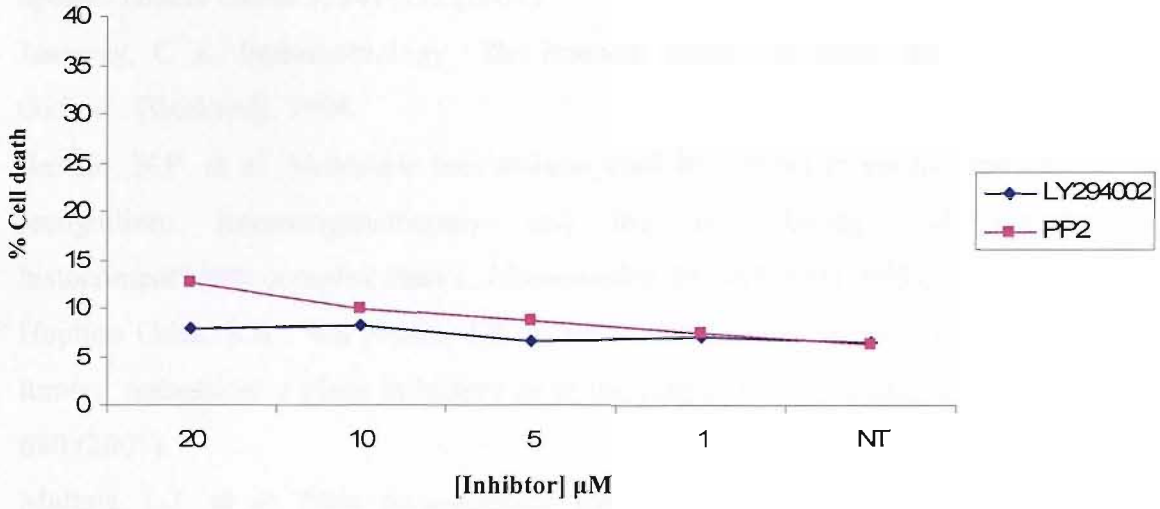

B)

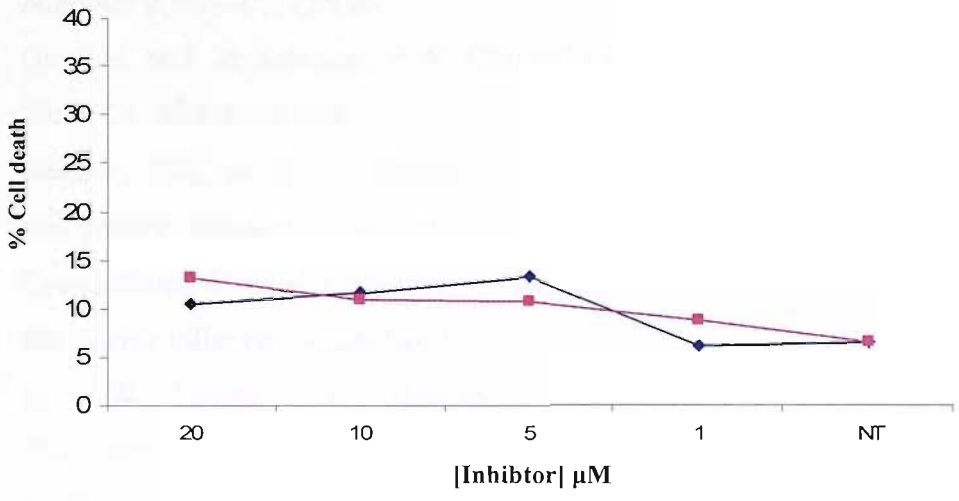

Figure 2: Cytotoxicity curves of kinase inhibitors LY294002 and PP2. $1x10^5$ Daudi **(A)** or Raji **(B)** cells were incubated or not with various concentrations of LY294002 (PI3K inhibitor) or PP2 (Src kinase inhibitor) for 24 hours at 37°C. Cells were then harvested and assessed for cell death via Annexin V/PI assay as outlined in Section 2.14.1.

REFERENCES

1. Ambrose, E.J. Biology of cancer. 2nd ed. Chichester : Ellis Horwood, 1975
2. William Roger, W. The principles of cancer and tumour formation. Cambridge : Chadwyck-Healey Ltd. 1997.
3. Hennessy, B.T., Hanrahan, E.O. & Daly, P.A. Non-Hodgkin lymphoma: an update. *Lancet Oncol* 5, 341-353 (2004).
4. Janeway, C A. Immunobiology : the immune system in health and disease. Oxford : Blackwell, 1994.
5. Restifo, N.P. et al. Molecular mechanisms used by tumors to escape immune recognition: immunogenetherapy and the cell biology of major histocompatibility complex class I. *J Immunother* 14, 182-190 (1993).
6. Hoption Cann, S.A., van Netten, J.P. & van Netten, C. Dr William Coley and tumour regression: a place in history or in the future. *Postgrad Med J* 79, 672-680 (2003).
7. Maltais, L.J. et al. New nomenclature for Fc receptor-like molecules. *Nat Immunol* 7, 431-432 (2006).
8. Glennie, M.J. & Johnson, P.W. Clinical trials of antibody therapy. *Immunol Today* 21, 403-410 (2000).
9. Meeker, T.C. et al. A clinical trial of anti-idiotype therapy for B cell malignancy. *Blood* 65, 1349-1363 (1985).
10. Grundemann, C. et al. Cutting edge: identification of e-cadherin as a ligand for the murine killer cell lectin-like receptor g1. *J Immunol* 176, 1311-1315 (2006).
11. Li, Y.W., Lawrie, D.K., Thammana, P., Moore, G.P. & Shearman, C.W. Construction, expression and characterization of a murine/human chimeric antibody with specificity for hepatitis B surface antigen. *Mol Immunol* 27, 303-311 (1990).
12. Tao, M.H., Canfield, S.M. & Morrison, S.L. The differential ability of human IgG1 and IgG4 to activate complement is determined by the COOH-terminal sequence of the CH2 domain. *J Exp Med* 173, 1025-1028 (1991).
13. Reth, M., Wienands, J., Tsubata, T. & Hombach, J. Identification of components of the B cell antigen receptor complex. *Adv Exp Med Biol* 292, 207-214 (1991).
14. Harnett, M.M., Katz, E. & Ford, C.A. Differential signalling during B-cell maturation. *Immunol Lett* 98, 33-44 (2005).

15. Antony, P. et al. B-cell antigen receptor activates transcription factors NFAT (nuclear factor of activated T-cells) and NF-kappaB (nuclear factor kappaB) via a mechanism that involves diacylglycerol. *Biochem Soc Trans* 32, 113-115 (2004).
16. Antony, P. et al. B cell receptor directs the activation of NFAT and NF-kappaB via distinct molecular mechanisms. *Exp Cell Res* 291, 11-24 (2003).
17. Winslow, M.M., Neilson, J.R. & Crabtree, G.R. Calcium signalling in lymphocytes. *Curr Opin Immunol* 15, 299-307 (2003).
18. Fluckiger, A.C. et al. Btk/Tec kinases regulate sustained increases in intracellular Ca2+ following B-cell receptor activation. *Embo J* 17, 1973-1985 (1998).
19. Wang, L.D. & Clark, M.R. B-cell antigen-receptor signalling in lymphocyte development. *Immunology* 110, 411-420 (2003).
20. Pasquet, J.M. et al. Phosphatidylinositol 3,4,5-trisphosphate regulates Ca(2+) entry via btk in platelets and megakaryocytes without increasing phospholipase C activity. *Embo J* 19, 2793-2802 (2000).
21. Gratacap, M.P. et al. Phosphatidylinositol 3,4,5-trisphosphate-dependent stimulation of phospholipase C-gamma2 is an early key event in FcgammaRIIA-mediated activation of human platelets. *J Biol Chem* 273, 24314-24321 (1998).
22. Ishiai, M. et al. BLNK required for coupling Syk to PLC gamma 2 and Rac1-JNK in B cells. *Immunity* 10, 117-125 (1999).
23. Yang, C. & Kazanietz, M.G. Divergence and complexities in DAG signaling: looking beyond PKC. *Trends Pharmacol Sci* 24, 602-608 (2003).
24. Singh, D.K. et al. The strength of receptor signaling is centrally controlled through a cooperative loop between Ca2+ and an oxidant signal. *Cell* 121, 281-293 (2005).
25. Bolland, S., Pearse, R.N., Kurosaki, T. & Ravetch, J.V. SHIP modulates immune receptor responses by regulating membrane association of Btk. *Immunity* 8, 509-516 (1998).
26. Cornall, R.J. et al. Polygenic autoimmune traits: Lyn, CD22, and SHP-1 are limiting elements of a biochemical pathway regulating BCR signaling and selection. *Immunity* 8, 497-508 (1998).

27. Hashimoto, A., Hirose, K., Kurosaki, T. & Iino, M. Negative control of store-operated Ca2+ influx by B cell receptor cross-linking. *J Immunol* 166, 1003-1008 (2001).
28. Ishibashi, K., Suzuki, M., Sasaki, S. & Imai, M. Identification of a new multigene four-transmembrane family (MS4A) related to CD20, HTm4 and beta subunit of the high-affinity IgE receptor. *Gene* 264, 87-93 (2001).
29. Liang, Y. & Tedder, T.F. Identification of a CD20-, FcepsilonRIbeta-, and HTm4-related gene family: sixteen new MS4A family members expressed in human and mouse. *Genomics* 72, 119-127 (2001).
30. Einfeld, D.A., Brown, J.P., Valentine, M.A., Clark, E.A. & Ledbetter, J.A. Molecular cloning of the human B cell CD20 receptor predicts a hydrophobic protein with multiple transmembrane domains. *Embo J* 7, 711-717 (1988).
31. Tedder, T.F. et al. Cloning of a complementary DNA encoding a new mouse B lymphocyte differentiation antigen, homologous to the human B1 (CD20) antigen, and localization of the gene to chromosome 19. *J Immunol* 141, 4388-4394 (1988).
32. Polyak, M.J. & Deans, J.P. Alanine-170 and proline-172 are critical determinants for extracellular CD20 epitopes; heterogeneity in the fine specificity of CD20 monoclonal antibodies is defined by additional requirements imposed by both amino acid sequence and quaternary structure. *Blood* 99, 3256-3262 (2002).
33. Ernst, J.A. et al. Isolation and characterization of the B-cell marker CD20. *Biochemistry* 44, 15150-15158 (2005).
34. Adra, C.N. et al. Cloning of the cDNA for a hematopoietic cell-specific protein related to CD20 and the beta subunit of the high-affinity IgE receptor: evidence for a family of proteins with four membrane-spanning regions. *Proc Natl Acad Sci U S A* 91, 10178-10182 (1994).
35. Thevenin, C., Lucas, B.P., Kozlow, E.J. & Kehrl, J.H. Cell type- and stage-specific expression of the CD20/B1 antigen correlates with the activity of a diverged octamer DNA motif present in its promoter. *J Biol Chem* 268, 5949-5956 (1993).
36. Himmelmann, A. et al. PU.1/Pip and basic helix loop helix zipper transcription factors interact with binding sites in the CD20 promoter to help confer lineage-

and stage-specific expression of CD20 in B lymphocytes. *Blood* 90, 3984-3995 (1997).

37. Crepieux, P., Coll, J. & Stehelin, D. The Ets family of proteins: weak modulators of gene expression in quest for transcriptional partners. *Crit Rev Oncog* 5, 615-638 (1994).
38. Nutt, S.L., Eberhard, D., Horcher, M., Rolink, A.G. & Busslinger, M. Pax5 determines the identity of B cells from the beginning to the end of B-lymphopoiesis. *Int Rev Immunol* 20, 65-82 (2001).
39. Katopodis, O. et al. Expansion of CD8+ T cells that express low levels of the B cell-specific molecule CD20 in patients with multiple myeloma. *Br J Haematol* 120, 478-481 (2003).
40. Yokose, N. et al. CD20-positive T cell leukemia/lymphoma: case report and review of the literature. *Ann Hematol* 80, 372-375 (2001).
41. Dancescu, M., Wu, C., Rubio, M., Delespesse, G. & Sarfati, M. IL-4 induces conformational change of CD20 antigen via a protein kinase C-independent pathway. Antagonistic effect of anti-CD40 monoclonal antibody. *J Immunol* 148, 2411-2416 (1992).
42. Edwards, C.K., 3rd PEGylated recombinant human soluble tumour necrosis factor receptor type I (r-Hu-sTNF-RI): novel high affinity TNF receptor designed for chronic inflammatory diseases. *Ann Rheum Dis* 58 Suppl 1, I73-81 (1999).
43. Sivaraman, S. et al. Effect of interferon-alpha on CD20 antigen expression of B-cell chronic lymphocytic leukemia. *Cytokines Cell Mol Ther* 6, 81-87 (2000).
44. Wojciechowski, W., Li, H., Marshall, S., Dell'Agnola, C. & Espinoza-Delgado, I. Enhanced expression of CD20 in human tumor B cells is controlled through ERK-dependent mechanisms. *J Immunol* 174, 7859-7868 (2005).
45. Bubien, J.K., Zhou, L.J., Bell, P.D., Frizzell, R.A. & Tedder, T.F. Transfection of the CD20 cell surface molecule into ectopic cell types generates a Ca2+ conductance found constitutively in B lymphocytes. *J Cell Biol* 121, 1121-1132 (1993).
46. Leveille, C., R, A.L.-D. & Mourad, W. CD20 is physically and functionally coupled to MHC class II and CD40 on human B cell lines. *Eur J Immunol* 29, 65-74 (1999).

47. Petrie, R.J. & Deans, J.P. Colocalization of the B cell receptor and CD20 followed by activation-dependent dissociation in distinct lipid rafts. *J Immunol* 169, 2886-2891 (2002).
48. Li, H., Ayer, L.M., Lytton, J. & Deans, J.P. Store-operated cation entry mediated by CD20 in membrane rafts. *J Biol Chem* 278, 42427-42434 (2003).
49. de Petris, S. Preferential distribution of surface immunoglobulins on microvilli. *Nature* 272, 66-68 (1978).
50. Greicius, G. et al. Microvilli structures on B lymphocytes: inducible functional domains? *Int Immunol* 16, 353-364 (2004).
51. Shan, D., Ledbetter, J.A. & Press, O.W. Apoptosis of malignant human B cells by ligation of CD20 with monoclonal antibodies. *Blood* 91, 1644-1652 (1998).
52. Chan, H.T. et al. CD20-induced lymphoma cell death is independent of both caspases and its redistribution into triton X-100 insoluble membrane rafts. *Cancer Res* 63, 5480-5489 (2003).
53. Tedder, T.F., Klejman, G., Schlossman, S.F. & Saito, H. Structure of the gene encoding the human B lymphocyte differentiation antigen CD20 (B1). *J Immunol* 142, 2560-2568 (1989).
54. Holder, M., Grafton, G., MacDonald, I., Finney, M. & Gordon, J. Engagement of CD20 suppresses apoptosis in germinal center B cells. *Eur J Immunol* 25, 3160-3164 (1995).
55. Golay, J.T., Clark, E.A. & Beverley, P.C. The CD20 (Bp35) antigen is involved in activation of B cells from the G0 to the G1 phase of the cell cycle. *J Immunol* 135, 3795-3801 (1985).
56. Shan, D., Ledbetter, J.A. & Press, O.W. Signaling events involved in anti-CD20-induced apoptosis of malignant human B cells. *Cancer Immunol Immunother* 48, 673-683 (2000).
57. Uchida, J. et al. Mouse CD20 expression and function. *Int Immunol* 16, 119-129 (2004).
58. Parekh, A.B. & Putney, J.W., Jr. Store-operated calcium channels. *Physiol Rev* 85, 757-810 (2005).
59. Mori, Y. et al. Transient receptor potential 1 regulates capacitative Ca(2+) entry and Ca(2+) release from endoplasmic reticulum in B lymphocytes. *J Exp Med* 195, 673-681 (2002).

60. Grafton, G., Stokes, L., Toellner, K.M. & Gordon, J. A non-voltage-gated calcium channel with L-type characteristics activated by B cell receptor ligation. *Biochem Pharmacol* 66, 2001-2009 (2003).
61. Genot, E.M. et al. Phosphorylation of CD20 in cells from a hairy cell leukemia cell line. Evidence for involvement of calcium/calmodulin-dependent protein kinase II. *J Immunol* 151, 71-82 (1993).
62. Janas, E., Priest, R., Wilde, J.I., White, J.H. & Malhotra, R. Rituxan (anti-CD20 antibody)-induced translocation of CD20 into lipid rafts is crucial for calcium influx and apoptosis. *Clin Exp Immunol* 139, 439-446 (2005).
63. Hofmeister, J.K., Cooney, D. & Coggeshall, K.M. Clustered CD20 induced apoptosis: src-family kinase, the proximal regulator of tyrosine phosphorylation, calcium influx, and caspase 3-dependent apoptosis. *Blood Cells Mol Dis* 26, 133-143 (2000).
64. Montero, M., Garcia-Sancho, J. & Alvarez, J. Inhibition of the calcium store-operated calcium entry pathway by chemotactic peptide and by phorbol ester develops gradually and independently along differentiation of HL60 cells. *J Biol Chem* 268, 26911-26919 (1993).
65. Unruh, T.L. et al. Cholesterol depletion inhibits src family kinase-dependent calcium mobilization and apoptosis induced by rituximab crosslinking. *Immunology* 116, 223-232 (2005).
66. Deans, J.P., Robbins, S.M., Polyak, M.J. & Savage, J.A. Rapid redistribution of CD20 to a low density detergent-insoluble membrane compartment. *J Biol Chem* 273, 344-348 (1998).
67. Cragg, M.S. et al. Complement-mediated lysis by anti-CD20 mAb correlates with segregation into lipid rafts. *Blood* 101, 1045-1052 (2003).
68. Li, H. et al. The CD20 calcium channel is localized to microvilli and constitutively associated with membrane rafts: antibody binding increases the affinity of the association through an epitope-dependent cross-linking-independent mechanism. *J Biol Chem* 279, 19893-19901 (2004).
69. Pizzo, P. & Viola, A. Lymphocyte lipid rafts: structure and function. *Curr Opin Immunol* 15, 255-260 (2003).
70. Pizzo, P. & Viola, A. Lipid rafts in lymphocyte activation. *Microbes Infect* 6, 686-692 (2004).

71. Simons, K. & Vaz, W.L. Model systems, lipid rafts, and cell membranes. *Annu Rev Biophys Biomol Struct* 33, 269-295 (2004).
72. Filatov, A.V., Shmigol, I.B., Kuzin, II, Sharonov, G.V. & Feofanov, A.V. Resistance of cellular membrane antigens to solubilization with Triton X-100 as a marker of their association with lipid rafts--analysis by flow cytometry. *J Immunol Methods* 278, 211-219 (2003).
73. Melkonian, K.A., Ostermeyer, A.G., Chen, J.Z., Roth, M.G. & Brown, D.A. Role of lipid modifications in targeting proteins to detergent-resistant membrane rafts. Many raft proteins are acylated, while few are prenylated. *J Biol Chem* 274, 3910-3917 (1999).
74. Polyak, M.J., Tailor, S.H. & Deans, J.P. Identification of a cytoplasmic region of CD20 required for its redistribution to a detergent-insoluble membrane compartment. *J Immunol* 161, 3242-3248 (1998).
75. Wolven, A., van't Hof, W. & Resh, M.D. Analysis of myristoylated and palmitoylated Src family proteins. *Methods Mol Biol* 84, 261-266 (1998).
76. Brdicka, T. et al. Phosphoprotein associated with glycosphingolipid-enriched microdomains (PAG), a novel ubiquitously expressed transmembrane adaptor protein, binds the protein tyrosine kinase csk and is involved in regulation of T cell activation. *J Exp Med* 191, 1591-1604 (2000).
77. Bollinger, C.R., Teichgraber, V. & Gulbins, E. Ceramide-enriched membrane domains. *Biochim Biophys Acta* 1746, 284-294 (2005).
78. Bezombes, C. et al. Rituximab antiproliferative effect in B-lymphoma cells is associated with acid-sphingomyelinase activation in raft microdomains. *Blood* 104, 1166-1173 (2004).
79. Brown, D. GPI-anchored proteins and detergent-resistant membrane domains. *Braz J Med Biol Res* 27, 309-315 (1994).
80. Shogomori, H. & Brown, D.A. Use of detergents to study membrane rafts: the good, the bad, and the ugly. *Biol Chem* 384, 1259-1263 (2003).
81. Chamberlain, L.H. Detergents as tools for the purification and classification of lipid rafts. *FEBS Lett* 559, 1-5 (2004).
82. Brown, D. Structure and function of membrane rafts. *Int J Med Microbiol* 291, 433-437 (2002).

83. Trujillo, M.A., Jiang, S.W., Tarara, J.E. & Eberhardt, N.L. Clustering of the B cell receptor is not required for the apoptotic response. *DNA Cell Biol* 22, 513-523 (2003).

84. Kalia, L.V. & Salter, M.W. Interactions between Src family protein tyrosine kinases and PSD-95. *Neuropharmacology* 45, 720-728 (2003).

85. Polyak, M.J., Ayer, L.M., Szczepek, A.J. & Deans, J.P. A cholesterol-dependent CD20 epitope detected by the FMC7 antibody. *Leukemia* 17, 1384-1389 (2003).

86. Cragg, M.S., Walshe, C.A., Ivanov, A.O. & Glennie, M.J. The biology of CD20 and its potential as a target for mAb therapy. *Curr Dir Autoimmun* 8, 140-174 (2005).

87. Weeds, A. Actin-binding proteins--regulators of cell architecture and motility. *Nature* 296, 811-816 (1982).

88. Fujiwara, T., Ritchie, K., Murakoshi, H., Jacobson, K. & Kusumi, A. Phospholipids undergo hop diffusion in compartmentalized cell membrane. *J Cell Biol* 157, 1071-1081 (2002).

89. Fernandez, E.M., O'Toole, P.J., Morrison, I.E., Cherry, R.J. & Fernandez, N. Interaction of HLA-DR with actin microfilaments. *Hum Immunol* 64, 327-337 (2003).

90. Melamed, I. & Gelfand, E.W. Microfilament assembly is involved in B-cell apoptosis. *Cell Immunol* 194, 136-142 (1999).

91. Mathas, S., Rickers, A., Bommert, K., Dorken, B. & Mapara, M.Y. Anti-CD20- and B-cell receptor-mediated apoptosis: evidence for shared intracellular signaling pathways. *Cancer Res* 60, 7170-7176 (2000).

92. Bourget, I., Breittmayer, J.P., Grenier-Brossette, N. & Cousin, J.L. CD20 monoclonal antibodies down-regulate IgM at the surface of B cells. *Eur J Immunol* 23, 768-771 (1993).

93. Fujieda, S., Sugimoto, C., Seki, M., Sunaga, H. & Saito, H. CD40 stimulation inhibits cell growth and Fas-mediated apoptosis in a thyroid cancer cell line. *Oncol Res* 10, 433-439 (1998).

94. Anolik, J., Looney, R.J., Bottaro, A., Sanz, I. & Young, F. Down-regulation of CD20 on B cells upon CD40 activation. *Eur J Immunol* 33, 2398-2409 (2003).

95. Mone, A.P. et al. HuIDI0 induces apoptosis concurrent with activation of the AKT survival pathway in human chronic lymphocytic leukemia cells. *Blood* 103, 1846-1854 (2004).

96. Mimori, K. et al. Costimulatory signals distinctively affect CD20- and B-cell-antigen-receptor-mediated apoptosis in Burkitt's lymphoma/leukemia cells. *Leukemia* 17, 1164-1174 (2003).

97. Deans, J.P. et al. Association of tyrosine and serine kinases with the B cell surface antigen CD20. Induction via CD20 of tyrosine phosphorylation and activation of phospholipase C-gamma 1 and PLC phospholipase C-gamma 2. *J Immunol* 151, 4494-4504 (1993).

98. Deans, J.P. et al. Association of 75/80-kDa phosphoproteins and the tyrosine kinases Lyn, Fyn, and Lck with the B cell molecule CD20. Evidence against involvement of the cytoplasmic regions of CD20. *J Biol Chem* 270, 22632-22638 (1995).

99. Matsuoka, H., Nada, S. & Okada, M. Mechanism of Csk-mediated down-regulation of Src family tyrosine kinases in epidermal growth factor signaling. *J Biol Chem* 279, 5975-5983 (2004).

100. Ohtake, H., Ichikawa, N., Okada, M. & Yamashita, T. Cutting Edge: Transmembrane phosphoprotein Csk-binding protein/phosphoprotein associated with glycosphingolipid-enriched microdomains as a negative feedback regulator of mast cell signaling through the FcepsilonRI. *J Immunol* 168, 2087-2090 (2002).

101. Press, O.W., Howell-Clark, J., Anderson, S. & Bernstein, I. Retention of B-cell-specific monoclonal antibodies by human lymphoma cells. *Blood* 83, 1390-1397 (1994).

102. McLaughlin, P. et al. Rituximab chimeric anti-CD20 monoclonal antibody therapy for relapsed indolent lymphoma: half of patients respond to a four-dose treatment program. *J Clin Oncol* 16, 2825-2833 (1998).

103. Armitage, J.O. & Weisenburger, D.D. New approach to classifying non-Hodgkin's lymphomas: clinical features of the major histologic subtypes. Non-Hodgkin's Lymphoma Classification Project. *J Clin Oncol* 16, 2780-2795 (1998).

104. Stern, M. & Herrmann, R. Overview of monoclonal antibodies in cancer therapy: present and promise. *Crit Rev Oncol Hematol* 54, 11-29 (2005).

105. Maloney, D.G., Smith, B. & Rose, A. Rituximab: mechanism of action and resistance. *Semin Oncol* 29, 2-9 (2002).

106. Colombat, P. et al. Rituximab (anti-CD20 monoclonal antibody) as single first-line therapy for patients with follicular lymphoma with a low tumor burden: clinical and molecular evaluation. *Blood* 97, 101-106 (2001).

107. Piro, L.D. et al. Extended Rituximab (anti-CD20 monoclonal antibody) therapy for relapsed or refractory low-grade or follicular non-Hodgkin's lymphoma. *Ann Oncol* 10, 655-661 (1999).

108. Czuczman, M.S., Weaver, R., Alkuzweny, B., Berlfein, J. & Grillo-Lopez, A.J. Prolonged clinical and molecular remission in patients with low-grade or follicular non-Hodgkin's lymphoma treated with rituximab plus CHOP chemotherapy: 9-year follow-up. *J Clin Oncol* 22, 4711-4716 (2004).

109. Friedberg, J.W. et al. Combination immunotherapy with rituximab and interleukin 2 in patients with relapsed or refractory follicular non-Hodgkin's lymphoma. *Br J Haematol* 117, 828-834 (2002).

110. Witzig, T.E. et al. Treatment with ibritumomab tiuxetan radioimmunotherapy in patients with rituximab-refractory follicular non-Hodgkin's lymphoma. *J Clin Oncol* 20, 3262-3269 (2002).

111. Liu, S.Y. et al. Follow-up of relapsed B-cell lymphoma patients treated with iodine-131-labeled anti-CD20 antibody and autologous stem-cell rescue. *J Clin Oncol* 16, 3270-3278 (1998).

112. Vose, J.M. et al. Phase II study of rituximab in combination with chop chemotherapy in patients with previously untreated, aggressive non-Hodgkin's lymphoma. *J Clin Oncol* 19, 389-397 (2001).

113. Horning, S.J. Treatment approaches to the low-grade lymphomas. *Blood* 83, 881-884 (1994).

114. Mothersill, C. & Seymour, C.B. Radiation-induced bystander effects--implications for cancer. *Nat Rev Cancer* 4, 158-164 (2004).

115. Coleman, M. et al. Epratuzumab: targeting B-cell malignancies through CD22. *Clin Cancer Res* 9, 3991S-3994S (2003).

116. Jensen, M.C., Cooper, L.J., Wu, A.M., Forman, S.J. & Raubitschek, A. Engineered CD20-specific primary human cytotoxic T lymphocytes for targeting B-cell malignancy. *Cytotherapy* 5, 131-138 (2003).

117. Haidar, J.H. et al. Loss of CD20 expression in relapsed lymphomas after rituximab therapy. *Eur J Haematol* 70, 330-332 (2003).

118. Golay, J. et al. Biologic response of B lymphoma cells to anti-CD20 monoclonal antibody rituximab in vitro: CD55 and CD59 regulate complement-mediated cell lysis. *Blood* 95, 3900-3908 (2000).

119. Beum, P.V., Kennedy, A.D., Williams, M.E., Lindorfer, M.A. & Taylor, R.P. The shaving reaction: rituximab/CD20 complexes are removed from mantle cell lymphoma and chronic lymphocytic leukemia cells by THP-1 monocytes. *J Immunol* 176, 2600-2609 (2006).

120. Gong, Q. et al. Importance of cellular microenvironment and circulatory dynamics in B cell immunotherapy. *J Immunol* 174, 817-826 (2005).

121. Akhtar, S. & Maghfoor, I. Rituximab plus CHOP for diffuse large-B-cell lymphoma. *N Engl J Med* 346, 1830-1831; author reply 1830-1831 (2002).

122. Treon, S.P. et al. Tumor cell expression of CD59 is associated with resistance to CD20 serotherapy in patients with B-cell malignancies. *J Immunother* 24, 263-271 (2001).

123. Howard, O.M. et al. Rituximab and CHOP induction therapy for newly diagnosed mantle-cell lymphoma: molecular complete responses are not predictive of progression-free survival. *J Clin Oncol* 20, 1288-1294 (2002).

124. Leandro, M.J., Edwards, J.C., Cambridge, G., Ehrenstein, M.R. & Isenberg, D.A. An open study of B lymphocyte depletion in systemic lupus erythematosus. *Arthritis Rheum* 46, 2673-2677 (2002).

125. Manfredi, R. et al. Rituximab alone proves effective in the treatment of refractory, severe stage III AIDS-related non-Hodgkin's paediatric lymphoma. *Aids* 17, 2146-2148 (2003).

126. Leandro, M.J., Edwards, J.C. & Cambridge, G. Clinical outcome in 22 patients with rheumatoid arthritis treated with B lymphocyte depletion. *Ann Rheum Dis* 61, 883-888 (2002).

127. Di Gaetano, N. et al. Complement activation determines the therapeutic activity of rituximab in vivo. *J Immunol* 171, 1581-1587 (2003).

128. Manches, O. et al. In vitro mechanisms of action of rituximab on primary non-Hodgkin lymphomas. *Blood* 101, 949-954 (2003).

129. Byrd, J.C. et al. The mechanism of tumor cell clearance by rituximab in vivo in patients with B-cell chronic lymphocytic leukemia: evidence of caspase activation and apoptosis induction. *Blood* 99, 1038-1043 (2002).

130. Bonavida, B. & Vega, M.I. Rituximab-mediated chemosensitization of AIDS and non-AIDS non-Hodgkin's lymphoma. *Drug Resist Updat* 8, 27-41 (2005).
131. Jazirehi, A.R. & Bonavida, B. Cellular and molecular signal transduction pathways modulated by rituximab (rituxan, anti-CD20 mAb) in non-Hodgkin's lymphoma: implications in chemosensitization and therapeutic intervention. *Oncogene* 24, 2121-2143 (2005).
132. Hsu, F.J. & Komarovskaya, M. CTLA4 blockade maximizes antitumor T-cell activation by dendritic cells presenting idiotype protein or opsonized anti-CD20 antibody-coated lymphoma cells. *J Immunother* 25, 455-468 (2002).
133. Palomba, M.L. et al. CD8+ T-cell-dependent immunity following xenogeneic DNA immunization against CD20 in a tumor challenge model of B-cell lymphoma. *Clin Cancer Res* 11, 370-379 (2005).
134. Hamaguchi, Y. et al. The peritoneal cavity provides a protective niche for B1 and conventional B lymphocytes during anti-CD20 immunotherapy in mice. *J Immunol* 174, 4389-4399 (2005).
135. Gelderman, K.A., Tomlinson, S., Ross, G.D. & Gorter, A. Complement function in mAb-mediated cancer immunotherapy. *Trends Immunol* 25, 158-164 (2004).
136. Oglesby, T.J., Allen, C.J., Liszewski, M.K., White, D.J. & Atkinson, J.P. Membrane cofactor protein (CD46) protects cells from complement-mediated attack by an intrinsic mechanism. *J Exp Med* 175, 1547-1551 (1992).
137. Harjunpaa, A., Junnikkala, S. & Meri, S. Rituximab (anti-CD20) therapy of B-cell lymphomas: direct complement killing is superior to cellular effector mechanisms. *Scand J Immunol* 51, 634-641 (2000).
138. Harjunpaa, A. et al. Complement activation in circulation and central nervous system after rituximab (anti-CD20) treatment of B-cell lymphoma. *Leuk Lymphoma* 42, 731-738 (2001).
139. Idusogie, E.E. et al. Mapping of the C1q binding site on rituxan, a chimeric antibody with a human IgG1 Fc. *J Immunol* 164, 4178-4184 (2000).
140. Kennedy, A.D. et al. An anti-C3b(i) mAb enhances complement activation, C3b(i) deposition, and killing of CD20+ cells by rituximab. *Blood* 101, 1071-1079 (2003).
141. Cragg, M.S. & Glennie, M.J. Antibody specificity controls in vivo effector mechanisms of anti-CD20 reagents. *Blood* 103, 2738-2743 (2004).

142. Weng, W.K. & Levy, R. Expression of complement inhibitors CD46, CD55, and CD59 on tumor cells does not predict clinical outcome after rituximab treatment in follicular non-Hodgkin lymphoma. *Blood* 98, 1352-1357 (2001).

143. Bannerji, R. et al. Apoptotic-regulatory and complement-protecting protein expression in chronic lymphocytic leukemia: relationship to in vivo rituximab resistance. *J Clin Oncol* 21, 1466-1471 (2003).

144. Hamaguchi, Y., Xiu, Y., Komura, K., Nimmerjahn, F. & Tedder, T.F. Antibody isotype-specific engagement of Fcgamma receptors regulates B lymphocyte depletion during CD20 immunotherapy. *J Exp Med* 203, 743-753 (2006).

145. Herlyn, D. & Koprowski, H. IgG2a monoclonal antibodies inhibit human tumor growth through interaction with effector cells. *Proc Natl Acad Sci U S A* 79, 4761-4765 (1982).

146. Kaminski, M.S., Kitamura, K., Maloney, D.G., Campbell, M.J. & Levy, R. Importance of antibody isotype in monoclonal anti-idiotype therapy of a murine B cell lymphoma. A study of hybridoma class switch variants. *J Immunol* 136, 1123-1130 (1986).

147. Catalfamo, M. & Henkart, P.A. Perforin and the granule exocytosis cytotoxicity pathway. *Curr Opin Immunol* 15, 522-527 (2003).

148. Uchida, J. et al. The innate mononuclear phagocyte network depletes B lymphocytes through Fc receptor-dependent mechanisms during anti-CD20 antibody immunotherapy. *J Exp Med* 199, 1659-1669 (2004).

149. Clynes, R.A., Towers, T.L., Presta, L.G. & Ravetch, J.V. Inhibitory Fc receptors modulate in vivo cytoxicity against tumor targets. *Nat Med* 6, 443-446 (2000).

150. Dall'Ozzo, S. et al. Rituximab-dependent cytotoxicity by natural killer cells: influence of FCGR3A polymorphism on the concentration-effect relationship. *Cancer Res* 64, 4664-4669 (2004).

151. Farag, S.S. et al. Fc gamma RIIIa and Fc gamma RIIa polymorphisms do not predict response to rituximab in B-cell chronic lymphocytic leukemia. *Blood* 103, 1472-1474 (2004).

152. Choi, C., Jeong, E. & Benveniste, E.N. Caspase-1 mediates Fas-induced apoptosis and is up-regulated by interferon-gamma in human astrocytoma cells. *J Neurooncol* 67, 167-176 (2004).

153. Martelli, A.M. et al. Nuclear apoptotic changes: an overview. *J Cell Biochem* 82, 634-646 (2001).

154. Thornberry, N.A. & Lazebnik, Y. Caspases: enemies within. *Science* 281, 1312-1316 (1998).
155. Cragg, M.S. et al. Complement mediated cell death is associated with DNA fragmentation. *Cell Death Differ* 7, 48-58 (2000).
156. Sakahira, H., Enari, M. & Nagata, S. Cleavage of CAD inhibitor in CAD activation and DNA degradation during apoptosis. *Nature* 391, 96-99 (1998).
157. Adams, J.M. & Cory, S. The Bcl-2 protein family: arbiters of cell survival. *Science* 281, 1322-1326 (1998).
158. Opferman, J.T. & Korsmeyer, S.J. Apoptosis in the development and maintenance of the immune system. *Nat Immunol* 4, 410-415 (2003).
159. Deans, J.P., Li, H. & Polyak, M.J. CD20-mediated apoptosis: signalling through lipid rafts. *Immunology* 107, 176-182 (2002).
160. van der Kolk, L.E. et al. CD20-induced B cell death can bypass mitochondria and caspase activation. *Leukemia* 16, 1735-1744 (2002).
161. Ghetie, M.A., Bright, H. & Vitetta, E.S. Homodimers but not monomers of Rituxan (chimeric anti-CD20) induce apoptosis in human B-lymphoma cells and synergize with a chemotherapeutic agent and an immunotoxin. *Blood* 97, 1392-1398 (2001).
162. Cardarelli, P.M. et al. Binding to CD20 by anti-B1 antibody or F(ab')(2) is sufficient for induction of apoptosis in B-cell lines. *Cancer Immunol Immunother* 51, 15-24 (2002).
163. Tutt, A.L. et al. Monoclonal antibody therapy of B cell lymphoma: signaling activity on tumor cells appears more important than recruitment of effectors. *J Immunol* 161, 3176-3185 (1998).
164. Weiss, L.M., Warnke, R.A., Sklar, J. & Cleary, M.L. Molecular analysis of the t(14;18) chromosomal translocation in malignant lymphomas. *N Engl J Med* 317, 1185-1189 (1987).
165. Clybouw, C. et al. EBV infection of human B lymphocytes leads to down-regulation of Bim expression: relationship to resistance to apoptosis. *J Immunol* 175, 2968-2973 (2005).
166. Alas, S., Emmanouilides, C. & Bonavida, B. Inhibition of interleukin 10 by rituximab results in down-regulation of bcl-2 and sensitization of B-cell non-Hodgkin's lymphoma to apoptosis. *Clin Cancer Res* 7, 709-723 (2001).

167. Loomis, R., Carbone, R., Reiss, M. & Lacy, J. Bcl-2 antisense (G3139, Genasense) enhances the in vitro and in vivo response of Epstein-Barr virus-associated lymphoproliferative disease to rituximab. *Clin Cancer Res* 9, 1931-1939 (2003).

168. Sanchez-Beato, M., Sanchez-Aguilera, A. & Piris, M.A. Cell cycle deregulation in B-cell lymphomas. *Blood* 101, 1220-1235 (2003).

169. Yin, Y., Liu, Y.X., Jin, Y.J., Hall, E.J. & Barrett, J.C. PAC1 phosphatase is a transcription target of p53 in signalling apoptosis and growth suppression. *Nature* 422, 527-531 (2003).

170. Erenpreisa, J. & Cragg, M.S. Mitotic death: a mechanism of survival? A review. *Cancer Cell Int* 1, 1 (2001).

171. Proskuryakov, S.Y., Gabai, V.L., Konoplyannikov, A.G., Zamulaeva, I.A. & Kolesnikova, A.I. Immunology of apoptosis and necrosis. *Biochemistry (Mosc)* 70, 1310-1320 (2005).

172. Kemp, T.J., Kim, J.S., Crist, S.A. & Griffith, T.S. Induction of necrotic tumor cell death by TRAIL/Apo-2L. *Apoptosis* 8, 587-599 (2003).

173. Sakon, S. et al. NF-kappaB inhibits TNF-induced accumulation of ROS that mediate prolonged MAPK activation and necrotic cell death. *Embo J* 22, 3898-3909 (2003).

174. Trubiani, O., Bosco, D. & Di Primio, R. Interferon-gamma (IFN-gamma) induces programmed cell death in differentiated human leukemic B cell lines. *Exp Cell Res* 215, 23-27 (1994).

175. Jaattela, M. & Tschopp, J. Caspase-independent cell death in T lymphocytes. *Nat Immunol* 4, 416-423 (2003).

176. Engedal, N. & Saatcioglu, F. Ceramide-induced cell death in the prostate cancer cell line LNCaP has both necrotic and apoptotic features. *Prostate* 46, 289-297 (2001).

177. Shinoura, N., Yoshida, Y., Asai, A., Kirino, T. & Hamada, H. Relative level of expression of Bax and Bcl-XL determines the cellular fate of apoptosis/necrosis induced by the overexpression of Bax. *Oncogene* 18, 5703-5713 (1999).

178. Manshouri, T. et al. Circulating CD20 is detectable in the plasma of patients with chronic lymphocytic leukemia and is of prognostic significance. *Blood* 101, 2507-2513 (2003).

179. Leist, M. & Jaattela, M. Four deaths and a funeral: from caspases to alternative mechanisms. *Nat Rev Mol Cell Biol* 2, 589-598 (2001).

180. Daniels, I., Abulayha, A.M., Thomson, B.J. & Haynes, A.P. Caspase-independent killing of Burkitt lymphoma cell lines by rituximab. *Apoptosis* (2006).

181. Selenko, N. et al. Cross-priming of cytotoxic T cells promoted by apoptosis-inducing tumor cell reactive antibodies? *J Clin Immunol* 22, 124-130 (2002).

182. Szollosi, J., Horejsi, V., Bene, L., Angelisova, P. & Damjanovich, S. Supramolecular complexes of MHC class I, MHC class II, CD20, and tetraspan molecules (CD53, CD81, and CD82) at the surface of a B cell line JY. *J Immunol* 157, 2939-2946 (1996).

183. Kucharczak, J., Simmons, M.J., Fan, Y. & Gelinas, C. To be, or not to be: NF-kappaB is the answer--role of Rel/NF-kappaB in the regulation of apoptosis. *Oncogene* 22, 8961-8982 (2003).

184. Karin, M. & Lin, A. NF-kappaB at the crossroads of life and death. *Nat Immunol* 3, 221-227 (2002).

185. Khoshnan, A. et al. The NF-kappa B cascade is important in Bcl-xL expression and for the anti-apoptotic effects of the CD28 receptor in primary human CD4+ lymphocytes. *J Immunol* 165, 1743-1754 (2000).

186. Vega, M.I. et al. Rituximab inhibits p38 MAPK activity in 2F7 B NHL and decreases IL-10 transcription: pivotal role of p38 MAPK in drug resistance. *Oncogene* 23, 3530-3540 (2004).

187. Jazirehi, A.R., Huerta-Yepez, S., Cheng, G. & Bonavida, B. Rituximab (chimeric anti-CD20 monoclonal antibody) inhibits the constitutive nuclear factor-{kappa}B signaling pathway in non-Hodgkin's lymphoma B-cell lines: role in sensitization to chemotherapeutic drug-induced apoptosis. *Cancer Res* 65, 264-276 (2005).

188. Laemmli, U.K. Cleavage of structural proteins during the assembly of the head of bacteriophage T4. *Nature* 227, 680-685 (1970).

189. Pfeiffer, A. et al. Lipopolysaccharide and ceramide docking to CD14 provokes ligand-specific receptor clustering in rafts. *Eur J Immunol* 31, 3153-3164 (2001).

190. Szollosi, J. et al. Fluorescence energy transfer measurements on cell surfaces: a critical comparison of steady-state fluorimetric and flow cytometric methods. *Cytometry* 5, 210-216 (1984).

191. McManus, M.T. & Sharp, P.A. Gene silencing in mammals by small interfering RNAs. *Nat Rev Genet* 3, 737-747 (2002).

192. Glennie, M.J., McBride, H.M., Worth, A.T. & Stevenson, G.T. Preparation and performance of bispecific F(ab' gamma)2 antibody containing thioether-linked Fab' gamma fragments. *J Immunol* 139, 2367-2375 (1987).

193. Smith, P.K. et al. Measurement of protein using bicinchoninic acid. *Anal Biochem* 150, 76-85 (1985).

194. Vermes, I., Haanen, C., Steffens-Nakken, H. & Reutelingsperger, C. A novel assay for apoptosis. Flow cytometric detection of phosphatidylserine expression on early apoptotic cells using fluorescein labelled Annexin V. *J Immunol Methods* 184, 39-51 (1995).

195. Nicoletti, I., Migliorati, G., Pagliacci, M.C., Grignani, F. & Riccardi, C. A rapid and simple method for measuring thymocyte apoptosis by propidium iodide staining and flow cytometry. *J Immunol Methods* 139, 271-279 (1991).

196. Roos, D. & Voetman, A.A. Preparation and cryopreservation of cytoplasts from human phagocytes. *Methods Enzymol* 132, 250-257 (1986).

197. Armati-Gulson, P.J., Lisak, R.P., Kuchmy, D. & Pollard, J. 51Cr release cytotoxicity radioimmunoassay to detect immune cytotoxic reactions to rat Schwann cells in vitro. *Neurosci Lett* 35, 321-326 (1983).

198. Vugmeyster, Y. & Howell, K. Rituximab-mediated depletion of cynomolgus monkey B cells in vitro in different matrices: possible inhibitory effect of IgG. *Int Immunopharmacol* 4, 1117-1124 (2004).

199. Carroll, M.C. The complement system in regulation of adaptive immunity. *Nat Immunol* 5, 981-986 (2004).

200. Teeling, J.L. et al. Characterization of new human CD20 monoclonal antibodies with potent cytolytic activity against non-Hodgkin lymphomas. *Blood* 104, 1793-1800 (2004).

201. Kono, H. et al. FcgammaRIIB Ile232Thr transmembrane polymorphism associated with human systemic lupus erythematosus decreases affinity to lipid rafts and attenuates inhibitory effects on B cell receptor signaling. *Hum Mol Genet* 14, 2881-2892 (2005).

202. Poloso, N.J., Muntasell, A. & Roche, P.A. MHC class II molecules traffic into lipid rafts during intracellular transport. *J Immunol* 173, 4539-4546 (2004).
203. Karacsonyi, C., Bedke, T., Hinrichsen, N., Schwinzer, R. & Lindner, R. MHC II molecules and invariant chain reside in membranes distinct from conventional lipid rafts. *J Leukoc Biol* 78, 1097-1105 (2005).
204. Carafoli, E. Calcium signaling: a tale for all seasons. *Proc Natl Acad Sci U S A* 99, 1115-1122 (2002).
205. Grynkiewicz, G., Poenie, M. & Tsien, R.Y. A new generation of Ca2+ indicators with greatly improved fluorescence properties. *J Biol Chem* 260, 3440-3450 (1985).
206. Mills, D.M., Stolpa, J.C. & Cambier, J.C. Cognate B cell signaling via MHC class II: differential regulation of B cell antigen receptor and MHC class II/Ig-alpha beta signaling by CD22. *J Immunol* 172, 195-201 (2004).
207. Hederer, R.A. et al. The CD45 tyrosine phosphatase regulates Campath-1H (CD52)-induced TCR-dependent signal transduction in human T cells. *Int Immunol* 12, 505-516 (2000).
208. Hoth, M. & Penner, R. Depletion of intracellular calcium stores activates a calcium current in mast cells. *Nature* 355, 353-356 (1992).
209. Toth, S., Csermely, P., Beregi, E., Szkladanyi, A. & Szabo, L.D. Decreased cytosolic free calcium concentration of aged human lymphocytes in resting state. *Compr Gerontol [A]* 3 Suppl, 16-22 (1989).
210. Vigorito, E., Clayton, E. & Turner, M. BCR activation of PI3K is Vav-independent in murine B cells. *Biochem Soc Trans* 32, 781-784 (2004).
211. Kohno, M. & Pouyssegur, J. Pharmacological inhibitors of the ERK signaling pathway: application as anticancer drugs. *Prog Cell Cycle Res* 5, 219-224 (2003).
212. Simon, C., Goepfert, H. & Boyd, D. Inhibition of the p38 mitogen-activated protein kinase by SB 203580 blocks PMA-induced Mr 92,000 type IV collagenase secretion and in vitro invasion. *Cancer Res* 58, 1135-1139 (1998).
213. Ebel, C., Schmidt, R.E. & Hundt, M. Signal transduction via both human low-affinity IgG Fc receptors, Fc gamma RIIa and Fc gamma RIIIb, depends on the activity of different families of intracellular kinases. *Immunobiology* 203, 616-628 (2001).

214. Curnow, S.J., Glennie, M.J. & Stevenson, G.T. Cytoplasmic calcium fluxes induced in cytotoxic effector cells by engagement of Fc gamma receptors I, II, and III. *Scand J Immunol* 36, 221-231 (1992).

215. van de Winkel, J.G., Tax, W.J., Jacobs, C.W., Huizinga, T.W. & Willems, P.H. Cross-linking of both types of IgG Fc receptors, Fc gamma RI and Fc gamma RII, enhances intracellular free Ca2+ in the monocytic cell line U937. *Scand J Immunol* 31, 315-325 (1990).

216. Dighiero, G. CLL Biology and Prognosis. *Hematology (Am Soc Hematol Educ Program)*, 278-284 (2005).

217. Flaswinkel, H., Weiser, P., Kim, K.M. & Reth, M. Signaling and internalisation function of the B cell antigen receptor complex. *Adv Exp Med Biol* 365, 1-8 (1994).

218. Amaral, M.C., Casillas, A.M. & Nel, A.E. Contrasting effects of two tumour promoters, phorbol myristate acetate and okadaic acid, on T-cell responses and activation of p42 MAP-kinase/ERK-2. *Immunology* 79, 24-31 (1993).

219. Aggarwal, B.B. et al. Nuclear transcription factor NF-kappa B: role in biology and medicine. *Indian J Exp Biol* 42, 341-353 (2004).

220. Kriehuber, E. et al. Balance between NF-kappaB and JNK/AP-1 activity controls dendritic cell life and death. *Blood* 106, 175-183 (2005).

221. Vega, M.I., Jazirehi, A.R., Huerta-Yepez, S. & Bonavida, B. Rituximab-induced inhibition of YY1 and Bcl-xL expression in Ramos non-Hodgkin's lymphoma cell line via inhibition of NF-kappa B activity: role of YY1 and Bcl-xL in Fas resistance and chemoresistance, respectively. *J Immunol* 175, 2174-2183 (2005).

222. Johnson, S.A. et al. Phosphorylated immunoreceptor signaling motifs (ITAMs) exhibit unique abilities to bind and activate Lyn and Syk tyrosine kinases. *J Immunol* 155, 4596-4603 (1995).

223. Kneitz, C., Wilhelm, M. & Tony, H.P. Effective B cell depletion with rituximab in the treatment of autoimmune diseases. *Immunobiology* 206, 519-527 (2002).

224. Eisenberg, R. SLE - Rituximab in lupus. *Arthritis Res Ther* 5, 157-159 (2003).

225. Murphy, S.B., Harris, A. & Williams, D.L. Chromosomal translocations and timing of malignant transformation in Burkitt's lymphoma. *N Engl J Med* 311, 195-196 (1984).

226. Cuomo, L. et al. Expression of the Epstein-Barr virus (EBV)-encoded membrane protein LMP1 impairs the in vitro growth, clonability and

tumorigenicity of an EBV-negative Burkitt lymphoma line. *Int J Cancer* 51, 949-955 (1992).

227. Fratelli, M., Galli, G., Minto, M. & Pasinetti, G.M. Role of clusterin in cell adhesion during early phases of programmed cell death in P19 embryonic carcinoma cells. *Biochim Biophys Acta* 1311, 71-76 (1996).
228. Dumont, F.J., Fischer, P. & Sirotina, A. Increased LFA-1-mediated homotypic cell adhesion is associated with the G1 growth arrest induced by rapamycin in a T cell lymphoma. *Exp Cell Res* 219, 146-158 (1995).
229. van Kooyk, Y. & Figdor, C.G. Signalling and adhesive properties of the integrin leucocyte function-associated antigen 1 (LFA-1). *Biochem Soc Trans* 25, 515-520 (1997).
230. Chen, R.H., Wang, W.J. & Kuo, J.C. The tumor suppressor DAP-kinase links cell adhesion and cytoskeleton reorganization to cell death regulation. *J Biomed Sci*, 1-7 (2006).
231. Gourlay, C.W. & Ayscough, K.R. The actin cytoskeleton in ageing and apoptosis. *FEMS Yeast Res* 5, 1193-1198 (2005).
232. Bubb, M.R., Senderowicz, A.M., Sausville, E.A., Duncan, K.L. & Korn, E.D. Jasplakinolide, a cytotoxic natural product, induces actin polymerization and competitively inhibits the binding of phalloidin to F-actin. *J Biol Chem* 269, 14869-14871 (1994).
233. Sugidachi, A. et al. Inhibition of rat platelet aggregation by mycalolide-B, a novel inhibitor of actin polymerization with a different mechanism of action from cytochalasin-D. *Thromb Haemost* 79, 614-619 (1998).
234. Coue, M., Brenner, S.L., Spector, I. & Korn, E.D. Inhibition of actin polymerization by latrunculin A. *FEBS Lett* 213, 316-318 (1987).
235. Misaghi, S., Pacold, M.E., Blom, D., Ploegh, H.L. & Korbel, G.A. Using a small molecule inhibitor of peptide: N-glycanase to probe its role in glycoprotein turnover. *Chem Biol* 11, 1677-1687 (2004).
236. Hanke, J.H. et al. Discovery of a novel, potent, and Src family-selective tyrosine kinase inhibitor. Study of Lck- and FynT-dependent T cell activation. *J Biol Chem* 271, 695-701 (1996).
237. Springer, T.A. & Wang, J.H. The three-dimensional structure of integrins and their ligands, and conformational regulation of cell adhesion. *Adv Protein Chem* 68, 29-63 (2004).

238. Hynes, R.O. Integrins: bidirectional, allosteric signaling machines. *Cell* 110, 673-687 (2002).

239. Miletic, A.V., Swat, M., Fujikawa, K. & Swat, W. Cytoskeletal remodeling in lymphocyte activation. *Curr Opin Immunol* 15, 261-268 (2003).

240. Ramanarayanan, J., Hernandez-Ilizaliturri, F.J., Chanan-Khan, A. & Czuczman, M.S. Pro-apoptotic therapy with the oligonucleotide Genasense (oblimersen sodium) targeting Bcl-2 protein expression enhances the biological anti-tumour activity of rituximab. *Br J Haematol* 127, 519-530 (2004).

241. Rose, A.L., Smith, B.E. & Maloney, D.G. Glucocorticoids and rituximab in vitro: synergistic direct antiproliferative and apoptotic effects. *Blood* 100, 1765-1773 (2002).

242. Breckenridge, D.G., Germain, M., Mathai, J.P., Nguyen, M. & Shore, G.C. Regulation of apoptosis by endoplasmic reticulum pathways. *Oncogene* 22, 8608-8618 (2003).

243. Wossning, T. & Reth, M. B cell antigen receptor assembly and Syk activation in the S2 cell reconstitution system. *Immunol Lett* 92, 67-73 (2004).

244. Kurosaki, T. et al. Role of the Syk autophosphorylation site and SH2 domains in B cell antigen receptor signaling. *J Exp Med* 182, 1815-1823 (1995).

245. Gallo, E.M., Cante-Barrett, K. & Crabtree, G.R. Lymphocyte calcium signaling from membrane to nucleus. *Nat Immunol* 7, 25-32 (2006).

246. Pedersen, I.M., Buhl, A.M., Klausen, P., Geisler, C.H. & Jurlander, J. The chimeric anti-CD20 antibody rituximab induces apoptosis in B-cell chronic lymphocytic leukemia cells through a p38 mitogen activated protein-kinase-dependent mechanism. *Blood* 99, 1314-1319 (2002).

247. Cittera, E. et al. Rituximab induces different but overlapping sets of genes in human B-lymphoma cell lines. *Cancer Immunol Immunother* 54, 273-286 (2005).